UNIVERSIDAD AUTONOMA DE MADRID

Departamento de Bioquímica

TESIS DOCTORAL

EFECTOS ADVERSOS DE LA RAPAMICINA EN LAS ACCIONES DE LA INSULINA Y LA NOREPINEFRINA EN LOS ADIPOCITOS MARRONES

ESTER GARCÍA-CASARRUBIOS PIMENTEL

Madrid, 2017

DEPARTAMENTO DE BIOQUIMICA

FACULTAD DE MEDICINA

UNIVERSIDAD AUTONOMA DE MADRID

EFECTOS ADVERSOS DE LA RAPAMICINA EN LAS ACCIONES DE LA INSULINA Y LA NOREPINEFRINA EN LOS ADIPOCITOS MARRONES

Memoria presentada por la licenciada en Biología
Ester García-Casarrubios Pimentel para optar al grado de
Doctor por la Universidad Autónoma de Madrid

Directoras de Tesis: Ángela Mª Martínez Valverde
María Jesús Obregón Perea

Instituto de Investigaciones Biomédicas "Alberto Sols" de Madrid,
CSIC-UAM

Madrid, 2017

Ángela Mª Martínez Valverde, Investigadora Científica del Consejo Superior de Investigaciones Científicas en el Instituto de Investigaciones Biomédicas "Alberto Sols" de Madrid (CSIC-UAM)

María Jesús Obregón Perea, Profesora de Investigación del Consejo Superior de Investigaciones Científicas en el Instituto de Investigaciones Biomédicas "Alberto Sols" de Madrid (CSIC-UAM)

CERTIFICAN: que Ester García-Casarrubios Pimentel, Licenciada en Biología por la Universidad de Alcalá de Henares, ha realizado bajo su dirección el trabajo de investigación titulado:

"EFECTOS ADVERSOS DE LA RAPAMICINA EN LAS ACCIONES DE LA INSULINA Y LA NOREPINEFRINA EN LOS ADIPOCITOS MARRONES"

Las que suscriben consideran el trabajo realizado satisfactorio y apto para ser presentado como Tesis Doctoral en el Departamento de Bioquímica de la Universidad Autónoma de Madrid.

Y para que conste donde proceda, expiden el presente certificado.

Madrid, 31 de Marzo de 2017

Fdo. Ángela Mª Martínez Valverde
Directora de la tesis

Fdo. María Jesús Obregón Perea
Directora de la tesis

Esta Tesis doctoral ha sido financiada por un contrato predoctoral asociado al proyecto MOIR-CM S2010/BMD2423 (Comunidad de Madrid) concedido a Ángela Mª Martínez Valverde (Subproyecto HEPIR) y María Jesús Obregón Perea (Subproyecto ADIPOGEN), así como por los proyectos SAF2012-33283 concedido a Ángela Mª Martínez Valverde y SAF2012-32491 concedido a María Jesús Obregón Perea por el Ministerio de Economía y Competitividad.

“Quise la sabiduría más que la salud y la belleza,
y me propuse tenerla por luz.
Con ella me vinieron todos los bienes juntos.
La quise y la rondé desde muchacho,
enamorado de su hermosura”
Sb 7, 10-11

“La ciencia, a pesar de sus progresos increíbles, no puede ni podrá nunca explicarlo todo. Cada vez ganará nuevas zonas a lo que hoy parece inexplicable.
Pero las rayas fronterizas del saber, por muy lejos que se eleven, siempre tendrán delante un infinito mundo de misterio”
Gregorio Marañón

A mis padres

A mi hermana

A Miguel, a

Pablo y al Futuro

Agradecimientos

Agradecimientos

Agradecimientos

Al final lo he/hemos conseguido; tras mucho esfuerzo aquí está la recompensa al trabajo, dedicación, tiempo, paciencia y apoyo de muchas personas. Esta tesis es tan mía como vuestra, por eso espero estéis orgullosos y la disfrutéis tanto como yo.

Quería agradecer en primer lugar a María Jesús y Ángela la oportunidad que me dieron de poder realizar una tesis doctoral, era un objetivo desde hacía muchos años y sin ellas no hubiera sido posible. María Jesús, he aprendido muchísimo de tu rigor científico y te agradezco la ayuda que siempre has estado dispuesta a ofrecer. Ángela, me llevo aprendida la perseverancia en el trabajo y un buen número de horas de cultivos que me hicieron disfrutar mucho.

Gracias al personal que compone el IIBm: limpieza, recepción, personal de cultivos, cocina y lavado, animalario, mantenimiento, residuos, almacén, informática, microscopía, gestión y administración. Mención especial para el personal de Protección Radiológica: mil gracias por todo, siempre habéis facilitado mucho la tarea y me llevo un recuerdo estupendo de la "temida radiactividad".

Por supuesto merecen un gracias inmenso los compañeros de otros laboratorios con quienes he compartido risas, momentos de crisis y mucha sabiduría: Sol, Elvira y Yuri, ¡enhorabuena doctores! Mónica, Bárbara, María, Carla, Anita, Patricia: gracias por todo.

Lo bueno de haber pertenecido a dos labos es que los compañeros de trabajo son el doble! En el 2.8, muchas gracias Rosa y Raquel por hacer que el inicio fuese más fácil, por resolver tantas dudas y estar siempre dispuestas a tender una mano. Nuria, muchas gracias por la ayuda en la recta final; espero que te vaya muy bien, da gusto tenerte en el laboratorio. Laura, yo no sé qué habría hecho sin ti, eres mi mano derecha; toda tu dedicación, tu buen hacer, tu disposición, tus ganas de aprender y en muchas ocasiones tus ánimos han dado como resultado este trabajo. Más allá de lo profesional estoy muy satisfecha de

poder afirmar que me llevo una amiga. Te deseo mucha suerte en el futuro, llegarás a cualquier meta que te propongas porque tu tenacidad es digna de admirar. Gracias por tanto.

Para el 1.10 no encuentro palabras que resuman estos años, han sido tantas cosas las compartidas a nivel profesional y personal que me quedaría corta. A quienes salieron del labo antes de acabar esta tesis, en especial a Dani. A todo el grupo actual, espero que os vaya bien. Mª Ángeles, gracias por tantas PCRs y bufferes, un placer aprender de ti. Andrea, espero que nos avises cuando leas porque me encantaría compartir contigo también ese capítulo de tu vida. Vir, Pirindola, has sido modelo de entrega incondicional por los amigos, tu paciencia infinita y tu estado de paz general son un ejemplo a seguir. Bea, lo que más me alegra de todo es haber compartido contigo 9 meses maravillosos; gracias por los consejos y por estar siempre dispuesta a escuchar. Ana, yo no sé cómo agradecerte tanto, a modo de resumen te diré que nos debemos un abrazo; qué suerte tienen los compañeros de tu nuevo laboratorio.

Quería agradecer al laboratorio de J.C. Prieto en la UAH y de A.Pandiella en el CIC de Salamanca la oportunidad de empezar en ciencia. Lo que allí aprendí no tiene precio; gracias Elena, Sabia, Flor, Stela y Carla por enseñarme de ciencia y de vida; con vosotras se cumple eso de que la distancia no importa. Eva y Laura, gracias por los inicios.

A los amigos de "fuera de la ciencia": Santiagueros, Culillos, Baena, Irene, Borja y Marta, Josema y MºCarmen,…Gracias por cada vez que preguntabais "¿Cómo va la investigación?", por escuchar hablar de adipocitos aunque no entendierais nada, por el apoyo en los momentos bajos y las risas compartidas, por comprender las ausencias y el silencio…en definitiva gracias por formar parte de mi vida.

Y reservo para el final lo más importante de mi vida, mi familia; porque sin ellos nada tiene sentido.

Pati, gracias; este 2017 es un año grande para nosotras, culminan proyectos importantes y se abre un futuro por delante en el que nos seguiremos teniendo la una a la otra. Cuantas veces en los momentos de desánimo he pensado en tu fortaleza y he tirado hacia delante. Tenemos mucho que celebrar, y siempre juntas.

Papá y Mamá, el apoyo incondicional y el amor infinito son vuestra bandera y aquí solo puedo agradeceros una pequeñísima parte de lo que habéis hecho por nosotras. "Lo que se empieza se termina", esta frase me ha empujado en los momentos difíciles y al final aquí está el resultado. Sin vosotros esta tesis no sería una realidad, como tantas otras cosas en mi vida. Gracias, os quiero muchísimo.

Miguel, qué difícil agradecerte tanto…Las horas de estudio, las tardes de silencio, el tiempo que parecía perdido, el apoyo incondicional ante cualquier proyecto…Eres la persona que vio los inicios y con la que quiero compartir de forma especial el gusto del trabajo terminado. Gracias por estos años y de antemano por todo lo que nos queda por vivir. ¡Lo hemos conseguido Pequeño!

Pablo, espero que algún día estés orgulloso de mí. Gracias por cada sonrisa y cada beso, tienen un efecto mágico; nos debemos unas cuantas sesiones de columpios. Te quiero, eres nuestro motor. Al Futuro, te esperamos con ilusión.

A Ti, gracias por la vida.

Agradecimientos

Resumen

Resumen

La diabetes post-trasplante (del inglés NODAT) es un desorden metabólico que afecta al 40% de los pacientes en tratamiento con inmunosupresores como la rapamicina (también conocido como sirolimus) ó la ciclosporina A. En los últimos años se ha investigado el efecto de los inmunosupresores sobre la acción de la insulina en tejidos periféricos como el músculo esquelético, el hígado y el tejido adiposo blanco. Sin embargo, el efecto de los inmunosupresores sobre las acciones de la insulina y la termogénesis en el tejido adiposo marrón (BAT) no ha sido estudiado.

En esta Tesis Doctoral hemos analizado el impacto de la rapamicina en la señalización de la insulina, en la expresión de genes termogénicos y en la respiración mitocondrial en los adipocitos marrones. Los adipocitos marrones tratados durante 16 horas con rapamicina presentaban disminuída la expresión proteica de IRS1 (sustrato del receptor de la insulina 1) y la fosforilación de Akt (proteína kinasa B) mediadas por la insulina. En consecuencia, la translocación de GLUT4 a la membrana plasmática y la captación de glucosa disminuían en presencia de rapamicina. También detectamos una activación temprana de la proteína quinasa JNK, así como un incremento en la fosforilación del residuo Serina 307 del IRS1. Además, encontramos que los efectos negativos de la rapamicina en la señalización de la insulina en los adipocitos marrones se revertían parcialmente con un inhibidor de JNK. Experimentos in vivo evidenciaron que ratas tratadas durante 3 semanas con rapamicina presentaban anulada la fosforilación de Akt mediada por insulina en el BAT. En relación con la función termogénica de los adipocitos marrones, hemos demostrado que la rapamicina inhibe la cascada de señalización inducida por norepinefrina (NE) o por el agonista adrenérgico β3 CL316243 tal como revelaba el análisis de la fosforilación de HSL (hormona sensible a hormonas), la liberación de glicerol y de ácidos grasos libres, la expresión de PGC-1α (coactivador 1α del receptor nuclear PPARγ) y los niveles de UCP1 (proteína desacoplante 1). Además, el tratamiento con rapamicina de los adipocitos marrones disminuyó la respiración basal mitocondrial, el flujo de protones y la capacidad máxima respiratoria. Por último, la actividad de la desiodasa-2 se inhibió en los adipocitos marrones tratados con rapamicina, indicando que la acción de las hormonas tiroideas sobre la termogénesis también se veía negativamente afectada por la rapamicina.

Como conclusión, este trabajo demuestra que los adipocitos marrones son células diana del efecto de la rapamicina, sugiriendo que la resistencia a la insulina en el BAT juega un papel importante en el desarrollo de la NODAT.

Summary

Summary

Summary

New onset diabetes after transplantation (NODAT) is a metabolic disorder that affects 40% of patients on immunosuppressive agents (IA) treatment such as rapamycin (also known as sirolimus) or ciclosporin A. IAs negatively modulate insulin actions in peripheral tissues including skeletal muscle, liver and white fat. However, the effects of IAs on insulin sensitivity and thermogenesis in brown adipose tissue (BAT) have not been investigated. We have analyzed the impact of rapamycin on insulin signaling, thermogenic gene-expression and mitochondrial respiration in BAT. Treatment of brown adipocytes with rapamycin for 16 h significantly decreased insulin receptor substrate 1 (IRS1) protein expression and insulin-mediated protein kinase B (Akt) phosphorylation. Consequently, both insulin-induced glucose transporter 4 (GLUT4) translocation to the plasma membrane and glucose uptake were decreased. Early activation of the N-terminal Janus activated kinase (JNK) was also observed, thereby increasing IRS1 Serine 307 phosphorylation. These effects of rapamycin on insulin signaling in brown adipocytes were partly prevented by a JNK inhibitor. In vivo treatment of rats with rapamycin for three weeks abolished insulin-mediated Akt phosphorylation in BAT. Rapamycin also inhibited norepinephrine (NE) or CL CL316243-induced HSL phosphorylation and lipolysis, the expression of peroxisome proliferator-activated receptor γ coactivator 1α (PGC-1α) and uncoupling protein 1 (UCP-1) in brown adipocytes. Importantly, basal mitochondrial respiration, proton leak and maximal respiratory capacity were significantly decreased in brown adipocytes treated with rapamycin. Also, the analysis of type II deiodinase enzymatic activity revealed that it was decreased by rapamycin, indicating that the effect of thyroid hormones in brown adipocytes was negatively affected by rapamycin.

In conclusion, we have demonstrated for the first time the important role of brown adipocytes as target cells of rapamycin, suggesting that insulin resistance in BAT might play a major role in NODAT development.

Summary

Índice

Índice

Índice

Abreviaturas

ACC	Acetil-Coenzima A carboxilasa
ADN	Ácido desoxirribonucleico
ADNc	Ácido desoxirribonucleico complementario
ADRβ3	Receptor adrenérgico β3
AIs	Agentes inmunosupresores
Akt	Proteína quinasa B
AMPc	Adenosín monofosfato cíclico
ANOVA	Análisis de la varianza
ARN	Ácido ribonucleico
ARNm	Ácido ribonucleico mensajero
ATP	Adenosín trifosfato
BAT	Tejido adiposo marrón (*Brown adipose tissue*)
BCA	Ácido bicinconínico
BEA	Butanol: Etanol: Amoniaco
BMP7	Proteína morfogénica de hueso tipo 7 (*Bone morphogenetic protein 7*)
BSA	Albúmina sérica bovina
C/EBPs	Proteínas de unión a secuencias amplificadoras CCAAT (*CCAAT-enhancer-binding proteins*)
CNIO	Centro nacional de investigaciones oncológicas
CT	Tomografía computarizada
D2 o Dio2	Iodotironina desiodasa tipo 2
DAPI	4´,6-diamino-2-fenilindo
DEPC	Dietilpirocarbonato

Deptor	del inglés *DEP-domain containing mTOR-interacting protein*
DMEM	Medio Eagle modificado por Dulbecco
DMSO	Dimetilsulfóxido
DTT	Ditiotreitol
4EBP	Proteína de unión del factor eucariotico de inicio de la traducción (*Eukaryotic initiation factor 4E (Eif4e)- binding protein*)
ECL	Sistema intensificador de quimioluminiscencia para Western-Blot
EDTA	Ácido etilén-diaminotetracético
EGTA	Ácido trietilénglicol tetracético
ERK	Quinasa regulada por mitógenos
FAS	Ácido graso sintasa
FBS	Suero fetal bovino
FCCP	Carbonyl cyanide-4-(trifluoromethoxy) phenylhydrazone
FFAs	Ácidos grasos libres
18F-FDG	^{18}F-fluorodesoxiglucosa
FGF21	Factor de crecimiento de fibroblastos 21 (*Fibroblast growth factor 21*)
FKBP-12	Proteína de unión a FK de 12 kDa
GK	Glucoquinasa
GLUTs	Transportadores de glucosa
GTP	Guanosin-5´-trifosfato
HSL	Lipasa sensible a hormonas
IBMX	Isobutil metil xantina
IGF1-1R	Receptor del factor de crecimiento insulínico tipo 1

IIBm	Instituto de investigaciones biomédicas de Madrid
IL-6	Interleuquina 6
IR	Receptor de insulina
IRS 1 y 2	Sustratos 1 y 2 del receptor de la insulina
JNK	Quinasa c-Jun N-terminal
kDa	Kilodalton
KRB	Tampón bicarbonato de Krebs-Ringer
KRP	Tampón fostato de Krebs-Ringer
LPL	Lipoproteína lipasa
ME	Enzima málica
mLST8	del inglés *Mammalian lethal with SEC13 protein 8*
mSIN	del inglés *Mammalian stress-activated protein kinase interacting protein*
mTOR	Diana de rapamicina en celulas de mamífero (*Mammalian target of rapamycin)*
mTORC1/2	Complejo 1/2 de la diana de rapamicina en células de mamífero
$Myf5^{+/-}$	Factor miogénico 5 positivo/negativo
NEFA	Ácidos grasos no esterificados
NCS	Suero neonatal bovino
NE	Norepinefrina
NODAT	Diabetes de nueva aparición post-transplante (*New-onset diabetes after transplantation)*
OCR	Ratio de consumo de oxígeno
PBS	Tampón fosfato salino

PCR	Reacción en cadena de la polimerasa
PDK1	Quinasa tipo 1 dependiente de fosfoinosítidos (*Phosphoinoisitide-dependent kinase l*)
PET	Tomografía por emisión de positrones
PFA	Paraformaldehido
PGC1α	Coactivador -1α del receptor PPARγ
PIP_2	Fosfatidil-inositol 4, 5 bifosfato
PIP_3	Fosfatidil inositol 3, 4, 5 trifosfato
PI3K	Fosfatidilinositol -3 quinasa
PKA	Proteína quinasa A
PMSF	Fluoruro de fenil metil sulfonilo
PPARγ	Receptor γ activado por proliferador de peroxisomas
PRAS40	Sustrato de Akt de 40 kDa rico en prolina
PRDM16	Proteína que contiene el dominio 16 (*Homologous domain-containing protein-16*)
PRIP	del inglés *Phospholipase C-related catalytically inactive protein*
PTP1B	Proteína tirosina fosfatasa 1B (*Protein tyrosine phosphatase 1B)*
PTU	Propiltiouracilo
p38-MAPK	Proteína quinasa activada por mitógenos p38
PVDF	Polifluoruro de vinilo
Raptor	del inglés *Regulatory-associated protein of mTOR*
Rheb	del inglés *Ras homolog enriched in brain*
Rictor	del inglés *Rapamacyn-insensitive companion of mTOR*
Rpm	Revoluciones por minuto

RT-PCR	Retrotranscripción inversa previa a PCR
S6K1	Proteína quinasa ribosomal S6
SDS-PAGE	Electroforesis en geles de poliacrilamida con Dodecil sulfato sódico
SEM	Error estándar de la media
Ser	Serina
SOCS	Proteínas supresoras de la señalización de citoquinas (*Suppressor of cytokine signaling proteins)*
T_3	Triiodotironina
T_4	Tetraiodotironina
TAGs	Triacilgliceridos
TBS	Buffer salino Tris
TCA	Ácido tricloroacetico
Thr	Treonina
Tris	Tris-(hidroximetil)-amino metano
TNF-α	Factor de necrosis tumoral tipo α
TSC2	Complejo de esclerosis tuberosa tipo 2 (*Tuberous Sclerosis Complex 2*)
TTBS	Buffer salino Tris con Tween 20
Tyr	Tirosina
UCP1	Proteína desacoplante 1 (*Uncoupling protein 1*)
UI	Unidades internacionales
VEGF	Factor de crecimiento del endotelio vascular
WAT	Tejido adiposo blanco (*White adipose tissue*)
WT	Genotipo salvaje o silvestre

Introducción

1. EL TEJIDO ADIPOSO

El tejido adiposo, cuyas células principales son los adipocitos, es un órgano ampliamente desarrollado tanto en hombres como en mujeres, alcanzando un peso de 3-4.5 kg en individuos sanos, pero pudiendo llegar hasta 45 kg en personas con obesidad severa (Tran y Kahn, 2010). Sin embargo, solo un tercio del tejido adiposo está compuesto por adipocitos maduros funcionales, mientras que el resto del tejido lo conforman vasos sanguíneos, células endoteliales, preadipocitos, fibras nerviosas, macrófagos y tejido muscular.

Todo organismo requiere energía para llevar a cabo sus funciones vitales y, por ello, es necesario poder almacenarla para su utilización cuando sea necesario. Hasta hace pocos años se consideraba que la función principal del tejido adiposo era la de almacenar energía en forma de lípidos en los adipocitos. Sin embargo, actualmente se sabe que el tejido adiposo no tiene únicamente esta función, sino que también ejerce un papel relevante en la regulación de la temperatura corporal, así como del metabolismo energético sistémico y, que además, es un órgano endocrino (Trayhurn, 2005). Estas funciones son posibles debido, en parte, a la gran vascularización que presenta este tejido (Honek et al., 2014), a la inervación simpática (Bartness et al., 2010) y a los nódulos linfoides que están relacionados con funciones inmunológicas vinculadas al tejido adiposo.

Distinguimos dos tipos principales de tejido adiposo: el blanco y el marrón. Ambos deben su denominación a la coloración que presentan y su localización, función y morfología son diferentes. De hecho, sus funciones principales son opuestas: el tejido adiposo blanco (WAT, del inglés *white adipose tissue*) se encarga de almacenar la energía en forma de triglicéridos (TAGs) que son procesados por las lipasas durante la lipolisis, proceso que permite la liberación de los ácidos grasos libres (FFAs) a la circulación para ser transportados a otros tejidos donde serán metabolizados Por el contrario, el tejido adiposo marrón (BAT, del inglés *brown adipose tissue*) utiliza los lípidos acumulados para obtener energía en forma de calor en el proceso conocido como termogénesis sin tiriteo o "*non-shivering thermogenesis*" (Cinti, 2012) y su coloración se debe a la acumulación de mitocondrias y, por tanto, de citocromos respiratorios en su citoplasma.

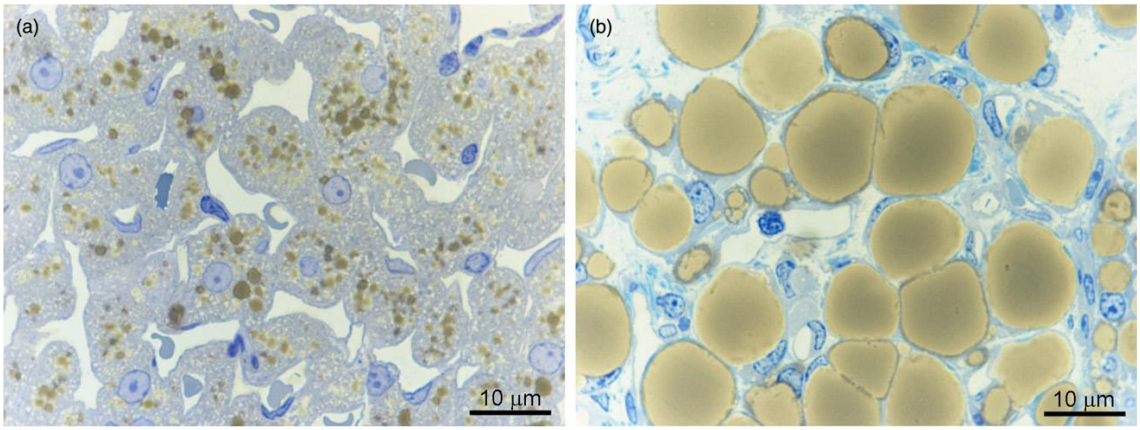

Figura 1. Morfología diferencial entre los adipocitos marrones (a) y los adipocitos blancos (b). En las imágenes se observa como los adipocitos marrones presentan múltiples gotas lipídicas en su citoplasma mientras que en los adipocitos blancos el citoplasma está ocupado mayoritariamente por una única gran gota lipídica. (Adaptado de Smorlesi et al., 2012)

1.1 Tejido Adiposo Blanco

El tejido adiposo blanco (WAT) es conocido clásicamente por almacenar lípidos en forma de TAGs. Tiene una localización amplia dentro del organismo en depósitos que varían según las especies. En la especie humana encontramos un marcado dimorfismo sexual: en los varones se localiza en la nuca, tríceps, deltoides y región abdominal, mientras que en las mujeres abunda en el pecho, muslos y nalgas (Paniagua Gómez-Álvarez, 2004). Además, también hay dimorfismo sexual en cuanto a la cantidad de tejido, pudiendo representar entre el 9-18% del peso corporal en hombres y entre el 4-28% en mujeres (Moreno, 2005).

De forma general podemos clasificar el WAT en subcutáneo o visceral según su localización anatómica (Smith et al., 2001; Gesta et al., 2007), manifestando ambas localizaciones diferencias funcionales, metabólicas y endocrinas. Así, un aumento del WAT visceral se asocia con alteraciones metabólicas, principalmente dislipemia y resistencia a la insulina que puede conducir al desarrollo de diabetes mellitus tipo II (Misra et al., 1997) y a un mayor riesgo de daño cardiovascular. Por el contrario, un aumento de la grasa subcutánea se relaciona con una mejor sensibilidad a insulina (Oh et al., 2017).

Los adipocitos blancos son células de gran tamaño (hasta 200 µm de diámetro), redondeadas y capaces de aumentar su volumen para albergar una única gota de grasa en su citoplasma. Cuando están cargados de lípidos, su núcleo queda desplazado hacia la membrana plasmática, al igual que el resto de orgánulos (Figura 1). Estas células presentan pocas mitocondrias (Luo y Liu, 2016) y la inervación simpática noradrenérgica contacta directamente con los capilares, no con la membrana plasmática de los adipocitos (Bartness y Bamshad, 1998), mientras que en el BAT dicha inervación llega a la membrana plasmática del adipocito (De Matteis et al., 1998).

Además de su función de almacenaje, el WAT es reconocido por su papel de aislante térmico y de soporte para estructuras como la piel y los tegumentos (Ali et al., 2013). Así mismo, cada vez queda más patente su papel como órgano endocrino debido a la secreción de hormonas (denominadas adipoquinas) como la adipsina, leptina, adiponectina, resistina y citoquinas, entre otras moléculas. (Rodríguez et al., 2015; Frühbeck et al., 2001).

1.2 Tejido Adiposo Marrón

El tejido adiposo marrón (BAT) es menos conocido aunque en las últimas décadas su estudio está siendo muy exhaustivo. Clásicamente su presencia se asociaba a animales hibernantes (Cannon y Nedergaard, 1986) y a mamíferos neonatales puesto que su función es la de proporcionar calor y así mantener la temperatura corporal de las crías recién nacidas hasta que su metabolismo alcanza la capacidad de regularla adecuadamente. Cuando este tejido no se activa sufre una involución perdiendo su función termogénica. Por tanto, hasta hace pocos años se consideraba que el BAT era un tejido únicamente fundamental para mantener la temperatura en animales hibernantes, pequeños mamíferos y en la etapa neonatal de los mamíferos, en especies como la humana (Cannon y Nedergaard, 1986), pero su papel en el adulto era desconocido. Sin embargo, diversos grupos de investigación buscaron técnicas para intentar detectar depósitos de BAT en adultos y comprobar que este se encontrase activo (Nedergaard et al., 2007). De esta manera, se encontró BAT en niños recién nacidos (Lean, 1989), en pacientes con feocromocitomas (Riquier et al., 1982; Fukuchi et al., 2004) y también en adultos expuestos al frio de modo constante (Huttunen et al., 1981). Fue en 2009 cuando se publicaron tres artículos simultáneos (Cypess et al., 2009; van

Marken Lichtenbelt et al., 2009; Virtanen et al., 2009) en los que se evidenciaba la presencia de depósitos activos de BAT en individuos adultos (Figura 2). Su localización es semejante a la encontrada en animales hibernantes: en la zona interescapular, en depósitos axilares, cervicales, perirrenales, inguinales, rodeando la glándula tiroides, la tráquea y el esófago, a ambos lados de la columna vertebral, sobre el corazón y riñón y en torno a grandes vasos como la aorta (Hany et al., 2002; Cannon y Nedergaard, 2004; Becker et al., 2016). Esta distribución permite exportar el máximo calor generado en el BAT y así calentar los órganos vitales como el corazón y riñones. En uno de estos estudios se encontraba un leve dimorfismo sexual ya que parecía que las mujeres presentaban una mayor masa de BAT y con mayor actividad. Asimismo, la actividad del tejido era inversamente proporcional a la edad del individuo y a su índice de masa corporal, por lo que podría haber una correlación inversa entre obesidad y actividad del BAT (Cypess et al., 2009). Además, en otro estudio se observó que el BAT estaba más activo a temperaturas bajas (van Marken Lichtenbelt et al., 2009), por lo que se afirmaba su papel fundamental en la termorregulación.

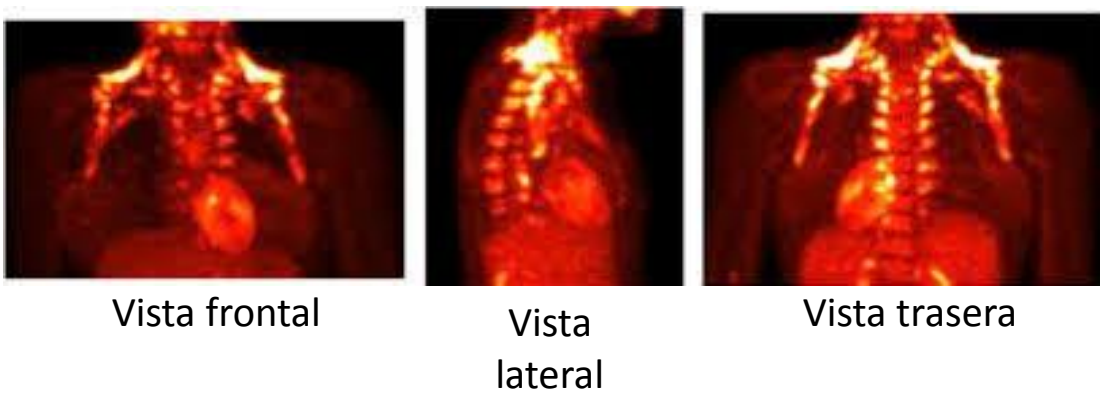

Figura 2. Activación metabólica del BAT supraclavicular. En adultos se analizó la activación del BAT mediante tomografía por emisión de positrones (PET) combinada con tomografía computarizada (CT), previa administración al paciente del trazador ^{18}F-fluorodesoxiglucosa (18F-FDG). Se observó una mayor captación de glucosa en la región supraclavicular (mayor brillo en la imagen) correspondiente al BAT (Adaptado de Virtanen, 2016).

El BAT está formado por adipocitos marrones, cuya morfología es distinta a la de los adipocitos blancos: albergan en su citoplasma múltiples gotas lipídicas de menor tamaño que rodean el núcleo y los orgánulos celulares y son fácilmente accesibles (Saely et al., 2012) (Figura 1). Además, los adipocitos marrones presentan un gran número de mitocondrias con las crestas de la membrana interna muy desarrolladas (Trayhurn y Nicholls, 1986). Tienen forma poliédrica y su diámetro oscila entre 20-45 µm; en la membrana plasmática presentan receptores adrenérgicos y el estímulo principal para su activación se produce por la vía simpática, en concreto mediante la norepinefrina (NE) (Martinez-de Mena y Obregón, 2005). El BAT presenta elevada vascularización que es muy necesaria para el intercambio de calor (Bargut et al., 2016) y de moléculas entre este tejido y el resto del organismo: hormonas, oxigeno, catecolaminas. De hecho, estudios recientes muestran la importancia del factor de crecimiento del endotelio vascular (VEGF) para el correcto desarrollo y funcionamiento del BAT (Bagchi et al., 2013).

Como se ha mencionado, la función principal del BAT es la generación de energía en forma de calor evitando el tiriteo (*non-shivering thermogenesis*). Esto se consigue desacoplando la fosforilación oxidativa y la cadena de transporte de electrones de la membrana interna de la mitocondria, en respuesta a la NE, de modo que al final de la misma se genere calor en lugar de ATP. La proteína encargada de dicho desacoplamiento es la proteína desacoplante (*uncoupling protein 1*, UCP1) (Figura 3).

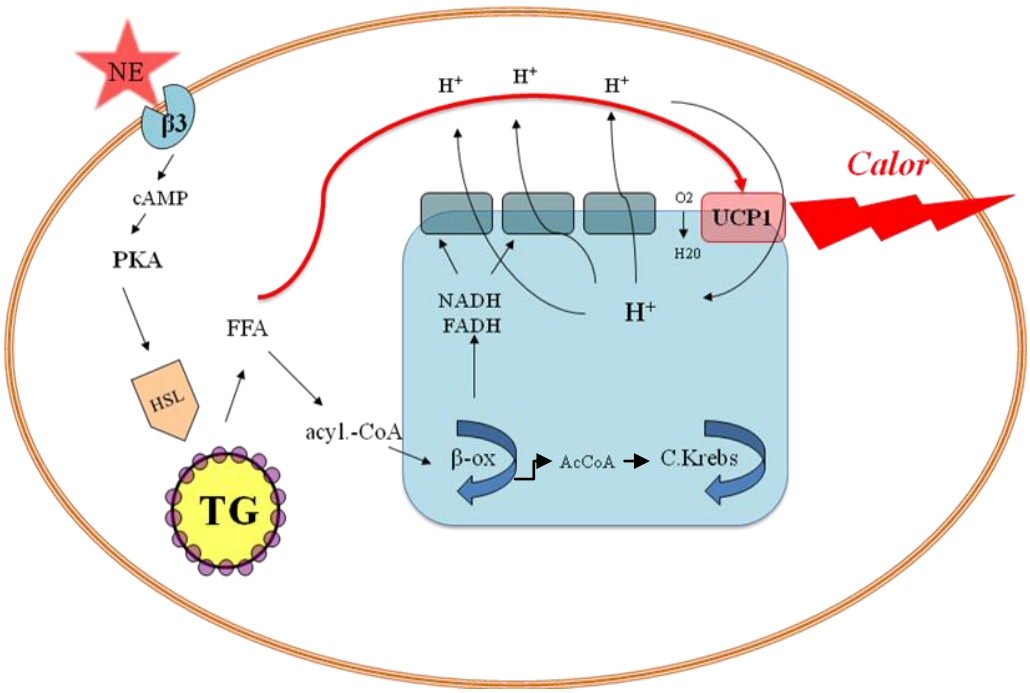

Figura 3. Vía de activación de la UCP1 en el BAT. Los receptores térmicos cutáneos detectan el frío, activan el hipotálamo y se pone en marcha el sistema simpático liberando NE que activa los receptores adrenérgicos de tipo β3 (ADRβ3) en el adipocito marrón. Esto provoca la liberación de FFAs en el citoplasma por activación de las lipasas, mediada por la proteína quinasa A (PKA) (Ravnskjaer et al., 2015), que activan a la UCP1 para desacoplar la cadena de transporte electrones y obtener energía en forma de calor. (Adaptado de Cannon y Nedergaard, 2004). Además, estudios moleculares han demostrado que la PKA fosforila a la p38-MAPK (Proteína quinasa activada por mitógenos p38) que conduce a la activación del factor de transcripción PGC1α (Coactivador de PPARγ-1α) en el núcleo y esto se traduce en un aumento de la biogénesis mitocondrial y en la inducción de la transcripción del gen *Ucp1* (Cao et al., 2004; Betz y Enerbäck, 2015).

Estudios realizados en el BAT de roedores durante el periodo perinatal han revelado que la diferenciación de los adipocitos marrones comprende un programa de diferenciación adipogénica que conlleva un aumento de las enzimas que sintetizan lípidos como la ACC (Acetil CoA carboxilasa) y la FAS (Ácido graso sintasa) y un programa termogénico caracterizado por inducir las proteínas implicadas en la

termogénesis (PGC1-α, UCP1 entre otras). A medida que avanza el desarrollo intrauterino, el preadipocito marrón pierde la capacidad de dividirse y comienza a sintetizar lípidos, transcribiéndose los genes que codifican para los enzimas lipogénicos (*Fasn*, *Acc*, *Me* (Enzima málica)) (Lorenzo et al., 1988), aumenta el número y tamaño de las mitocondrias y éstas desarrollan múltiples crestas en la membrana interna (Cinti, 2001), aumenta la expresión del gen *Ucp1* (Porras et al., 1989) y, finalmente, en el momento del nacimiento el BAT se encuentra plenamente funcional.

Otro marcador característicocaracterístico del BAT y que es clave para su diferenciación es la proteína PRDM16 (Proteína que contiene el dominio 16, del inglés *homologous domain-containing protein-16*). Se trata de un factor de transcripción ampliamente expresado en el BAT, no así en el WAT de tal manera que si un preadipocito expresa PRDM16 se promueve la inducción de PGC1α, UCP1 y Desiodasa 2 (Dio2). En ratones en los cuales se sobreexpresaba PRDM16 se observó la estimulación de los adipocitos marrones. Por el contrario, al silenciar este factor de transcripción mediante RNA de interferencia se provocó una disminución casi completa de las características propias del adipocito marrón (Seale et al., 2007). PRDM16 también se ha identificado en adultos humanos, lo que vuelve a corroborar la presencia de este tejido y su actividad a lo largo de toda la vida (Virtanen et al., 2009; Lidell et al., 2013).

También son marcadores propios de BAT la LPL (Lipoproteína lipasa), Dio2 que regula la concentración de T3 (Triiodotironina) que está presente en el tejido adiposo marrón (Obregón, 2014), BMP7 (Proteína morfogenica del hueso 7) que como se detalla a continuación promueve la diferenciación de los adipocitos marrones (Ravussin y Galgani, 2011).

En los últimos años se ha estudiado el origen del WAT y BAT, identificándose los marcadores propios de cada uno de ellos (Gesta et al., 2007; Timmons et al., 2007). Estos trabajos han establecido que los adipocitos blancos y marrones no tienen un linaje común, ya que los adipocitos marrones provienen de células progenitoras $Myf5^{+}$ (Factor de transcripción miogénico 5), al igual que los mioblastos, pero no así los adipocitos blancos que son $Myf5^{-}$ (Sanchez-Gurmaches y Guertin, 2014). Para la diferenciación de los precursores $Myf5^{+}$ a los adipocitos marrones se requiere del factor BMP7, que a su vez activa a PRDM16 que tiene un papel fundamental en este proceso. De esta manera,

PRDM16 se une a PGC1α, PPARγ (Receptor γ activado por proliferadores de peroxisomas) y otros miembros de la familia de los C/EBPs (Proteina de unión a secuencias amplificadoras CCAAT) aumentando la transcripción de éstos y así promoviendo la diferenciación hacia el fenotipo de adipocitos marrones (Ravussin y Galgani, 2015). A nivel molecular, BMP7 activa a p38-MAPK promoviendo la biogénesis mitocondrial por lo que se acentúa así la funcionalidad del tejido (Lin et al., 2014). De esta manera, el BAT está plenamente activo al nacer, puesto que como se ha indicado anteriormente su función es clave en esos primeros momentos de vida postnatal (Obregón et al., 1987). Por el contrario, el WAT empieza a diferenciarse durante la gestación, alcanzando su máximo desarrollo en época postnatal (Gesta et al., 2007). Por último, también es importante destacar el papel de la T_3 en el proceso de diferenciación de los adipocitos marrones y en la activación del gen *Ucp1* a nivel de su promotor (Obregon et al., 1987; Rabelo et al., 1997).

1.3 Papel del BAT en el control metabólico mediado por la insulina

Además de la función termogénica, el BAT desempeña un papel importante en la regulación de la homeostasis metabólica y del balance energético del organismo. Dentro del propio BAT, en relación al metabolismo lipídico, se sabe que una activación aguda a través de los receptores ADRβ provoca un aumento de los niveles de AMP cíclico (AMPc) que a su vez inducen la activación de la lipolisis por medio de la fosforilación y activación de la HSL (lipasa sensible a hormonas) causando la liberación de FFAs. Como se ha indicado, éstos son utilizados como sustratos para la respiración mitocondrial, al ser oxidados, resultando en la activación de la UCP1 (Trayhurn y Milner, 1989).

Respecto al metabolismo glucídico, se conoce que el BAT es sensible a la insulina en relación con la captación de glucosa (Valverde et al., 2005), aunque hay estudios que también demuestran que los adipocitos marrones son capaces de utilizar la glucosa sin necesidad de ser estimulados por insulina, sino por la NE vía receptores ADRβ3 (Inokuma et al., 2005), lo que provoca una captación de glucosa mediante el transportador GLUT1, en lugar de GLUT4 que es la isoforma sensible a la insulina (Dallner et al., 2006).

La señalización de la insulina en los diferentes tejidos periféricos es crucial para una correcta homeostasis glucídica del organismo. En los últimos años se han definido los nodos principales donde esta ruta puede verse alterada y/o modulada (Figura 4): a nivel de receptor de insulina (IR) en la membrana citoplasmática, en la unión con las proteínas sustrato del receptor de la insulina (IRSs), en la activación de la fosfatidil-inositol 3-quinasa (PI3K) o en la activación de la proteína quinasa B (Akt) (Taniguchi et al., 2006). El establecimiento de estos nodos críticos de la señalización de la insulina ha sido posible gracias a la generación de modelos murinos genéticamente modificados donde estas proteínas se encontraban eliminadas o sobreexpresadas.

Tras la unión de la insulina, el IR fosforila a las proteínas IRS (principalmente 1 y 2) en múltiples residuos tirosina (Tyr). Las proteínas IRS son proteínas embarcadero (del inglés *docking protein*) y que a su vez activan dos vías de señalización paralelas: la vía de la PI3K-Akt (responsable de las acciones metabólicas de la insulina) y la vía de Ras/MAPK (que regula la expresión de genes relacionados con el control del crecimiento celular y la diferenciación) (Avruch, 1998). Tanto el IR como el IRS1 son regulados negativamente por la proteína tirosina fosfatasa 1B (PTP1B) al ser defosforilados en residuos Tyr claves en el dominio catalítico del IR ó en los residuos de unión a la PI3K en el caso del IRS1 (Ramachandran y Kennedy, 2003). Trabajos realizados en modelos in vivo en ratones deficiente en el gen *Ptpn1* han demostrado una mejora de la señalización en la cascada de la insulina tanto en el hígado como en el músculo esquelético (Haj et al., 2005; González-Rodríguez et al., 2012). Las proteínas de la familia SOCS (Proteínas supresoras de la señalización de citoquinas), particularmente SOCS3, cuya expresión se incrementa tras el tratamiento con citoquinas, también regulan negativamente la ruta de señalización de la insulina interfiriendo con la interacción del IR con IRS1 (Emanuelli et al., 2001).

La fosforilación en residuos serina (Ser) del IRS1 es otro punto clave en la regulación negativa de la señalización de la insulina. La activación de ciertas proteínas Ser/Treonina (Thr) quinasas en respuesta a estímulos de estrés metabólico como ERK (Quinasa regulada por mitógenos), S6K1 (Proteína quinasa ribosomal S6) y JNK (Quinasa c-Jun N-terminal), que además se activan también en respuesta a la insulina, conduce a la fosforilación del IRS1 en residuos Ser, como mecanismo de retroalimentación negativa (en inglés *negative feedback*), ya que resulta en un cambio

de conformación del IRS1 que impide su fosforilación en residuos Tyr mediada por el IR (Aguirre et al., 2000; Copps y White, 2012).

Además de la regulación negativa sobre la cascada de la insulina mediada por fosforilación en Ser del IRS1, también se ha descrito una regulación negativa por modulación de sus niveles proteicos. Se sabe que niveles bajos del IRS1 en tejido adiposo blanco son indicadores de resistencia a la insulina (Carvalho et al., 1999; Hirashima et al., 2003). Ratones deficientes en el gen *Irs1* presentan alterada la ruta de la señalización de la insulina en músculo esquelético y desarrollan resistencia a la insulina (Araki et al., 1994). Además, los preadipocitos marrones inmortalizados procedentes de estos animales son incapaces de alcanzar su diferenciación terminal (Fasshauer et al., 2001; Tseng et at., 2005). Estos y otros estudios relevantes que se detallarán a lo largo de esta Tesis han evidenciado que el IRS1 es una molécula clave en la transducción de la señal de la insulina en los adipocitos marrones (Valverde et al., 1999).

El siguiente nodo crítico de la ruta de señalización de la insulina es la regulación de la PI3K, enzima que fosforila el fosfolípido de membrana PIP_2 (fosfatidilinositol 4,5 bisfosfato) generando el segundo mensajero PIP_3 (fosfatidilinositol 3, 4 ,5 trifosfato). El PIP_3 se une a proteínas con dominio PH, entre las que se encuentra la PDK1 (Quinasa tipo 1 dependiente de fosfoinositidos) que es la proteína responsable de activar Akt mediante fosforilación de dicha quinasa en el residuo Thr 308 (Alessi et al., 1997). A continuación, se requiere también la fosforilación del residuo Ser 473 de Akt para una completa activación. Se postula que la proteína Rictor del complejo mTOR podría ser la encargada de fosforilar el residuo Ser 473 de PDK1 en adipocitos y otros tipos celulares (Sarbassov et al., 2005).

La fosforilación de Akt regula diversas acciones metabólicas, relacionadas con la insulina, induciendo la fosforilación de sucesivas proteínas de la cadena de señalización. En relación con el tema de estudio de esta Tesis, se conoce que Akt fosforila al inhibidor de mTOR (del inglés *Mammalian target of rapamycin*) TSC2 (Complejo de esclerosis tuberosa tipo 2) inhibiéndola a su vez y provocando así la activación del complejo mTOR (Harris y Lawrence, 2003). Una vez activado mTOR, éste regula la síntesis de proteínas mediante la fosforilación de la proteína S6K1 y del factor de

transcripción 4EBP (Proteína de unión del factor eucariótico de inicio de la traducción) (Figuras 4 y 6).

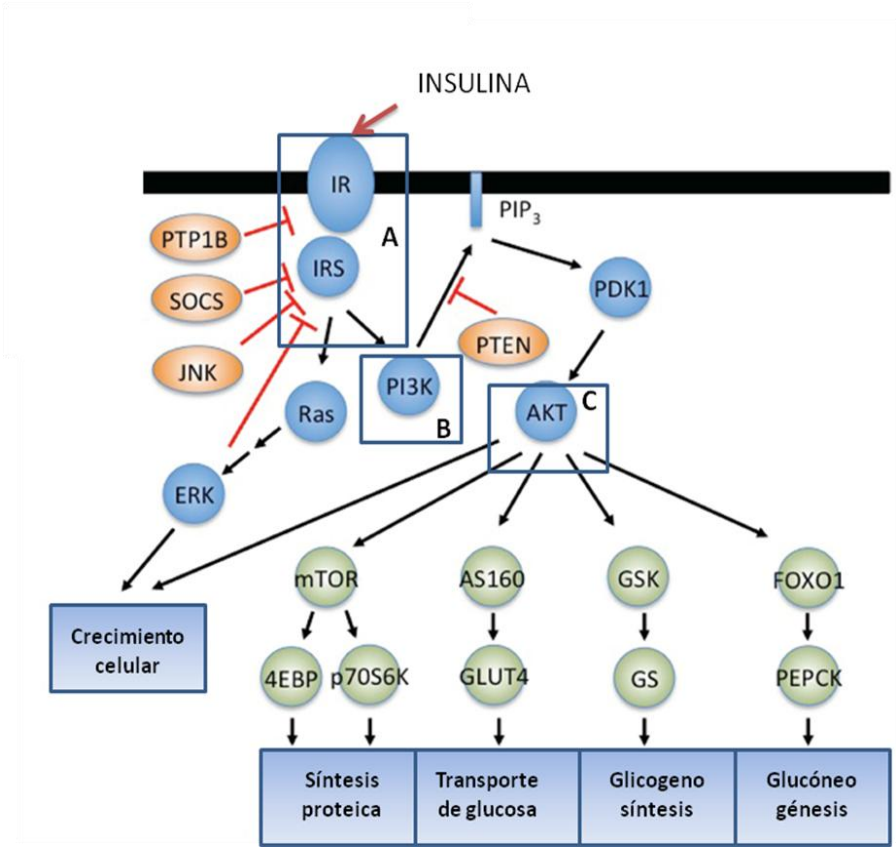

Figura 4. Ruta de la señalización de la insulina. La insulina se une al IR, que a su vez se activa por autofosforilación en residuos Tyr y se une con las proteínas IRS (nodo A). En consecuencia, se activa la PI3K (nodo B) y finalmente la Akt (nodo C) que es moduladora del crecimiento y supervivencia celular, la síntesis proteica, el transporte de glucosa al interior de la célula por el transportador GLUT4 y la síntesis de glucógeno (Adaptado de Taniguchi et al., 2006).

Cabe destacar que la importancia del IR en la señalización de la insulina en el BAT se demostró mediante la generación de ratones deficientes para el IR que presentan una disminución de la masa del BAT interescapular y una disminución a la tolerancia a la glucosa debido a un defecto en la secreción de la insulina. Estos resultados han evidenciado que el IR es necesario tanto para el desarrollo del BAT como para mantener la homeostasis glucídica del organismo (Guerra et al., 2001). Además, un estudio posterior demostró que estos ratones cuando se alimentan con una dieta rica en grasa presentan un aumento de la adiposidad visceral y un aumento de la secreción de adipoquinas inflamatorias (Gómez-Hernández et al., 2012).

2. EL COMPLEJO mTOR

El complejo mTOR es una proteína con actividad Ser/Thr quinasa de 2549 aminoácidos y 290 kDa (revisado por Hay y Sonenberg, 2004; Fingar y Blenis, 2004) que controla la síntesis proteica y la proliferación celular. Su cascada de señalización está involucrada en procesos metabólicos relacionados con la adipogénesis (Fernandez-Veledo et al., 2013) y se sabe que está desregulada en pacientes con obesidad y diabetes tipo II (Laplante y Sabatini, 2009).

mTOR es el componente principal de los complejos multiproteicos mTORC1 (Complejo 1 de la diana de rapamicina en células de mamífero), vinculado con el estado energético de la célula, factores de crecimiento, niveles de oxigeno y aminoácidos y mTORC2 (Complejo 2 de la diana de rapamicina en células de mamífero), activado por factores de crecimiento y encargado de la regulación de la supervivencia celular, organización del citoesqueleto y metabolismo celular. mTOR posee un dominio catalítico flanqueado por las regiones FAT (FRAP, ATM, TRRAP) y FATC (FAT C-terminal) cerca de su región C-terminal, siendo el dominio FAT donde se localizan los sitios de interacción con el complejo FKBP12-rapamicina (Proteina de unión a FK de 12 kDa) (Stan et al., 1994) y con Rheb (*Ras homolog enriched in brain*). En el extremo N-terminal se localizan secuencias conservadas de α-hélice donde se encuentran los sitios de interacción con Raptor (*Regulatory-associated protein of mTOR*) y Rictor (*Rapamacyn-insensitive companion of mTOR*).

El complejo mTORC1 presenta los siguientes componentes: mTOR que es la subunidad catalítica, Raptor que es una proteína reguladora y ensambla todo el complejo, mLST8 (*Mammalian lethal with SEC13 protein 8*), PRAS40 (sustrato de Akt de 40 kDa, rico en prolina) y Deptor (*DEP-domain containing mTOR-interacting protein*), siendo estos últimos los responsables de la regulación negativa de mTORC1 (Wang et al., 2007; Peterson et al., 2009). En presencia de nutrientes y factores de crecimiento, la proteína PRAS40 está fosforilada e inhibida por Akt lo que implica una mayor actividad de mTORC1 (Sancak et al., 2007).

El complejo mTORC2 está compuesto por las proteínas Rictor, mSIN1 (*Mammalian stress-activated protein kinase interacting protein*) (estas dos proteínas se estabilizan mutuamente dando consistencia al complejo (Jacinto et al., 2006)), mTOR, Deptor

(regulador negativo de la actividad del complejo) y LST8 (Dibble y Cantley, 2015) (Figura 6).

Las proteínas que forman parte de la cascada de señalización de la insulina, como IR, IRS1, PI3K y Akt, son reguladores de los subcomplejos de mTOR. De hecho Akt fosforila a mTORC2 provocando su inhibición y activando así a mTORC1 (Inoki et al., 2002). A su vez, esta activación de mTORC1 reprime la señalización de la insulina limitando la activación de Akt mediante la fosforilación de la proteína S6K1 (Harrington et al., 2005) que tal como se ha indicado anteriormente es capaz de fosforilar el IRS1 en el residuo Ser 307 (Um et al., 2004) alcanzado así una autorregulación mediante retroalimentación negativa. Así, la activación sostenida de S6K1 produce una inhibición de la cascada de señalización de IRS1-PI3K provocando resistencia a la insulina. Estudios en ratones deficientes en la proteína S6K1 han demostrado que éstos presentan mayor sensibilidad a insulina, no desarrollan obesidad cuando se alimentan con una dieta rica en grasa y sus depósitos de grasa están disminuidos (Um et al., 2004).

Uno de los mecanismos reguladores negativos de la actividad del complejo mTORC1 es el complejo de esclerosis tuberosa o TSC que es un heterodímero compuesto por TSC1 y TSC2. A su vez, TSC2 es capaz de activar a la actividad GTPasa intrínseca de Rheb, inactivándolo (Long et al., 2005) y, por tanto, inhibiendo la actividad de mTORC1 ya que se necesita que Rheb esté ligado a GTP y por tanto activo.

S6K1 es una Ser/Thr quinasa activada por PI3K y Akt (Chung et al., 1994) y tiene una función primordial en la síntesis proteica y en el crecimiento celular mediada por mTOR. S6K1 posee un dominio de activación y un dominio hidrofóbico similares a los de Akt y su activación depende de la fosforilación de la Thr 389 (en el dominio hidrofóbico) llevada a cabo por mTORC1 (Pearson et al., 1995). Esta activación de S6K1 parece ser la responsable del crecimiento y progresión del ciclo celular (Fingar et al., 2004). Por otro lado, como la activación prolongada de S6K1 produce la inhibición de la cascada de la señalización de la insulina a nivel de IRS1-PI3K provocando resistencia a insulina, es necesario un control muy fino tanto de la intensidad como de la duración de la cascada de la insulina puesto que se trata de una compleja red de múltiples regulaciones cascadas arriba y abajo.

Se ha demostrado que en el BAT mTORC2 es necesario para la captación de glucosa vía estimulación adrenérgica (Olsen et al., 2014) debido a un aumento en la transcripción del transportador de glucosa GLUT1 y a su síntesis de novo por aumento de los niveles de AMPc, lo que provocaría su translocación a la membrana plasmática. De igual manera, el tratamiento crónico con la rapamicina inhibe también al subcomplejo mTORC2 (Sarbassov et al., 2006) impidiendo la captación de glucosa mediada por la estimulación adrenérgica.

Otro aspecto importante a destacar es el papel del complejo mTOR en la diferenciación adipogénica mediante la inducción de Akt. De hecho, el tratamiento con rapamicina, al inhibir mTORC1, provoca el mismo efecto con respecto a la incapacidad de diferenciación de los preadipocitos marrones que una reducción en los niveles de ARNm de PPARγ (Zhang et al., 2009). Cabe señalar que la rapamicina es un inhibidor agudo de mTORC1 pero no así de mTORC2 aunque algunos autores cuestionan dicha especificidad (Zeng et al., 2007).

3. EFECTO DE LOS INMUNOSUPRESORES SOBRE LA SENSIBILIDAD A LA INSULINA: DIABETES DE NUEVA GENERACIÓN POST-TRANSPLANTE (NODAT).

Los inmunosupresores son compuestos ampliamente utilizados en pacientes sometidos a trasplantes y otras patologías como el cáncer. Aunque son beneficiosos para estos estados puntuales de salud, de forma general los agentes inmunosupresores (AIs) provocan en el organismo una desregulación del metabolismo que se manifiesta en dislipidemia, hipertensión y diabetes de nueva generación post-trasplante (NODAT, del inglés *New Onset of Diabetes after Transplant*) (Galindo et al., 2016). Como se detallará más adelante, en la actualidad el término NODAT hace referencia a un conjunto de alteraciones en el metabolismo de la glucosa que se asemejan a la diabetes mellitus tipo II aunque tiene diferente aparición, duración y severidad (Hecking et al., 2013).

Uno de los inmunosupresores de amplio uso en la clínica es la rapamicina o sirolimus (Figura 5). Esta molécula es un ligando del complejo mTOR y ha desplazado en su uso clínico a otros fármacos debido a que minimiza efectos secundarios como neurotoxicidad, dilipidemia e hipertensión (Mota, 2005), aunque aumenta el riesgo de padecer daños cardiovasculares (Watt, 2011).

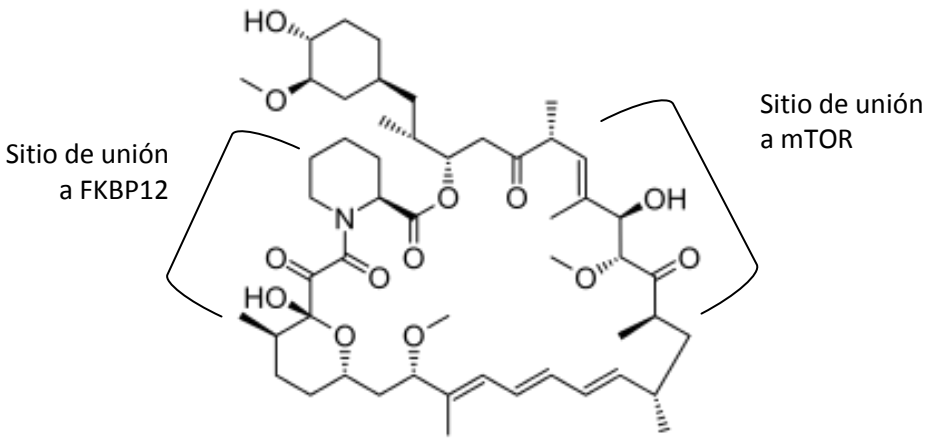

Figura 5. Estructura molecular de rapamicina o sirolimus. Esta molécula se extrae del hongo *Streptomyces hygroscopicus* e inhibe el complejo mTOR (Adaptado de Fuhrmann et al., 2014)

Fue precisamente la rapamicina la molécula que permitió diferenciar los subcomplejos de mTOR. Tras penetrar en la célula, se une al receptor citoplasmático FKBP12 e interacciona con el dominio FRB de mTORC1 (Guertin y Sabatini, 2009). En tratamientos agudos mTORC1 es más sensible a rapamicina que mTORC2, aunque como se mencionará más adelante, estos datos son controvertidos. En cualquier caso lo que está comprobado es que rapamicina inhibe la actividad de la proteína quinasa S6K1 porque evita su fosforilación mediada por mTORC1 en el residuo Thr 389 (Pearson et al., 1995) (Figura 6).

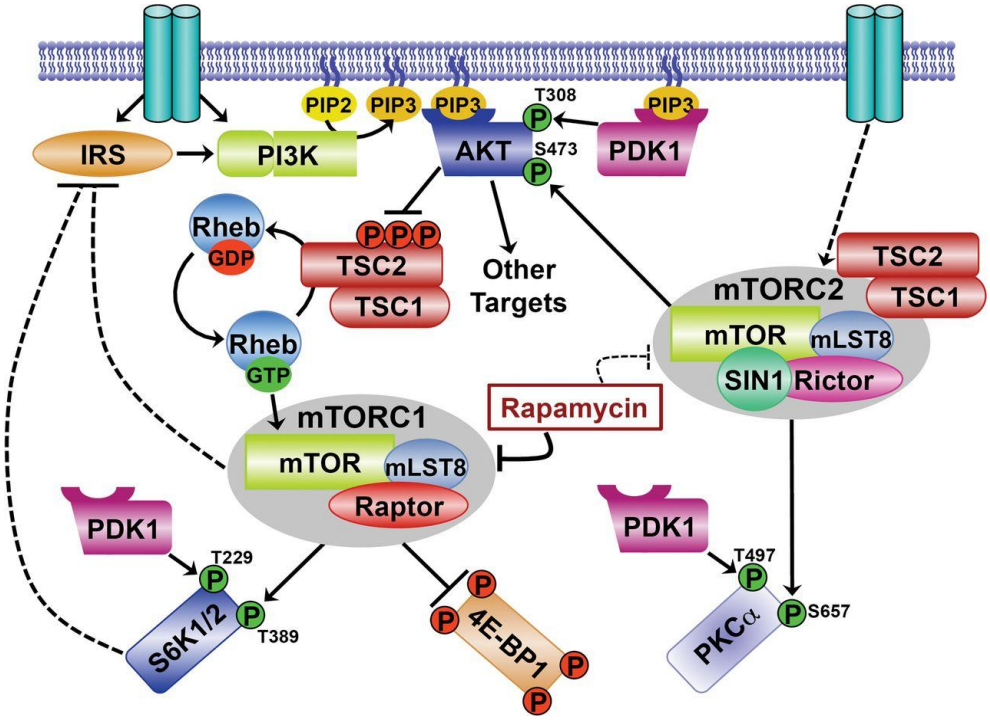

Figura 6. **Modelo de la regulación y efectos de complejo mTOR** (Huang et al., 2009).

A diferencia de otros AIs, la rapamicina no inhibe la calcineurina sino que se une a FKBP12 formando un complejo que bloquea a su vez al complejo mTORC1 que además de las funciones celulares descritas anteriormente regula procesos importantes en las células del sistema inmune impidiendo, por ejemplo, la proliferación de los linfocitos T (Guertin y Sabatini, 2009). Cabe señalar por otra parte los AIs inhibidores de calcineurina (que se pueden administrar a los pacientes combinados con la rapamicina), que actúan inhibiendo esta enzima lo que provoca que no se active la IL-2 y disminuya el crecimiento y la diferenciación de linfocitos T (Lopes et al., 2013).

Respecto al metabolismo lipídico, el uso de rapamicina provoca dislipemias (Lopes et al., 2014a) ya que la inhibición de mTORC1 con rapamicina impide la fosforilación de Akt y por tanto la síntesis lipídica de novo (Porstmann et al., 2005). En referencia al metabolismo de la glucosa y las acciones insulínicas, se conoce que la rapamicina provoca un descenso de la sensibilidad a insulina en tejidos periféricos como el musculo esquelético, hígado y WAT (esta última referencia a WAT es aplicable a roedores y a humanos) y que también disminuye la captación de glucosa e inhibe la señal de insulina

en los adipocitos blancos indicando todo ello que rapamicina tiene un papel importante en la aparición de la resistencia a insulina (Lopes et al., 2014a).

La aparición de NODAT puede considerarse como un síndrome metabólico padecido por numerosos pacientes tras recibir un tratamiento crónico con inmunosupresores. Se manifiesta pocos meses después del trasplante y sus características clínicas dependen del agente inmunosupresor empleado, de las posibles combinaciones de éstos e incluso de los orígenes demográficos de los pacientes (Dirks et al., 2004). Previo al desarrollo de NODAT, los pacientes pueden manifestar hipertrigliceridemia y se consideran factores de riesgo la edad y la obesidad (Gyurus et al., 2011). En pacientes que ya padecen NODAT, la rapamicina suprime la señalización de la insulina, inhibe la síntesis de GLUT1, dificulta la translocación de GLUT4 e impide la respuesta adecuada de las células β del páncreas (Han et al., 2016).

A pesar de las evidencias del uso de la rapamicina, así como de otros inmunosupresores en relación con desórdenes metabólicos en pacientes crónicos, no se conoce aún el mecanismo molecular definitivo responsable de dichas alteraciones. Se han publicado estudios donde la rapamicina disminuye la represión de la señalización de la ruta IRS1-PI3K-Akt en estados de incremento de la actividad de mTORC1-S6K1, lo que conduce a una mejora de la fosforilación de Akt y de la captación de glucosa en el musculo esquelético y en el WAT (Tremblay et al., 2005). Otros estudios además reflejan que el uso combinado de rapamicina con inhibidores de calcineurina como la ciclosporina mejoran el metabolismo glucídico in vivo (Egidi et al., 2003). Sin embargo, la combinación de rapamicina con inhibidores de calcineurina también se asocia con la resistencia a insulina y a un mayor riesgo de padecer NODAT (Teutonico et al., 2005), por lo que no se pueden afirmar todavía unos mecanismos moleculares claros. Otros estudios describen que el tratamiento con rapamicina inhibe o al menos disminuye la fosforilación de Akt en el residuo Ser 473 (por mTORC2) sin afectar la fosforilación en Thr 308 por PDK1 (Sarbassov et al., 2006; Pereira et al., 2012). Usada en tratamientos agudos, la rapamicina inhibe mTORC1, mientras que en tratamientos crónicos también se ve inhibido mTORC2, y, por tanto la fosforilación de Akt en Ser 473 (Hagan et al., 2008) lo que repercute en un descenso de la captación de la glucosa por las células. También está documentado que el tratamiento con rapamicina, al bloquear la acción de mTORC1, inhibe la fosforilación de S6K1 (Pearson et al., 1995).

Otra proteína clave en relación a los adipocitos que se ve alterada por el tratamiento con rapamicina es PGC1α, ya que se ha descrito que disminuye su expresión, al menos en el músculo esquelético, siendo también responsable de un descenso de la sensibilidad a insulina por su vinculación con la expresión de GLUT4 (Michael et al., 2001).

Aunque la rapamicina no afecta a la expresión de genes de proteínas involucradas en gluconeogénesis hepática, si parece que provoca una disminución en la expresión de la glucoquinasa (GK) que es el enzima responsable de la fosforilación de la glucosa a glucosa-6-fosfato,, disminuyendo la disposición de glucosa en el hígado (Lopes et al., 2014a). Otro de los síntomas de diabetes y por tanto de NODAT es la aparición de glucosuria. En este sentido, la rapamicina a priori causa menos daños renales y nefrotoxicidad que ciclosporina A pero se ha encontrado un aumento del aclaramiento renal de glucosa en pacientes tratados con este agente inmunosupresor (Franz et al., 2010).

Por tanto un esclarecimiento de los mecanismos moleculares alterados en NODAT debido al uso de AIs es de vital importancia para poder desarrollar nuevas combinaciones farmacológicas que atenúen los efectos metabólicos que conducen a la aparición de dichas patologías.

Objetivos

En esta Tesis doctoral se ha analizado la repercusión del tratamiento con rapamicina sobre las respuestas de los adipocitos marrones en relación con la sensibilidad a la insulina y la activación de la termogénesis inducida por norepinefrina con el fin de establecer la implicación del tejido adiposo marrón en el desarrollo de NODAT.

Para ello se plantearon los siguientes objetivos:

1. Generar líneas celulares inmortalizadas de adipocitos marrones de rata y ratón que permitieran realizar estudios de señalización celular.

2. Analizar los efectos del tratamiento de los adipocitos marrones con rapamicina a distintos tiempos sobre la ruta de señalización de la insulina que es responsable de la estimulación de la captación de glucosa en dichas células.

3. Identificar los moduladores negativos de la señalización de la insulina que son sensibles al efecto de la rapamicina.

4. Analizar el efecto del tratamiento con rapamicina sobre las respuestas de los adipocitos marrones al tratamiento con norepinefrina focalizándonos en la lipolisis y en la expresión de los genes termogénicos *Ucp1* y *Pgc1a*.

5. Analizar el efecto del tratamiento con rapamicina en la respiración mitocondrial en los adipocitos marrones

Materiales y Métodos

1. CULTIVOS CELULARES

1.1 Generación de líneas celulares de preadipocitos marrones inmortalizados a partir del BAT de ratas y ratones lactantes

- **Animales de experimentación**

Tanto nuestro grupo como otros grupos de investigación habían generado líneas celulares inmortalizadas de adipocitos marrones a partir de embriones o ratas/ratones recién nacidos (Lorenzo et al., 1996; Klein et al., 2002; Miranda et al., 2010). En esta Tesis por primera vez hemos generado líneas celulares de adipocitos marrones de animales lactantes de aproximadamente 20 días de vida. Las ratas eran de la raza Sprague-Dawley y los ratones eran de la cepa C57Bl/6 x 129/Sv de genotipo salvaje (WT). Aunque no forman parte de esta Tesis, también generamos líneas celulares de adipocitos marrones de genotipo PTP1B KO (deficientes en el gen *ptpn1*) y SIRT1 Tg (con sobre-expresión moderada del gen *Sir2*). Éstos últimos (Pfluger et al., 2008) fueron cedidos por el Dr. Manuel Serrano (CNIO, Madrid).

Los animales se mantuvieron estabulados en el animalario del Instituto de Investigaciones Biomédicas Alberto Sols (IIBm) en las condiciones establecidas de 22 ± 2º C y 45-55% de humedad con alternancia de ciclos diurnos y nocturnos de 12 horas y administración "ad libitum" de agua y alimento (pienso de mantenimiento A04-10 de SAFE, Panlab).

- **Medios de cultivo de los preadipocitos marrones**

Medio de dispersión: es el medio en el que se digiere el BAT una vez extraído. Dicho medio contiene DMEM (Medio Eagle modificado por Dulbecco) suplementado con Hepes 10 mM, penicilina 50 UI, estreptomicina 50 µg/ml, BSA (Albúmina sérica bovina) 1.5 % y Colagenasa A (Sigma) al 0.2% (2 mg/ml) procedente de *Clostridium histolyticum*.

Medio de proliferación: es el medio en el que se siembran las células extraídas del BAT para promover su proliferación. Está compuesto por DMEM suplementado con

Hepes 10 mM, penicilina 50 UI, estreptomicina 50 µg/ml, suero neonatal bovino (NCS) al 10%, insulina 3 nM y acido ascórbico 15 µM.

Medio de mantenimiento: Es el medio en que se mantienen las líneas celulares de preadipocitos marrones una vez inmortalizadas. Está compuesto por: DMEM suplementado con FBS (Suero fetal bovino) al 10%, Hepes 10 mM, penicilina 50 UI, estreptomicina 50 µg/ml. Se utilizará para la expansión y el mantenimiento de las líneas celulares.

Medio de congelación: está compuesto por FBS y DMSO (Dimetilsulfóxido) al 12%

PBS (Tampón salino de fosfato) **1X:** es el tampón salino que se utiliza para lavar las células y se suplementa con Hepes 10 mM, penicilina 50 UI y estreptomicina 50 µg/ml.

Todos los medios y soluciones que entran en contacto con las células deben ser estériles y ser preparados en las cabinas de flujo laminar para evitar contaminaciones. En el caso del medio de dispersión también es necesaria su filtración primero con filtros de 0.45 µm y posteriormente con filtros de 0.22 µm de tamaño de poro (Millipore).

- **Cultivos primarios de preadipocitos marrones**

La extracción del BAT se realizó en la sala de cultivos celulares del animalario del IIBm en la cabina de flujo laminar para evitar posibles contaminaciones. Los animales se sacrificaron por dislocación cervical tanto en el caso de las ratas como en de los ratones. A continuación, los animales se sumergían en una solución desinfectante (Hibitane diluido 1/100) y tras cortar la piel se extraía el BAT interescapular en condiciones estériles usando todo el material de cirugía desinfectado con etanol.

Una vez extraído el BAT de 10-12 animales, se troceaba con ayuda de tijeras y se añadía a viales que contenían medio de dispersión con colagenasa previamente filtrado a través de filtros de 0.4 y 0.22 µm en los cuales se realizaba la digestión enzimática. Los viales se incubaron durante 30 minutos en un baño a 37ºC con agitación vigorosa. Cada 10 minutos los viales se agitaban en un vórtex durante 10 segundos.

Una vez terminada la digestión, ya en el cuarto de cultivos del IIBm se procedió a un primer filtrado de la mezcla a través de una membrana de nylon de tamaño de poro de 250 µm, para eliminar el BAT no digerido. El filtrado se dejaba reposar durante 30 minutos en la cabina de cultivos para separar los adipocitos ya maduros que contienen gran cantidad de gotas de grasa y flotan formando una capa superficial de color blanquecino. Con ayuda de una aguja espinal se recogía el infranadante (medio que queda por debajo de la capa de adipocitos flotantes) y se volvía a filtrar, esta vez por una membrana de nylon de 25 µm de tamaño de poro.

El filtrado se repartió en tubos de cristal estériles que se centrifugaron durante 10 minutos a 720 x g. En los tubos centrifugados se distingue una capa superficial de grasa y un precipitado con los preadipocitos, hematíes y otras células de tamaño inferior a 25 µm. Los tubos se agitaron suavemente para despegar la capa de grasa adherida a la pared, que se desechaba junto con el sobrenadante. El precipitado se lavaba con medio DMEM (suplementado con Hepes 10 mM, penicilina 50 UI y estreptomicina 50 µg/ml).

Los tubos se centrifugaron de nuevo durante 10 minutos a 720 x g y los precipitados obtenidos contenían los preadipocitos marrones. Tras desechar el sobrenadante, el precipitado de células se resuspendía en medio de proliferación y se sembraba en placas de 6 pocillos (150.000 células/pocillo). Las placas se mantenían en un incubador a 37ºC, 5% de CO_2 y con una humedad del 80%.

Transcurridas 24 horas de la siembra, los preadipocitos se lavaron con DMEM (suplementado con Hepes 10 mM, penicilina 50 UI, estreptomicina 50 µg/ml) y se siguieron cultivando en medio de proliferación. Para los cultivos primarios, las células alcanzan la confluencia en el día 4 y a partir de entonces comienza el periodo de diferenciación que se mantiene hasta el día 7, a partir del cual se realizan los tratamientos indicados.

- **Generación de las líneas de preadipocitos marrones inmortalizados**

Una vez que las células en cultivo primario alcanzaron el 60% de confluencia se eliminó el medio de cultivo y se lavaron con medio DMEM de lavado. A continuación, se procedió a la inmortalización de los cultivos primarios mediante la infección con partículas retrovirales portadoras de la construcción pBabe Antígeno T puro (pBabe

LTAg puro) en presencia de polibreno 4 μg/ml, policatión que favorece la entrada de las partículas virales al interior de la célula. La preparación de las partículas retrovirales se detalla más adelante. La proteína antígeno T del virus del polisoma SV40 proporciona a las células la capacidad de propagarse indefinidamente así como la inhibición del crecimiento celular por contacto tras alcanzar la confluencia.

Las células permanecieron en contacto con las partículas retrovirales entre 48-72 horas. Transcurrido ese tiempo, se retiraron las partículas retrovirales y se procedió a la selección de las células infectadas con el antibiótico de selección que en nuestro caso era puromicina usada a 1 μg/ml, ya que únicamente las células infectadas con la construcción retroviral pBabe LTAg puro eran resistentes a este antibiótico. Una vez finalizado el proceso de selección trabajamos con clones de células inmortalizadas. Durante esta Tesis se han generado 3 líneas independientes de preadipocitos marrones de rata y 8 líneas independientes de preadipocitos marrones de ratón (Figura 7).

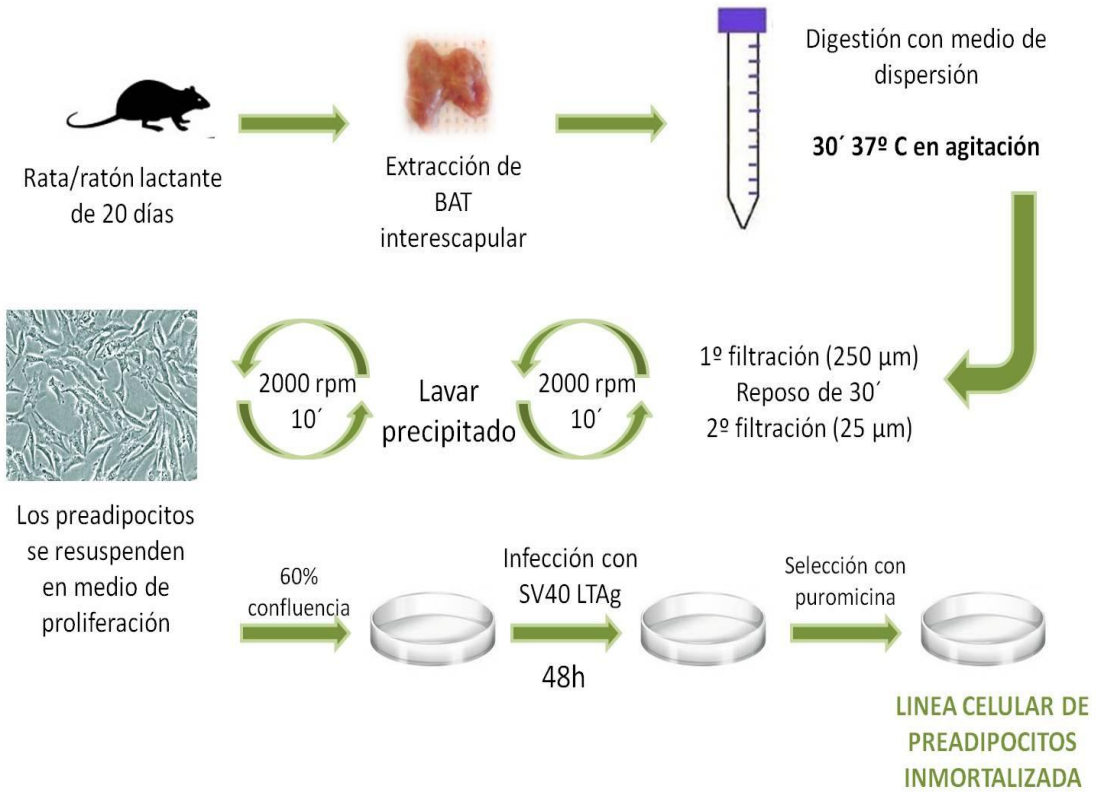

Figura 7. Esquema de la obtención de líneas celulares inmortalizadas de preadipocitos a partir de ratas/ratones lactantes.

- **Obtención de los retrovirus**

Las construcciones retrovirales se transfectaron en células denominadas "empaquetadoras" con el fin de dotar a la partícula viral de una envoltura que le permita infectar a las células diana. Para ello, se transfectaron las células empaquetadoras de la línea celular Bosc-23 por el método del fosfato cálcico de acuerdo con el protocolo descrito en el kit de transfección de la casa comercial Stratagene para células de mamífero que seguía los siguientes pasos:

- Preparación de la suspensión de ADN plasmídico para transfectar por permeabilización con $CaPO_4$

Se transfectaron 3 μg de ADN plasmídico por placa de cultivo de 6 cm de diámetro. Se calculó la cantidad necesaria de ADN plasmídico, se llevó a un volumen final de 225 μl con agua estéril y a continuación se añadieron 25 μl de la Solución 1 ($CaCl_2$ 2,5 M). Paralelamente, en un tubo de 10 ml se añadieron 250 μl de la Solución 2 (BBS pH 6,95: ácido N, N-bis (2-hidroxietil)-2-aminoetanosulfónico 50 mM, NaCl 280 mM, Na_2HPO_4 1,5 mM). Sobre la Solución 2 se añadió, gota a gota, la suspensión de ADN al tiempo que se gaseaba con nitrógeno. La mezcla se incubó 30 minutos a temperatura ambiente.

El gaseo con el nitrógeno favorece la formación del precipitado de $CaPO_4$, lo que a su vez facilita la transfección al mejorar la adsorción del ADN a la membrana celular, y al impedir la digestión del ADN por desoxirribonucleasas.

- Preparación de las células.

Las células empaquetadoras Bosc-23 se crecieron en medio de cultivo DMEM suplementado con un 10% de FBS hasta que alcanzaron una confluencia del 60-80%. En ese momento, se retiró el medio y se lavaron las células dos veces con PBS 1X atemperado. A continuación, se añadieron 2 ml de medio de cultivo DMEM suplementado al 5% con FBS modificado (MBS de la casa comercial Stratagene). De esta manera, las células quedaron listas para recibir el ADN.

- Adición de la suspensión de ADN plasmídico e incubación.

Una vez transcurridos los 30 minutos de incubación de la suspensión del ADN, esta adquirió un aspecto turbio debido a la formación de los precipitados. Lentamente y gota a gota, se añadieron 500 µl de la suspensión a cada placa de cultivo, mientras que se agitaban ligeramente con el fin de conseguir una mejor distribución del ADN.

Una vez añadido el ADN, las células se incubaron durante 4 horas a 37ºC y un 5% de CO_2. Transcurrido ese tiempo, se aspiró el medio de las placas por vacío y se lavaron las células tres veces con PBS atemperado libre de iones magnesio y calcio con el fin de eliminar los precipitados. A continuación, se les añadió el medio de cultivo DMEM suplementado al 10% con FBS.

Al día siguiente de la transfección, se retiró el medio de cultivo por vacío y se añadieron 3 ml de medio fresco. Las células se incubaron en estas condiciones durante 24 horas, transcurridas las cuales se recogió el medio de cultivo que contenía las partículas virales secretadas por las células Bosc-23. Este medio se filtró con filtros de 45 µm para eliminar posibles restos celulares y a continuación se congeló en nitrógeno líquido. La suspensión viral se conservó a –80ºC hasta el momento de su utilización.

- **Mantenimiento de las líneas celulares**

La generación de estas líneas celulares facilita el trabajo ya que evita tener que utilizar un número elevado y constante de animales de experimentación y pone las células a disposición del estudio siempre que sean requeridas. Sin embargo, se corre el riesgo de contaminación de la línea celular normalmente con micoplasma. Para ello, es necesario extremar la esterilidad en cada manejo de las placas de cultivo y si se detecta la contaminación (se observa suciedad en las placas, células muertas flotando y pierden la capacidad de diferenciación) se procede a tratar las placas con ciclinas (el protocolo se detallará más adelante). Cuando las células llegan a un número superior de 10-15 pases dejan de diferenciar correctamente por lo que se deben descartar y utilizar un nuevo vial congelado de un pase bajo.

Las líneas celulares de preadipocitos marrones se preservaron congeladas en nitrógeno líquido. Para ello, las células se despegan de las placas de cultivo con una solución de tripsina-EDTA (Gibco) durante 3-5 minutos tras los cuales se detiene la

tripsinización con medio de congelación (FBS-DMSO al 12%). La congelación se realiza de manera gradual primero a -20ºC durante 4-6 horas, a continuación a -80ºC durante 24-48 horas tras las cuales los viales de células se mantienen en tanques de nitrógeno líquido a -170ºC.

La descongelación de las células se realiza en el baño a 37ºC sumergiendo el vial cuidando de no sobrepasar la tapa. Cuando el vial está descongelado se recoge su contenido con una pipeta y se añade sobre una placa de 10 cm que contiene el medio de proliferación y así se mantenían las células hasta llegar a pase 15. Una vez al mes se realiza un test de micoplasmas para confirmar que las células estaban libres de contaminación. Para ello, se recoge 1 ml del medio que había estado en contacto con las células durante 2 días, se hierve a 95ºC durante 5 minutos y se centrifuga a 20000 x g durante 5 segundos. El sobrenadante se recoge y se utiliza para realizar una reacción de PCR en el servicio de cultivos del IIBm.

En el caso de que las células estuvieran infectadas con micoplasmas pero que procedieran de un pase bajo se procedía a realizar un tratamiento con ciclinas. Se aspiraba el medio de las placas y se añadía DMEM completo con BM Cyclin 1 (Roche) a 10 µg/ml dejando actuar durante 3 días tras los cuales se retiraba el medio y se añadía medio con BM Cyclin 2 (Roche) 5 µg/ml durante 4 días. Este procedimiento se repetía de nuevo y una vez finalizado se comprobaba mediante una nueva reacción de PCR que el tratamiento había sido efectivo.

1.2 Diferenciación de los preadipocitos marrones inmortalizados.

- **Medios de cultivo**

Medio de proliferación: es en el que se siembran los preadipocitos después de descongelarlos o tras cada pase para amplificarlos, ya descrito anteriormente.

Medio de diferenciación: Se compone de DMEM (Gibco) suplementado con FBS (Gibco) 20%, Hepes 1 mM, penicilina 50 UI, estreptomicina 50 µg/ml, insulina 20 nM y T_3 1 nM.

Medio de inducción: se prepara sobre el medio de diferenciación suplementado con dexametasona 0.5 µM, indometacina 0.125 µM, IBMX (Isobutilmetil xantina) 0.5 mM y rosiglitazona 1 µM.

- **Procedimiento**

Cuando los preadipocitos marrones sembrados en placas de 10 cm alcanzaban una confluencia celular del 80%, las placas se lavaban con PBS, se tripsinizaban tal como se ha indicado anteriormente y se contaban con la cámara de Neubauer para sembrar 100.000 células por pocillo en una placa de 6 pocillos ó 50.000 células en placas de 12 pocillos. Esta siembra se realizaba en el medio de diferenciación descrito anteriormente. A las 24 horas de la siembra se procedía al cambio de medio y los preadipocitos se mantenían con el medio de inducción durante 36 horas. Tras este periodo, se lavaban las placas con PBS y se añadía de nuevo medio de diferenciación que era renovado cada 48 horas. A día 6-7 de diferenciación (comenzando a contar desde el día que se añadía el medio de inducción), se observaba que las células habían diferenciado a adipocitos marrones maduros que contenían en el citoplasma múltiples gotas de lípidos (Figura 8). En este momento se realizaban los experimentos con los adipocitos marrones diferenciados tal como se detallará en la sección de Resultados.

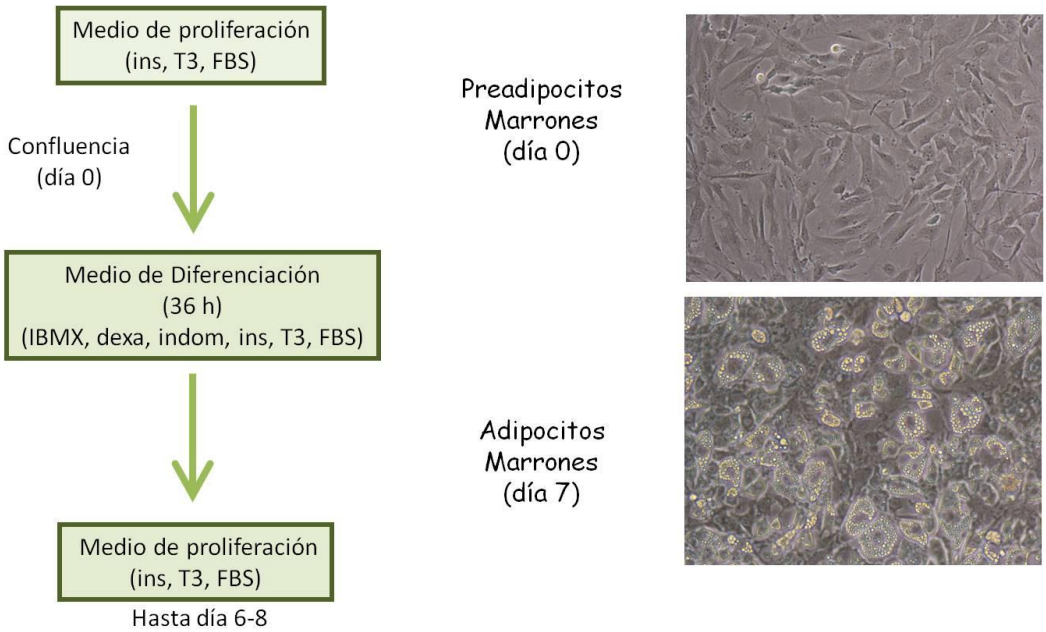

Figura 8. Esquema del proceso de diferenciación de las líneas celulares de preadipocitos marrones inmortalizadas.

Para comprobar que las líneas celulares generadas habían diferenciado correctamente se procedía a analizar la expresión de la FAS, un marcador clave de diferenciación adipogénica, y de la UCP1 como marcador de la diferenciación termogénica (Figura 9).

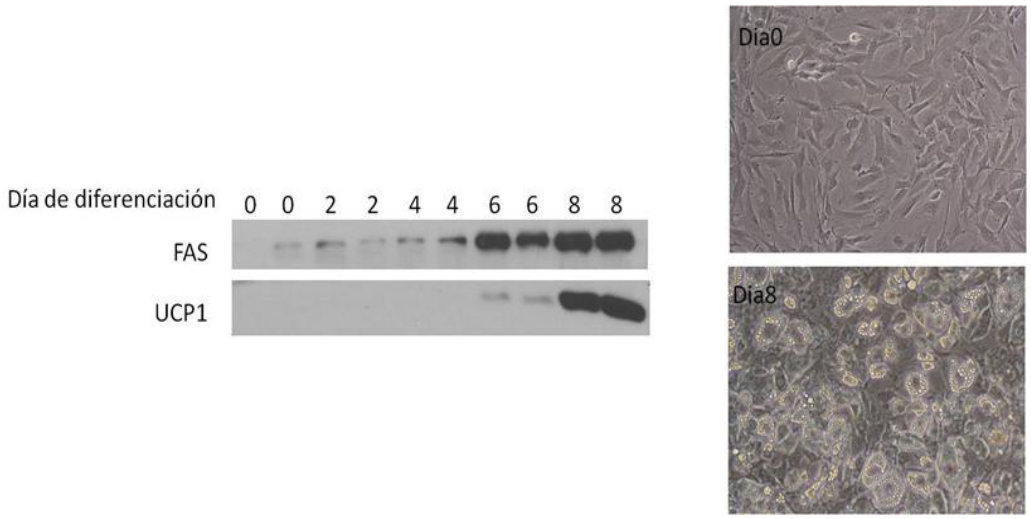

Figura 9. Inducción de marcadores termogénicos y adipogénicos en el tiempo tras aplicar protocolo de diferenciación a las líneas de preadipocitos marrones inmortalizados procedentes de ratas lactantes.

Algunos experimentos fueron realizados en cultivos primarios de adipocitos marrones de rata para descartar que los datos obtenidos se debieran a posibles efectos de los protocolos de inmortalización y diferenciación que se aplicaban a las líneas celulares. Para ello, se obtuvo el BAT de ratas lactantes de aproximadamente 20 días de vida tal como se ha descrito anteriormente, se aislaron los preadipocitos marrones, se sembraron y se dejaron diferenciar espontáneamente durante 8 días, tras los cuales se observaba que los adipocitos marrones presentan multitud de gotas lipídicas en su citoplasma. Las estimulaciones con los diferentes compuestos de estudio se realizaron en DMEM (Gibco) con NCS al 10% (NCS hipotiroideo si se añadía T_3), Hepes 10 mM, penicilina 50 UI y estreptomicina 50 µg/ml, suplementado con insulina 3 nM y acido ascórbico 15 µM.

2. TRATAMIENTO IN VIVO CON RAPAMICINA EN RATAS WISTAR

Ratas Wistar macho de 10 semanas de edad, obtenidas de Charles Rivers Lab. Inc. (Barcelona) se mantuvieron en cajas ventiladas (2 animales por caja) bajo un ritmo de 12 horas de luz y 12 de oscuridad y con una dieta estándar (IPM-R20, Letica, Barcelona) con acceso libre a agua. Los animales fueron tratados con 1 mg/kg de peso/día de rapamicina (Rapamune®, Laboratorios Pfizer, Lisboa), mimetizando así la dosis clínica que previamente había sido estudiada (Fuhrmann et al., 2014). El tratamiento se administró por vía oral durante 3 semanas y se midió el peso corporal a diario. Al finalizar el tratamiento, se inyectó a los animales intraperitonealmente 10 U/kg de insulina recombinante humana (Actrapid) y se sacrificaron 10 minutos más tarde mediante dislocación cervical. Tras el sacrificio el BAT se extrajo inmediatamente para analizar la señalización de la insulina. La concentración en sangre de rapamicina se comprobó mediante un inmunoensayo utilizando métodos (Flex Reagent) y equipos (Dimension®-RxL, Siemens) automáticos.

Todos los estudios con animales se realizaron siguiendo los protocolos aprobados por la Normativa Nacional y de la Unión Europea sobre el Cuidado de Animales.

3. ANALISIS DE LA EXPRESION DE PROTEÍNAS

La expresión de las proteínas se analizó mediante Western Blot.

Las proteínas fueron extraídas a partir de cultivos de líneas celulares inmortalizadas o del BAT de animales de experimentación. Para extraer las proteínas de cada pocillo de una placa de 6 pocillos utilizamos 100 µl de tampón de lisis compuesto por Tris-HCl 10 mM, EDTA 5 mM, NaCl 50 mM, $Na_4P_2O_7$ 30 mM, NaF 50 mM, Na_3VO_4 100 µM, Tritón X-100 1%, PMSF 1 mM, leupeptina 10 µg/ml, aprotinina 10 µg/ml a pH 7,6). Para extraer las proteínas del BAT lisamos 40 mg de tejido en 400 µl de tampón de lisis compuesto por Hepes 50 mM, Tritón X-100 1%, $Na_4P_2O_7$ 50 mM, NaF 0.1 M, EDTA 10 mM, Na_3VO_4 10 mM, PMSF 1 mM, leupeptina 10 µg/ml, aprotinina 10 µg/ml.

En el caso de las líneas celulares, los pocillos se lavaron con PBS y las células se lisaron en hielo con el tampón de lisis. El lisado se centrifugó a 17.000 x g durante 10 minutos a 4ºC. Tras la centrifugación se recogía el sobrenadante, intentando evitar

recoger la capa de grasa que queda en la superficie. Si la capa de grasa se mezclaba con el sobrenadante se procedió a realizar una segunda e incluso una tercera centrifugación. A continuación, se valoraba la concentración de proteínas del lisado mediante el método de Bradford (Bio-Rad) y utilizando BSA 1µg/µl para hacer la curva patrón. Una vez valoradas las muestras, éstas se almacenaron a -80ºC o directamente se prepararon los extractos.

Los extractos se prepararon para una concentración final de proteína de 15-50 µg en el tampón de carga (Tris 100 mM, glicerol 10%, SDS 4%, azul de bromofenol 0.2%, β-mercaptoetanol 2 mM). Las muestras se calentaron durante 5 minutos a 95ºC y se utilizaban en el momento o se congelaban a -20ºC.

El BAT obtenidos de las ratas se homogenizaba con un Polytron (PT 1200E, Kinematica AG) en el tampón de lisis y manteniendo siempre el tejido en hielo. Posteriormente, los extractos se centrifugaron a 40.000 x g durante 30 minutos a 4ºC (también se evitaba recoger la capa de grasa). Seguidamente se valoraba la concentración de proteína por el método de BCA (Ácido bicinconínico, Thermofisher) usando como estándar BSA (1µg/µl). Las muestras se prepararon en tampón de carga de la misma manera que los lisados procedentes de cultivos celulares.

Las muestras se cargaron en geles de SDS-PAGE (Electroforesis en gel de poliacrilamida con Dodecil sulfato sódico), con porcentajes de acrilamida entre 8-12% (BioRad), junto con una solución estándar con proteínas de peso molecular conocido que permite identificar las proteínas objeto de estudio. A continuación, se realizaba la electroforesis y se transferían las proteínas a membranas de PVDF (Polifluoruro de vinilo, Merk-Millipore) previamente activadas con metanol. Las membranas se bloqueaban con BSA al 3% (p/v) a temperatura ambiente durante una hora y se incuban durante toda la noche con los anticuerpos correspondientes (Figura 10) diluidos en TTBS (Buffer salino Tris con Tween 20) (Tween-20 al 0,05% (v/v), Tris-HCl 10 mM, NaCl 150 mM, pH 7.5)

ANTICUERPO	REFERENCIA	LABORATORIO
Anti-pJNK (Thr 183/Tyr 185)	#4668	Cell Signaling Technology
Anti-pHSL(Ser 660)	#4126	
Anti-Akt	#9272	
Anti-pIR (Tyr 1162/Tyr 1163)	sc-25103-R	Santa Cruz Biotechnology
Anti-IR	sc-711	
Anti-JNK	sc-571	
Anti-pAkt1/2/3 (Ser 473)	sc-7985-R	
Anti-pAkt1/2/3 (Thr 308)	sc-16646-R	
Anti-pS6K1 (Thr 339)	sc-11759	
Anti-caveolin-1	sc-894	
goat anti-mouse IgG-HRP	sc-2005	
goat anti-rabbit IgG-HRP	sc-2004	
Anti-IRS1	06-248	Merck Millipore
Anti-pIRS1 (Ser 307)	07-247	
Anti-IRS2		M.White (Harvard Medical School, USA)
Anti-GLUT-4	AB 1346	Chemicon
Anti-UCP1	ab23841	Abcam
Anti-αTubulina	A5441	Sigma-Aldrich

Figura 10. Listado de anticuerpos utilizados en los ensayos de Western Blot

Tras repetidos lavados de las membranas con TTBS, éstas eran incubadas con los anticuerpos secundarios (Figura 10). Las bandas correspondientes a las proteínas reconocidas por los anticuerpos se visualizaban mediante ECL (Sistema intensificador de quimioluminiscencia para Western-Blot, Merck-Millipore) y revelándolas en películas radiográficas (Kodak) que posteriormente fueron densitometradas con el programa Image J.

4. ENSAYO DE PCR CUANTITATIVA EN TIEMPO REAL

Las placas del cultivo se llevaron a una campana extractora de gases donde se les añadió 1 ml de Trizol® (Invitrogen) con el fin de conseguir la lisis celular y la solubilización del ARN. Con ayuda de una pipeta se homogeneizó la muestra y se recogieron los lisados en tubos Eppendorff estériles de 1.5 ml que se mantuvieron en hielo. El proceso de extracción se podía parar en este momento conservando las muestras a -80ºC, o bien continuar con la fase de extracción del ARN propiamente dicha.

A los lisados celulares obtenidos en el paso anterior, se les añadió 200 µl de cloroformo y se agitaron vigorosamente durante 15 segundos con la ayuda de un agitador mecánico. A continuación, las muestras se dejaron reposar durante 3 minutos a temperatura ambiente tras los cuales se centrifugaron a 17.000 x g durante 15 minutos a 4ºC, obteniéndose dos fases. En la fase superior o fase acuosa se encuentra el ARN mientras que el ADN y las proteínas se encuentran en la fase inferior y en la interfase, respectivamente.

Con la ayuda de una pipeta, se recogió la fase acuosa de cada una de las muestras y se llevó a un tubo nuevo estéril para proceder a la precipitación del ARN con un volumen igual de alcohol isopropílico. Los tubos se agitaron vigorosamente con un agitador mecánico y se mantuvieron a temperatura ambiente 10 minutos. A continuación, las muestras se centrifugaron de nuevo a 17.000 x g durante 15 minutos a 4ºC y como resultado de la centrifugación se obtuvo un precipitado blanco de ARN. El sobrenadante se eliminó por vacío y el precipitado se lavó con 1 ml de etanol al 75% en agua estéril tratada con dietilpirocarbonato (DEPC). Por último, los tubos se centrifugaron a 17.000 x g durante 5 minutos a 4ºC tras los cuales el sobrenadante se eliminó por aspiración con una bomba de vacío y se dejó secar el precipitado al aire durante 10-15 minutos para resuspender el ARN en un volumen conocido (aproximadamente de 20 µl) de agua estéril tratada con DEPC. Finalmente, para asegurar la completa solubilidad del precipitado de ARN, los tubos se calentaron a 60ºC durante 5 minutos. De la muestra resuspendida se tomó una alícuota para determinar, con el uso de un Nanodrop, la cantidad de ARN obtenido y su pureza. Utilizando 1 µg del ARN extraído se obtuvo el ADNc mediante la técnica de RT-PCR usando los reativos iScript (BioRad) y utilizando el termociclador 2400 (Perkin Elmer). Las muestras se amplificaron por triplicado siguiendo el siguiente programa: 50ºC durante 2

minutos, 95ºC durante 10 minutos; 40 ciclos de 15 segundos a 95ºC y un minuto a 60ºC.

El ADNc fue amplificado y cuantificado por hibridación con las sondas TaqMan-Applied Biosystems para rata de *Ucp1* (marcada con FAM, Rn00562126-m1) y de *Pgc1a* (con FAM, Rn00580241-m1). La expresión de cada gen referida por el valor "Ct" (ciclo de amplificación requerido para alcanzar un umbral mínimo establecido) se normalizó con el valor "Ct" de la sonda control Ubiquitina (marcada con VIC, Rn01789812) aplicando la fórmula $2^{-\Delta\Delta Ct}$, que nos indica la expresión "relativa" del ARNm en número de veces de incremento o disminución (fold-change) $2^{-\Delta\Delta Ct}$: Dif expresión = $2^{-(\text{Ct gen de interés - Ct gen control})}$

Una de las ventajas de la tecnología TaqMan es que tanto la sonda del gen control (marcado con VIC) como la del gen a analizar (marcado con FAM) ocupan el mismo pocillo en la placa y esto nos permite corregir cualquier error individual en cada pocillo. Las sondas de hibridación TaqMan presentan también la ventaja de su elevada especificidad: poseen un fluoróforo en el extremo 5´ y una molécula en el 3´ que bloquea la fluorescencia (quencher); la sonda hibrida con la región a amplificar por PCR y cuando la polimerasa lleva a cabo la reacción elimina la molécula de 3´y permite obtener fluorescencia del extremo 5´que podemos detectar y cuantificar.

5. MEDICION DE LA CAPTACION DE GLUCOSA

Los adipocitos marrones diferenciados en placas de 12 pocillos se trataron tal como se indica en la sección de Resultados y se cultivaron en medio DMEM en ausencia de suero durante 2 horas. A continuación, las células se lavaron 3 veces con el tampón KRP (Tampón fosfato de Krebs-Ringer) (NaCl 135 mM, KCl 5.4 mM, $CaCl_2$ 1.4 mM, $MgSO_4$ 1.4 mM, $Na_4P_2O_7$ 10 mM) y se incubaron con 500 µl de este mismo tampón durante 15 minutos a 37ºC. Seguidamente, las células se estimulaban con insulina (10 nM) durante 10 minutos tras los cuales se añadía una mezcla con 50 mM glucosa y 0,5 mCi/ml [^{3}H] 2-deoxiglucosa.

Transcurridos 5 minutos de incubación, se lavaron las células de nuevo dos veces con el tampón KRP, se solubilizaron con 500 µl de SDS al 1% (p/v) incubándolas

durante 2 horas a 37ºC. Finalmente, se homogenizaba bien el lisado con ayuda de una jeringa y se tomaban 100 µl del mismo que se diluyeron en 4.5 ml de liquido de centelleo para su lectura en el contador de centelleo. Paralelamente, se valoraban las proteínas utilizando como estándar BSA y el reactivo BCA (Thermofisher). Este protocolo ha sido puesto a punto a partir de otros anteriores desarrollados en nuestro laboratorio (Valverde et al., 1998).

6. ANALISIS DE LA TRANSLOCACION DEL GLUT4 A LA MEMBRANA PLASMATICA

Los adipocitos marrones cultivados en placas de 12 pocillos fueron lavados con PBS y recogidos en tampón de homogenización (Tris-HCl 20 mM, EGTA 2 mM, EDTA 2 mM, PMSF (Fluoruro de fenil metil sulfonilo) 1 mM, β-mercaptoetanol 10 mM, aprotinina 10 µg/ml, leupeptina 10 µg/ml) pH 7.4. Tras incubar las muestras durante 10 minutos en hielo, se procedía a la homogenización en un potter de vidrio. A continuación, el homogenado se centrifugaba a 500 x g durante 5 minutos a 4ºC para precipitar los núcleos celulares. El sobrenadante obtenido se centrifugaba a 100.000 x g durante 30 minutos a 4ºC obteniendo un precipitado con la fracción de membrana plasmática y un sobrenadante con la fracción de membrana interna. El precipitado se lavaba 3 veces y se añadía tampón de homogenización suplementado con Tritón X-100 al 1% (p/v). Tras una incubación de una hora en hielo, se procedía a centrifugar la solución a 100.000 x g durante 15 minutos para separar la membrana plasmática (sobrenadante) del citoesqueleto (precipitado). La fracción de membrana plasmática se guardaba a -80ºC para posteriormente analizarse mediante Western blot con los anticuerpos anti-GLUT-4 y anti-caveolina 1 (proteína de membrana utilizada como control de carga).

7. ENSAYO DE LA LIPOLISIS

Tras los tratamientos correspondientes, se retiraba el medio de cultivo y los adipocitos marrones diferenciados se incubaban con tampón KRB (Tampón bicarbonato de Krebs-Ringer) (NaCl 118.5 mM, KCl 4.75 mM, $CaCl_2$ 1.92 mM, KH_4PO_4 1.19 mM, $MgSO_4$ $(H2O)_7$ 1.19 mM, $NaHCO_3$ 25 mM, Hepes 10 mM, D-Glucosa 6 mM, BSA 4%) con y sin NE 5 µM (Sigma) o el agonista β3 adrenérgico CL316243 2 µM (Sigma). Transcurridas 2 horas, se recogía el medio KRB de cada pocillo, manteniendo las placas con las células siempre en hielo, y se cuantificaba el glicerol y los ácidos grasos libres que las células habían liberado a dicho medio siguiendo el protocolo establecido por la casa comercial Wako. En paralelo se valoraban las proteínas mediante con el reactivo BCA (Thermofisher) para referir los niveles de glicerol o de ácidos grasos libres a la concentración de proteína de cada pocillo.

8. ANALISIS DE LA TRANSLOCACION DEL GLUT4 MEDIANTE INMUNOFLUORESCENCIA

Los preadipocitos marrones fueron sembrados y diferenciados en cristales circulares de vidrio sobre la base de los pocillos y, una vez diferenciados y tratados tal como se describe en el apartado de resultados, las células se fijaron con paraformaldehido (PFA) al 4% durante 15 minutos. Tras la fijación, se realizaban tres lavados con PBS para retirar el exceso de PFA y, a continuación, las células se permeabilizaban con Tritón X-100 al 0.1%. Se volvían a realizar 2 lavados con PBS y se procedía al bloqueo con PBS-BSA al 3% durante una hora a temperatura ambiente.

Una vez finalizado el bloqueo, los cristales se incubaron con el anticuerpo anti-GLUT4 (sc-56566, Santa Cruz) en PBS-BSA al 3% (p/v) a una dilución 1/25 (v/v) durante toda la noche a 4ºC. Tras realizar 3 lavados con BSA al 1%, muy cuidadosamente para no despegar la capa celular adherida a los cristales circulares, se procedía a la incubación con el anticuerpo secundario acoplado a Alexa 488 (Invitrogen) a la dilución 1/500 (v/v) en BSA al 3% y manteníamos la incubación durante 1 hora en oscuridad. Una vez finalizada esta incubación, los cristales se lavaron de nuevo con PBS-BSA al 1% y procedimos a teñir los núcleos con DAPI (4´,6-diamino-2-fenilindo). Los cristales circulares fueron fijados a los portas con ProLong

gold (Thermofisher), y se mantenían 24 horas a temperatura ambiente en oscuridad y otras 24 horas a 4ºC también en oscuridad. Finalmente, se observaba la inmunofluorescencia de la preparación en el microscopio Nikon Eclipse 90i y las imágenes se analizaban con el programa con el programa Nis elements (Nikon).

9. EVALUACION DE LA RESPIRACION MITOCONDRIAL DE LOS ADIPOCITOS MARRONES

Para determinar la tasa de consumo de oxigeno (OCR) realizada por los adipocitos marrones maduros se utilizó el Seahorse XF24 Extracellular Flux Analyzer (Seahorse Bioscience). Los adipocitos marrones fueron cultivados, diferenciados y tratados con rapamicina (Sigma) a la concentración de 100 nM durante 16 horas en placas de 24 pocillos específicas de Seahorse. Para la evaluación de un perfil bioenergético típico se utiliza oligomicina para bloquear la ATP sintasa; el desacoplante carbonyl cyanide-4-(trifluoromethoxy) phenylhydrazone (FCCP) para medir la capacidad respiratoria máxima, seguido de rotenona, el inhibidor del complejo 1 de la cadena respiratoria, y antimicina-A para finalmente medir sólo la actividad no mitocondrial (todos los reactivos utilizados eran de Sigma-Aldrich). Antes de la lectura las células se incubaron durante 1 hora en medio XF Assay Medium (Seahorse Bioscience) suplementado con glucosa 5 mM. Durante el ensayo, se inyectaron los siguientes compuestos a las concentraciones finales que se indican: 0.2 μM oligomicina, 0.2 μM FCCP, 1 μM rotenona y 1 μM antimicina-A. El OCR fue calculado midiendo la concentración de oxígeno del medio por unidad de tiempo (pmol/min) y normalizado por la concentración de proteína de cada pocillo. Los datos finales son la media de 8-10 pocillos ± SEM por unidad de tiempo de al menos 3 experimentos independientes.

10. ACTIVIDAD DE LA DESIODASA D2

Se determinó la actividad 5'-desiodasa Tipo II (D2) en los adipocitos marrones diferenciados midiendo la cantidad de ioduro producido usando como sustrato la T_4.

Las placas de cultivo con las células congeladas en hielo seco se homogenizaron en 1 ml de un tampón que contiene sacarosa 0.32 M, Hepes 10 mM, pH=7 y ditiotreitol (DTT) 10 mM que se añade en el momento de la homogenización. Es importante señalar que todo el proceso se realiza en hielo debido a que la actividad D2 se protege a 4ºC y por el DTT ya que su vida media es corta, de unos 30 minutos. La concentración de proteínas debe de ser de unos 100 µg por 50 µl del homogenado.

Para determinar la actividad D2 se usa como sustrato ^{125}I-T_4 (su síntesis se detalla más adelante). Se midió el yoduro radiactivo liberado a partir de ^{125}I-T_4. Antes de realizar el ensayo se purificaba la ^{125}I-T_4 mediante electroforesis en papel durante 5 min a 400 V usando acetato amónico ($C_2H_7O_2NH_4$) 50 mM, pH 6.8. El yoduro migra unos 3-4 cm, mientras que la ^{125}I-T_4 permanece en el origen. La ^{125}I-T_4 se eluye en una jeringa usando NaOH 0.04 N, añadiendo posteriormente los reactivos de la reacción (DTT, tampón Fosfato, T_4 y propiltiouracilo (PTU), se detalla más adelante). En este proceso se recupera aproximadamente el 50% de la ^{125}I-T_4 libre de yoduro (< del 1% de la radiactividad en forma de yoduro).

La actividad D2 se mide según el método de Leonard et al., 1983, modificado en el laboratorio (Martinez-de Mena y Obregón, 2005), a pH 7 en presencia de 50.000 cpm de ^{125}I-T_4 y T_4 2 nM, de PTU 1 mM y DTT 20-50 mM en un volumen total de 100 µl. También se añade T_3 1 µM para inhibir la desiodación interna de la T_4 en posición 5, así se inhibe la producción de rT_3 a partir de T_4 y la degradación de la T_3 formada. Tras una hora de incubación a 37°C la reacción se para añadiendo 50 µl de una mezcla de plasma: PTU 10 mM (1:1) y 350 µl de ácido tricloroacético (TCA) al 10 %, precipitando las proteínas por centrifugación.

El yoduro liberado se separa por cromatografía de intercambio iónico, pasando 400 µl del sobrenadante anterior por columnas Dowex 50W-X2 (Bio Rad), eluyendo el ioduro con 2 ml de ácido acético al 10%. A continuación se cuenta la radiactividad y se calcula la actividad enzimática como fentomoles (fmols) de I⁻/ hora/ por mg de proteína

y. se le resta la desiodación no enzimática (blanco= muestra que no contiene homogenado, sino buffer). El ensayo se realiza en duplicado o triplicado.

Se determinaron las proteínas en los homogenados usando el método de Lowry et al., 1951. Como el DTT de los homogenados interfiere en la reacción colorimétrica, las proteínas se precipitaron con TCA (Ácido tricloroacético) al 10 % y se resuspendieron en NaOH 0.4 N, usando BSA como estándar (5-90 µg BSA).

- **Obtención de ^{125}I-T_4 para determinar la actividad desiodasa D2**

Marcaje: Para la medir la actividad desiodasa se requiere ^{125}I-T_4 de alta actividad específica, que es sintetizada en el laboratorio.

El marcaje se realiza usando como substrato una yodotironina de un grado de yodación menor. Se usa T_3 para obtener T_4 marcada con I^{125}, oxidando el yoduro radiactivo al estado de yodo naciente con cloramina T, incorporándose el I^{125} a la T_3. La reacción contiene: 2 mCi de ^{125}I, 1 µg de T_3 y 50 µl de tampón fosfato 0.5 M, pH 7.5. Se añadieron 25 µg de cloramina T y la reacción se para a los 20 segundos con 240 µg de metabisulfito sódico ($Na_2S_2O_5$). Los productos de marcaje se separan mediante cromatografía en papel durante 16 horas usando como solvente BEA (Butanol: Etanol: Amoniaco ($C_4H_{10}O$: C_2H_5OH: NH_3) 0.5 N (5:1:2)). Una vez realizada la cromatografía, se corta y cuenta en tiras de 8 mm y se identifica la zona que contiene ^{125}I-T_4 que se eluye con metanol:amoniaco (CH_4O: NH_3) 2N (9:1), evaporándose el eluido metanólico a sequedad bajo corriente de N2 para evitar oxidaciones y reconstituyendo la ^{125}I-T_4 en etanol, a una concentración de 400.000 cpm/µl.

11. ANALISIS ESTADISTICO

El análisis estadístico de los datos se llevó a cabo con el programa Graph Pad Prism 5 (www.graphpad.com) expresando los resultados como la media ± SEM (error estándar de la media). Para comparar dos grupos utilizamos el análisis t-Student y para comparaciones múltiples se usó el test de ANOVA de una variable. El post-test utilizado para valorar las diferencias entre distintos grupos fue Bonferroni, El nivel de significación estadística se ha establecido cuando *$p<0.05$.

Resultados

1. Efecto de la rapamicina en la señalización de la insulina en los adipocitos marrones

Debido a que el efecto de diversos inmunosupresores sobre las acciones de la insulina había sido estudiado en tejidos como hígado, WAT o riñón (Smith et al., 2003; Zhang et al.; 2014; Pereira et al., 2014), pero no había estudios realizados sobre los efectos en el BAT, realizamos una primera aproximación analizando el impacto de la rapamicina en la señalización de la insulina en los adipocitos marrones. Para ello, se utilizaron las líneas inmortalizadas de preadipocitos marrones de rata lactante (18-20 días de vida) generadas en el laboratorio y descritas en Materiales y Métodos.

Los preadipocitos marrones se sembraron con una densidad de 150.000 células por pocillo (40.000 células/cm2) en placas de 12 pocillos. Tras seguir el protocolo de diferenciación descrito anteriormente (Miranda et al., 2010) se observaba que a partir del día 6 de diferenciación los adipocitos marrones contenían múltiples gotas lipídicas y adquirían una morfología poliédrica que los diferenciaba claramente de la forma alargada que presentan los preadipocitos. (Figura 11)

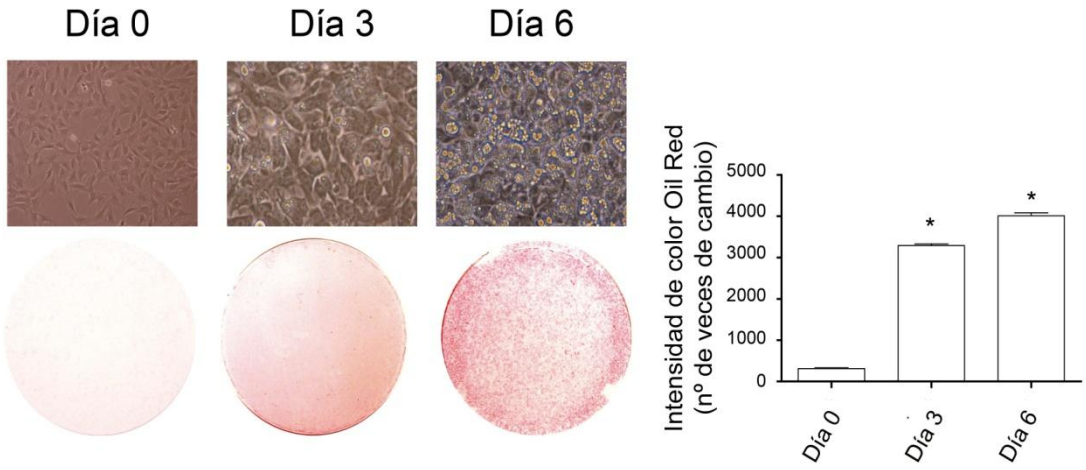

Figura 11. Diferenciación de los adipocitos marrones inmortalizados. Los adipocitos marrones se sembraron y se diferenciaron siguiendo el protocolo descrito en Materiales y Métodos. En la figura se muestran fotografías representativas de la diferenciación celular y la tinción con el colorante Oil Red O de pocillos independientes a los días 0 (preadipocitos), 3 y 6 de diferenciación. *$p < 0.05$ respecto a día 0.

Con el fin de corroborar la correcta diferenciación de los preadipocitos marrones a adipocitos marrones maduros analizamos la expresión de proteínas marcadoras de la adipogénesis como son la FAS, el transportador de glucosa GLUT4 y la proteína desacoplante UCP1 (Figura 12 y Figura 9 de Materiales y Métodos). De igual manera, valoramos también la expresión, en el transcurso de la diferenciación adipocítica de proteínas de la ruta de señalización de la insulina. Estudios anteriores (Entingh-Pearsall y Kahn, 2004) habían demostrado que en los preadipocitos marrones de rata hay una mayor expresión del IGF-1R mientras que el IR apenas se detecta. Sin embargo, en el transcurso de la diferenciación disminuye la expresión del IGF-1R y aumenta la del IR (Figura 12).

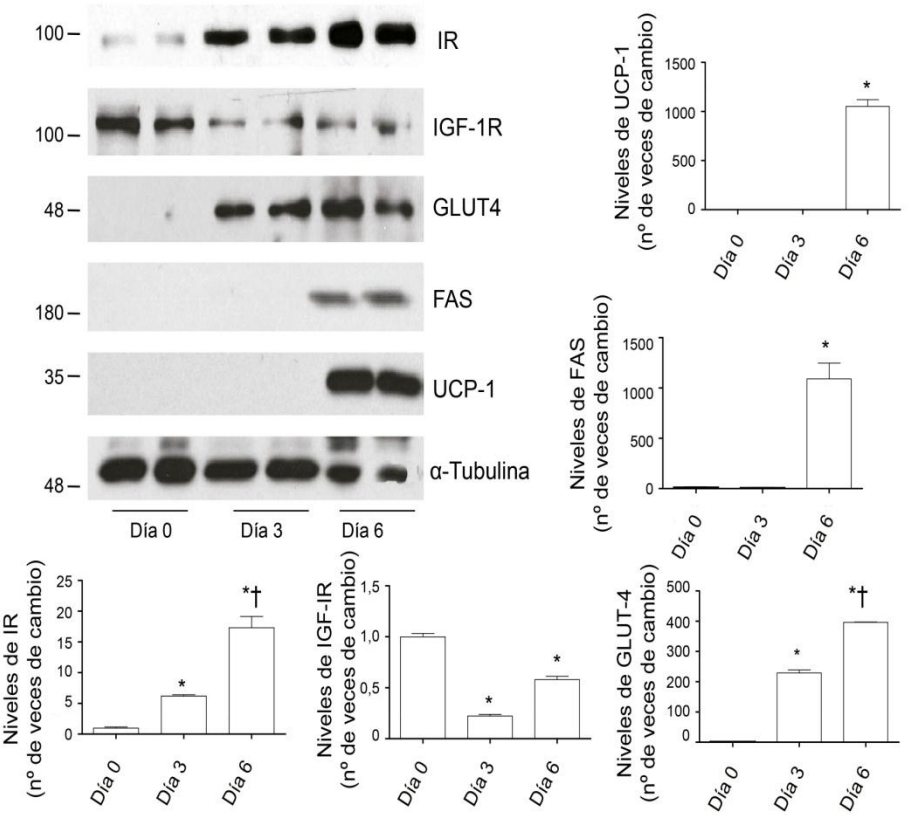

Figura 12. Expresión de proteínas marcadores de la diferenciación de los adipocitos marrones en la línea celular generada. Tras inducirse el proceso de diferenciación, se obtuvieron los lisados de los adipocitos a días 0 (preadipocitos), 3 y 6 para analizar la expresión de las proteínas FAS, GLUT4, UCP1, IR e IGF-1R mediante Western blot. Los resultados son representativos de 2 experimentos independientes realizados en 3 líneas diferentes de células inmortalizadas. Los resultados son la media ± SEM. *p < 0.05 respecto al día 0 y †p < 0.05 respecto al día 3.

Dentro de la cascada de señalización de la insulina, abordamos primero el estudio del efecto de la rapamicina sobre los niveles de la proteína IRS1 debido a su importancia en la diferenciación de los adipocitos marrones y en la señalización de la insulina en estas células (Fasshauer et al., 2001; Valverde et al., 1999a). Se analizaron los niveles de IRS1 en los adipocitos marrones diferenciados tras el tratamiento durante 16 horas con concentraciones crecientes de rapamicina desde 10 nM a 100 nM. Los resultados obtenidos muestran que los niveles proteicos de IRS1 descendieron en los adipocitos marrones cultivados con rapamicina de una manera dosis-dependiente, disminuyendo a valores apenas detectables a la concentración de 100 nM (Figura 13). Sin embargo, la expresión de las proteínas IRS2 y Akt no se vio afectada por el tratamiento con la rapamicina. Como control de la efectividad de la rapamicina analizamos la fosforilación de S6K1 con respecto a células sin tratar, que, como cabía esperar, disminuyó con el tratamiento de manera dosis-dependiente.

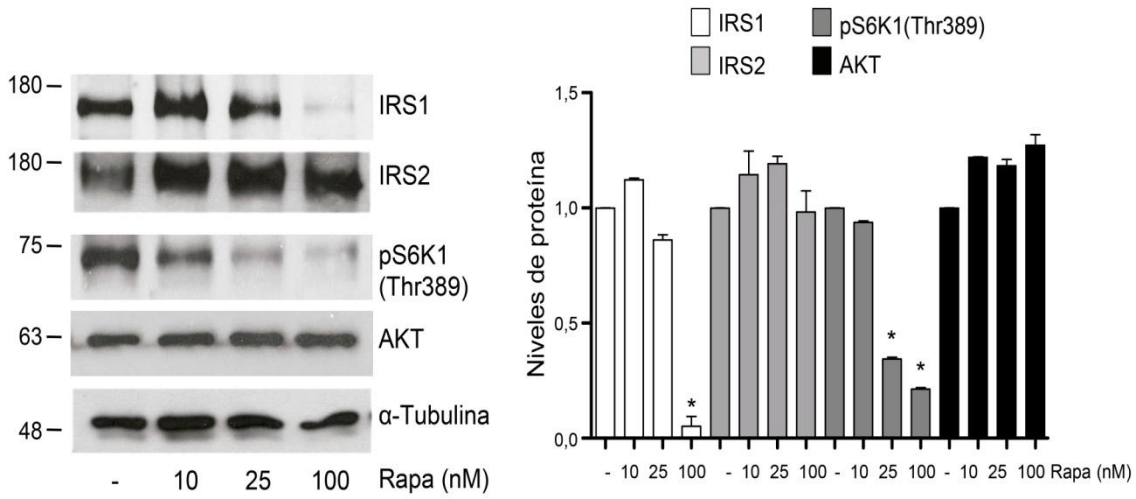

Fig 13. El tratamiento con rapamicina durante 16 horas induce la degradación del IRS1 en los adipocitos marrones. Los adipocitos marrones de rata fueron diferenciados durante 6 dias y cultivados en presencia de dosis crecientes de rapamicina (Rapa) durante 16 horas. Al finalizar el tratamiento, los adipocitos marroness fueron recogidos y se prepararon los lisados proteicos. Los niveles de proteínas se analizaron mediante Western Blot utilizando anticuerpos contra IRS1, IRS2, fosfo-S6K1 (Thr 389) y α-Tubulina, usada como control de carga. El resultado de 3 experimentos independientes se cuantificó densitomentrando las bandas obtenidas. Los resultados son las medias ± SEM. $^{*}p < 0.05$ respecto al basal sin estimulación.

A continuación se investigó el efecto de la rapamicina en la modulación de la señalización de la insulina en los adipocitos marrones. Para ello, se valoró la activación de la ruta de señalización mediada por el IR que conduce a la activación de Akt debido a su importante papel en la regulacion de la expresión de genes implicados en procesos relevantes en los adipocitos marrones como son la síntesis lipídica y la termogénesis (Valverde et al. 1999a; Valverde et al., 2003b).

Los adipocitos marrones fueron tratados durante 16 horas con concentraciones crecientes de rapamicina. A continuación, se deprivaron de suero durante 2 horas y se estimularon con insulina a la concentración de 10 nM durante 10 minutos. Tal como se muestra en la Figura 14, observamos un aumento de la fosforilación del IR en los residuos Tyr 1162/1163 del dominio catalítico con respecto a las células que no recibieron rapamicina, aunque este dato carece de significación estadística. Sin embargo, el pretratamiento con rapamicina disminuyó la fosforilación de Akt en los residuos Ser 473 y Thr 308 inducida por la insulina de manera dosis-dependiente (Figura 14).

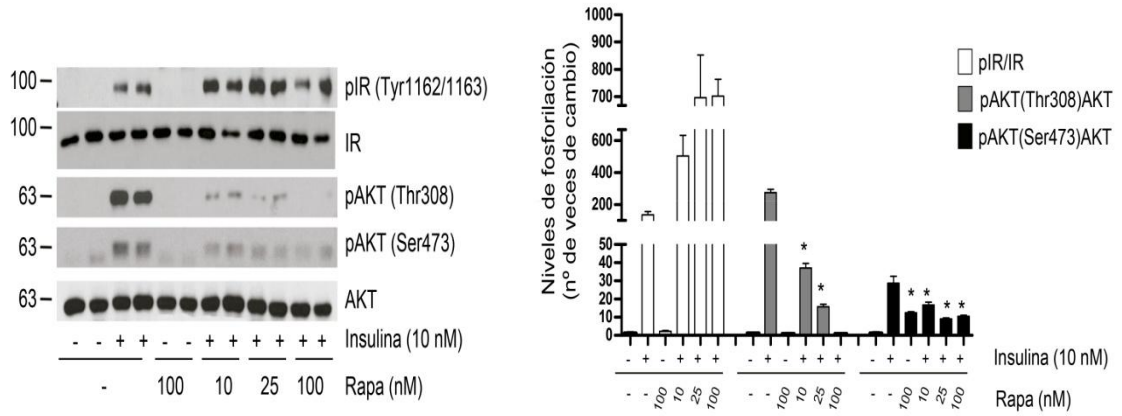

Fig 14. El tratamiento de 16 horas con rapamicina disminuyó la señalización de la insulina mediada por Akt en los adipocitos marrones. Los adipocitos marrones diferenciados se trataron con dosis crecientes de rapamicina y tras un ayuno de 2 horas se estimularon durante 10 minutos con insulina a la concentración de 10 nM. Se recogieron los lisados de proteínas y se analizaron mediante Western blot usando los siguentes anticuerpos: anti-fosfo IR (Tyr 1162/1163), anti-IR, anti-fosfo-Akt (Ser 473), anti-fosfo-Akt (Thr 308) y anti-Akt. Los resultados de 4 experimentos independientes se cuantificaron densitometrando las bandas obtenidas. Los resultados mostrados son las medias ± SEM. $^{*}p < 0.05$ respecto a células estimuladas con insulina que no habían sido tratadas con rapamicina.

A continuación, investigamos si la degradación de IRS1 que encontrabamos tras el tratamiento de los adipocitos marrones con rapamicina durante 16 horas era responsable de la disminución de la respuesta a la insulina en la fosforilación de Akt. Para ello, los adipocitos fueron tratados con rapamicina durante un tiempo corto de 45 minutos tras los cuales se evaluaron los niveles de IRS1, sin observarse modificaciones respecto a adipocitos marrones no tratados (Figura 15).

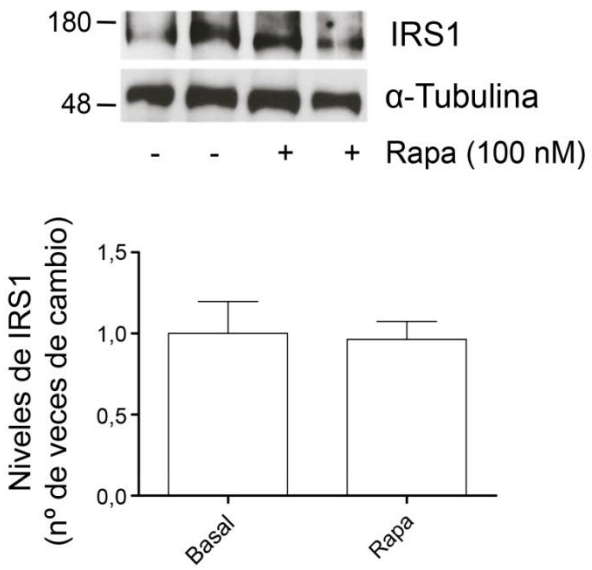

Fig 15. El tratamiento de los adipocitos marrones con rapamicina durante 45 minutos no altera los niveles de IRS1. Los adipocitos marrones diferenciados se cultivaron durante 45 minutos en presencia de rapamicina (100 nM). La proteína total se analizó por Western blot usando anticuerpos frente a IRS1 y α-Tubulina como control de carga.

En el siguiente experimento se trataron las celulas con rapamicina durante 45 minutos tras los cuales se añadió insulina a la concentración de 10 nM durante 10 minutos tras los cuales se analizó la fosforilación de Akt. Se comprobó que el pretratamiento con rapamicina durante un tiempo corto inhibía la fosforilación de S6K1 pero no disminuyó la fosforilación de Akt debida al estímulo de la insulina (Figura 16).

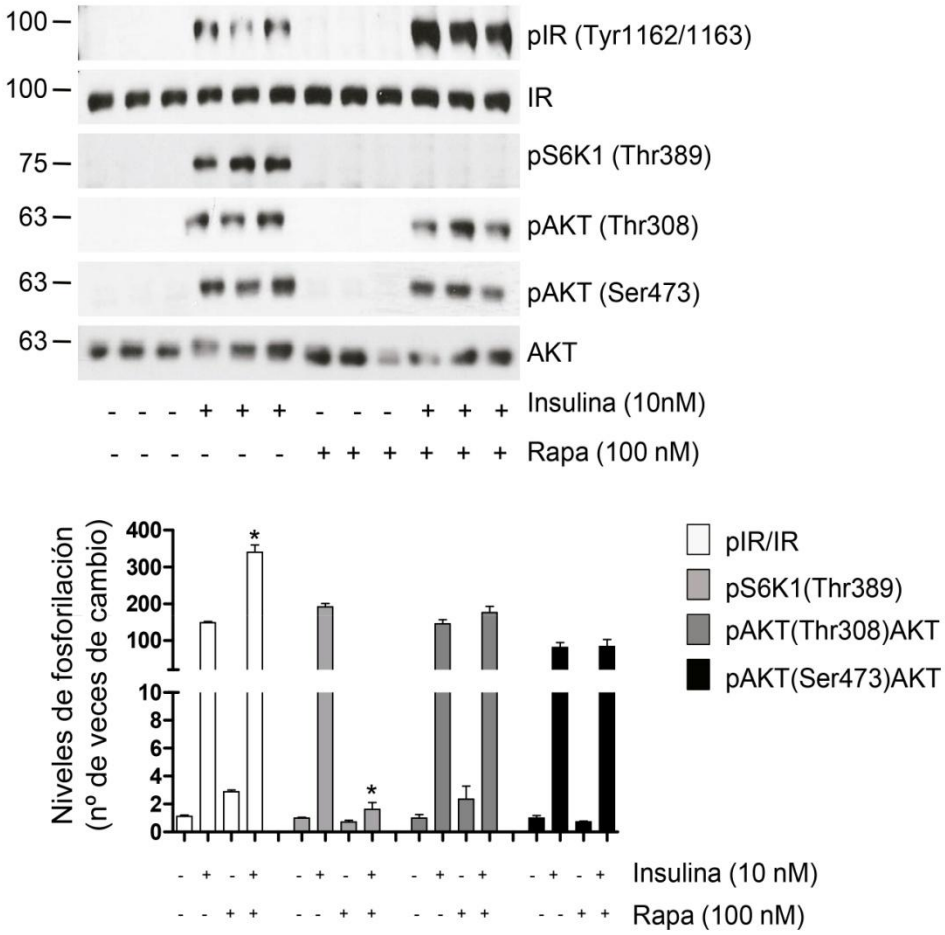

Figura 16. Tratamiento con rapamicina durante 45 minutos disminuye la fosforilación de S6K1 pero no compromete la señalización de la insulina en los adipocitos marrones a nivel de IR y Akt. Los adipocitos marrones diferenciados (dia 6) se cultivaron en presencia de rapamicina (100 nM) durante 45 minutos. A continuación, las células se estimularon durante 10 minutos con insulina (10 nM). Las proteinas se analizaron mediante Western blot usando anticuerpos siguientes: anti-fosfo-IR (Tyr 1162/1163), anti-IR, anti-fosfo-S6K1 (Thr 389), anti-fosfo-Akt (Ser 473), anti-fosfo-Akt (Thr 308) y anti-Akt. Los resultados de 3 experimentos independientes se cuantificaron densitomentrando las bandas obtenidas. Los resultados mostrados son las medias ± SEM. $^{*}p < 0.05$ respecto a las células estimuladas con insulina sin pretratamiento con rapamicina.

2. Efecto de la rapamicina sobre la captación de glucosa y la translocación del GLUT4 mediadas por la insulina en los adipocitos marrones.

Resultados previos habían demostrado que la insulina induce la captación de glucosa vía PI3K/Akt en cultivos primarios de adipocitos marrones fetales de rata (Hernández et al., 2001; Valverde et al., 1999b). Teniendo esto en cuenta, comprobamos el efecto de la rapamicina en la captación de glucosa en respuesta a la insulina en los adipocitos marrones. Las células fueron tratadas con rapamicina (100 nM) durante 16 horas tras las cuales se evaluó la captación de glucosa tras la estimulación durante 10 minutos con insulina (10 nM). Tal como se muestra en la Figura 17, se obtuvo un incremento de 2.5 veces en la captación de glucosa en las células estimuladas con insulina comparándolas con las no tratadas. Sin embargo, en adipocitos marrones que fueron pretratados con rapamicina durante 16 horas la captación de glucosa en respuesta a la insulina disminuyó de manera significativa con respecto a la de los adipocitos marrones que no habían recibido el pretratamiento con rapamicina.

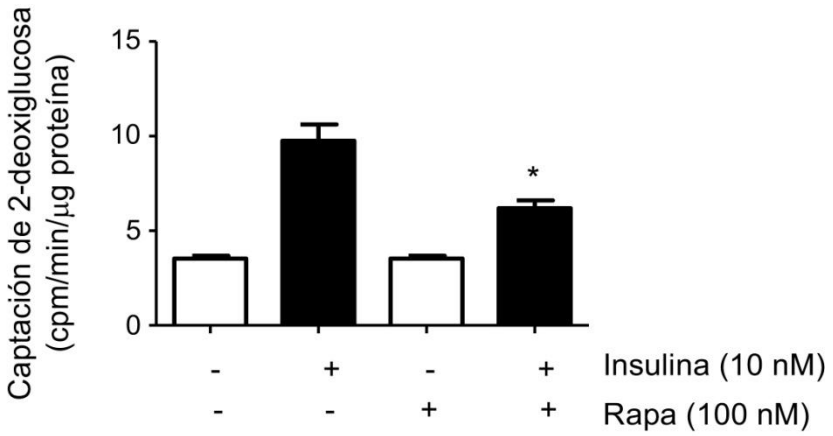

Figura 17. El tratamiento con rapamicina disminuye la captación de glucosa en respuesta a la insulina en los adipocitos marrones. La captación de 2-deoxy-D[1-^{3}H] fue medida tras la estimulación de los adipocitos marrones diferenciados con y sin pretratamiento con rapamicina (100 nM) durante 16 horas y posteriormente estimulados con insulina (10 nM) durante 10 minutos. Los resultados son la media de 4 experimentos independientes realizados por duplicado. *$p < 0.05$ respecto a células que no recibieron el pretratamiento con rapamicina.

En los adipocitos marrones pretratados con rapamicina se observó un descenso de la translocación del GLUT4 a la membrana plasmática, tal como se muestra en la Figura 18, hecho que no ocurría en las células que no habían recibido dicho pretratamiento. Dicha traslocación del GLUT4 a la membrana plasmática se analizó mediante Western blot (panel A) e inmunofluorescencia (panel B).

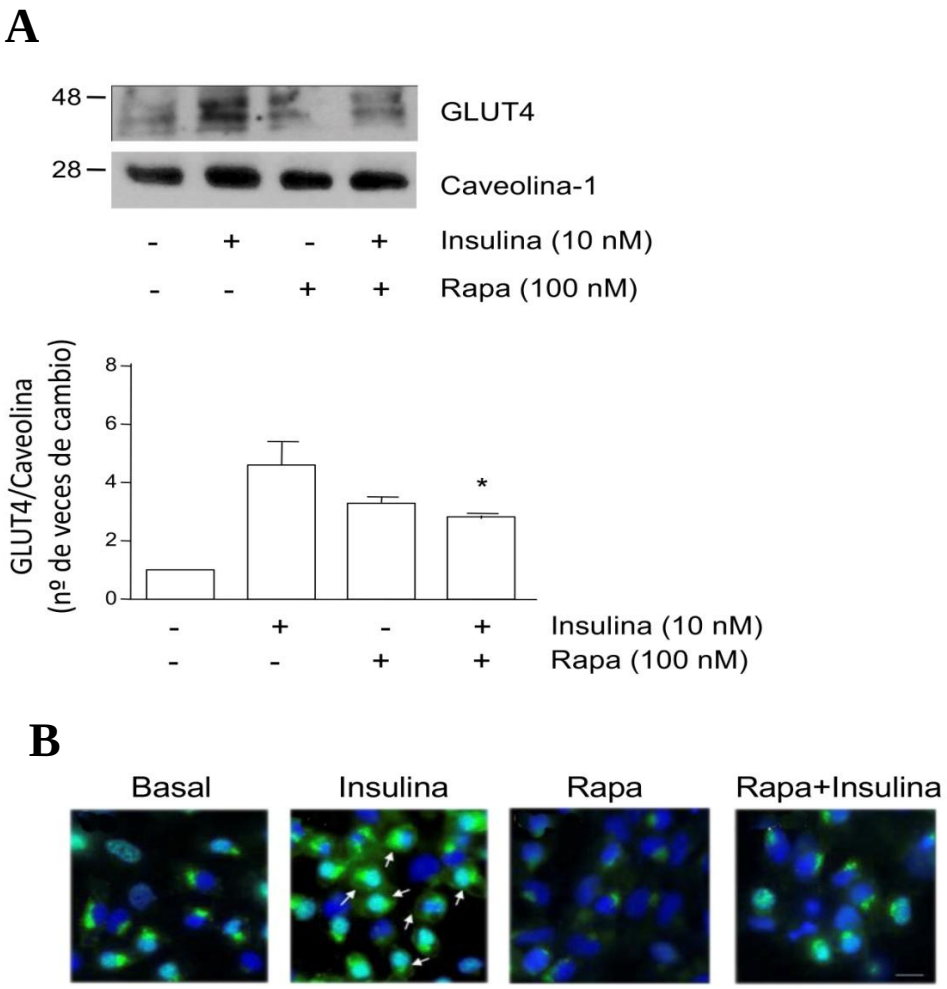

Figura 18. El pretratamiento con rapamicina disminuye la traslocación de GLUT4 a la membrana plasmática en respuesta a la insulina en los adipocitos marrones. A. Mediante Western blot se muestra la detección de GLUT4 en la membrana plasmática de los adipocitos marrones. Como control de carga de proteínas específicas de la membrana plasmática se utilizó caveolina-1. La gráfica representan la cuantificación de la translocación de GLUT4 a la membrana plasmática de los adipocitos marrones. Los resultados son la media ± SEM de 3 experimentos independientes. *$p < 0.05$ respecto a las células que no recibieron pretratamiento con rapamicina. **B**. Imágenes representativas del análisis de la traslocación del GLUT4 mediante inmunofluorescencia como señalan las puntas de flecha (escala 10 µm). Las imágenes son representativas de 5 experimentos independientes.

3. La rapamicina induce la fosforilación de JNK e IRS1 (Ser 307) en los adipocitos marrones.

La activación de la quinasa de estrés JNK inhibe la señalización de la insulina en tejidos periféricos debido a su capacidad de fosforilar al IRS1 en el residuo Ser 307, impidiendo la unión del IRS1 a la subunidad reguladora de la PI3K p85α y promoviendo la degradación del IRS1 mediante el sistema del proteasoma (Tanti y Jager, 2009; Pederson et al., 2001). Como en los experimentos anteriormente expuestos se observó que un pretratamiento con rapamicina durante 16 horas disminuía los niveles de la proteína IRS1, quisimos analizar la fosforilación de JNK (como un indicativo de su activación) en los adipocitos marrones diferenciados tratados con rapamicina (100 nM) durante varios periodos de tiempo.

Tal como se muestra en la Figura 19, el tratamiento de los adipocitos marrones con rapamicina inducía una rápida fosforilación de JNK con respecto a las células sin tratar, alcanzando el efecto máximo a los 30 minutos de estimulación. Además, los niveles de JNK total se mantuvieron estables durante el tratamiento (panel A). De igual manera, analizamos la fosforilación de p-38 MAPK, que no fue modulada por el tratamiento con rapamicina (resultados no mostrados).

Seguidamente quisimos analizar si la fosforilación de JNK mediada por la rapamicina provocaba la fosforilación del IRS1 en Ser 307. El análisis mediante Western blot reveló que los adipocitos marrones diferenciados tratados durante tiempos cortos con rapamicina presentaban una fosforilación del IRS1 en Ser 307, no variando los niveles de IRS1 totales (Figura 19, panel A). Para excluir que dicha fosforilación pudiera ser llevada a cabo por la S6K1 (Um et al., 2004) analizamos su fosforilación encontrando, tal como cabía esperar, que la rapamicina inhibía la fosforilación de S6K1 a partir de 15 minutos de tratamiento (Figura 19, panel B).

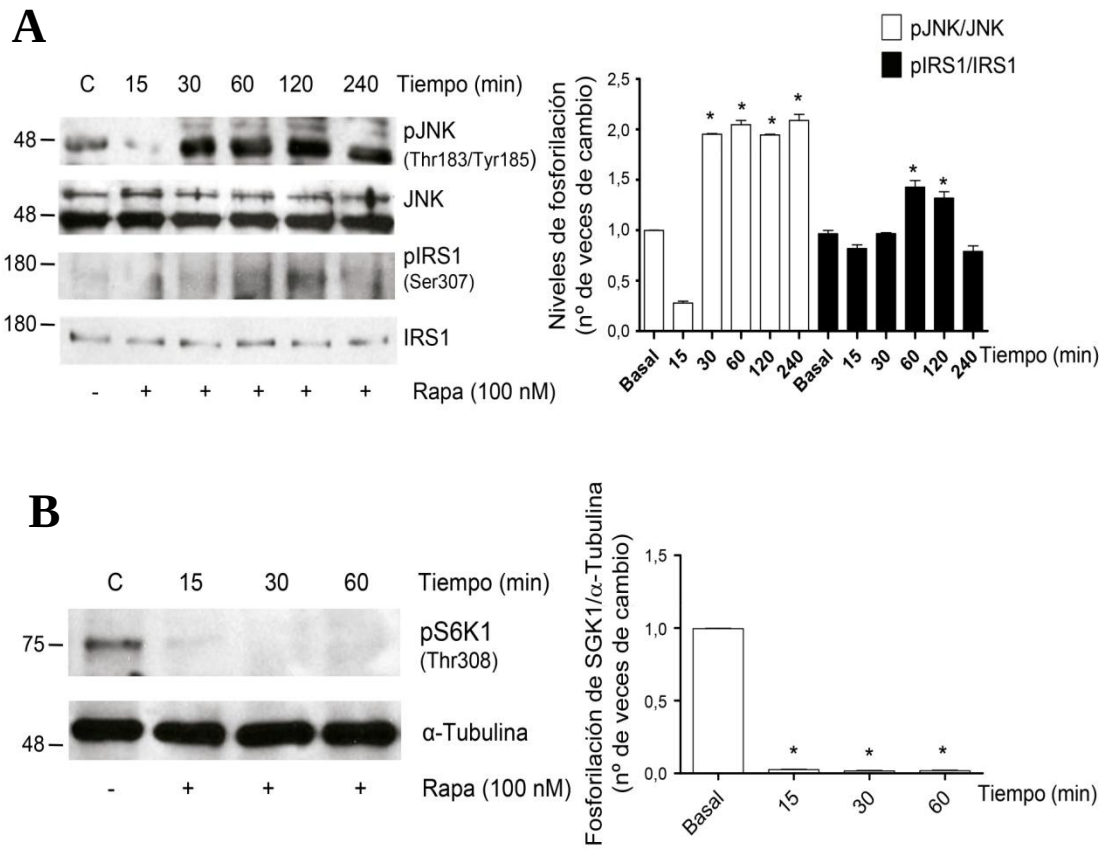

Figura 19. La rapamicina induce la activación de JNK y la fosforilación del IRS-1 (Ser 307) en los adipocitos marrones. Los adipocitos marrones diferenciados se estimularon con rapamicina a la concentración de 100 nM durante diferentes peridos de tiempo. Los extractos de proteína se analizaron mediante Western blot usando los anticuerpos anti-fosfo IRS-1 (Ser 307), anti-fosfo-JNK (Thr 183/ Tyr 185) y anti-fosfo-S6K1 (Thr 389), tomando como control de carga las proteínas totales. Se muestra un experimento representativo. Los resultados de densitometrar 3 experimentos independientes se muestran en las gráficas correspondientes. Los niveles de fosforilación están referidos a condiciones basales sin estimulacion. *$p < 0.05$

4. El tratamiento con rapamicina interfiere con la señalización de la insulina en cultivo primario de adipocitos marrones y en el BAT de rata.

Para confirmar que el efecto de la rapamicina sobre los adipocitos marrones diferenciados no era debido al protocolo de inmortalización, se plantearon experimentos con cultivos primarios de adipocitos marrones extraídos del BAT interescapular de ratas lactantes de 20 días de vida. Estos adipocitos marrones se diferencian espontáneamente a los 8 días de la siembra tal como se indica en Materiales y Métodos.

El pretratamiento de los adipocitos marrones primarios durante 16 horas con rapamicina a la concentración de 100 nM impidió la fosforilación de Akt en los residuos Ser 473 y Thr 308 mediada por insulina (10 nM) (Figura 20).

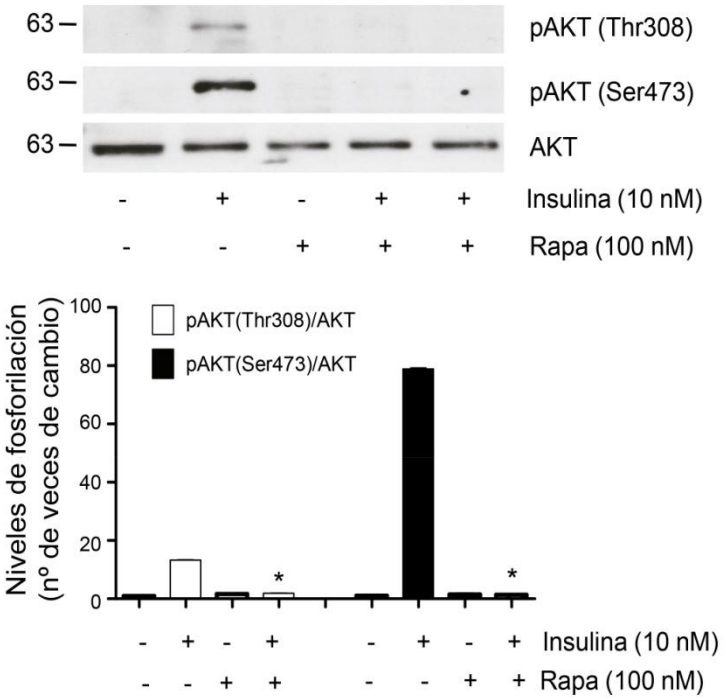

Figura 20. El tratamiento con rapamicina bloquea la fosforilación de Akt mediada por insulina en cultivo primario de adipocitos marrones de ratas lactantes. Se realizaron cultivos primarios de preadipocitos marrones de ratas lactantes tal como se describe en Materiales y Métodos. Una vez sembradas las células, éstas se dejaron diferenciar espontáneamente y seguidamente fueron tratadas con rapamicina a la concentración de 100 nM durante 16 horas y posteriormente estimuladas con insulina (10 nM) durante 10 minutos. Se analizaron las proteinas mediante Western blot con los anticuerpos anti-fosfo-Akt (Ser 473), anti-fosfo-Akt /Thr 308) y anti-Akt. Los resultados corresponden a la media ± SEM de tres experimentos independientes realizados por duplicado. *p < 0.05 respecto a celulas que no recibieron el pretratamiento con rapamicina.

Además, comprobamos que el pretratamiento con rapamicina inducía la fosforilación de JNK y del IRS en Ser 307, lo que excluía de nuevo la vinculación entre el protocolo de inmortalización de los adipocitos marrones y el efecto de la rapamicina (Figura 21).

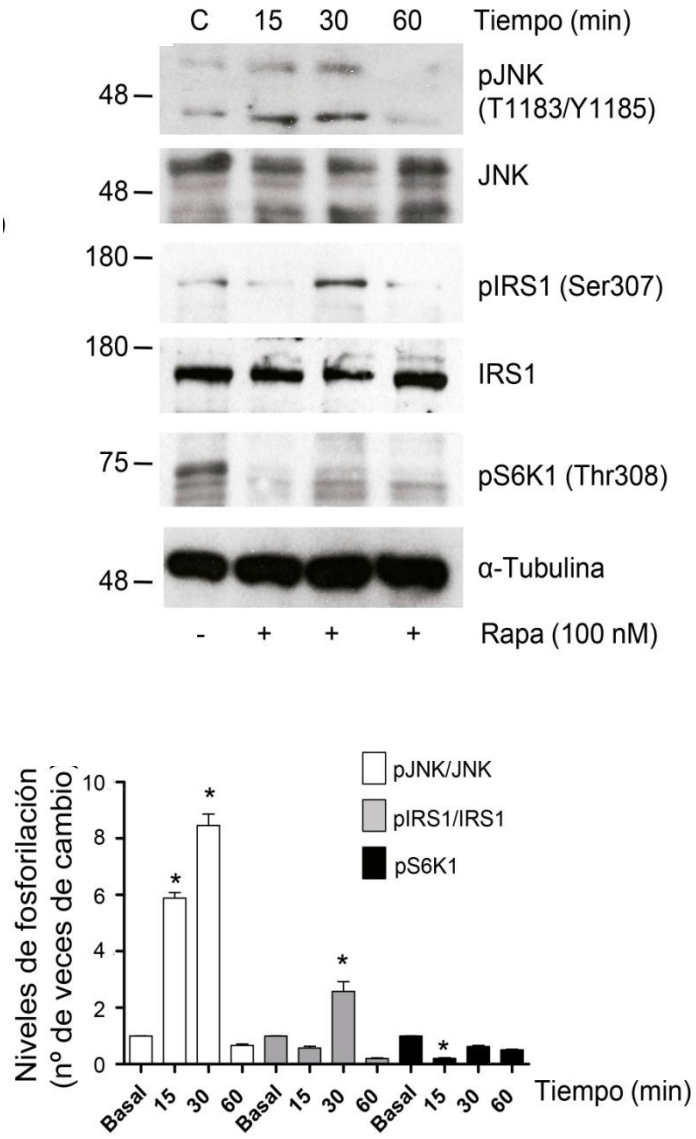

Figura 21. La rapamicina induce la fosforilación de JNK e IRS 1 (Ser 307) en cultivos primarios de adipocitos marrones de BAT de ratas lactantes. Una vez diferenciados, los adipocitos marrones primarios se trataron con rapamicina (100 nM) en los periodos de tiempo indicados. Se analizó mediante Western blot la fosforilación de JNK, IRS1 (Ser 307) y S6K1, referidos a las condiciones basales. Los resultados son la media ± SEM de 3 experimentos independientes. *p < 0.05 respecto a células sin tratamiento con rapamicina.

Recientemente se ha publicado que el tratamiento crónico de ratas Wistar con rapamicina provoca alteraciones en el metabolismo de la glucosa a nivel sistémico, en la sensibilidad a la insulina y en la señalización de la insulina en hígado, músculo esquelético y WAT (Lopes et al., 2014b). Para dilucidar el efecto de la rapamicina en el BAT in vivo se analizó la señalización de la insulina en ratas que habían recibido un tratamiento con rapamicina durante 3 semanas tal como se describe en Materiales y Métodos. La Figura 22 muestra que la fosforilación de Akt (en ambos residuos: Ser 473 y Thr 308) en respuesta a la insulina fue ampliamente atenuada en el BAT de ratas tratadas con rapamicina durante 3 semanas.

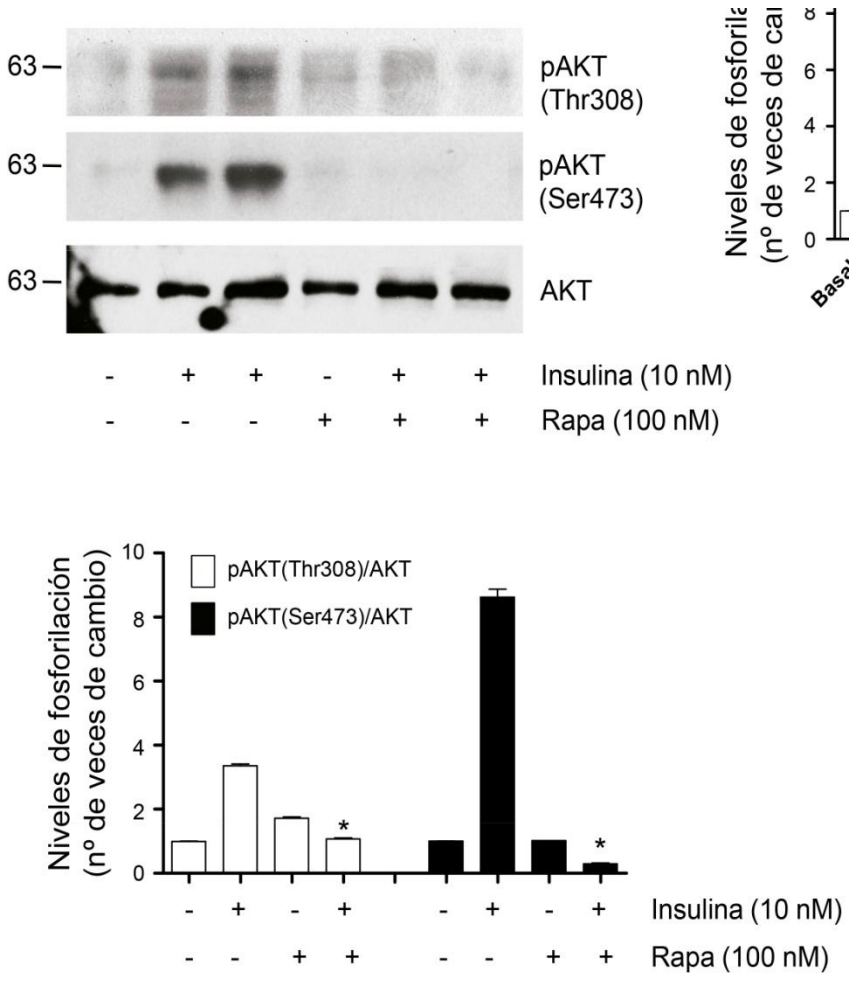

Figura 22: El tratamiento con rapamicina en ratas Wistar durante 3 semanas impidió la fosforilación de Akt mediada por la insulina. Ratas Wistar fueron tratadas con rapamicina y estimuladas con insulina como se describe en Materiales y Métodos. La fosforilación de Akt fue analizada en lisados de BAT mediante Western blot. Los niveles de fosforilacion se refieren a animales inyectados con el vehículo y estimulados con insulina. *$p < 0.05$ (n= 6 animales/ grupo).

5. La inhibicion de la JNK mejora el efecto de la rapamicina en la señalización de la insulina en los adipocitos marrones.

Teniendo en cuenta las premisas anteriores de que el pretratamiento con rapamicina fosforila la JNK y, en consecuencia, se ve afectada de manera negativa la señalizacion de la insulina en los adipocitos marrones, comprobamos si dicha inhibición de la casacada de señalización se debía a la activación temprana de JNK y la consiguiente fosforilación de IRS1 en Ser 307 que conlleva a su degradación (Pederson et al., 2001).

Para ello, tratamos a los adipocitos marrones con rapamicina en presencia o ausencia del inhibidor de JNK SP600125 durante 90 minutos, tiempo suficiente para detectar la fosforilación del IRS1 en el residuo Ser 307 (Figura 23) según los resultados mostrados en experimentos anteriores (Figura 19). La concentración de SP600125 en la que se observaba una inhibición de la fosforilación de JNK más eficiente fue 20 µM (Figura 24).

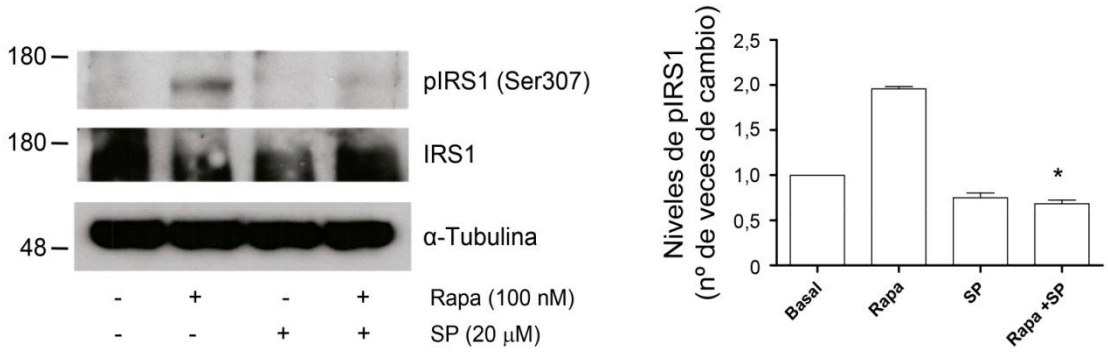

Figura 23. La inhibición de JNK mediante SP600125 impide la fosforilacion de IRS1 en Ser 307 inducida por rapamicina. Los adipocitos marrones diferenciados se trataron con rapamicina (100 nM) durante 90 minutos en ausencia ó presencia del inhibidor de JNK, SP600125, usado a 20 µM. Se analizó la fosforilación de IRS1 (Ser 307) mediante Western blot. La gráfica corresponde a la cuantificación de los resultados obtenidos en 3 experimentos independientes. *$p < 0.05$ con respecto a células sin tratar con SP600125.

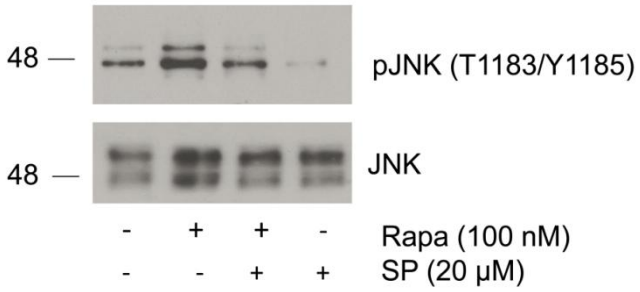

Figura 24. Efecto del inhibidor de JNK SP600125 sobre la fosforilación de JNK inducida por rapamicina. Los adipocitos marrones diferenciados fueron tratados durante 90 minutos con rapamicina 100 nM en presencia o ausencia del inhibidor de JNK SP600125 a la concentración de 20 µM. Se analizó la fosforilación de JNK (Thr 183/ Tyr 185) mediante Western blot, usándose los niveles totales de JNK total como control de carga. Se muestra un experimento representativo que fue corroborado por otros dos experimentos independientes en los que se obtuvo el mismo resultado.

A continuación analizamos los niveles totales del IRS1 tras el cotratamiento con rapamicina y SP600125 durante 16 horas. Tal como se muestra en la Figura 25, dicho cotratamiento preserva los niveles de la proteina IRS1

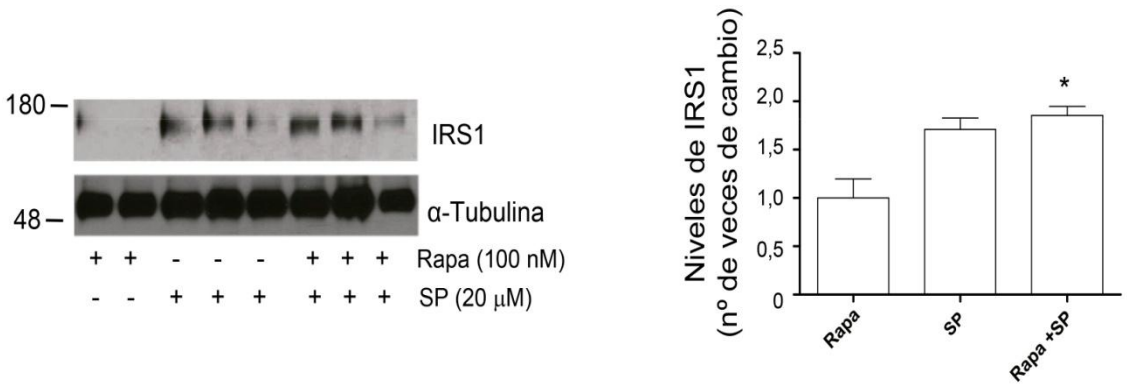

Figura 25. El cotratamiento con rapamicina y SP600125 preserva los niveles totales del IRS1 en los adipocitos marrones. Los adicpocitos marrones diferenciados se trataron con rapamicina (100 nM) durante 16 horas en presencia ó ausencia del inhibidor de JNK, SP600125, usado a 20 µM. La expresión del IRS1 se analizó mediante Western blot. Los resultados de 3 experimentos independientes se cuantificaron densitomentrando las bandas obtenidas. Los resultados mostrados son las medias ± SEM. Los niveles de IRS1 se refieren a los obtenidos con el tratamiento con rapamicina en ausencia de inhibidor (Rapa). *$p < 0.05$.

A continuación analizamos el efecto del cotratamiento de rapamicina y SP600125 durante 16 h sobre la señalización de la insulina y encontramos una mejora en el efecto de la insulina sobre la fosforilación de Akt tanto en el residuo Ser 473 como en el Thr 308 comparado con los adipocitos marrones tratados exclusivamente con rapamicina (Figura 26).

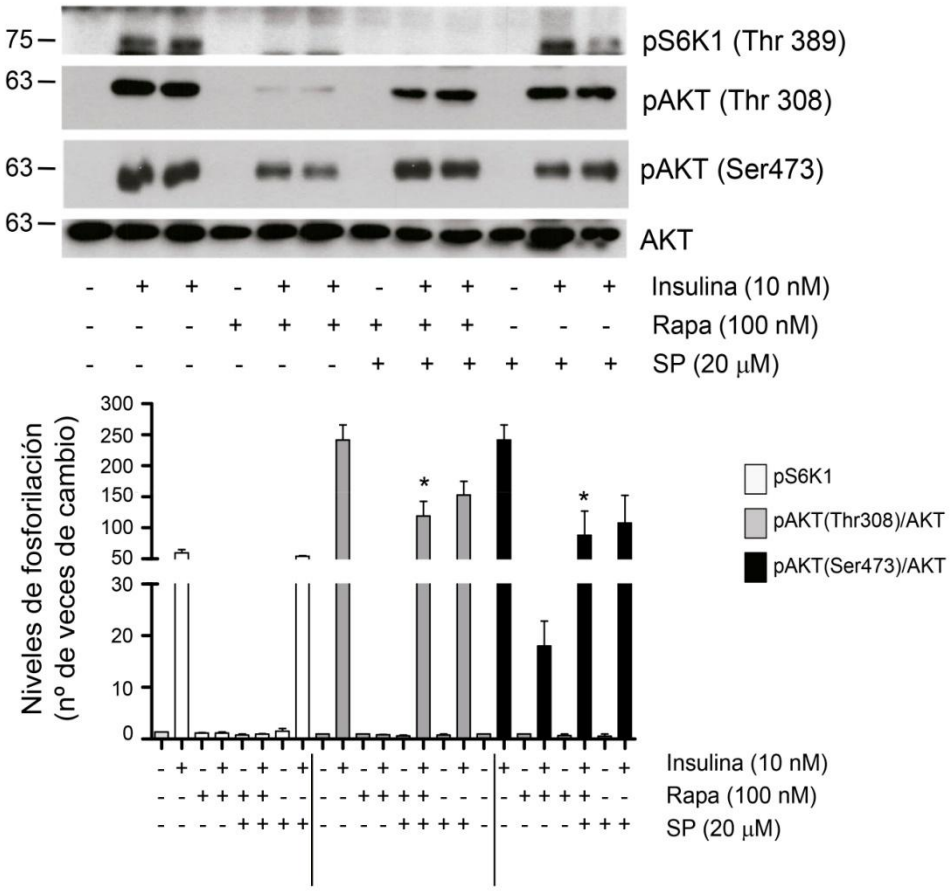

Figura 26. La inhibición de JNK con SP600125 mejora la sensibilidad a la insulina en los adipocitos marrones tratados con rapamicina. Tras 16 horas de tratamiento con rapamicina (100 nM) en presencia o ausencia de SP600125 (20 μM), los adipocitos marrones se estimularon con insulina (10 nM) durante 10 minutos. Los lisados celulares se analizaron mediante Western blot utilizando anticuerpos frente a fosfo-Akt (Ser 473), fosfo-Akt (Thr 308), Akt y fosfo-S6K1 (Thr 389). El resultado de 3 experimentos independientes se cuantificó mediante densitometría, mostrandose la media ± SEM de 3 experimentos independientes. *p< 0.05 respecto a células estimuladas con insulina y pretratadas con rapamicina en ausencia de SP600125 .

6. Efecto del tratamiento con rapamicina sobre la lipolisis y la expresión de *Ucp-1* inducidas por NE o por el agonista β3 adrenérgico CL316243.

El efecto de rapamicina sobre la estimulacion que provocan la NE y el agonista β3 CL316243 en la lipolisis en los adipocitos marrones fue evaluado ya que constituye un indicio temprano de la activación de la termogénesis.

Los adipocitos marrones diferenciados se estimularon con NE (5 µM) o CL316243 (2 µM) durante 4 horas. Para comprobar que estas células son sensibles a ambos estímulos por el aumento de la señalización β-adrenérgica analizamos la fosforilación de la HSL y la consiguiente liberación de glicerol al medio de cultivo celular. Tal como se muestra en la Figura 27, en las células pretratadas durante 16 horas con rapamicina se observó un descenso significativo del efecto de la NE y del CL316243 en la fosforilación de la HSL en el residuo Ser 660. Tal como cabía esperar, el pretratamiento con rapamicina disminuyó la lipolísis de los adipocitos marrones en respuesta a NE o CL316243.

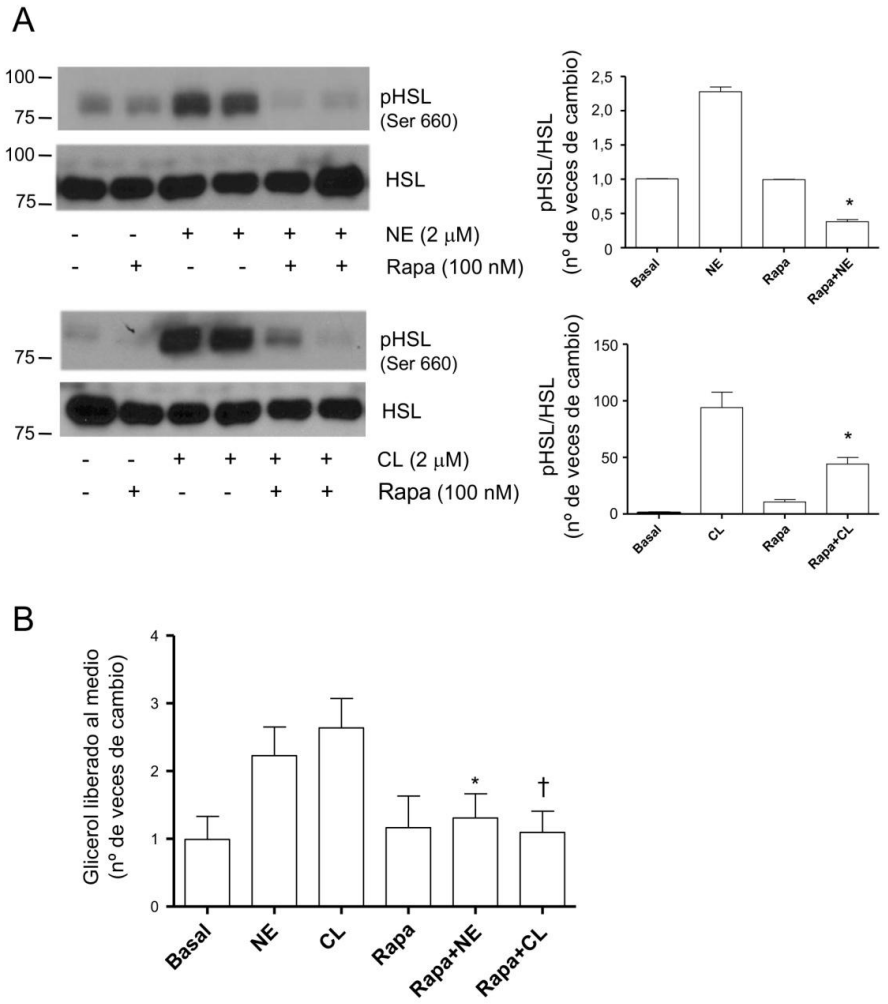

Figura 27. El tratamiento con rapamicina disminuye la lipolisis mediada por NE o CL316243 en los adipocitos marrones. A) Los adipocitos marrones se trataron con rapamicina (100 nM) durante 16 horas (o permanecieron sin tratar en el grupo control) y durante las ultimas 4 horas se simultaneó el tratamiento con NE a la concentración de 5 μM o con el agonista β3 CL316243 a la concentración de 2 μM. Analizamos la fosforilacion de HSL (Ser 660) mediante Western blot. Los resultados de 3 experimentos independientes se cuantificaron mostrando la media ± SEM. *p < 0.05 respecto a la estimulación con NE ó CL316243 en ausencia de rapamicina**. B)** En paralelo, medimos la liberación de glicerol al medio de cultivo como se detalla en Materiales y Métodos. Los resultados se expresan en referencia a la estimulación con NE o CL316243, donde *┼p <0.05 (n=3 experimentos independientes realizados por triplicado).

Estudios previos del laboratorio describieron que la combinación de NE y T_3 induce un aumento de los niveles del ARNm de *Ucp1* en cultivos primarios de adipocitos marrones de rata (Hernandez y Obregón, 2000). Teniendo esto en cuenta valoramos el efecto de la rapamicina sobre la expresión de genes termogénicos como son *Ucp1* y *Pgc1a* analizando sus niveles de ARNm.

Las células fueron tratadas con rapamicina durante 16 horas y durante las últimas 8 horas en presencia de NE a la concentración de 5 µM y de T_3 a la concentración de 1 nM. La rapamicina disminuyó drásticamente los niveles de ARNm de *Ucp1* y *Pgc1a*, que en ausencia de rapamicina aumentan 100 y 3.5 veces, respectivamente, con respecto a las células control sin estimulación (Figura 28).

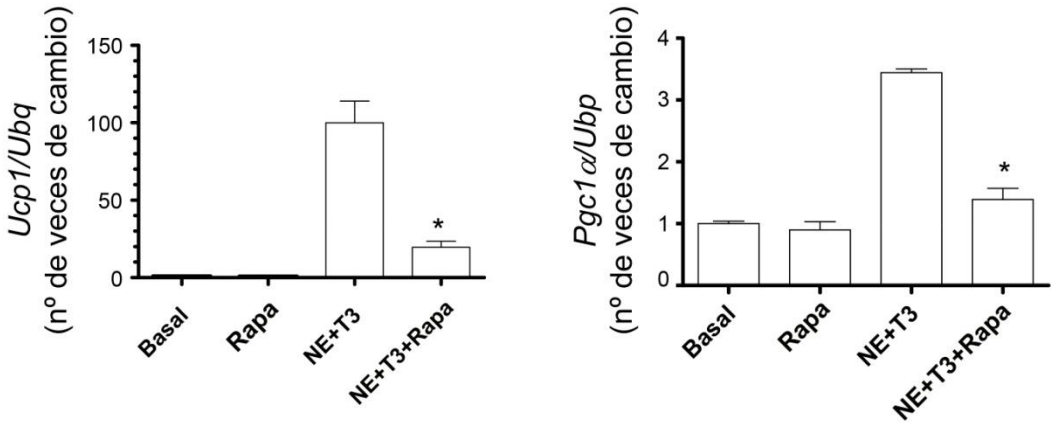

Figura 28. La rapamicina inhibe los niveles de ARNm de *Ucp1* y *Pgc1a* inducidos por la combinación de NE y T_3. Los adipocitos marrones diferenciados de rata se trataron con rapamicina (100 nM) durante 16 horas o permanecieron sin tratamiento, y durante las últimas 8 horas se trataron con la combinación de NE (5 µM) y T_3 (1nM). Los niveles de ARNm de *Ucp1* y *Pgc1α* se analizaron mediante RT-PCR. Los resultados muestran el número de veces que se incrementa la expresión de ambos ARNm en referencia a la combinación NE+T_3 en ausencia de rapamicina. *$p < 0.05$ (n= 3 experimentos independientes realizados por triplicado).

Debido a las dificultades para detectar la proteína UCP1 en los adipocitos marrones de rata estimulados con NE (Hernandez et al, 2011), analizamos el nivel de UCP1 en una linea de adipocitos marrones inmortalizados de ratón previamente generada en el laboratorio, tal y como se ha descrito en Materiales y Métodos, ya que los adipocitos de ratón muestran una mayor sensibilidad que los de rata. Tal como se muestra en la Figura 29, la expresión de la proteína UCP1 se elevaba con la estimulación de NE pero disminuía drasticamente tras el cotratamiento de los adipocitos marrones con rapamicina y NE.

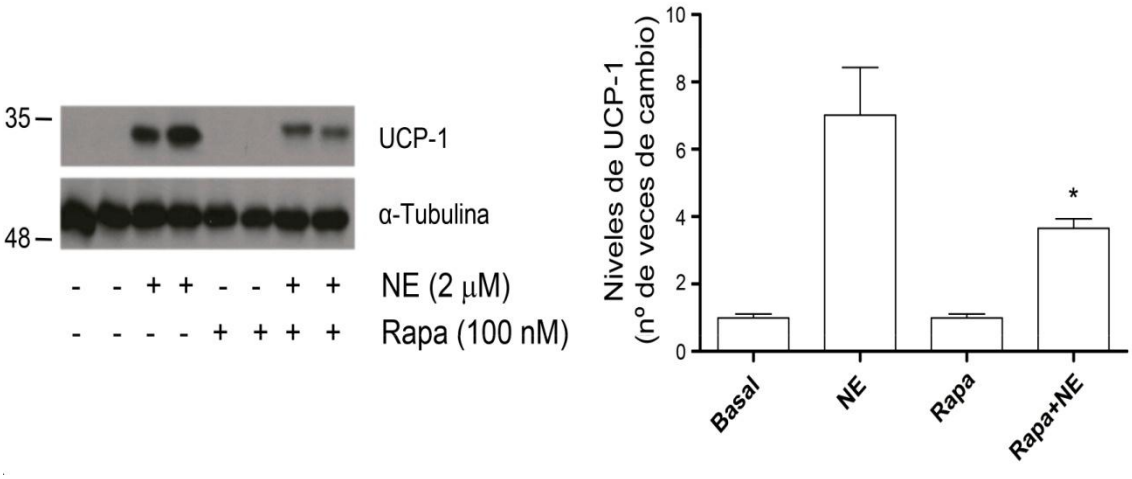

Figura 29. El tratamiento de los adipocitos marrones con rapamicina es capaz de revertir el efecto de la NE en la expresión de la proteína UCP1 en adipocitos marrones de ratón. Analizamos los niveles de la proteína UCP1 en adipocitos marrones de ratón diferenciados tratados con rapamicina (100 nM) durante 16 horas y estimulados con NE (5 μM) durante las ultimas 8 horas de tratamiento. Analizamos los niveles de α-Tubulina como control de carga. Los resultados mostrados son la media ± SEM de 3 experimentos independientes. *$p < 0.05$ respecto a las células estimuladas con NE sin recibir el pretratamiento con rapamicina (NE).

7. La rapamicina disminuye la respiración mitocondrial en los adipocitos marrones.

Para entender mejor cómo afectaba la rapamicina a la actividad mitocondrial en los adipocitos marrones procedimos a medir su perfil respiratorio usando el analizador de flujo extracelular XF24 (Seahorse Biosciences). Los adipocitos marrones se trataron con rapamicina a la concentración de 100 nM durante 16 horas tras las cuales se realizo la medición tal como se detalla en Materiales y Métodos. Como se observa en la Figura 30, el tratamiento con rapamicina disminuyó la respiración basal, el flujo de protones y la capacidad máxima de respiración de estas células.

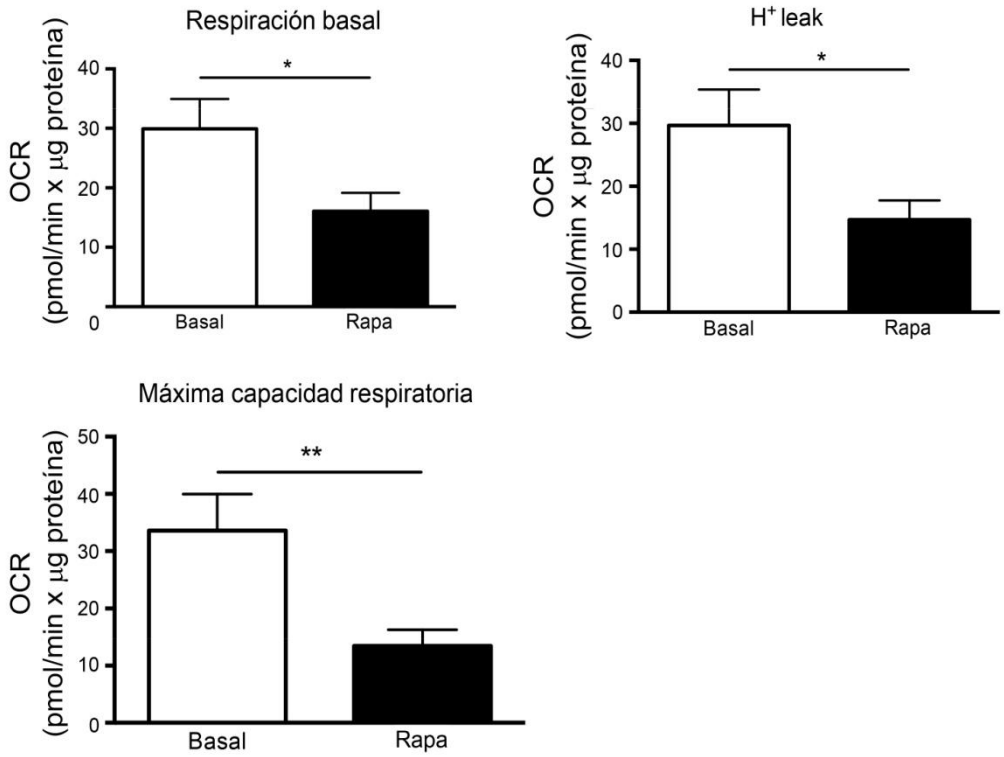

Figura 30. El tratamiento con rapamicina disminuye la respiracion basal, el flujo de protones y la tasa de respiración máxima en los adipocitos marrones. Mediante la tecnología Seahorse se cuantificaron estos tres parámetros, mostrando la media ± SEM. *p < 0.05 respecto a células tratadas con rapamicina (Rapa) (n= 9 valores de 3 experimentos independientes realizados por triplicado).

8. El tratamiento con rapamicina disminuye la actividad desiodasa D2 en adipocitos marrones estimulados con NE.

Estudios previos del laboratorio han demostrado que la T_3 es necesaria para una completa estimulación β-adrenérgica de los adipocitos marrones. En el BAT la T_3 es producida localmente por la enzima desiodasa D2, que es considerada un marcador de actividad termogénica del BAT (Martínez-de Mena y Obregón, 2005) . Teniendo esto en cuenta, estudiamos el efecto del tratamiento con rapamicina sobre la actividad D2. Los adipocitos marrones de rata se trataron con T_3 (1 nM) durante 24 horas, y la mitad de ellos con rapamicina (100 nM) durante 16 horas y se añadió NE durante las ultimas 8 h en la mitad de las muestras. Tras retirar el medio, se recogieron las celulas sobre nieve carbónica y se valoró la actividad D2 tal como se detalla en Materiales y Métodos, obteniendo como resultado que en los adipocitos marrones la rapamicina disminuye la actividad desiodasa D2 de forma significativa, cuando la D2 está estimulada adrenergicamente con NE (Figura 31), mientras que la actividad D2 basal (no estimulada con NE) no se ve afectada por la rapamicina (no se muestra). Este resultado es similar a lo encontrado en el ARNm de la *Ucp1* (Figura 29).

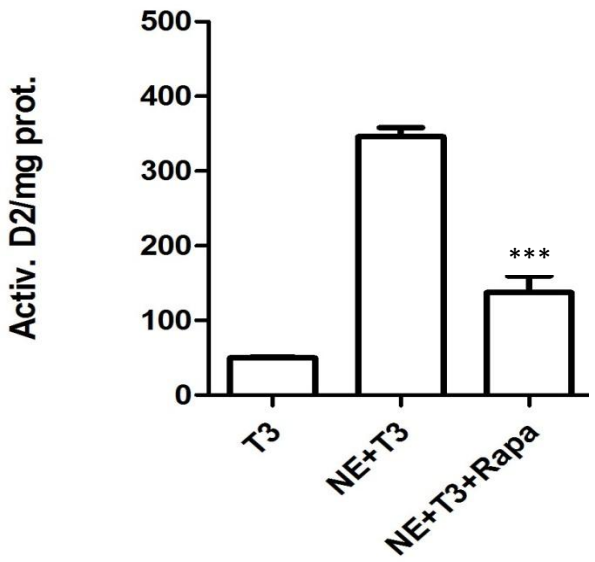

Figura 31. Efecto de la rapamicina sobre la actividad desiodasa D2 en los adipocitos marrones. La estimulación de la actividad D2 provocada por la estimulación con NE y T_3 disminuyó tras el tratamiento conjunto con NE, T_3 y Rapamicina. La actividad D2 basal no se afectó por la Rapamicina y T_3 (resultados no mostrados). Los datos están expresados en fentomoles de T_3 generados / h mU/ por mg de proteína. (n=3 / grupo). ***$p < 0.01$ respecto al tratamiento con NE+T_3.

Discusión

Nuestro país encabeza la lista europea de trasplantes anuales, con un total de 4.769 trasplantes en el año 2015. Por órganos, se realizaron 2.905 trasplantes renales, 1.162 hepáticos, 299 cardíacos, 294 pulmonares, 97 de páncreas y 12 intestinales, según datos de la Organización Nacional de Trasplantes (www.ont.es). El uso de inmunosupresores en pacientes trasplantados de órganos sólidos es imprescindible para garantizar que el nuevo órgano no sea rechazado por el receptor debido a la reacción del sistema inmune (Martín-Dávila et al., 2007). Los primeros inmunosupresores empleados en estos pacientes fueron los esteroides y la azatioprina, seguidos de los inhibidores de calcineurina (como ciclosporina A y tacrolimus) e inhibidores del complejo mTOR (como rapamicina, también conocida como sirolimus), pero pronto se comprobó que el uso de estos medicamentos provocaba, entre otros daños colaterales, alteraciones en el metabolismo lipídico y glucídico (Klintmalm y Nashan, 2014). De esta manera, entre las patologías secundarias derivadas del uso de los inmunosupresores se encuentra la diabetes post-trasplante (NODAT) debido a que los inmunosupresores como la rapamicina, modulan negativamente la señalización de la insulina en los tejidos periféricos relevantes como el músculo o el WAT (Deblon et al., 2012) debido a la inhibición del complejo mTORC1 (Magnusson et al., 2017), aunque un estudio reciente ha mostrado que en algunos modelos de ratones diabéticos el tratamiento con rapamicina podría mejorar la resistencia a insulina (Reifsnyder et al., 2016). También se han publicado estudios de administración conjunta de inhibidores de calcineurina y rapamicina, puesto que, como se ha indicado en la introducción, presentan diferente mecanismo de actuación y podrían ejercer efectos complementarios en referencia al metabolismo lipídico y glucídico para evitar la aparición de NODAT. Sin embargo, los resultados obtenidos con esta combinación no fueron beneficiosos ya que no se mejoró la supervivencia del injerto y, además, se acentuó la toxicidad renal (Bamgbola et al., 2016).

Estudios en adipocitos blancos maduros humanos procedentes de los depósitos subcutáneo y omental han demostrado que el tratamiento con rapamicina, tanto agudo como crónico, provoca un descenso de la captación de glucosa inducida por la insulina (Pereira et al., 2012). Otros estudios muy recientes muestran que ante la pérdida de funcionalidad del complejo mTORC1 en ratones con modificaciones génicas en Raptor, el BAT es incapaz de adaptarse al frio (Labbe et al., 2016) y se reduce su volumen así como su contenido lipídico (Lee et al., 2016), aunque parece que este efecto no es

tejido-específico, siendo necesarias nuevas evidencias experimentales para dilucidar el efecto de mTORC1 en el funcionamiento del BAT. Teniendo en cuenta estos estudios previos y debido a la falta de investigaciones sobre el efecto del inmunosupresor rapamicina en la señalización de la insulina y en la función termogénica del BAT, decidimos abordar este reto utilizando adipocitos marrones en cultivo.

El análisis de los efectos de la rapamicina sobre la ruta de señalización de la insulina en adipocitos marrones requería de un modelo in vitro que facilitara la experimentación a nivel mecanístico. Para ello, generamos líneas celulares inmortalizadas a partir del BAT interescapular de ratas y ratones de 20 días de vida, siendo esta edad una novedad en la generación de líneas celulares puesto que otros grupos de investigación las habían obtenido a partir de fetos o de animales recién nacidos (Lorenzo et al., 1996; Valverde et al., 1999a; Klein et al., 2002; Miranda et al., 2010). El uso de BAT de fetos o neonatos para generar líneas celulares inmortalizadas implica que, aunque el número de preadipocitos o de células precursoras es muy elevado, los adipocitos maduros no están cargados con suficientes lípidos de manera que en el proceso de aislamiento no flotan y no se puede alcanzar una correcta separación de adipocitos maduros y de precursores. Al generar líneas celulares a partir de BAT de animales lactantes, los adipocitos maduros presentan un elevado contenido lipídico de manera que flotan resultando muy fácil separarlos de los preadipocitos. Así, la población de preadipocitos obtenidos es más homogénea y presenta una mayor pureza, lo que permite que dichas células sean recogidas y sembradas fácilmente para comenzar con el protocolo de inmortalización para el establecimiento de la línea celular.

Una vez establecidas las líneas celulares de preadipocitos marrones procedentes de ratas lactantes, procedimos a su diferenciación a adipocitos marrones maduros. Para ello, seguimos el mismo protocolo experimental que el descrito previamente para inmortalizar los adipocitos marrones de ratones neonatos (Miranda et al., 2010).

Una vez diferenciados los preadipocitos marrones comprobamos que el protocolo de aislamiento, cultivo, inmortalización y diferenciación celular se había realizado de manera correcta mediante el análisis de los niveles de proteínas relevantes que se expresan en el BAT como son UCP1, marcadora de la función termogénica; FAS, marcadora de la diferenciación adipogénica; GLUT4 e IR, marcadores de sensibilidad a la insulina, y comprobamos que todos ellos se expresaron de modo gradual según

avanzaban los días de diferenciación. Además, analizamos los niveles del IGF-IR ya que se expresa altamente en los preadipocitos y fibroblastos y comprobamos que disminuían a medida que los preadipocitos se diferenciaban a adipocitos marrones maduros. Por tanto, los resultados de este análisis nos permitieron concluir que las líneas celulares inmortalizadas de preadipocitos marrones de rata lactante diferencian en condiciones experimentales similares a las de los preadipocitos marrones procedentes de ratones neonatos, adquiriendo un fenotipo de adipocitos marrones maduros que también caracterizamos por la presencia de numerosas gotas de grasa en el citosol.

Los resultados de este trabajo han demostrado por primera vez que los adipocitos marrones son sensibles a la acción de la rapamicina, ya que éste inmunosupresor afecta tanto a la señalización de la insulina como a la expresión de genes termogénicos inducida por NE. Estos resultados sugieren que la resistencia a insulina en adipocitos marrones puede jugar un papel importante en el desarrollo del NODAT. De hecho, estudios previos en ratones modificados genéticamente deficientes en el IR exclusivamente en adipocitos marrones (ratones BATIRKO) revelaron la importancia de mantener funcional la señalización de la insulina en el BAT para el control de la homeostasis glucídica del organismo, así como para controlar el balance energético. Estos ratones desarrollan intolerancia a la glucosa debido a un fallo en la secreción de insulina (Guerra et al., 2001) y aumentan de manera significativa su adiposidad visceral cuando son sometidos a una dieta rica en grasa (Gómez-Hernández et al., 2012). También es importante destacar que las alteraciones de la adiposidad y de la homeostasis glucídica en los ratones BATIRKO obesos eran debidas a un estado de inflamación crónica de bajo grado originado por un aumento de citoquinas y factores proinflamatorios como el TNFα, radicales libres de oxígeno e infiltración de macrófagos que a su vez dificulta la correcta señalización de la insulina y que se ha relacionado directamente con daños vasculares, obesidad y riesgos cardiovasculares (Gómez-Hernández et al., 2012; Apovian et al., 2008). Otra alteración a destacar en el ratón BATIRKO es el descenso de los niveles del factor de transcripción C/EBP-α (no así PPARγ), lo que indica la importancia de la señalización de la insulina para el correcto desarrollo de la adipogénesis en el BAT (Guerra et al., 2001).

La primera evidencia experimental que encontramos sobre el impacto negativo de la rapamicina sobre la señalización de la insulina en los adipocitos marrones fue el descenso en la expresión de la proteína IRS1 tras un tratamiento de 16 h con

rapamicina. Cabe destacar que las proteínas IRS son reguladores críticos de las rutas de señalización que permiten la diferenciación de los adipocitos marrones ya que resultados previos de nuestro laboratorio y otros indicaron que la deleción genética de *Irs1* en ratones suprime la fosforilación de Akt inducida por insulina en preadipocitos marrones, impidiendo así la diferenciación adipogénica y una adecuada respuesta termogénica (Valverde et al., 1999a; Valverde et al., 2003a; Tseng et al., 2004; Fasshauer et al., 2001)

El análisis de la señalización de la insulina tras un pretratamiento de 16 h con rapamicina reveló un descenso en la fosforilación de Akt, tanto en el residuo Ser 473 como en la Thr 308. Como consecuencia de este pretratamiento con rapamicina, se detectó una disminución de la translocación de GLUT4 a la membrana plasmática y un descenso en la captación de glucosa en los adipocitos marrones en respuesta a la insulina. Estos resultados no nos sorprendieron puesto que se ha demostrado que ambas son dependientes de la fosforilación de Akt inducida por la insulina (Huang y Czech, 2007). Estos resultados concuerdan con resultados previos observados in vivo en ratones o ex vivo en el WAT humano donde el pretratamiento con rapamicina disminuyó la translocación de GLUT4 a la membrana plasmática y la captación de glucosa inducidas por la insulina (Lopes et al., 2013; Pereira et al., 2012). Sin embargo, otros inmunosupresores como ciclosporina A (CsA) o FK506, no impiden la fosforilación de Akt pero aumentan la velocidad de endocitosis del GLUT4 (Fuhrmann et al., 2014). Resultados preliminares de nuestro laboratorio con adipocitos marrones tratados con éstos inmunosupresores han revelado que también son capaces de disminuir los niveles del IRS1, así como de impedir la fosforilación de Akt en respuesta a la insulina (resultados no mostrados).

Nuestros resultados también han demostrado una modulación diferencial de las proteínas IRS por el tratamiento con rapamicina ya que a diferencia de lo que ocurre con el IRS1, en los adipocitos marrones la expresión del IRS2 no se modifica tras el tratamiento con rapamicina durante 16 h. Esta especificidad en la modulación de las proteínas IRS por la rapamicina también se ha descrito por otros autores puesto que en adipocitos humanos de localización subcutánea disminuye la expresión de IRS2 (Pereira et al., 2012). Por tanto, nuestros datos apuntan a una especificidad celular de la rapamicina desencadenando la degradación del IRS1 en los adipocitos marrones o del IRS2 en los adipocitos blancos por la vía del proteasoma. Estos resultados refuerzan el

concepto que existe en el campo de la señalización de la insulina de la especificidad de las proteínas IRS1/2 para transducir la señalización celular iniciada por la activación del IR de manera diferencial en distintos tipos celulares, y podría ser de utilidad terapéutica para el tratamiento la resistencia a la insulina en patologías como NODAT.

A continuación, nos propusimos profundizar en los aspectos mecanísticos subyacentes al tratamiento con rapamicina que conlleva la disminución de los niveles del IRS1 en los adipocitos marrones. Para ello, analizamos la señalización celular desencadenada por la rapamicina a tiempos más cortos, es decir, tiempos anteriores a la visualización de la degradación del IRS1. Es ampliamente conocido que la fosforilación del IRS1 en el residuo Ser 307 regula negativamente la transducción de la señal de la insulina ya que inhibe la activación de la PI3K a través de la disrupción de la interacción entre el IRS1 y la subunidad reguladora de la PI3K p85α (Copps y White, 2012) y además dirige al IRS1 para su degradación en el sistema del proteosoma (Tanti y Jager, 2009). La fosforilación del IRS1 en el residuo Ser 307 puede inducirse por estrés celular, por la propia insulina (para frenar la señalización impidiendo de esta manera la activación sostenida del IR), por citoquinas proinflamatorias como el TNFα, lípidos y también por activación del complejo mTORC1, provocando resistencia a insulina (Pederson et al., 2001; Berg et al., 2002). Nuestros resultados en adipocitos marrones demostraron que el descenso de los niveles de IRS1 tras 16 h de tratamiento con rapamicina iba precedido por una fosforilación en el residuo Ser 307 a tiempos cortos de tratamiento (15 min-2 h). Estos datos sugieren que cuando se inhibe mTORC1 con rapamicina, otras Ser/Thr quinasas deben estar implicadas en este mecanismo de retroalimentación negativo. Entre los candidatos alternativos que podrían mediar esta fosforilación del IRS1 en Ser 307 en presencia de rapamicina postulamos a JNK debido a estudios anteriores que mostraban que es capaz de unirse al IRS1 y que su actividad quinasa fosforila al IRS1 en dicho residuo (Hilder et al., 2003; Kim et al., 2009). Además, JNK es activado por estímulos que inducen resistencia a la insulina como son la hiperinsulinemia, el exceso de nutrientes o el estrés oxidativo (Copps y White, 2012). Además, la regulación negativa de la cascada de señalización de la insulina por fosforilación del IRS1 en Ser 307 se ha estudiado en múltiples modelos animales y celulares. Por ejemplo, resultados de nuestro laboratorio donde se analizó la resistencia a la insulina en el hígado de ratones envejecidos demostraron que éstos animales

presentaban una elevación en los niveles de fosforilación de JNK así como mayores niveles de fosforilación del IRS1 en Ser 307 (Gonzalez-Rodriguez et al., 2012).

Cabe destacar que la fosforilación del IRS1 en Ser 307 se ha encontrado también en células de la retina (fotorreceptores) expuestas a un ambiente proinflamatorio (Arroba y Valverde, 2015). En este caso, dicha fosforilación, que también precedía a la degradación del IRS1, tenía consecuencias negativas en la fosforilación de Akt en respuesta al IGF-I cuya señalización es necesaria para el mantenimiento de la supervivencia de los fotorreceptores.

En nuestros experimentos observamos que en adipocitos marrones diferenciados, tanto en cultivos primarios como en líneas inmortalizadas, el tratamiento con rapamicina inducía rápidamente la fosforilación de JNK. Esta respuesta, que fue suprimida significativamente con el inhibidor de JNK SP600125, se correlacionaba con la fosforilación del IRS1 en Ser 307. Por tanto, el tratamiento con rapamicina además de inactivar directamente al complejo mTORC1, podría estar incrementando el estrés oxidativo provocando un aumento de las especies reactivas de oxigeno que activan a JNK que a su vez fosforila al IRS1 en Ser 307 de una manera independiente a mTORC1. En relación con estos resultados, se ha encontrado que en células cardiacas que carecen de mTORC1 se induce la activación de JNK, incrementa la apoptosis y disminuye la transcripción del factor HIF1-α, lo que conduce a un estado de hipoxia (Mazelin et al., 2016). En este mismo trabajo se vincula la importancia de mTORC1 con el metabolismo energético ya que el tejido cardiaco, al igual que el BAT, requiere de un aporte constante y elevado de energía obtenido por la fosforilación oxidativa en la mitocondria. Así, los ratones deficientes en mTORC1 en el tejido cardíaco presentaron alteraciones similares a las causadas por el tratamiento con rapamicina ya que reprimen la señalización de PPARα en relación al metabolismo de ácidos grasos en la mitocondria. Esta represión del metabolismo de ácidos grasos en la mitocondria también se ha encontrado en modelos animales de células cardíacas con Akt activado de forma constitutiva (Wende et al., 2015).

Aunque estos datos no se muestran en la sección de resultados, tras el tratamiento de los adipocitos marrones con rapamicina durante tiempos cortos no se activaban las quinasa ERK y p38-MAPK, por lo que descartamos su papel en la modulación de la señalización de la insulina por rapamicina en nuestras condiciones experimentales. Sin

embargo, otros grupos de investigación han encontrado que en los adipocitos blancos humanos procedentes de tejido omental y subcutáneo la fosforilación del IRS1 en Ser 307 se reduce significativamente después de un tratamiento con rapamicina tanto a tiempos cortos (13 minutos) como largos (20 horas), (Pereira et al., 2012), lo que demuestra que como se ha señalado anteriormente el efecto de la rapamicina puede tener especificidad celular y actuar de forma diferente en adipocitos blancos y marrones.

Además de los efectos de la rapamicina encontrados in vivo en el WAT, la rapamicina es capaz de inducir a nivel sistémico resistencia a la insulina e intolerancia a la glucosa, impidiendo la señalización de la insulina en otros tejidos como el musculo esquelético y el hígado en ratas Wistar tratadas durante 3 semanas con este compuesto (Lopes et al., 2014b). De acuerdo con estos estudios previos, nuestros resultados in vivo muestran que este mismo tratamiento también interfiere con la señalización de la insulina en el BAT impidiendo la fosforilación de Akt. Experimentos adicionales midiendo la captación de glucosa in vivo serían extraordinariamente interesantes para corroborar la relevancia fisiológica de nuestros resultados.

En los mamíferos, el BAT actúa como un regulador clave del metabolismo energético mediante la liberación de FFAs, inducida por la ruta β-adrenérgica a partir de TAG, en el proceso de lipolisis (Cannon y Nedergaard, 2004; Fedorenko et al., 2012). El BAT utiliza FFAs como sustratos oxidativos para la respiración así como para la activación alostérica de la UCP1. Se ha descrito que la lipolisis inducida por NE es capaz de provocar la activación de los receptores nucleares PPARα y PPARδ (Mottillo et al., 2012), lo que induce la expresión del gen *Ucp1* en el BAT. Nuestros resultados muestran que el tratamiento con rapamicina disminuye la activación de la lipolisis inducida por NE o CL316243. Este último es un agonista de ADRβ3 , ya que son estos receptores y no los ADRα los que median la señalización adrenérgica en el BAT (Hutchinson et al., 2005; Hutchinson y Bengtsson, 2006), mediante la inhibición de la fosforilación de la HSL en el residuo Ser 660. Resulta interesante el hecho de que en los adipocitos 3T3-L1 (modelo celular de adipocitos blancos) se observa el efecto contrario, es decir, un aumento de la fosforilación de HSL y de la lipolisis mediada por el tratamiento con rapamicina (Soliman et al., 2010). De igual manera, este efecto contrario también se ha descrito en el ratón deficiente de S6K1 (diana directa de mTORC1) que presentan un fenotipo delgado tras la alimentación con una dieta altamente lipídica (Um et al., 2004). Una posible explicación para estas diferencias

entre el WAT y el BAT podría implicar a diferentes moduladores de la fosforilación de HSL de una manera específica en cada tipo celular. En este sentido, la activación de la fosfatasa PP2A parece ser la responsable de la defosforilación de HSL en los adipocitos blancos aislados de rata (Wood et al., 1993), aunque otros autores han identificado a la proteína PRIP (del inglés *phospholipase C-related catalytically inactive protein*) como un modulador negativo de la termogénesis en los adipocitos marrones (Oue et al., 2016) por su capacidad de disminuir la fosforilación de la HSL y la lipolisis. Resultan igualmente interesantes los hallazgos recientes que identifican a la proteína Grb10 (del inglés *Growth factor receptor bound protein 10*) como un modulador negativo de mTORC1 en el BAT y en el WAT y cuya deficiencia suprime la lipolisis y reduce la función termogénica tanto en adipocitos blancos como marrones (Liu et al., 2014). El estudio en profundidad de estos y de otros posibles mecanismos por los cuales la lipolisis se modula de manera diferencial por la rapamicina en los adipocitos marrones y blancos en el contexto del NODAT es una línea de trabajo que merece continuarse en profundidad.

En el BAT, además de la lipolisis, la estimulación β-adrenérgica regula la termogénesis a través del control transcripcional de los genes implicados en dicho proceso. Nuestros resultados muestran claramente y por vez primera, la inhibición, mediada por rapamicina, de los niveles de ARNm de *Pgc1α* y *Ucp1* en los adipocitos marrones que deberían estar altamente inducidos por la acción de la NE. Se ha demostrado que la inhibición de mTORC1 por la rapamicina reduce la expresión génica de *Pgc1α* en el musculo esquelético de ratón así como la actividad mitocondrial mediante un mecanismo mediado por el factor de transcripción YY1 (ying y yang) (Cunningham et al., 2007). De esta manera, la inhibición de mTORC1 por rapamicina conduce a la incapacidad de YY1 para interactuar y ser coactivado por PGC-1α en el músculo esquelético (Blättler et al., 2012a). Además, en estas condiciones YY1 actúa como un represor transcripcional de ciertos genes de la señalización de la insulina (Blättler et al., 2012b). En el BAT, bajo condiciones de demanda energética mediada por la señalización adrenérgica, el YY1 aumenta la expresión del programa termogénico canónico uniéndose al promotor del gen de *Ucp1* y reclutando a PGC-1α (Blättler et al., 2012a). Nuestros experimentos sugieren que la disminución del RNA mensajero de *Pgc1α* y *Ucp1* tras el tratamiento con rapamicina en adipocitos marrones podría estar mediada por la represión de la interacción del eje YY1-PGC-1α vía mTORC1, lo que

finalmente provocaría la inhibición de los niveles de la proteína UCP1. Además, se conoce que moléculas mitocondriales dianas de PGC-1α que están involucradas en la fosforilación oxidativa, en el ciclo de los ácidos tricarboxílicos y en la respiración desacoplante son también inhibidas por rapamicina (Cunningham et al., 2007). De acuerdo con estos resultados, nuestros datos obtenidos mediante la tecnología Seahorse muestran claramente una reducción en la respiración basal, en el flujo de protones y en la respiración máxima en los adipocitos marrones tratados con rapamicina.

Asimismo hemos analizado otro marcador de la funcionalidad del BAT, la desiodasa tipo 2 o D2, que se ha comenzado a emplear recientemente como una diana que indica la activación del BAT. La D2 se activa con la estimulación adrenérgica de modo semejante a la UCP1 y su función es producir T_3 a nivel local, es decir para cubrir las necesidades del BAT y específicamente para la activación de la UCP1 y la mitocondriogénesis. Resultados anteriores del laboratorio demostraron que la expresión de la D2 es dependiente de insulina (Martínez-de Mena y Obregón, 2005). Nosotros hemos observado que la rapamicina inhibe la estimulación adrenérgica inducida por la NE. Esta inhibición implicaría que la cantidad de T_3 disponible en el adipocito marrón estaría disminuida, así como las funciones dependientes de T_3, como la lipogénesis y la termogénesis.

Nuestro trabajo ha demostrado que además de los adipocitos blancos, los adipocitos marrones son diana de la acción de la rapamicina ya que esta molécula tal como se esquematiza en la Figura 32 modula negativamente las acciones de la insulina y la NE. La activación del BAT se considera actualmente una herramienta con gran potencial para combatir la obesidad y otras complicaciones metabólicas en humanos (Saito et al., 2009). Por ello, es razonable proponer el uso de activadores del BAT descritos recientemente como el FGF21 (Hanssen et al., 2015) para el tratamiento de NODAT, esperando que en un futuro próximo se profundice en el estudio de estos mecanismos .

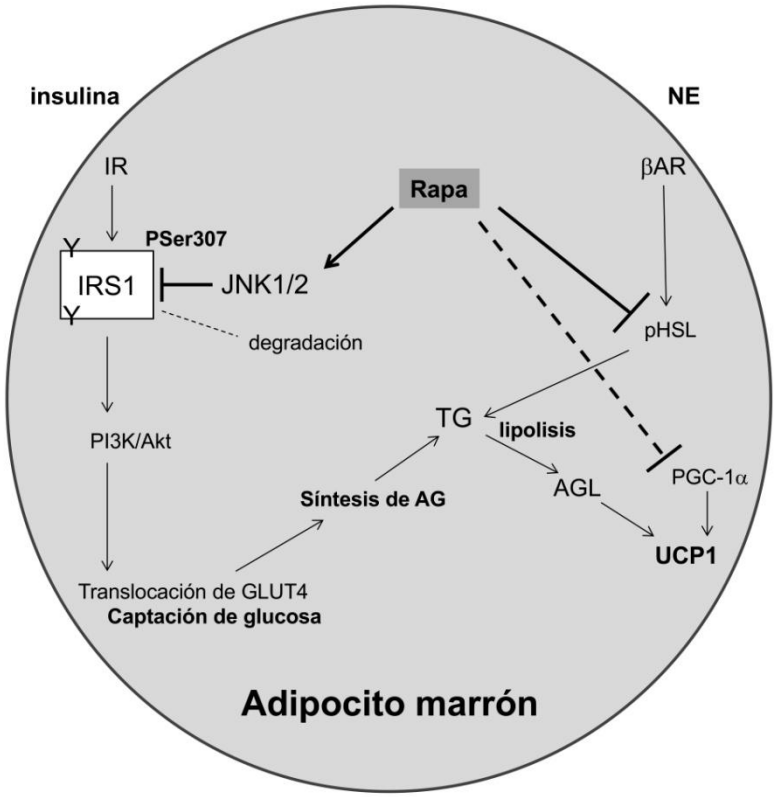

Figura 32. Propuesta de modelo de la señalización de la insulina en adipocitos marrones tras el tratamiento con rapamicina y NE.

Conclusiones

1. Las líneas celulares inmortalizadas generadas de adipocitos marrones de rata y ratón mantienen las respuestas a la insulina y la norepinefrina y, por tanto, son una herramienta óptima para su utilización en estudios de señalización celular ya que los resultados obtenidos han sido validados en cultivos primarios de adipocitos marrones.

2. La rapamicina regula de manera diferencia los niveles de IRS1 e IRS2 ya que el tratamiento de los adipocitos marrones con rapamicina durante 16 horas disminuye la expresión de IRS1 y la fosforilación de Akt en los residuos Ser 473 y Thr 308 de manera dependiente de la dosis, manteniéndose intactos los niveles de IRS2.

3. El tratamiento de los adipocitos marrones con rapamicina durante 16 h disminuye la translocación del GLUT4 a la membrana plasmática, así como la captación de glucosa en respuesta a la insulina.

4. El tratamiento de los adipocitos marrones con rapamicina durante tiempos cortos (15-60 minutos) induce la activación de la quinasa de estrés JNK, lo que, a su vez, conduce a la fosforilación del IRS1 en el residuo Ser 307.

5. La inhibición de JNK con el compuesto SP600125 suprime la fosforilación del IRS1 en el residuo Ser 307 en respuesta a la rapamicina en los adipocitos marrones, así como sus efectos negativos sobre la señalización de la insulina.

6. El tratamiento farmacológico con rapamicina en ratas durante 3 semanas suprime la fosforilación de Akt en respuesta a la insulina en el tejido adiposo marrón.

7. El tratamiento de los adipocitos marrones con rapamicina durante 16 horas disminuye la fosforilación de la lipasa sensible a hormonas (HSL) inducida por la norepinefrina y por el agonista adrenérgico β3 CL316243, lo que conlleva a una inhibición de la lipolisis.

8. El tratamiento de los adipocitos marrones con rapamicina durante 16 h disminuye los niveles de ARNm de *Ucp1* y *Pgc1α*, la expresión proteica de la UCP1 y la actividad desiodasa 2 inducidas por la norepinefrina.

9. El tratamiento de los adipocitos marrones con rapamicina durante 16 h reduce la respiración basal, el flujo de protones y la capacidad respiratoria máxima en la mitocondria.

Conclusión final: los adipocitos marrones son células sensibles al tratamiento con rapamicina, ya que tanto las respuestas a la insulina como a la norepinefrina se ven alteradas en presencia de este agente inmunosupresor. Por tanto, los resultados de esta Tesis Doctoral han puesto en evidencia por primera vez que el NODAT cursa con una pérdida de la funcionalidad de los adipocitos marrones, lo que sugiere la necesidad de nuevas estrategias terapéuticas dirigidas a preservar la actividad del tejido adiposo marrón en pacientes tratados con este agente inmunosupresor.

Bibliografía

AGUIRRE, V., UCHIDA, T., YENUSH, L., DAVIS, R. & WHITE, M. F. 2000. The c-Jun NH2-terminal Kinase Promotes Insulin Resistance during Association with Insulin Receptor Substrate-1 and Phosphorylation of Ser307. *Journal of Biological Chemistry,* 275**,** 9047-9054.

ALESSI, D. R., JAMES, S. R., DOWNES, C. P., HOLMES, A. B., GAFFNEY, P. R. J., REESE, C. B. & COHEN, P. 1997. Characterization of a 3-phosphoinositide-dependent protein kinase which phosphorylates and activates protein kinase B. *Current Biology,* 7**,** 261-269.

ALI, A. T., HOCHFELD, W. E., MYBURGH, R. & PEPPER, M. S. 2013. Adipocyte and adipogenesis. *European Journal of Cell Biology,* 92**,** 229-236.

APOVIAN, C. M., BIGORNIA, S., MOTT, M., MEYERS, M. R., ULLOOR, J., GAGUA, M., MCDONNELL, M., HESS, D., JOSEPH, L. & GOKCE, N. 2008. Adipose Macrophage Infiltration is Associated with Insulin Resistance and Vascular Endothelial Dysfunction in Obese Subjects. *Arteriosclerosis, thrombosis, and vascular biology,* 28**,** 1654-1659.

ARAKI E, LIPES MA, PATTI ME, BRÜNING JC, HAAG B 3RD, JOHNSON RS & CR., K. 1994. Alternative pathway of insulin signalling in mice with targeted disruption of the IRS-1 gene *Nature,* 10**,** 186-190.

ARROBA, A. & VALVERDE, Á. M. 2015. Inhibition of Protein Tyrosine Phosphatase 1B Improves IGF-I Receptor Signaling and Protects Against Inflammation-Induced Gliosis in the Retina. *Invest Ophthalmol Vis Sci,* 56**,** 8031-8044.

AVRUCH, J. 1998. Insulin signal transduction through protein kinase cascades. *Molecular and Cellular Biochemistry,* 182**,** 31-48.

BAGCHI, M., KIM, L. A., BOUCHER, J., WALSHE, T. E., KAHN, C. R. & D'AMORE, P. A. 2013. Vascular endothelial growth factor is important for brown adipose tissue development and maintenance. *The FASEB Journal,* 27**,** 3257-3271.

BAMGBOLA, O. 2016. Metabolic consequences of modern immunosuppressive agents in solid organ transplantation. *Therapeutic Advances in Endocrinology and Metabolism,* 7**,** 110-127.

BARGUT, T. C. L., AGUILA, M. B. & MANDARIM-DE-LACERDA, C. A. 2016. Brown adipose tissue: Updates in cellular and molecular biology. *Tissue and Cell*, 48, 452-460.

BARTNESS, T. J. & BAMSHAD, M. 1998. Innervation of mammalian white adipose tissue: implications for the regulation of total body fat. *American Journal of Physiology - Regulatory, Integrative and Comparative Physiology,* 275**,** 1399-1411.

BARTNESS, T. J., VAUGHAN, C. H. & SONG, C. K. 2010. Sympathetic and sensory innervation of brown adipose tissue. *International journal of obesity (2005),* 34**,** 36-42.

BECKER, A. S., NAGEL, H. W., WOLFRUM, C. & BURGER, I. A. 2016. Anatomical Grading for Metabolic Activity of Brown Adipose Tissue. *PLOS ONE,* 11**,** e0149458.

BERG, C. E., LAVAN, B. E. & RONDINONE, C. M. 2002. Rapamycin partially prevents insulin resistance induced by chronic insulin treatment. *Biochemical and Biophysical Research Communications,* 293**,** 1021-1027.

BETZ, M. J. & ENERBÄCK, S. 2015. Human Brown Adipose Tissue: What We Have Learned So Far. *Diabetes,* 64**,** 2352-2360.

BLÄTTLER, SHARON M., CUNNINGHAM, JOHN T., VERDEGUER, F., CHIM, H., HAAS, W., LIU, H., ROMANINO, K., RÜEGG, MARKUS A., GYGI, STEVEN P., SHI, Y. & PUIGSERVER, P. 2012a. Yin Yang 1 Deficiency in Skeletal Muscle Protects against Rapamycin-Induced Diabetic-like Symptoms through Activation of Insulin/IGF Signaling. *Cell Metabolism,* 15**,** 505-517.

BLÄTTLER, S. M., VERDEGUER, F., LIESA, M., CUNNINGHAM, J. T., VOGEL, R. O., CHIM, H., LIU, H., ROMANINO, K., SHIRIHAI, O. S., VAZQUEZ, F., RÜEGG, M. A., SHI, Y. & PUIGSERVER, P. 2012b. Defective Mitochondrial Morphology and Bioenergetic Function in Mice Lacking the Transcription Factor Yin Yang 1 in Skeletal Muscle. *Molecular and Cellular Biology,* 32**,** 3333-3346.

CANNON, B. & NEDERGAARD, J. 1986. Brown adipose tissue thermogenesis in neonatal and cold-adapted animals. *Biochemical Society Transactions,* 14**,** 233-236.

CANNON, B. & NEDERGAARD, J. 2004. Brown Adipose Tissue: Function and Physiological Significance. *Physiological Reviews,* 84**,** 277-359.

CAO, W., DANIEL, K. W., ROBIDOUX, J., PUIGSERVER, P., MEDVEDEV, A. V., BAI, X., FLOERING, L. M., SPIEGELMAN, B. M. & COLLINS, S. 2004. p38 Mitogen-Activated Protein Kinase Is the Central Regulator of Cyclic AMP-Dependent Transcription of the Brown Fat Uncoupling Protein 1 Gene. *Molecular and Cellular Biology,* 24**,** 3057-3067.

CARVALHO, E., JANSSON, P.-A., AXELSEN, M., ERIKSSON, J. W., HUANG, X., GROOP, L., RONDINONE, C., SJÖSTRÖM, L. & SMITH, U. 1999. Low cellular IRS 1 gene and protein expression predict insulin resistance and NIDDM. *The FASEB Journal,* 13**,** 2173-2178.

CHUNG J, GRAMMER TC, LEMON KP, KAZLAUSKAS A & J., B. 1994. PDGF- and insulin-dependent pp70S6k activation mediated by phosphatidylinositol-3-OH kinase. *Nature,* 370**,** 71-75.

CINTI, S. 2001. The adipose organ: morphological perspectives of adipose tissues. *Proceedings of the Nutrition Society,* 60**,** 319-328.

CINTI, S. 2012. The adipose organ at a glance. *Disease Models & Mechanisms,* 5**,** 588-594.

COPPS, K. D. & WHITE, M. F. 2012. Regulation of insulin sensitivity by serine/threonine phosphorylation of insulin receptor substrate proteins IRS1 and IRS2. *Diabetologia,* 55**,** 2565-2582.

CUNNINGHAM, J., RODGERS, JT., ARLOW, DH., VAZQUEZ, F., MOOTHA, VK. & PUIGSERVER, P. 2007. mTOR controls mitochondrial oxidative function through a YY1-PGC-1alpha transcriptional complex. *Nature,* 450**,** 736-740.

CYPESS , A. M., LEHMAN , S., WILLIAMS , G., TAL , I., RODMAN , D., GOLDFINE , A. B., KUO , F. C., PALMER , E. L., TSENG , Y.-H., DORIA , A., KOLODNY , G. M. & KAHN , C. R. 2009. Identification and Importance of Brown Adipose Tissue in Adult Humans. *New England Journal of Medicine,* 360**,** 1509-1517.

DALLNER, O. S., CHERNOGUBOVA, E., BROLINSON, K. A. & BENGTSSON, T. 2006. β3-Adrenergic Receptors Stimulate Glucose Uptake in Brown Adipocytes by Two Mechanisms Independently of Glucose Transporter 4 Translocation. *Endocrinology,* 147**,** 5730-5739.

DE MATTEIS, R., RICQUIER, D. & CINTI, S. 1998. TH-, NPY-, SP-, and CGRP-immunoreactive nerves in interscapular brown adipose tissue of adult rats acclimated at different temperatures: an immunohistochemical study. *Journal of neurocytology,* 12**,** 877-886.

DEBLON, N., BOURGOIN, L., VEYRAT-DUREBEX, C., PEYROU, M., VINCIGUERRA, M., CAILLON, A., MAEDER, C., FOURNIER, M., MONTET, X., ROHNER-JEANRENAUD, F. & FOTI, M. 2012. Chronic mTOR inhibition by rapamycin induces muscle insulin resistance despite weight loss in rats. *British Journal of Pharmacology,* 165**,** 2325-2340.

DIBBLE, C.C. & CANTTLEY, L.C. 2015. Regulation of mTORC1 by PI3K signaling. *Trends in Cell Biology,* 25, 545-555

DIRKS NL, HUTH B, YATES CR & B., M. 2004. Pharmacokinetics of immunosuppressants: a perspective on ethnic differences. *International Journal of Clinical Pharmacology and Therapeutics,* 42**,** 701-718.

EGIDI, M. F., COWAN, P. A., NASEER, A. & GABER, A. O. 2003. Conversion to sirolimus in solid organ transplantation: a Single-Center experience. *Transplantation Proceedings,* 35**,** 131-137.

EMANUELLI, B., PERALDI, P., FILLOUX, C., CHAVEY, C., FREIDINGER, K., HILTON, D. J., HOTAMISLIGIL, G. S. & VAN OBBERGHEN, E. 2001. SOCS-3 inhibits insulin signaling and is up-regulated in response to TNF-a in the adipose tissue of obese mice. *Journal of Biological Chemistry*, 276, 47944-47949.

ENTINGH-PEARSALL, A. & KAHN, C.R. 2004. Differential Roles of the Insulin and Insulin-like Growth Factor-I (IGF-I) Receptors in Response to Insulin and IGF-I. *Journal of Biological Chemistry,* 279, 38016-38024

FASSHAUER, M., KLEIN, J., KRIAUCIUNAS, K. M., UEKI, K., BENITO, M. & KAHN, C. R. 2001. Essential Role of Insulin Receptor Substrate 1 in Differentiation of Brown Adipocytes. *Molecular and Cellular Biology,* 21**,** 319-329.

FEDORENKO, A., LISHKO, POLINA V. & KIRICHOK, Y. 2012. Mechanism of Fatty-Acid-Dependent UCP1 Uncoupling in Brown Fat Mitochondria. *Cell,* 151**,** 400-413.

FERNANDEZ-VELEDO, S., VAZQUEZ-CARBALLO, A., VILA-BEDMAR, R., CEPERUELO-, MALLAFRE, V. & VENDRELL, J. 2013. Role of energy- and nutrient-sensing kinases AMP-activated protein kinase (AMPK) and mammalian target of rapamycin (mTOR) in adipocyte differentiation. *International Union of Biochemistry and Molecular Biology*, 65, 572-583.

FINGAR, D. & BLENIS, J. 2004. Target of rapamycin (TOR): an integrator of nutrient and growth factor signals and coordinator of cell growth and cell cycle progression. *Oncogene,* 23**,** 3151-3171.

FINGAR, D. C., RICHARDSON, C. J., TEE, A. R., CHEATHAM, L., TSOU, C. & BLENIS, J. 2004. mTOR Controls Cell Cycle Progression through Its Cell Growth Effectors S6K1 and 4E-BP1/Eukaryotic Translation Initiation Factor 4E. *Molecular and Cellular Biology,* 24**,** 200-216.

FRANZ, S., REGENITER, A., HOPFER, H., MIHATSCH, M. & DICKENMANN, M. 2010. Tubular Toxicity in Sirolimus- and Cyclosporine-Based Transplant Immunosuppression Strategies: An Ancillary Study From a Randomized Controlled Trial. *American Journal of Kidney Diseases,* 55**,** 335-343.

FRÜHBECK, G., GÓMEZ-AMBROSI, J., MURUZÁBAL, F. J. & BURRELL, M. A. 2001. The adipocyte: a model for integration of endocrine and metabolic signaling in energy metabolism regulation. *American Journal of Physiology - Endocrinology And Metabolism,* 280**,** 827-847.

FUHRMANN, A., LOPES, P. C., SERENO, J., PEDRO, J., ESPINOZA, D. O., PEREIRA, M. J., REIS, F., ERIKSSON, J. W. & CARVALHO, E. 2014. Molecular mechanisms underlying the effects of cyclosporin A and sirolimus on glucose and lipid metabolism in liver, skeletal muscle and adipose tissue in an in vivo rat model. *Biochemical Pharmacology,* 88**,** 216-228.

FUKUCHI, K., TATSUMI, M., ISHIDA, Y., OKU, N., HATAZAWA, J. & WAHL, R. L. 2004. Radionuclide Imaging Metabolic Activity of Brown Adipose Tissue in a Patient with Pheochromocytoma. *Exp Clin Endocrinol Diabetes,* 112**,** 601-603.

GALINDO, R. J., FRIED, M., BREEN, T. & TAMLER, R. 2016. Hyperglycemia management in patients with posttransplantation diabetes. *Endocrine Practice,* 22**,** 454-465.

GESTA, S., TSENG, Y.-H. & KAHN, C. R. 2007. Developmental Origin of Fat: Tracking Obesity to Its Source. *Cell,* 131**,** 242-256.

GÓMEZ-HERNÁNDEZ, A., OTERO, Y. F., HERAS, N. D. L., ESCRIBANO, Ó., CACHOFEIRO, V., LAHERA, V. & BENITO, M. 2012. Brown Fat Lipoatrophy and Increased Visceral Adiposity through a Concerted Adipocytokines Overexpression Induces Vascular Insulin Resistance and Dysfunction. *Endocrinology,* 153**,** 1242-1255.

GONZÁLEZ-RODRÍGUEZ, Á., MÁS-GUTIERREZ, J. A., MIRASIERRA, M., FERNANDEZ-PÉREZ, A., LEE, Y. J., KO, H. J., KIM, J. K., ROMANOS, E., CARRASCOSA, J. M., ROS, M., VALLEJO, M., RONDINONE, C. M. & VALVERDE, Á. M. 2012. Essential role of Protein Tyrosine Phosphatase 1B in Obesity-induced Inflammation and Peripheral Insulin Resistance during aging. *Aging Cell,* 11**,** 284-296.

GUERRA, C., NAVARRO, P., VALVERDE, A. M., ARRIBAS, M., BR, XFC, NING, J., KOZAK, L. P., KAHN, C. R. & BENITO, M. 2001. Brown adipose tissue–specific insulin receptor knockout shows diabetic phenotype without insulin resistance. *The Journal of Clinical Investigation,* 108**,** 1205-1213.

GUERTIN, D. A. & SABATINI, D. M. 2009. The Pharmacology of mTOR Inhibition. *Science Signaling,* 2**,** pe24.

GYURUS, E., KAPOSZTAS, Z. & KAHAN, B. D. 2011. Sirolimus Therapy Predisposes to New-Onset Diabetes Mellitus After Renal Transplantation: A Long-Term Analysis of Various Treatment Regimens. *Transplantation Proceedings,* 43**,** 1583-1592.

HAGAN, G. N., LIN, Y., MAGNUSON, M. A., AVRUCH, J. & CZECH, M. P. 2008. A Rictor-Myo1c Complex Participates in Dynamic Cortical Actin Events in 3T3-L1 Adipocytes. *Molecular and Cellular Biology,* 28**,** 4215-4226.

HAJ, F. G., ZABOLOTNY, J. M., KIM, Y.-B., KAHN, B. B. & NEEL, B. G. 2005. Liver-specific Protein-tyrosine Phosphatase 1B (PTP1B) Re-expression Alters Glucose Homeostasis of PTP1B–/–Mice. *Journal of Biological Chemistry,* 280**,** 15038-15046.

HAN, E., KIM, M. S., KIM, Y. S. & KANG, E. S. 2016. Risk assessment and management of post-transplant diabetes mellitus. *Metabolism - Clinical and Experimental,* 65**,** 1559-1569.

HANSSEN, M. J. W., BROEDERS, E., SAMMS, R. J., VOSSELMAN, M. J., VAN DER LANS, A. A. J. J., CHENG, C. C., ADAMS, A. C., VAN MARKEN LICHTENBELT, W. D. & SCHRAUWEN, P. 2015. Serum FGF21 levels are associated with brown adipose tissue activity in humans. *Scientific Reports,* 5**,** 10275.

HANY, T. F., ESMAIEL, G., EHAB M. KAMEL, ALFRED BUCK, HIMMS-HAGEN, J. & SCHULTHESS1, G. K. V. 2002. Brown adipose tissue: a factor to consider in symmetrical tracer uptake in the neck and upper chest region. *European Journal of Nuclear Medicine,* 29**,** 1393-1398.

HARRINGTON, L. S., FINDLAY, G. M. & LAMB, R. F. 2005. Restraining PI3K: mTOR signalling goes back to the membrane. *Trends in Biochemical Sciences,* 30**,** 35-42.

HARRIS, T. E. & LAWRENCE, J. C. 2003. TOR Signaling. *Science's STKE,* 2003**,** re15.

HAY, N. & SONENBERG, N. 2004. Upstream and downstream of mTOR. *Genes & Development,* 18**,** 1926-1945.

HECKING, M., WERZOWA, J., HAIDINGER, M., HÖRL, W. H., PASCUAL, J., BUDDE, K., LUAN, F. L., OJO, A., DE VRIES, A. P. J., PORRINI, E., PACINI, G., PORT, F. K., SHARIF, A., SÄEMANN, M. D. & GROUP, E.-N.-O. D. A. T. W. 2013. Novel views on new-onset diabetes after transplantation: development, prevention and treatment. *Nephrology Dialysis Transplantation,* 28**,** 550-566.

HERNANDEZ, A., MARTINEZ DE MENA, R., MARTIN, E. & OBREGON, M. 2011. Differences in the Response of UCP1 mRNA to Hormonal Stimulation Between Rat and Mouse Primary Cultures of Brown Adipocytes. *Cellular Physiology and Biochemistry,* 28**,** 969-980.

HERNÁNDEZ, A. & OBREGÓN, M. J. 2000. Triiodothyronine amplifies the adrenergic stimulation of uncoupling protein expression in rat brown adipocytes. *American Journal of Physiology - Endocrinology And Metabolism,* 278**,** 769-777.

HERNANDEZ, R., TERUEL, T. & LORENZO, M. 2001. Akt mediates insulin induction of glucose uptake and up-regulation of GLUT4 gene expression in brown adipocytes. *FEBS Letters,* 494**,** 225-231.

HILDER, T. L., TOU, J. C. L., GRINDELAND, R. E., WADE, C. E. & GRAVES, L. M. 2003. Phosphorylation of insulin receptor substrate-1 serine 307 correlates with JNK activity in atrophic skeletal muscle. *FEBS Letters,* 553**,** 63-67.

HIRASHIMA, Y., TSURUZOE, K., KODAMA, S., IGATA, M., TOYONAGA, T., UEKI, K., KAHN, C. & ARAKI, E. 2003. Insulin down-regulates insulin receptor substrate-2 expression through the phosphatidylinositol 3-kinase/Akt pathway. *Journal of Endocrinology,* 179**,** 253-266.

HONEK, J., LIM, S., FISCHER, C., IWAMOTO, H., SEKI, T. & CAO, Y. 2014. Brown adipose tissue, thermogenesis, angiogenesis: pathophysiological aspects. *Hormone Molecular Biology and Clinical Investigation,* 19**,** 5-11.

HUANG, J. & MANNING, BD. 2009. A complex interplay between Akt, TSC2 and the two mTOR complexes. *Biochemical Society Transactions,* 37**,** 217-222.

HUANG, S. & CZECH, M. P. 2007. The GLUT4 Glucose Transporter. *Cell Metabolism,* 5**,** 237-252.

HUTCHINSON, D. S. & BENGTSSON, T. 2006. AMP-Activated Protein Kinase Activation by Adrenoceptors in L6 Skeletal Muscle Cells. *Diabetes,* 55**,** 682-690.

HUTCHINSON, D. S., CHERNOGUBOVA, E., DALLNER, O. S., CANNON, B. & BENGTSSON, T. 2005. β-Adrenoceptors, but not α-adrenoceptors, stimulate AMP-activated protein kinase in brown adipocytes independently of uncoupling protein-1. *Diabetologia,* 48**,** 2386-2395.

HUTTUNEN P, HIRVONEN J & V., K. 1981. The occurrence of brown adipose tissue in outdoor workers. *European Journal of Applied Physiology and Occupational Physiology,* 46**,** 339-345.

INOKI, K., LI, Y., ZHU, T., WU, J. & GUAN, K. L. 2002. TSC2 is phosphorylated and inhibited by Akt and suppresses mTOR signalling. *Nature Cell Biology,* 4**,** 648-657.

INOKUMA, K.-I., OGURA-OKAMATSU, Y., TODA, C., KIMURA, K., YAMASHITA, H. & SAITO, M. 2005. Uncoupling Protein 1 Is Necessary for Norepinephrine-Induced Glucose Utilization in Brown Adipose Tissue. *Diabetes,* 54**,** 1385-1391.

JACINTO, E., FACCHINETTI, V., LIU, D., SOTO, N., WEI, S., JUNG, S. Y., HUANG, Q., QIN, J. & SU, B. 2006. SIN1/MIP1 Maintains rictor-mTOR Complex Integrity and Regulates Akt Phosphorylation and Substrate Specificity. *Cell,* 127**,** 125-137.

KIM, T., WAYNE LEITNER, J., ADOCHIO, R. & DRAZNIN, B. 2009. Knockdown of JNK rescues 3T3-L1 adipocytes from insulin resistance induced by mitochondrial dysfunction. *Biochemical and Biophysical Research Communications,* 378**,** 772-776.

KLEIN, J., FASSHAUER, M., KLEIN, H. H., BENITO, M. & KAHN , C. R. 2002. Novel adipocyte lines from brown fat: a model system for the study of differentiation, energy metabolism, and insulin action. *BioEssays,* 24**,** 382-388.

KLINTMALM, G. B. & NASHAN, B. 2014. The Role of mTOR Inhibitors in Liver Transplantation: Reviewing the Evidence. *Journal of Transplantation,* 2014**,** 845438.

LABBÉ, S.M., MOUCHIROUD, M., CARON, A. SECCO, B., FREINKMAN, E., LAMOUREUX, G., GELINAS, Y., LACOMPTE, R., BOSSE, Y., CHIMIN, P., FESTUCIOA W.T., RICHARD, D. & LAPLANTE, M. 2016. mTORC1 is Required for Brown Adipose Tissue Recruitment and Metabolic Adaptation to Cold. *Scientific Reports*, 6, 37223.

LAPLANTE, M. & SABATINI, D. M. 2009. An emerging role of mTOR in lipid biosynthesis. *Current Biology,* 19**,** 1046-1052.

LEAN, M. E. J. 1989. Brown adipose tissue in humans. *Proceedings of the Nutrition Society,* 48**,** 243-256.

LEE, P. L., TANG, Y., LI, H. & GUERTIN, D. A. 2016. Raptor/mTORC1 loss in adipocytes causes progressive lipodystrophy and fatty liver disease. *Molecular Metabolism,* 5**,** 422-432.

LEONARD JL., MELLEN, SA. & Larsen PR. 1983 Thyroxine 5-deiodinase activity in brown adipose tissue. *Endocrinology* ,112, 1153–1155.

LIDELL, M. E., BETZ, M. J., LEINHARD, O. D., HEGLIND, M., ELANDER, L., SLAWIK, M., MUSSACK, T., NILSSON, D., ROMU, T., NUUTILA, P., VIRTANEN, K. A., BEUSCHLEIN, F., PERSSON, A., BORGA, M. & ENERBACK, S. 2013. Evidence for two types of brown adipose tissue in humans. *Nat Med,* 19**,** 631-634.

LIN, J.-C., TARN, W.-Y. & HSIEH, W.-K. 2014. Emerging role for RNA binding motif protein 4 in the development of brown adipocytes. *Biochimica et Biophysica Acta (BBA) - Molecular Cell Research,* 1843**,** 769-779.

LIU, M., BAI, J., HE, S., VILLARREAL, R., HU, D., ZHANG, C., YANG, X., LIANG, H., SLAGA, THOMAS J., YU, Y., ZHOU, Z., BLENIS, J., SCHERER, PHILIPP E., DONG, LILY Q. & LIU, F. 2014. Grb10 Promotes Lipolysis and Thermogenesis by Phosphorylation-Dependent Feedback Inhibition of mTORC1. *Cell Metabolism,* 19**,** 967-980.

LONG, X., LIN, Y., ORTIZ-VEGA, S., YONEZAWA, K. & AVRUCH, J. 2005. Rheb Binds and Regulates the mTOR Kinase. *Current Biology,* 15**,** 702-713.

LOPES, P., FUHRMANN, A., SERENO, J., PEREIRA, M. J., NUNES, P., PEDRO, J., MELÃO, A., REIS, F. & CARVALHO, E. 2013. Effects of Cyclosporine and Sirolimus on Insulin-Stimulated Glucose Transport and Glucose Tolerance in a Rat Model. *Transplantation Proceedings,* 45**,** 1142-1148.

LOPES, P. C., FUHRMANN, A., CARVALHO, F., SERENO, J., SANTOS, M. R., PEREIRA, M. J., ERIKSSON, J. W., REIS, F. & CARVALHO, E. 2014a. Cyclosporine A enhances gluconeogenesis while sirolimus impairs insulin signaling in peripheral tissues after 3 weeks of treatment. *Biochemical Pharmacology,* 91**,** 61-73.

LOPES, P. C., FUHRMANN, A., SERENO, J., ESPINOZA, D. O., PEREIRA, M. J., ERIKSSON, J. W., REIS, F. & CARVALHO, E. 2014b. Short and long term in vivo effects of Cyclosporine A and Sirolimus on genes and proteins involved in lipid metabolism in Wistar rats. *Metabolism - Clinical and Experimental,* 63**,** 702-715.

LORENZO, M., RONCERO, C., FABREGAT, I. & BENITO, M. 1988. Hormonal regulation of rat foetal lipogenesis in brown-adipocyte primary cultures. *Biochemical Journal,* 251**,** 617-620.

LORENZO, M., VALVERDE, A., TERUEL, T., ALVAREZ, A. & BENITO, M. 1996. p21ras induced differentiation-related gene expression in fetal brown adipocyte primary cells and cell lines. *Cell Growth Differ,* 7**,** 1251-1259.

LOWRY, OH., ROSEBROUGH, NJ., FARR, AL. & RANDALL, RJ. 1951. Protein measurement with the Folin phenol reagent. *Journal of Biological Chemistry*, 193, 265-275

LUO, L. & LIU, M. 2016. Adipose tissue in control of metabolism. *Journal of Endocrinology,* 231**,** 77-99.

MAGNUSSON, R., GUSTAFSSON, M., CEDERSUND, G., STRÅLFORS, P. & NYMAN, E. 2017. Cross-talks via mTORC2 can explain enhanced activation in response to insulin in diabetic patients. *Bioscience Reports,* 37, 20160514

MARTÍN-DÁVILA, P., BLANES, M. & JESÚS FORTÚN, J. 2007. Inmunosupresión e infección en el paciente trasplantado. *Enfermedades infecciosas y Microbiología Clínica,* 25**,** 143-154.

MARTINEZ-DEMENA, R. & OBREGÓN, M.-J. 2005. Insulin increases the adrenergic stimulation of 5' deiodinase activity and mRNA expression in rat brown adipocytes; role of MAPK and PI3K. *Journal of Molecular Endocrinology,* 34**,** 139-151.

MAZELIN, L., PANTHU, B., NICOT, A.-S., BELOTTI, E., TINTIGNAC, L., TEIXEIRA, G., ZHANG, Q., RISSON, V., BAAS, D., DELAUNE, E., DERUMEAUX, G., TAILLANDIER, D., OHLMANN, T., OVIZE, M., GANGLOFF, Y.-G. & SCHAEFFER, L. 2016. mTOR inactivation in myocardium from infant mice rapidly leads to dilated cardiomyopathy due to translation defects and p53/JNK-mediated apoptosis. *Journal of Molecular and Cellular Cardiology,* 97**,** 213-225.

MICHAEL, L. F., WU, Z., CHEATHAM, R. B., PUIGSERVER, P., ADELMANT, G., LEHMAN, J. J., KELLY, D. P. & SPIEGELMAN, B. M. 2001. Restoration of insulin-sensitive glucose transporter (GLUT4) gene expression in muscle cells by the transcriptional coactivator PGC-1. *Proceedings of the National Academy of Sciences of the United States of America,* 98**,** 3820-3825.

MIRANDA, S., GONZÁLEZ-RODRÍGUEZ, Á., REVUELTA-CERVANTES, J., RONDINONE, C. M. & VALVERDE, Á. M. 2010. Beneficial effects of PTP1B deficiency on brown adipocyte differentiation and protection against apoptosis induced by pro- and anti-inflammatory stimuli. *Cellular Signalling,* 22**,** 645-659.

MISRA, A., GARG, A., ABATE, N., PESHOCK, R. M., STRAY-GUNDERSEN, J. & GRUNDY, S. M. 1997. Relationship of Anterior and Posterior Subcutaneous Abdominal Fat to Insulin Sensitivity in Nondiabetic Men. *Obesity Research,* 5**,** 93-99.

MORENO, B. 2005. *La Obesidad en el Tercer Milenio*, Ed. Médica Panamericana, 3-11

MOTA, A. 2005. Sirolimus: a new option in transplantation. *Expert Opinion on Pharmacotherapy,* 6**,** 479-487.

MOTTILLO, E. P., BLOCH, A. E., LEFF, T. & GRANNEMAN, J. G. 2012. Lipolytic Products Activate Peroxisome Proliferator-activated Receptor (PPAR) α and δ in Brown Adipocytes to Match Fatty Acid Oxidation with Supply. *Journal of Biological Chemistry,* 287**,** 25038-25048.

NEDERGAARD, J., BENGTSSON, T. & CANNON, B. 2007. Unexpected evidence for active brown adipose tissue in adult humans. *American Journal of Physiology - Endocrinology And Metabolism,* 293**,** 444-452.

OBREGON, M.J. 2014. Adipose tissues and thyroid hormones. *Frontiers in Physiology,* 5**,** 479 (1-12)

OBREGON, M.-J., PITAMBER, R., JACOBSSON, A., NEDERGAARD, J. & CANNON, B. 1987. Euthyroid status is essential for the perinatal increase in thermogenin mRNA in brown adipose tissue of rat pups. *Biochemical and Biophysical Research Communications,* 148**,** 9-14.

OH, K.-J., LEE, D., KIM, W., HAN, B., LEE, S. & BAE, K.-H. 2017. Metabolic Adaptation in Obesity and Type II Diabetes: Myokines, Adipokines and Hepatokines. *International Journal of Molecular Sciences,* 18**,** 8.

OLSEN, J. M., SATO, M., DALLNER, O. S., SANDSTRÖM, A. L., PISANI, D. F., CHAMBARD, J.-C., AMRI, E.-Z., HUTCHINSON, D. S. & BENGTSSON, T. 2014. Glucose uptake in brown fat cells is dependent on mTOR complex 2–promoted GLUT1 translocation. *The Journal of Cell Biology,* 207**,** 365-374.

OUE, K., ZHANG, J., HARADA-HADA, K., ASANO, S., YAMAWAKI, Y., HAYASHIUCHI, M., FURUSHO, H., TAKATA, T., IRIFUNE, M., HIRATA, M. & KANEMATSU, T. 2016. Phospholipase C-related Catalytically Inactive Protein Is a New Modulator of Thermogenesis Promoted by β-Adrenergic Receptors in Brown Adipocytes. *Journal of Biological Chemistry,* 291**,** 4185-4196.

PANIAGUA GÓMEZ-ÁLVAREZ, R. 2004. *Citología e Histología Animal y Vegetal*, Ed.McGraw-Hill. 577-609

PEARSON, R. B., DENNIS, P. B., HAN, J. W., WILLIAMSON, N. A., KOZMA, S. C., WETTENHALL, R. E. & THOMAS, G. 1995. The principal target of rapamycin-induced p70s6k inactivation is a novel phosphorylation site within a conserved hydrophobic domain. *The EMBO Journal,* 14**,** 5279-5287.

PEDERSON, T. M., KRAMER, D. L. & RONDINONE, C. M. 2001. Serine/Threonine Phosphorylation of IRS-1 Triggers Its Degradation. *Possible Regulation by Tyrosine Phosphorylation,* 50**,** 24-31.

PEREIRA, M. J., PALMING, J., RIZELL, M., AURELIANO, M., CARVALHO, E., SVENSSON, M. K. & ERIKSSON, J. W. 2012. mTOR inhibition with rapamycin causes impaired insulin signalling and glucose uptake in human subcutaneous and omental adipocytes. *Molecular and Cellular Endocrinology,* 355**,** 96-105.

PEREIRA, M. J., PALMING, J., RIZELL, M., AURELIANO, M., CARVALHO, E., SVENSSON, M. K. & ERIKSSON, J. W. 2014. Cyclosporine A and Tacrolimus Reduce the Amount of GLUT4 at the Cell Surface in Human Adipocytes: Increased Endocytosis as a Potential Mechanism for the Diabetogenic Effects of Immunosuppressive Agents. *The Journal of Clinical Endocrinology & Metabolism,* 99**,** 1885-1894.

PETERSON, T. R., LAPLANTE, M., THOREEN, C. C., SANCAK, Y., KANG, S. A., KUEHL, W. M., GRAY, N. S. & SABATINI, D. M. 2009. DEPTOR is an mTOR Inhibitor Whose Frequent Overexpression in Multiple Myeloma Cells Promotes their Survival. *Cell,* 137**,** 873-886.

PFLUGER, P. T., HERRANZ, D., VELASCO-MIGUEL, S., SERRANO, M. & TSCHÖP, M. H. 2008. Sirt1 protects against high-fat diet-induced metabolic damage. *Proceedings of the National Academy of Sciences of the United States of America,* 105**,** 9793-9798.

PORRAS, A., FERNÁNDEZ, M. & BENITO, M. 1989. Adrenergic regulation of the uncoupling protein expression in foetal rat brown adipocytes in primary culture. *Biochemical and Biophysical Research Communications,* 163**,** 541-547.

PORSTMANN, T., GRIFFITHS, B., CHUN, Y.-L., DELPUECH, O., GRIFFITHS, J. R., DOWNWARD, J. & SCHULZE, A. 2005. PKB/Akt induces transcription of enzymes involved in cholesterol and fatty acid biosynthesis via activation of SREBP. *Oncogene***,** 6465-6481.

RABELO, R. R., SCHIFMAN, A., RUBIO, A., SHENG, X. & SILVA, J. E. 1995. Delineation of thyroid hormone-responsive sequences within a critical enhancer in the rat uncoupling protein gene. *Endocrinology,* 136**,** 1003-1013.

RAMACHANDRAN, C. & KENNEDY, B. P. 2003. Protein Tyrosine Phosphatase 1B: A Novel Target for Type 2 Diabetes and Obesity. *Current Topics in Medicinal Chemistry,* 3**,** 749-757.

RAVNSKJAER, K., MADIRAJU, A. & MONTMINY, M. 2015. Role of the cAMP Pathway in Glucose and Lipid Metabolism. *Handbook of Experimental Farmacology*, 233, 29-49.

RAVUSSIN, E. & GALGANI, J. E. 2011. The Implication of Brown Adipose Tissue for Humans. *Annual Review of Nutrition,* 31**,** 33-47.

REIFSNYDER, P. C., FLURKEY, K., TE, A. & HARRISON, D. E. 2016. Rapamycin treatment benefits glucose metabolism in mouse models of type 2 diabetes. *Aging (Albany NY),* 8**,** 3120-3130.

RICQUIER, D., NECHAD, M. & MORY, G. 1982. Ultrastructural and biochemical characterization of human brown adipose tissue in pheochromocytoma. *Journal of Clinical Endocrinology and Metabolism,* 54**,** 803-807.

RODRÍGUEZ, A., EZQUERRO, S., MÉNDEZ-GIMÉNEZ, L., BECERRIL, S. & FRÜHBECK, G. 2015. Revisiting the adipocyte: a model for integration of cytokine signaling in the regulation of energy metabolism. *American Journal of Physiology - Endocrinology And Metabolism,* 309**,** 691-714.

SAELY, C. H., GEIGER, K. & DREXEL, H. 2012. Brown versus White Adipose Tissue: A Mini-Review. *Gerontology,* 58**,** 15-23.

SAITO, M., OKAMATSU-OGURA, Y., MATSUSHITA, M., WATANABE, K., YONESHIRO, T., NIO-KOBAYASHI, J., IWANAGA, T., MIYAGAWA, M., KAMEYA, T., NAKADA, K., KAWAI, Y. & TSUJISAKI, M. 2009. High Incidence of Metabolically Active Brown Adipose Tissue in Healthy Adult Humans. *Effects of Cold Exposure and Adiposity,* 58**,** 1526-1531.

SANCAK, Y., THOREEN, C. C., PETERSON, T. R., LINDQUIST, R. A., KANG, S. A., SPOONER, E., CARR, S. A. & SABATINI, D. M. 2007. PRAS40 Is an Insulin-Regulated Inhibitor of the mTORC1 Protein Kinase. *Molecular Cell,* 25**,** 903-915.

SANCHEZ-GURMACHES, J. & GUERTIN, D. A. 2014. Adipocyte lineages: Tracing back the origins of fat. *Biochimica et Biophysica Acta (BBA) - Molecular Basis of Disease,* 1842**,** 340-351.

SARBASSOV, D. D., ALI, S. M., SENGUPTA, S., SHEEN, J.-H., HSU, P. P., BAGLEY, A. F., MARKHARD, A. L. & SABATINI, D. M. 2006. Prolonged Rapamycin Treatment Inhibits mTORC2 Assembly and Akt/PKB. *Molecular Cell,* 22**,** 159-168.

SARBASSOV, D. D., GUERTIN, D. A., ALI, S. M. & SABATINI, D. M. 2005. Phosphorylation and Regulation of Akt/PKB by the Rictor-mTOR Complex. *Science,* 307**,** 1098-1101.

SEALE, P., KAJIMURA, S., YANG, W., CHIN, S., ROHAS, L., ULDRY, M., TAVERNIER, G., LANGIN, D. & SPIEGELMAN, B. M. 2007. Transcriptional Control of Brown Fat Determination by PRDM16. *Cell metabolism,* 6**,** 38-54.

SMITH J.M, N. T. L., MCDONALD R.A. 2003. Current immunosuppressive agents: efficacy, side effects and utilization. *Pediatric Clinics of North America,* 50**,** 1283-1300.

SMITH, S. R., LOVEJOY, J. C., GREENWAY, F., RYAN, D., DEJONGE, L., DE LA BRETONNE, J., VOLAFOVA, J. & BRAY, G. A. 2001. Contributions of total body fat, abdominal subcutaneous adipose tissue compartments, and visceral adipose tissue to the metabolic complications of obesity. *Metabolism - Clinical and Experimental,* 50**,** 425-435.

SMORLESI, A., A;, F., GIORDANO, A. & CINTI, S. 2012. The adipose organ: white-brown adipocyte plasticity and metabolic inflammation. *Obesity Rewiews,* 13**,** 83-96.

SOLIMAN, G. A., ACOSTA-JARQUEZ, H. A. & FINGAR, D. C. 2010. mTORC1 inhibition via rapamycin promotes triacylglycerol lipolysis and release of free fatty acids un 3T3-L1 adipocytes. *Lipids,* 45**,** 1089-1100.

STAN, R., MCLAUGHLIN, M. M., CAFFERKEY, R., JOHNSON, R. K., ROSENBERG, M. & LIVI, G. P. 1994. Interaction between FKBP12-rapamycin and TOR involves a conserved serine residue. *Journal of Biological Chemistry,* 269**,** 32027-30.

TANIGUCHI, C. M., EMMANUELLI, B. & KAHN , C. R. 2006. Critical nodes in signalling pathways: insights into insulin action. *Nature reviews. Molecular Cell Biology,* 7**,** 85-96.

TANTI, J.F. & JAGER, J. 2009. Cellular mechanism of insulin resistance: role of stress-regulated serine kinases and insuline receptor substrates (IRS) serine phosphorylation. *Current Opinion in Pharmacology,* 9**,** 753-762.

TEUTONICO, A., SCHENA, P. F. & DI PAOLO, S. 2005. Glucose Metabolism in Renal Transplant Recipients: Effect of Calcineurin Inhibitor Withdrawal and Conversion to Sirolimus. *Journal of the American Society of Nephrology,* 16**,** 3128-3135.

TIMMONS, J. A., WENNMALM, K., LARSSON, O., WALDEN, T. B., LASSMANN, T., PETROVIC, N., HAMILTON, D. L., GIMENO, R. E., WAHLESTEDT, C., BAAR, K., NEDERGAARD, J. & CANNON, B. 2007. Myogenic gene expression signature establishes that brown and white adipocytes originate from distinct cell lineages. *Proceedings of the National Academy of Sciences of the United States of America,* 104**,** 4401-4406.

TRAN, T. T. & KAHN, C. R. 2010. Transplantation of Adipose Tissue and Adipose-Derived Stem Cells as a Tool to Study Metabolic Physiology and for Treatment of Disease. *Nature reviews. Endocrinology,* 6**,** 195-213.

TRAYHURN, P. 2005. The biology of obesity. *Proceedings of the Nutrition Society,* 64**,** 31-38.

TRAYHURN, P. & NICHOLLS, D.G. 1986. *Brown Adipose Tissue*. Ed . Arnold, 1-30.

TRAYHURN, P. & MILNER, R. 1989. A commentary on the interpretation of in vitro biochemical measures of brown adipose tissue thermogenesis *Canadian Journal of Physiology and Pharmacology,* 67**,** 811-819.

TREMBLAY, F. D. R., GAGNON, A., VEILLEUX, A., SORISKY, A. & MARETTE, A. 2005. Activation of the Mammalian Target of Rapamycin Pathway Acutely Inhibits Insulin Signaling to Akt and Glucose Transport in 3T3-L1 and Human Adipocytes. *Endocrinology,* 146**,** 1328-1337.

TSENG, Y.-H., KRIAUCIUNAS, K. M., KOKKOTOU, E. & KAHN, C. R. 2004. Differential Roles of Insulin Receptor Substrates in Brown Adipocyte Differentiation. *Molecular and Cellular Biology,* 24**,** 1918-1929.

TSENG YH, BUTTE AJ, KOKKOTOU E, YECHOOR VK, TANIGUCHI CM, KRIAUCIUNAS KM, CYPESS AM, NIINOBE M, YOSHIKAWA K, PATTI ME & CR., K. 2005. Prediction of preadipocyte differentiation by gene expression reveals role of insulin receptor substrates and necdin *Nature Cell Biology,* 7**,** 601-611.

UM, S. H., FRIGERIO, F., WATANABE, M., PICARD, F., JOAQUIN, M., STICKER, M., FUMAGALLI, S., ALLEGRINI, PR., KOZMA SC., AUWERX, J. & GEORGE THOMAS 2004. Absence of S6K1 protects against age- and diet-induced obesity while enhancing insulin sensitivity. *Nature,* 431**,** 200-205.

VALVERDE, A. M., ARRIBAS, M., MUR, C., NAVARRO, P., PONS, S., CASSARD-DOULCIER, A.-M., KAHN, C. R. & BENITO, M. 2003a. Insulin-induced Up-regulated Uncoupling Protein-1 Expression Is Mediated by Insulin Receptor Substrate 1 through the Phosphatidylinositol 3-Kinase/Akt Signaling Pathway in Fetal Brown Adipocytes. *Journal of Biological Chemistry,* 278**,** 10221-10231.

VALVERDE, A. M. & BENITO, M. 2005. The Brown Adipose Cell: A Unique Model for Understanding the Molecular Mechanism of Insulin Resistance. *Mini-Reviews in Medicinal Chemistry,* 5**,** 269-278.

VALVERDE, A. M., BURKS, D. J., FABREGAT, I., FISHER, T. L., CARRETERO, J., WHITE, M. F. & BENITO, M. 2003b. Molecular Mechanisms of Insulin Resistance in IRS-2-Deficient Hepatocytes. *Diabetes,* 52**,** 2239-2248.

VALVERDE, A. M., KAHN, C. R. & BENITO, M. 1999a. Insulin signaling in insulin receptor substrate (IRS)-1-deficient brown adipocytes: requirement of IRS-1 for lipid synthesis. *Diabetes,* 48**,** 2122-2131.

VALVERDE, A. M., NAVARRO, P., BENITO, M. & LORENZO, M. 1998. H-ras Induces Glucose Uptake in Brown Adipocytes in an Insulin- and Phosphatidylinositol 3-Kinase-Independent Manner. *Experimental Cell Research,* 243**,** 274-281.

VALVERDE, A. M., NAVARRO, P., TERUEL, T., CONEJO, R., BENITO, M. & LORENZO, M. 1999b. Insulin and insulin-like growth factor I up-regulate GLUT4 gene expression in fetal brown adipocytes, in a phosphoinositide 3-kinase-dependent manner. *Biochemical Journal,* 337**,** 397-405.

VAN MARKEN LICHTENBELT , W. D., VANHOMMERIG , J. W., SMULDERS , N. M., DROSSAERTS , J. M. A. F. L., KEMERINK , G. J., BOUVY , N. D., SCHRAUWEN , P. & TEULE , G. J. J. 2009. Cold-Activated Brown Adipose Tissue in Healthy Men. *New England Journal of Medicine,* 360**,** 1500-1508.

VIRTANEN, K. A. 2016. The rediscovery of BAT in adult humans using imaging. *Best Practice & Research Clinical Endocrinology & Metabolism,* 30**,** 471-477.

VIRTANEN , K. A., LIDELL , M. E., ORAVA , J., HEGLIND , M., WESTERGREN , R., NIEMI , T., TAITTONEN , M., LAINE , J., SAVISTO , N.-J., ENERBÄCK , S. & NUUTILA , P. 2009. Functional Brown Adipose Tissue in Healthy Adults. *New England Journal of Medicine,* 360**,** 1518-1525.

WANG, L., HARRIS, T. E., ROTH, R. A. & LAWRENCE , J. C. 2007. PRAS40 Regulates mTORC1 Kinase Activity by Functioning as a Direct Inhibitor of Substrate Binding. *Journal of Biological Chemistry,* 282**,** 20036-20044.

WATT, K. D. 2011. Metabolic syndrome: is immunosupression to blame? *Liver Transplantation,* 3**,** 38-42.

WENDE, A. R., O'NEILL, B. T., BUGGER, H., RIEHLE, C., TUINEI, J., BUCHANAN, J., TSUSHIMA, K., WANG, L., CARO, P., GUO, A., SLOAN, C., KIM, B. J., WANG, X., PEREIRA, R. O., MCCRORY, M. A., NYE, B. G., BENAVIDES, G. A., DARLEY-USMAR, V. M., SHIOI, T., WEIMER, B. C. & ABEL, E. D. 2015. Enhanced Cardiac Akt/Protein Kinase B Signaling Contributes to Pathological Cardiac Hypertrophy in Part by Impairing Mitochondrial Function via Transcriptional Repression of Mitochondrion-Targeted Nuclear Genes. *Molecular and Cellular Biology,* 35**,** 831-846.

WOOD, S. L., EMMISON, N., BORTHWICK, A. C. & YEAMAN, S. J. 1993. The protein phosphatases responsible for dephosphorylation of hormone-sensitive lipase in isolated rat adipocytes. *Biochemical Journal,* 295**,** 531-535.

ZENG, Z., SARBASSOV, D. D., SAMUDIO, I. J., YEE, K. W. L., MUNSELL, M. F., ELLEN JACKSON, C., GILES, F. J., SABATINI, D. M., ANDREEFF, M. & KONOPLEVA, M. 2007. Rapamycin derivatives reduce mTORC2 signaling and inhibit AKT activation in AML. *Blood,* 109**,** 3509-3512.

ZHANG, H. H., HUANG, J., DÜVEL, K., BOBACK, B., WU, S., SQUILLACE, R. M., WU, C.-L. & MANNING, B. D. 2009. Insulin Stimulates Adipogenesis through the Akt-TSC2-mTORC1 Pathway. *PLOS ONE,* 4**,** e6189.

ZHANG, Y., BOKOV, A., GELFOND, J., SOTO, V., IKENO, Y., HUBBARD, G., DIAZ, V., SLOANE, L., MASLIN, K., TREASTER, S., RÉNDON, S., VAN REMMEN, H., WARD, W., JAVORS, M., RICHARDSON, A., AUSTAD, S. N. & FISCHER, K. 2014. Rapamycin Extends Life and Health in C57BL/6 Mice. *The Journals of Gerontology Series A: Biological Sciences and Medical Sciences,* 69A**,** 119-130.

Anexo

Artículos Publicados

Biochimica et Biophysica Acta 1861 (2016) 1929–1941

Contents lists available at ScienceDirect

Biochimica et Biophysica Acta

journal homepage: www.elsevier.com/locate/bbalip

Rapamycin negatively impacts insulin signaling, glucose uptake and uncoupling protein-1 in brown adipocytes

Ester García-Casarrubios [a,1], Carlos de Moura [a,b,1], Ana I Arroba [a,c,1], Nuria Pescador [c], María Calderon-Dominguez [d,e], Laura Garcia [a], Laura Herrero [d,e], Dolors Serra [d,e], Susana Cadenas [f,g], Flavio Reis [b,h], Eugenia Carvalho [b,i,j,*], Maria Jesus Obregon [a], Ángela M Valverde [a,c,**]

[a] Institute of Biomedicine Alberto Sols (CSIC/UAM), E-28029 Madrid, Spain
[b] Center for Neuroscience and Cell Biology, University of Coimbra, E-3000 Coimbra, Portugal
[c] Centro de Investigación Biomédica en Red de Diabetes y Enfermedades Metabólicas Asociadas (CIBERDEM), Instituto de Salud Carlos III, Spain
[d] Department of Biochemistry and Physiology, Institut de Biomedicina de la Universitat de Barcelona (IBUB), Universitat de Barcelona, E-08028 Barcelona, Spain
[e] Centro de Investigación Biomédica en Red de Fisiopatología de la Obesidad y la Nutrición (CIBEROBN), Instituto de Salud Carlos III, E-28029 Madrid, Spain
[f] Centro de Biología Molecular "Severo Ochoa" (CSIC-UAM) and Departamento de Biología Molecular, Universidad Autónoma de Madrid, 28049 Madrid, Spain
[g] Instituto de Investigación Sanitaria Princesa (IIS-IP), 28006 Madrid, Spain
[h] Laboratory of Pharmacology and Experimental Therapeutics, Institute for Biomedical Imaging and Life Sciences (IBILI), Faculty of Medicine, University of Coimbra, E-3000-548 Coimbra, Portugal
[i] Department of Geriatrics, University of Arkansas for Medical Sciences, Little Rock, AR 72202, United States
[j] Arkansas Children's Research Institute, Little Rock, AR 72202, United States

ARTICLE INFO

Article history:
Received 9 June 2016
Received in revised form 20 September 2016
Accepted 22 September 2016
Available online 26 September 2016

Keywords:
NODAT
Brown adipocytes
Insulin signaling
Thermogenesis
Bioenergetics

ABSTRACT

New onset diabetes after transplantation (NODAT) is a metabolic disorder that affects 40% of patients on immunosuppressive agent (IA) treatment, such as rapamycin (also known as sirolimus). IAs negatively modulate insulin action in peripheral tissues including skeletal muscle, liver and white fat. However, the effects of IAs on insulin sensitivity and thermogenesis in brown adipose tissue (BAT) have not been investigated. We have analyzed the impact of rapamycin on insulin signaling, thermogenic gene-expression and mitochondrial respiration in BAT. Treatment of brown adipocytes with rapamycin for 16 h significantly decreased insulin receptor substrate 1 (IRS1) protein expression and insulin-mediated protein kinase B (Akt) phosphorylation. Consequently, both insulin-induced glucose transporter 4 (GLUT4) translocation to the plasma membrane and glucose uptake were decreased. Early activation of the N-terminal Janus activated kinase (JNK) was also observed, thereby increasing IRS1 Ser 307 phosphorylation. These effects of rapamycin on insulin signaling in brown adipocytes were partly prevented by a JNK inhibitor. In vivo treatment of rats with rapamycin for three weeks abolished insulin-mediated Akt phosphorylation in BAT. Rapamycin also inhibited norepinephrine (NE)-induced lipolysis, the expression of peroxisome proliferator-activated receptor γ coactivator 1α (PGC-1α) and uncoupling protein (UCP)-1 in brown adipocytes. Importantly, basal mitochondrial respiration, proton leak and maximal respiratory capacity were significantly decreased in brown adipocytes treated with rapamycin. In conclusion, we demonstrate, for the first time the important role of brown adipocytes as target cells of rapamycin, suggesting that insulin resistance in BAT might play a major role in NODAT development.

1. Introduction

Immunosuppressive therapy accounts for the remarkable success attained in organ transplant survival. On the other hand, some immunosuppressive agents (IAs) have shown several metabolic side effects such as hypertension, dyslipidemia and new onset diabetes after transplant (NODAT) [1]. NODAT has been defined as a heterogeneous condition of abnormal glucose tolerance with variable onset, duration and severity, with similar diagnosis criteria as type 2 diabetes mellitus (T2D). It is also referred to as post-transplantation diabetes mellitus (PTDM) sharing characteristics with T2D, but the pathophysiology may differ [2], recommending particular diagnosis and attention [3].

Abbreviations: NODAT, new onset diabetes after transplantation; IAs, immunosuppressive agents; BAT, brown adipose tissue; Akt, protein kinase B; mTOR, mammalian target of rapamycin; GLUT4, glucose transporter 4; IRS, insulin receptor substrate; JNK, N-terminal Janus activated kinase; NE, norepinephrine; UCP-1, uncoupling protein-1; Ser, serine; Thr, threonine.

* Correspondence to: E. Carvalho, Center for Neuroscience and Cell Biology, Rua Larga, E-3004-517 Coimbra, Portugal.
** Correspondence to: Á. M. Valverde, Instituto de Investigaciones Biomédicas Alberto Sols, C/ Arturo Duperier 4, 28029 Madrid, Spain.
E-mail addresses: ecarvalh@cnc.uc.pt (E. Carvalho), avalverde@iib.uam.es (Á.M. Valverde).
[1] Equal contributors.

http://dx.doi.org/10.1016/j.bbalip.2016.09.016
1388-1981/

Rapamycin, the mammalian target of rapamycin (mTOR) inhibitor, has been used in clinical practice as an alternative to classical IAs such as steroids, mycophenolate mofetil and calcineurin inhibitors to minimize their serious side-effects, including nephrotoxicity, hypertension, dyslipidemia, insulin resistance and NODAT [4–6], increasing the risk of cardiovascular disease [7]. Despite its higher immunosuppressive capacity, rapamycin is also associated with several severe side effects; however, the molecular mechanisms remain to be elucidated [8–9].

Studies from our group and others have shown that rapamycin reduces insulin sensitivity in peripheral tissues, including liver and muscle in rodents and white adipose tissue (WAT) in both human and rodents [10–14]. Although the precise mechanisms remain to be elucidated, rapamycin treatment impairs lipolysis, insulin-stimulated glucose uptake and inhibits insulin signaling in white adipocytes, playing a major role in rapamycin-induced insulin resistance [10,13,15–16]. However, no studies have yet been performed to address the effects of rapamycin in brown adipose tissue (BAT).

Despite having been considered an irrelevant tissue in adult humans for a long time, consistent results have now revealed the metabolic relevance of BAT, in particular its important role in the regulation of thermogenesis and energy homeostasis [17–18]. BAT contains uncoupling protein-1 (UCP-1), which uncouples oxidative phosphorylation releasing energy stored in the mitochondrial proton electrochemical gradient as heat in response to catecholamines. In addition, BAT is a major site for lipid metabolism, fatty acids being the main fuel to maintain the thermogenic capacity of the tissue [19]. High metabolic activity from BAT has been identified mainly in the cervical and supraclavicular areas in adult humans by ^{18}F-deoxyglucose (FDG)-positron emission tomography (PET)-computed tomography (CT) [20–27]. These studies demonstrate that BAT is not only present but it is indeed active in adult humans with significant importance in whole-body glucose homeostasis when activated. In addition, subcutaneous white adipocytes can gain a browning phenotype after severe adrenergic stress [28].

Growing evidence shows that impaired BAT function is also involved in the development of insulin resistance. In particular, BAT lipoatrophy can induce visceral adiposity, severe glucose intolerance, high postprandial glucose levels and a defect in acute insulin secretion [29–30]. Moreover, these effects might be linked to mTOR, as suggested using adipocyte-specific mTOR-knockout mice with both mTORC1 and mTORC2 complexes deleted [31]. This study showed that ablation of mTOR, a critical regulator of adipogenesis and systemic energy metabolism, decreased both BAT and WAT mass and caused insulin resistance in mice.

While many studies have evaluated the effect of IAs, in particular rapamycin, in WAT, no studies have tested the effects of rapamycin in BAT. Therefore, the goal of this work was to analyze the impact of rapamycin in insulin sensitivity, thermogenic gene expression and mitochondrial respiration in brown adipocytes.

2. Materials and methods

2.1. Reagents and antibodies

Cell culture reagents were from Invitrogen (Carlsbad, CA, USA). Insulin, NE and CL316243 were from Sigma (Sigma-Aldrich, Saint Louis, MO, USA). The anti-Large T antigen (LTAg) antibody was kindly provided by J. de Caprio (Dana Farber Cancer Institute, Boston, MA). Anti-phospho JNK (Thr 183/Tyr 185) (#4668), anti-phospho HSL (Ser 660) (#4126) and anti-Akt (#9272) antibodies were from Cell Signaling Technology (MA, USA). Rapamycin, anti-phospho IR (Tyr 1162/Tyr 1163) (sc-25103-R), anti-IR (sc-711), anti-JNK (sc-571), anti-phospho Akt1/2/3 (Ser 473) (sc-7985-R), anti-phospho Akt1/2/3 (Thr 308) (sc-16646-R), anti-phospho S6K1 (Thr 389) (sc-11759) and anti-caveolin-1 (sc-894) antibodies were from Santa Cruz (Palo Alto, CA, USA). Anti-IRS1 (06-248) and anti-phospho IRS1 (Ser 307) (07-247) antibodies were from Merck Millipore (Merck KGaA, Darmstadt, Germany). The anti-IRS2 antibody was a gift of M. White (Boston Children's Hospital, Boston, USA). The anti-GLUT-4 (AB 1346) antibody was purchased from Chemicon (Chemicon International, CA, USA). The anti-UCP-1 antibody was purchased from Abcam (Cambridge, UK). SP600125 was purchased from Calbiochem (Merck KGaA, Darmstadt, Germany).

2.2. Generation of an immortalized brown preadipocyte cell line from suckling rats

Brown preadipocytes were isolated from the interscapular BAT of 20-day old suckling Sprague-Dawley rats as previously described [32]. Briefly, after digestion with collagenase A, mature brown adipocytes were allowed to float and then discarded. The infranatant was filtered through a 25 μm silk filter and then centrifuged. Brown preadipocytes were seeded in DMEM supplemented with 10% neonatal calf serum (NCS), 3 nM insulin, 10 mM HEPES, 50 IU penicillin, 50 μg/ml streptomycin and 15 μM ascorbic acid. Precursor cells proliferate actively under these conditions. Once brown preadipocytes reached 50–60% confluence, these cells were infected with retroviral particles encoding SV40 Large T antigen. For this, viral Bosc-23 packaging cells were transfected at 70% confluence by calcium phosphate coprecipitation with 3 μg/6 cm-dish of the puromycin-resistance retroviral vector pBabe encoding attenuated SV40 Large T antigen (kindly provided by J. de Caprio, Dana Farber Cancer Institute, Boston, MA). Then, primary brown preadipocytes were infected with polybrene (4 μg/ml)-supplemented virus for 48 h followed by selection with puromycin (1 μg/ml) for a further 2 weeks. Five different pools of immortalized cells, generated in independent infections, were expanded.

2.3. Differentiation of brown preadipocytes

For differentiation, immortalized brown preadipocytes were grown in DMEM supplemented with 20% fetal calf serum (FCS), 20 nM insulin and 1 nM triiodothyronine (T3) (differentiation medium, DM) until reaching confluence as previously described [33]. Next, the cells were cultured for two days in induction medium (IM) consisting of differentiation medium supplemented with 0.5 μM dexamethasone, 0.125 μM indomethacin and 0.5 mM isobutyl-methyl-xanthine (IBMX). Then, cells were cultured in DM until day 6 that exhibited a fully differentiated phenotype with numerous multilocular lipid droplets in their cytoplasm. To evaluate lipid droplets accumulation, Oil Red O staining was performed. Differentiated brown adipocytes were fixed in 10% paraformaldehyde for 30 min at room temperature. Then, cells were washed with PBS and subsequently rinsed in 60% isopropanol for 5 min to facilitate the staining of neutral lipids and stained with filtered Oil Red O working solution (0.3% Oil Red O in isopropanol) for 15 min. The excess of Oil Red O was removed by rinsing the culture dishes with water for several times.

2.4. Preparation of protein extracts and Western blot

Cells were scraped off in ice-cold PBS, pelleted by centrifugation at 4000 ×*g* for 10 min at 4 °C and resuspended in buffer containing 10 mM Tris-HCl, 5 mM EDTA, 50 mM NaCl, 30 mM disodium pyrophosphate, 50 mM NaF, 100 μM Na3VO4, 1% Triton X-100, 1 mM phenylmethylsulfonyl fluoride, 10 μg/ml leupeptin and 10 μg/ml aprotinin pH 7.6 (lysis buffer). Cell lysates were clarified by centrifugation at 12,000 ×*g* for 10 min at 4 °C. Protein content was determined by the Bradford method, using the Bio-Rad reagent and BSA as the standard. After SDS-PAGE, proteins were transferred to Immobilon membranes (Merck-Millipore), blocked using 5% non-fat dried milk or 3% bovine serum albumin (BSA) in 10 mM Tris-HCl, 150 mM NaCl pH 7.5, and incubated overnight with the antibodies indicated in 0.05% Tween-20, 10 mM Tris-HCl, 150 mM NaCl pH 7.5. Immunoreactive bands were visualized using the ECL Western blotting protocol (Merck-Millipore).

2.5. Quantitative real-time PCR

Total RNA was extracted with Trizol (Invitrogen). Complementary DNA (cDNA) was synthesized by reverse transcription PCR (RT-PCR) from 1 μg of RNA using iScript cDNA synthesis kit (BioRad, Hercules, CA). For qPCR, each cDNA sample was run in an ABI 7300 in triplicate well, in the following PCR program: 50 °C for 2 min, 94 °C for 10 min, and 30 cycles of 97 °C for 30 s followed by 60 °C for 1 min. Rat *Ucp1* mRNA was quantified using specific FAM™ dye-labeled TaqMan® probes for rat *Ucp1* (Rn00562126-m1; Gene expression assays, Applied Biosystems, Foster City, CA) and rat *Pgc1a* (Rn00580241_m1; Gene expression assays, Applied Biosystems, Foster City, CA). Results were normalized using VIC® dye-labeled TaqMan® probe for rat ubiquitin (Rn01789812-g1, Applied Biosystems).

2.6. Measurement of glucose uptake

At the end of the culture, differentiated brown adipocytes were serum-deprived for 2 h. Then, cells were washed with ice-cold Krebs-Ringer-phosphate buffer (KRP) (135 mM NaCl, 5.4 mM KCl, 1.4 mM $CaCl_2$, 1.4 mM $MgSO_4$, 10 mM sodium pyrophosphate, pH 7.4) and incubated with 1 ml KRP buffer with or without insulin for 10 min at 37 °C. 2-Deoxy-D [1-^{3}H]glucose (500 nCi/ml) was added to this solution, and the incubation was continued for 5 min at 37 °C. The cells were then washed with ice-cold KRP buffer and solubilized in 1 ml 1% SDS, as previously described [34–36]. Glucose uptake was expressed as pmoles per mg protein.

2.7. Analysis of GLUT4 translocation to the plasma membrane

Cells were washed with ice-cold PBS and scraped into homogenization buffer containing 20 mm Tris-HCl, 2 mm EGTA, 2 mm EDTA, 1 mm phenylmethylsulfonyl fluoride, 10 mm β-mercaptoethanol, 10 μg/ml aprotinin, and 10 μg/ml leupeptin (pH 7.4). After 10-min incubation, cells were homogenized with 30 strokes of a Dounce homogenizer using a tight-fitting pestle. Nuclei were pelleted by centrifugation at 500 ×g for 5 min, and the low-speed supernatant was centrifuged at 100,000 ×g for 30 min. The high-speed supernatant constituted the internal membrane fraction and the pellet which contained the plasma membrane fraction was washed three times and extracted in ice-cold homogenization buffer containing 1% Triton X-100 for 60 min. The Triton-soluble component (plasma membrane fraction) was separated from the Triton-insoluble material (cytoskeletal fraction) by centrifugation at 100,000 ×g for 15 min. The plasma membrane fraction was kept at −70 °C before protein quantification and Western blotting with antibodies against GLUT4 and caveolin-1, a plasma membrane protein used as the loading control.

2.8. Immunofluorescence and confocal imaging

Brown preadipocytes were differentiated on glass coverslips, fixed in 4% paraformaldehyde and processed for immunofluorescence. Briefly, anti-GLUT4 (sc-56566, Santa Cruz) primary antibody was applied for 1 h at 37 °C in PBS-1% BSA at 1/50 dilution. The secondary antibody used was Alexa 488 goat anti-mouse (Invitrogen) at 1/500 dilution. Cell nuclei were counterstained with DAPI (Sigma). Immunofluorescence was examined in a Nikon Eclipse 90i microscope with imaging software Nis elements.

2.9. In vivo treatment

Ten weeks old male Wistar rats, obtained from Charles River Lab. Inc. (Barcelona, Spain), housed (two animals per cage) in individually ventilated cages racks and subjected to 12/12 h dark/light cycles and given standard laboratory rat chow (IPM-R20, Letica, Barcelona, Spain) and free access to tap water, were treated with 1 mg/kg body weight (BW)/day of rapamycin (Rapamune®, Laboratorios Pfizer Lda., Lisbon, Portugal), thus mimicking a clinical relevant dose, as previously described [10]. Treatment was performed by oral gavage, daily, for 3 weeks, and body weight was monitored daily. At the end of the treatment, animals were intraperitoneally injected 10 U/kg of human recombinant insulin (Actrapid) and sacrificed 10 min latter by cervical dislocation. BAT was removed and used to analyze insulin signaling. Rapamycin blood concentrations were assessed by immunoassay using automatic methods (Flex reagent) and equipment (Dimension®-RxL, Siemens, Germany). Animal studies were conducted using protocols approved by to the National and European Community Council Directives on Animal Care.

2.10. Homogenization and preparation of tissue extracts

Frozen BAT samples were homogenized in 16 volumes (w/v) of ice-cold lysis buffer containing 50 mM Tris-HCl, 1% Triton X-100, 2 mM EGTA, 10 mM EDTA acid, 100 mM NaF, 1 mM Na4P2O7, 2 mM Na3VO4, 100 μg/ml phenylmethylsulfonyl fluoride, 1 μg/ml aprotinin, 1 μg/ml pepstatin A and 1 μg/ml leupeptin. Samples were homogenized in the same lysis buffer using the Brinkmann PT 10/35 Polytron. Extracts were kept ice-cold at all times. Tissue extracts were cleared by centrifugation at 40,000 ×*g* for 20 min at 4 °C. The supernatant was aliquoted and stored at −70 °C.

2.11. Measurement of glycerol release

After treatment of brown adipocytes with NE or the β3 agonist CL316243, cell medium was removed and glycerol content was measured using a commercial kit (Biosystems, Barcelona, Spain) according to the manufacturer's instructions. Samples were normalized by the protein concentration of each well.

2.12. Evaluation of mitochondrial respiration in brown adipocytes

The Seahorse XF24 Extracellular Flux Analyzer (Seahorse Bioscience, www.seahorsebio.com) was used to measure oxygen consumption rate (OCR) in brown adipocytes. Cells were differentiated in customized Seahorse 24-well plates and treated with 100 nM rapamycin for 16 h. Before the measurement, cells were incubated for 1 h with XF Assay Medium (Seahorse Bioscience) plus 5 mM glucose. OCR was calculated by plotting the O_2 tension of media as a function of time (pmol/min), and data were normalized by the protein concentration measured in each individual well. The results were quantified as the mean of 8–10 wells ± standard error of the mean (SEM) per time point in at least three independent experiments.

2.13. Statistical analysis

Results are given as mean ± SEM using GraphPad Prism, version 5 (GraphPad Software, San Diego, CA, USA). Statistical analyses using the Student's *t*-test were performed when two groups were considered. For multiple group comparisons, the One-Way ANOVA test, followed by the post hoc Bonferroni's Multiple Comparison was used. Differences were considered significant when $^*p < 0.05$.

3. Results

3.1. Effect of rapamycin on insulin signaling cascade in brown adipocytes

To study the impact of rapamycin on insulin-mediated signaling in brown adipocytes, we generated an immortalized preadipocyte cell line from the interscapular BAT of 20-day old suckling rats. Brown preadipocytes were seeded and differentiated as described in Materials and methods. At day 6, cells reached a fully differentiated phenotype as shown by the accumulation of multilocular lipid droplets

(Supplementary Fig. 1A), as well as by the expression of adipogenic markers such as fatty acid synthase (FAS), GLUT4 and the thermogenic marker UCP-1 (Supplementary Fig. 1B). As reported in mouse brown preadipocytes [37], before differentiation, rat brown preadipocytes presented low IR expression, gradually increasing during differentiation in a time-dependent manner. Conversely, the expression of the IGF-IR was higher in brown preadipocytes, decreased at day 3 of differentiation and remained low at day 6.

IRS1 is a critical node in the insulin signaling cascade in brown adipocytes [38–40]. Thus, we analyzed IRS1 protein levels in differentiated brown adipocytes treated with rapamycin (10–100 nM) for 16 h. As shown in Fig. 1A, IRS1 protein expression decreased in brown adipocytes incubated with rapamycin in a dose-dependent manner. Notably, after 100 nM rapamycin treatment, IRS1 was barely detected whereas the expression levels of IRS2 and Akt were not altered. The effect of rapamycin at the doses used in brown adipocytes was assessed by the inhibition of S6K1 phosphorylation, a direct mTORC1 substrate, compared to untreated cells.

Next, we investigated the effect of rapamycin on the modulation of insulin signaling in brown adipocytes, including the activation of Akt that regulates adipogenic- and thermogenic-related gene expression downstream of IRS1 [38,40–41]. Pretreatment of brown adipocytes with rapamycin for 16 h increased tyrosine phosphorylation of the IR upon insulin stimulation, although not reaching statistical significance

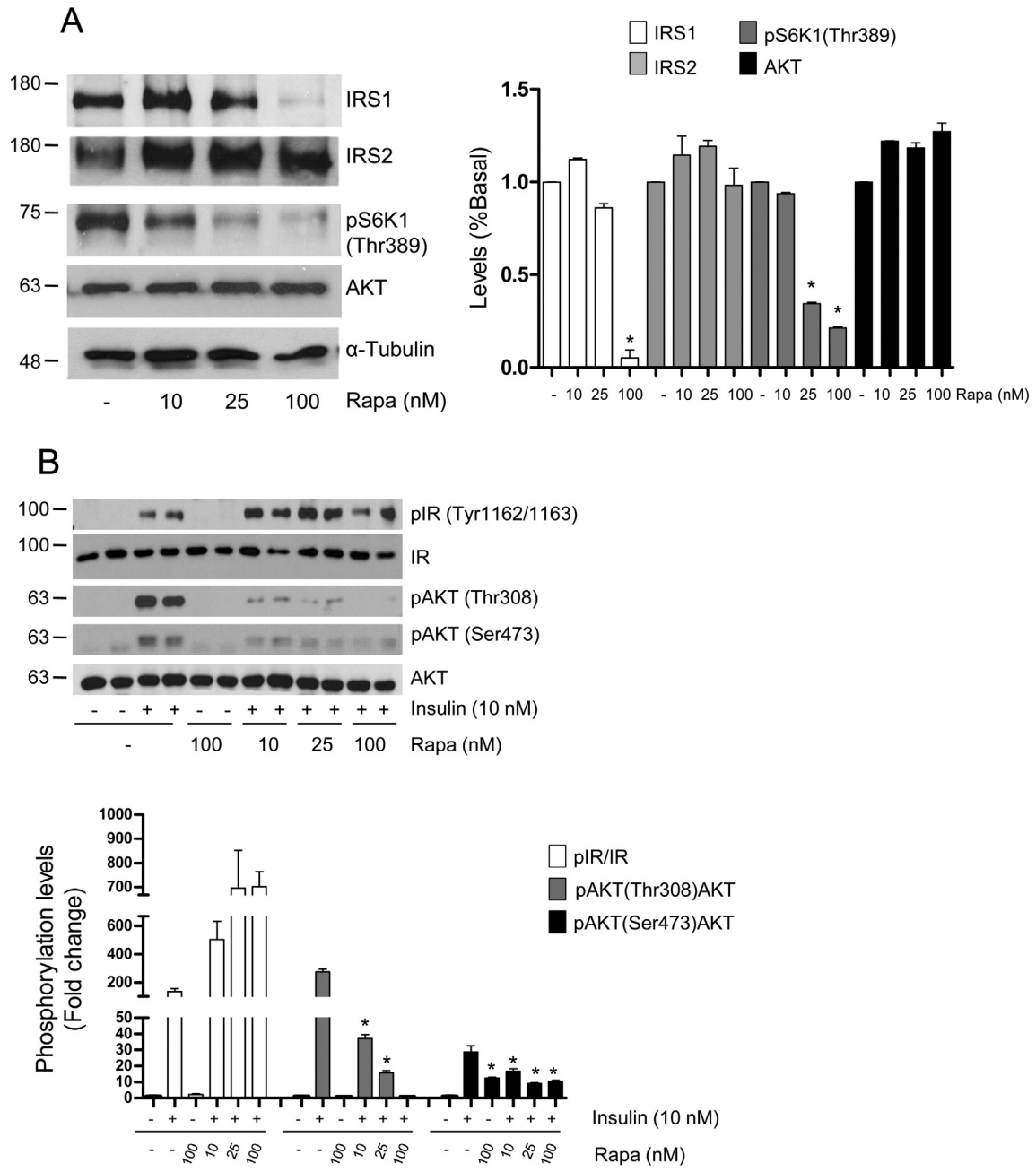

Fig. 1. Long-term treatment with rapamycin induced IRS1 degradation and impaired Akt-mediated insulin signaling in brown adipocytes. A. Differentiated rat brown adipocytes (day 6) were cultured in the presence of several doses of rapamycin (Rapa) for 16 h. At the end of the culture time, brown adipocytes were harvested and whole cell lysates were prepared. Total protein was analyzed by Western blot using antibodies against IRS1, IRS2, Akt, phospho-S6K1 (Thr 389) and α-Tubulin as loading control. Results of 3 independent experiments were quantified by scanning densitometry. Results are means ± SEM. *$p < 0.05$, versus basal. B. Differentiated brown adipocytes were treated with different doses of rapamycin or left untreated. Then, cells were serum-deprived for 2 h and further stimulated with 10 nM insulin for 10 min. Total protein was analyzed by Western blot using anti-phospho IR (Tyr 1162/1163), anti-IR, anti-phospho-Akt (Ser 473), anti-phospho-Akt (Thr 308) and anti-Akt specific antibodies. Results of 4 independent experiments were quantified by scanning densitometry. Results are means ± SEM. *$p < 0.05$ versus insulin-stimulated cells without rapamycin treatment.

(Fig. 1B). However, rapamycin significantly decreased insulin-induced Akt phosphorylation at both Ser 473 (regulatory domain) and Thr 308 (catalytic domain) residues in a dose-dependent manner.

Furthermore, we addressed the question of whether or not the decrease in IRS1 protein levels by the long-term rapamycin (16 h) treatment of brown adipocytes was responsible for the decreased insulin-induced Akt phosphorylation. To this aim, brown adipocytes were treated with rapamycin or vehicle for 45 min and IRS1 protein levels were analyzed. No differences in IRS1 protein levels were observed between the 2 groups of cells (Fig. 2A). In another experiment, cells were treated with rapamycin for 45 min followed by 10 min insulin stimulation and Akt phosphorylation was evaluated. Rapamycin pretreatment for 45 min inhibited S6K1 phosphorylation, but failed to decrease insulin-mediated Akt phosphorylation (Fig. 2B).

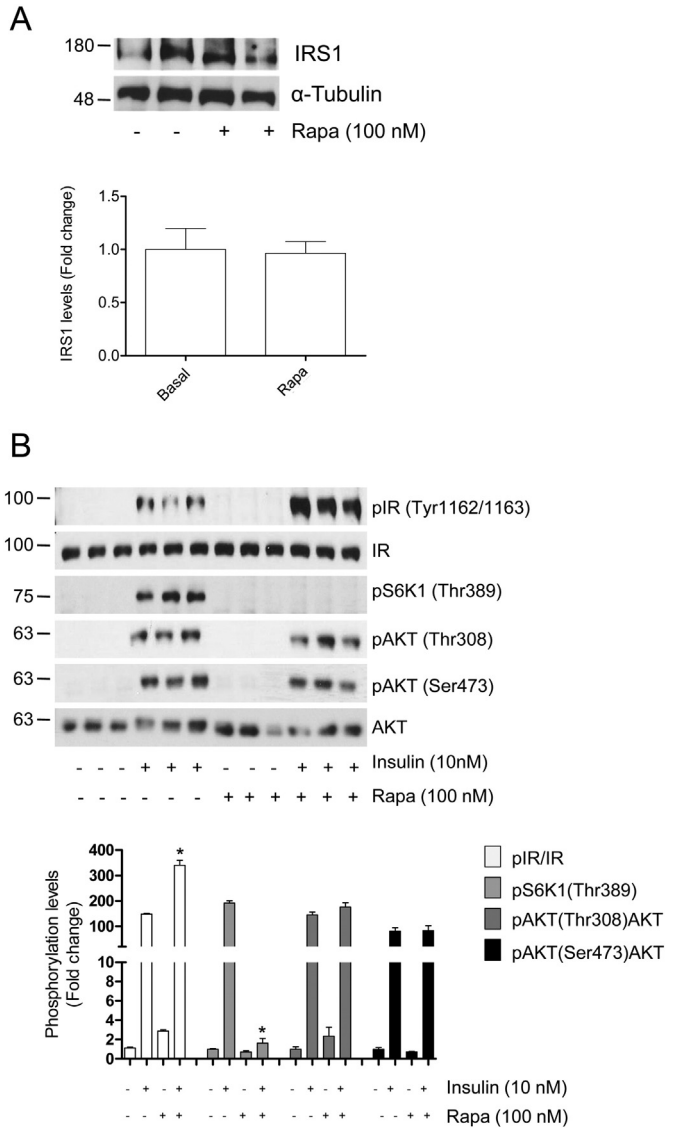

Fig. 2. Short-term treatment with rapamycin did not impair insulin signaling in brown adipocytes. A. Differentiated rat brown adipocytes were cultured in the presence of 100 nM rapamycin for 45 min. Total protein was analyzed by Western blot using antibodies against IRS1 and α-Tubulin as loading control. B. Differentiated rat brown adipocytes (day 6) were cultured in the presence of 100 nM rapamycin (Rapa) for 45 min or left untreated. Then, cells were stimulated with 10 nM insulin for 10 min. Total protein was analyzed by Western blot using antibodies against phospho IR (Tyr 1162/1163), IR, phospho-S6K1 (Thr 389), phospho-Akt (Ser 473), phospho-Akt (Thr 308) and Akt. Results from 3 independent experiments were quantified by scanning densitometry. Results are means ± SEM. *p < 0.05 versus insulin-stimulated cells.

3.2. Effect of rapamycin on insulin-induced glucose uptake and GLUT4 translocation in brown adipocytes

Since insulin induces glucose uptake in a PI 3-kinase/Akt-dependent manner in primary fetal brown adipocytes [42–43], we assessed the effect of rapamycin on insulin-induced glucose uptake in brown adipocytes. Differentiated brown adipocytes were pretreated with 100 nM rapamycin for 16 h and glucose uptake was measured after insulin stimulation for 10 min, resulting in a 2.5-fold increase in glucose uptake compared to control cells (Fig. 3A). Interestingly, this response was

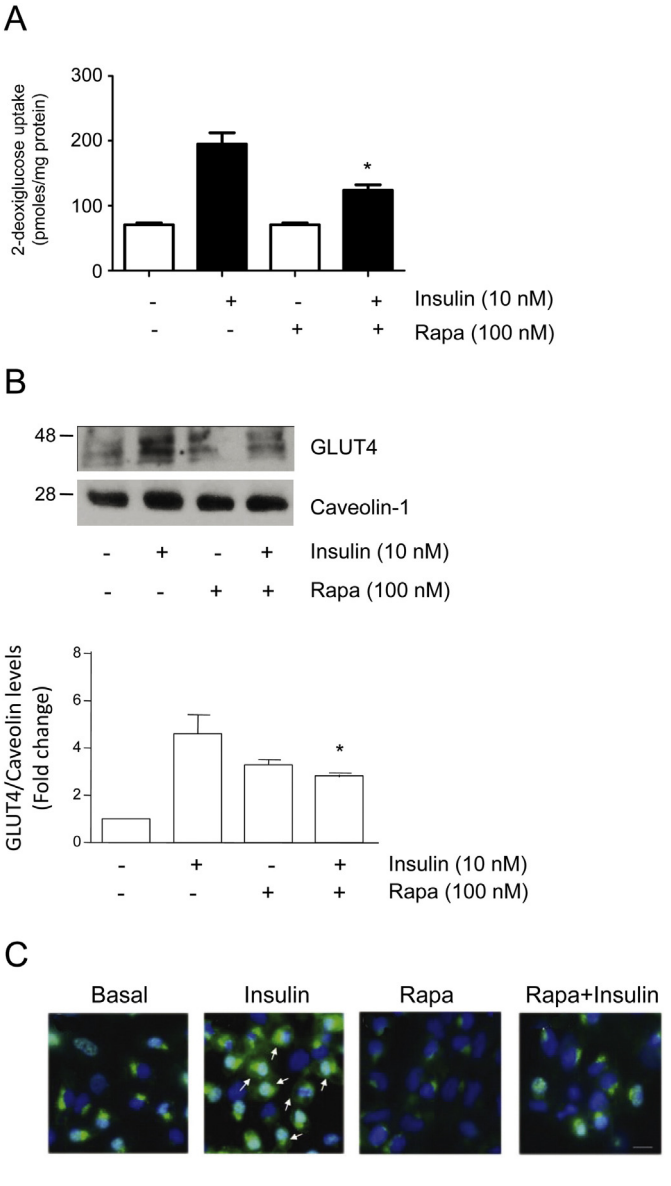

Fig. 3. Rapamycin decreased insulin-induced glucose uptake and GLUT4 translocation. A. 2-Deoxy-D[1-^{3}H]glucose uptake was measured following stimulation of differentiated brown adipocytes with or without rapamycin (Rapa) for 16 h and insulin for 10 min. Results are expressed as pmoles per mg protein and are means ± SEM of 4 independent experiments performed in duplicate. *p < 0.05 versus insulin-stimulated cells. B. Representative Western blot detecting GLUT4 in plasma membrane extracts using caveolin-1 as a plasma membrane loading control. The graph represents the quantification of GLUT4 translocation to the plasma membrane. Results are means ± SEM of 3 independent experiments. *p < 0.05 versus insulin-stimulated cells. C. Immunofluorescence of GLUT4 in the conditions indicated. GLUT4 located at the plasma membrane is indicated by arrows (scale bar 10 μm). Representative images of 5 independent experiments are shown.

significantly decreased in cells pretreated for 16 h with rapamycin. In addition, GLUT4 translocation to the plasma membrane was evaluated by subcellular fractionation and Western blot using caveolin-1 as the loading control [44]. Insulin stimulation increased GLUT4 protein content at the plasma membrane, an effect that was significantly decreased by rapamycin (Fig. 3B). Immunofluorescence analysis depicts a rapid insulin-induced GLUT4 translocation to the plasma membrane in brown adipocytes, whereas it was accumulated in the internal compartments in non-treated cells (Fig. 3C). In contrast, GLUT4 was barely observed at the plasma membrane in brown adipocytes treated with rapamycin prior to insulin stimulation.

3.3. Rapamycin rapidly induced the phosphorylation of c-Jun NH(2)-terminal kinase (JNK) and IRS1 at Ser 307 in brown adipocytes

Activation of stress kinases, particularly JNK, has been shown to inhibit insulin-mediated signaling in peripheral tissues by its ability to induce IRS1 phosphorylation at Ser 307, thereby uncoupling IRS1 from the IR and promoting IRS1 protein degradation [45]. Since rapamycin treatment for 16 h led to reduction in IRS1 protein levels (Fig. 1A), we analyzed JNK phosphorylation in differentiated brown adipocytes treated with 100 nM rapamycin for various time-periods. Rapamycin induced a rapid response in JNK phosphorylation as compared to untreated cells with a maximal effect observed at 30 min, whereas total levels of JNK were unchanged (Fig. 4). By contrast, p38 MAPK phosphorylation was not modulated by rapamycin treatment (data not shown).

To evaluate whether rapamycin-mediated JNK activation was able to phosphorylate IRS1 at Ser residues, we performed Western blot analysis with a phospho-specific anti-IRS1 Ser 307 antibody. In agreement with JNK phosphorylation, treatment of differentiated brown adipocytes with rapamycin for short time periods induced IRS1 phosphorylation at Ser 307 (Fig. 4), while total IRS1 levels remained unchanged. Notably, rapamycin inhibited S6K1 phosphorylation as early as after 15 min of treatment.

3.4. Rapamycin impaired insulin signaling in primary brown adipocytes and BAT from rats

To confirm that the effect of rapamycin on insulin signaling in differentiated brown adipocytes was not due to the immortalization protocol, we tested primary brown adipocytes isolated from 20 day-old suckling rats and allowed them to differentiate spontaneously for 8 days. As shown in Fig. 5A, insulin-mediated Akt phosphorylation was impaired in primary brown adipocytes pretreated with 100 nM rapamycin for 16 h. In addition, rapid JNK and IRS1 (Ser 307) phosphorylation was detected upon rapamycin stimulation, thus excluding effects related to the immortalization of brown preadipocytes (Fig. 5B).

We have recently reported that chronic treatment of Wistar rats with rapamycin resulted in alterations in whole body glucose tolerance, insulin sensitivity and insulin signaling in liver, skeletal muscle and white fat [12]. To get further insights on the effects of rapamycin in BAT in vivo, we analyzed insulin signaling. Akt phosphorylation in response to insulin at both Ser 473 and Thr 309 residues was totally blunted in BAT of rats treated with rapamycin for 3 weeks (Fig. 5C).

3.5. Inhibition of JNK ameliorated the effects of rapamycin in insulin signaling in brown adipocytes

We tested whether rapamycin-mediated inhibition of insulin signaling in brown adipocytes was dependent on the early activation of JNK-

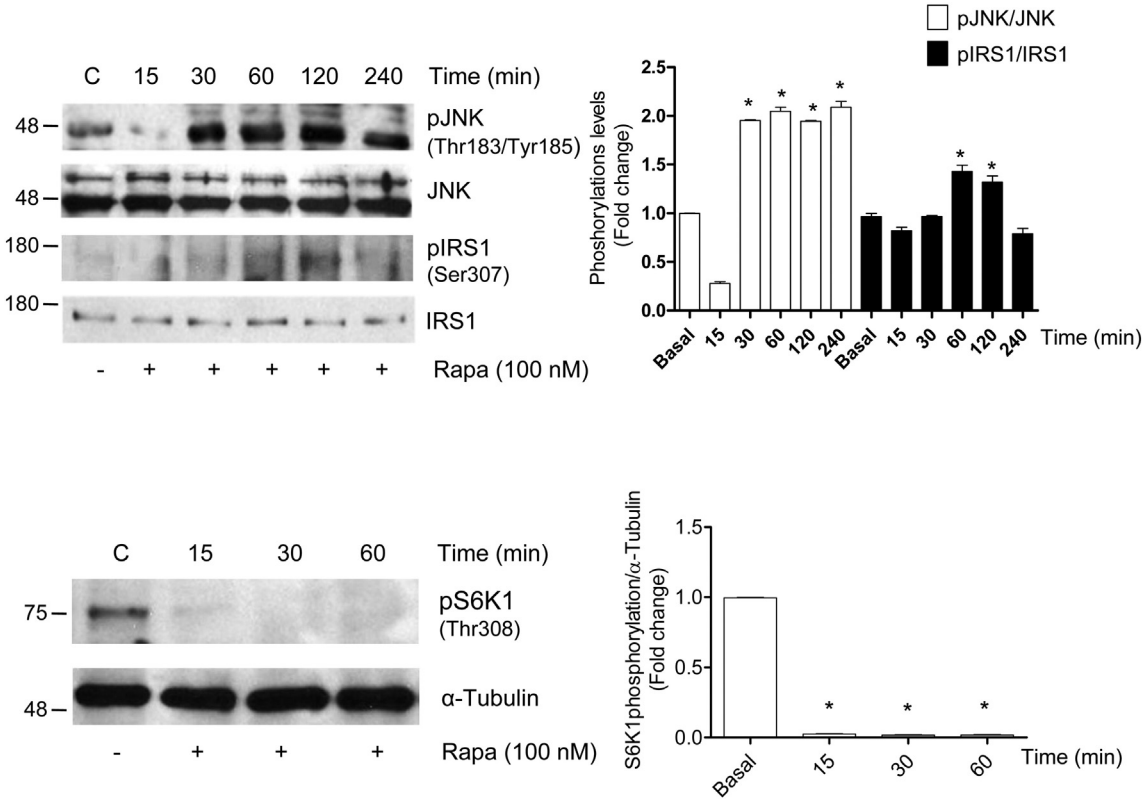

Fig. 4. Rapamycin induced the activation of JNK and phosphorylation of IRS1 at Ser 307 in brown adipocytes. Differentiated brown adipocytes were stimulated with 100 nM rapamycin (Rapa) at the indicated time-periods. Protein extracts were separated by SDS-PAGE and the phosphorylation of IRS1 (Ser 307) and JNK (Thr 183/Tyr 185) was analyzed by Western blot with the corresponding antibodies. Total levels of IRS1 and JNK were also analyzed. Phosphorylation of S6K1 at Thr 389 was analyzed by Western blot. A representative experiment is shown. Results from 3 independent experiments were quantified by scanning densitometry. Phosphorylated levels are referred to the basal (non-stimulated) condition. *$p < 0.05$.

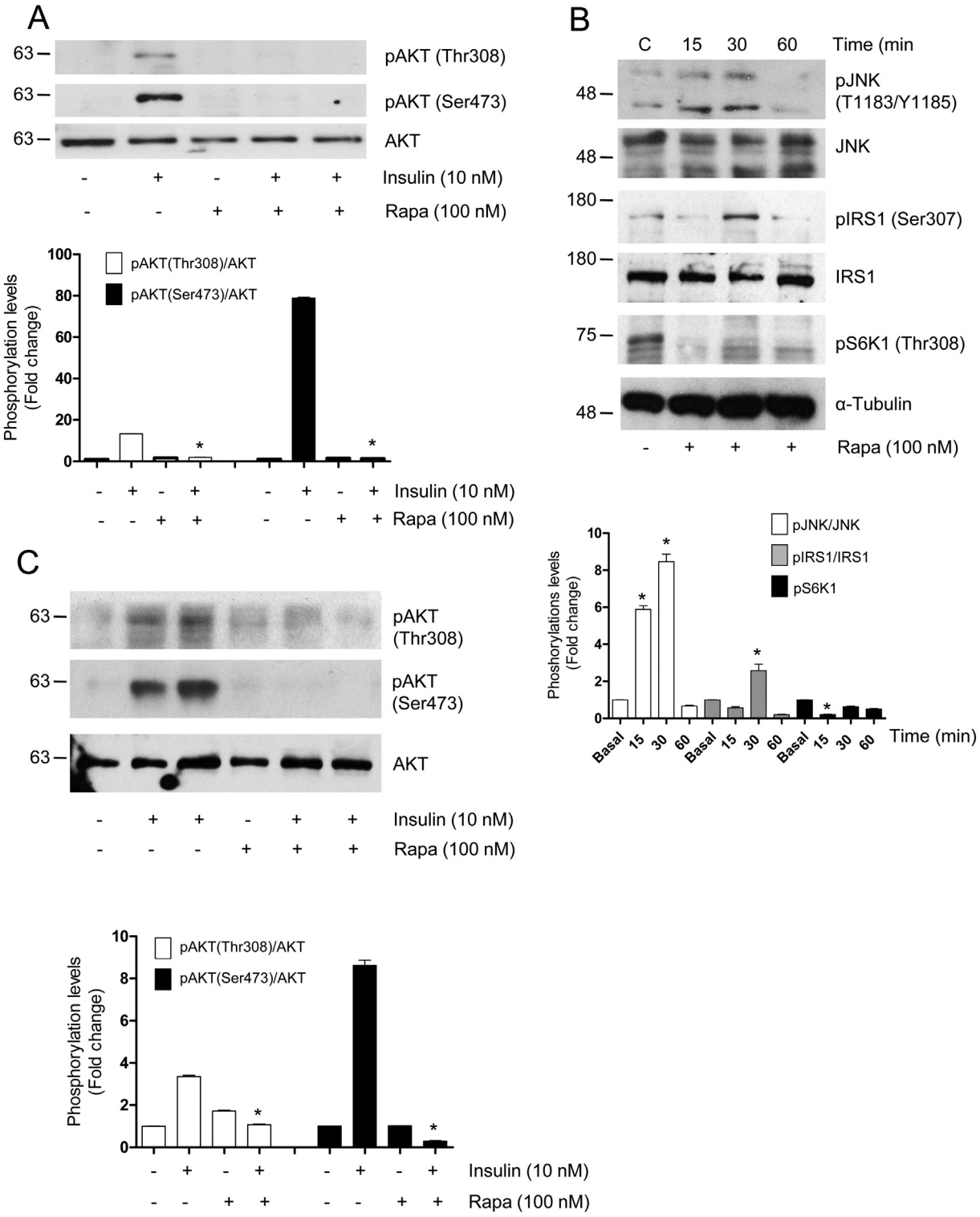

Fig. 5. Rapamycin induced the phosphorylation of JNK and IRS1 (Ser 307) and impaired insulin-mediated Akt phosphorylation in primary brown adipocytes and in BAT from rats. Primary brown preadipocytes were differentiated as described in Materials and methods. A. Cells were treated with rapamycin (Rapa) (100 nM) for 16 h and subsequently stimulated with insulin (10 nM) for 10 min. Total protein was analyzed by Western blot using antibodies against phospho-Akt (Ser 473), phospho-Akt (Thr 308) and Akt. Results of 3 independent experiments performed in duplicate were quantified by scanning densitometry. Results are means ± SEM. *$p < 0.05$ versus insulin-stimulated cells. B. Differentiated primary brown adipocytes were stimulated with 100 nM rapamycin at the indicated time-periods. The phosphorylation of IRS1 (Ser 307), JNK (Thr 183/Tyr 185) and S6K1 (Thr 389) was analyzed by Western blot. Results from 3 independent experiments were quantified by scanning densitometry. Phosphorylated levels are referred to the basal condition. *$p < 0.05$. C. Wistar rats were treated with rapamycin and stimulated with insulin as described in Materials and methods. Phosphorylation of Akt at Ser 473 and Thr 308 residues was analyzed in BAT lysates by Western blot. Phosphorylated levels are referred to the animals injected with vehicle. *$p < 0.05$ versus controls ($n = 6$ animals/group).

mediated IRS1 Ser 307 phosphorylation that leads to its degradation, as previously described [46]. Therefore, cells were treated with rapamycin in the absence or presence of the JNK inhibitor SP600125 [47] for 90 min, time at which IRS1 phosphorylation at Ser 307 was detected (Fig. 4). In brown adipocytes, SP600125 efficiently inhibited JNK phosphorylation at 20 μM concentration (Supplementary Fig. 2). As shown

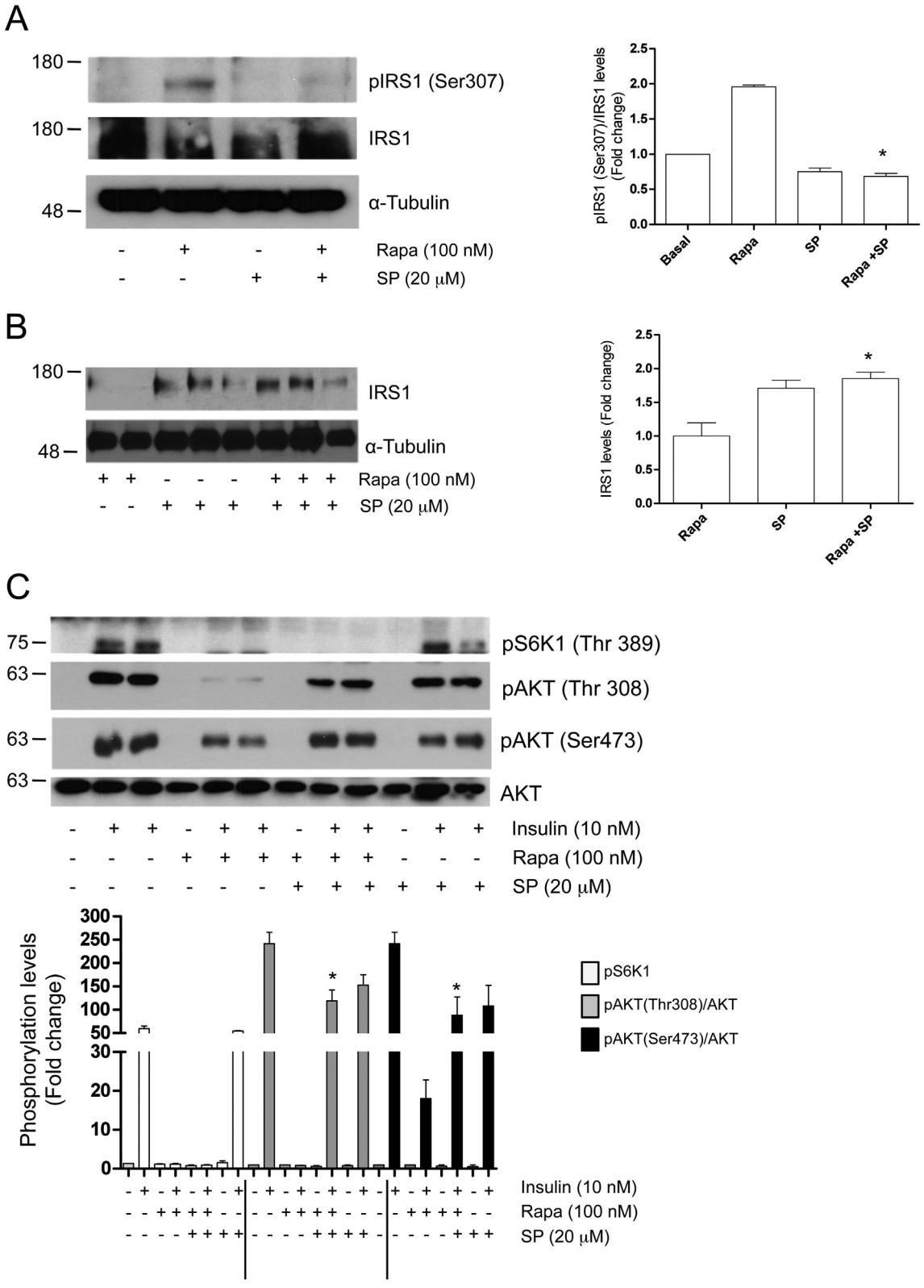

Fig. 6. Inhibition of JNK improved insulin sensitivity in rapamycin-treated brown adipocytes. A. Differentiated brown adipocytes were treated for 90 min with rapamycin (Rapa) (100 nM) in the absence or presence of the JNK inhibitor SP600125 (20 μM). Phosphorylation of IRS1 (Ser 307) was analyzed by Western blot. Results from 3 independent experiments were quantified by scanning densitometry. Phosphorylated levels are referred to the basal condition. *$p < 0.05$. B. Differentiated brown adipocytes were treated for 16 h with rapamycin (100 nM) in the absence or presence of the JNK inhibitor SP600125 (10 μM). IRS1 expression was analyzed by Western blot. Results from 3 independent experiments were quantified by scanning densitometry. IRS1 levels are referred to the rapamycin condition. *$p < 0.05$. C. After 16 h of treatment as described in B, cells were stimulated with 10 nM insulin for 10 min. Total protein was analyzed by Western blot using antibodies against phospho-Akt (Ser 473), phospho-Akt (Thr 308), Akt and phospho-S6K1 (Thr 389). Results of 3 independent experiments were quantified by scanning densitometry. Results are means ± SEM. *$p < 0.05$ versus insulin-stimulated cells pretreated with rapamycin.

in Fig. 6A, IRS1 Ser 307 phosphorylation induced by rapamycin was notably reduced in the presence of SP600125. Also, the co-treatment with rapamycin and SP600125 for 16 h preserved IRS1 protein levels (Fig. 6B) and enhanced insulin-stimulated Akt phosphorylation at both Ser 473 and Thr 308 residues compared to the response of brown adipocytes treated with rapamycin alone (Fig. 6C).

3.6. Rapamycin decreased NE- or β3 agonist CL316243-induced increase in lipolysis and UCP-1 expression in brown adipocytes

The effect of rapamycin on NE and β3 agonist CL316243-stimulated lipolysis was evaluated as an early trigger of thermogenesis activation. Differentiated brown adipocytes were stimulated with either NE or CL316243 at 5 and 2 μM concentrations, respectively, for 4 h. Brown adipocytes were sensitive to both NE and CL316243 in inducing early β-adrenergic signaling, as shown by the increase in hormone-sensitive lipase (HSL) phosphorylation and, consequently, by the release of glycerol to the culture medium (Fig. 7A and B). Pretreatment of brown adipocytes with rapamycin for 16 h significantly decreased the effects of NE and CL316243 on both responses.

The combination of NE plus triiodothyronine (T3) stimulates *Ucp1* mRNA levels in primary rat brown adipocytes [48], thus, the effect of rapamycin on thermogenic gene expression was tested by measuring *Ucp1* and *Pgc1a* mRNA levels. Cells were treated with rapamycin for 16 h

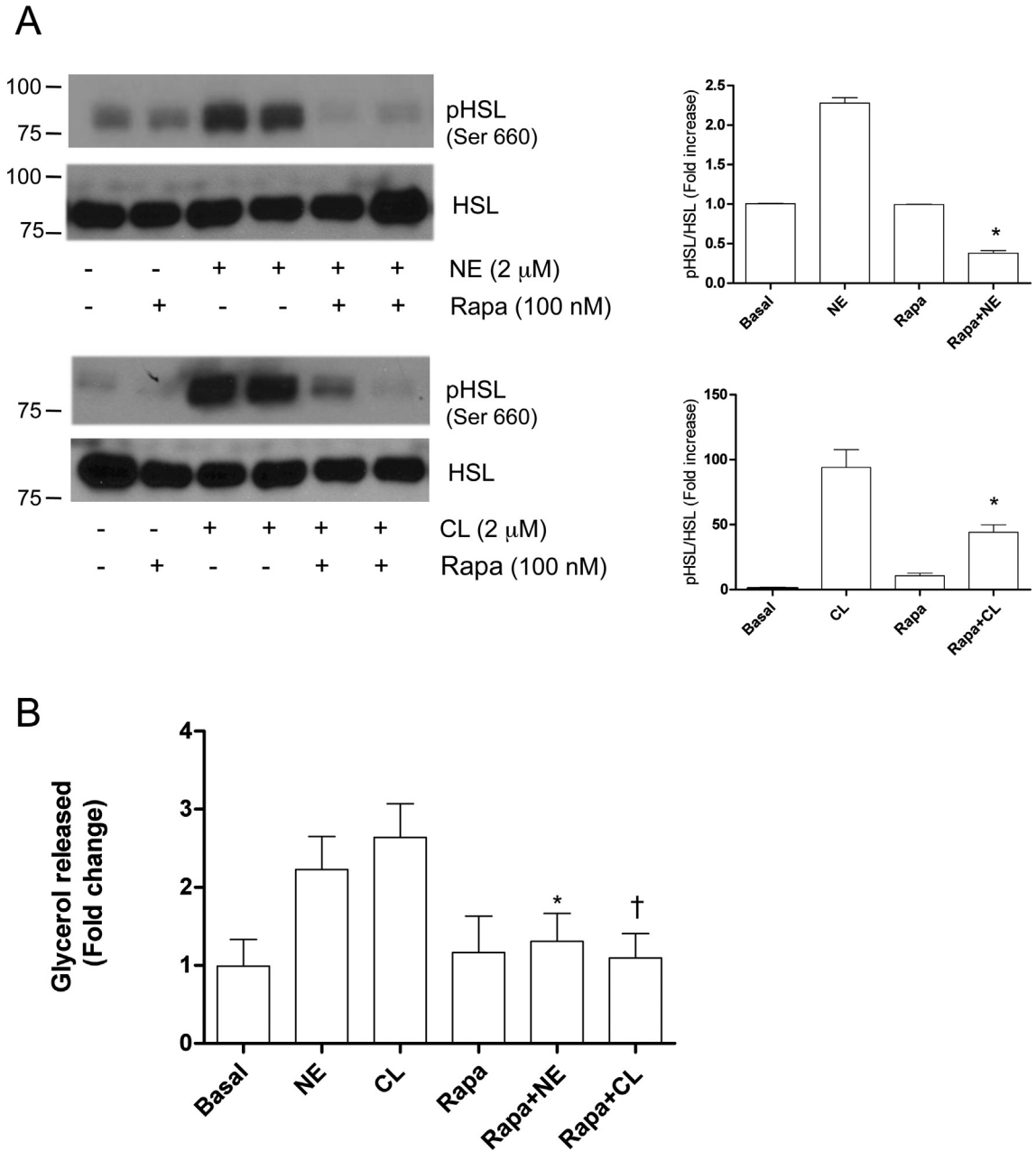

Fig. 7. Rapamycin decreased NE or CL316243-mediated lipolysis in brown adipocytes. Brown adipocytes were treated with rapamycin (Rapa) (100 nM) for 16 h or remained untreated and subsequently stimulated with NE (5 μM) of the β3 agonist CL316243 (2 μM) for a further 4 h. A. Phosphorylation of HSL (Ser 660) was analyzed by Western blot. Results of 3 independent experiments were quantified by scanning densitometry. Results are means ± SEM. *$p < 0.05$ versus NE or CL316243-stimulated cells. B. Glycerol released to the culture medium was measured as described in Materials and methods. Results are expressed as fold change and referred to NE or CL316243-stimulated cells (*†$p < 0.05$) ($n = 3$ independent experiments performed in triplicate).

before addition of NE (5 μM) for 8 h. As shown in Fig. 8A, treatment with NE induced about a 30-fold increase in *Ucp1* and a 3.5-fold increase in *Pgc1a* mRNA levels over basal levels and this effect was blunted by rapamycin.

Due to difficulties in detecting UCP-1 protein in NE-stimulated rat brown adipocytes [48], we performed this analysis in mouse immortalized brown adipocytes previously generated in our laboratory [33], that show higher sensitivity than those isolated from rats [48]. Fig. 8B shows

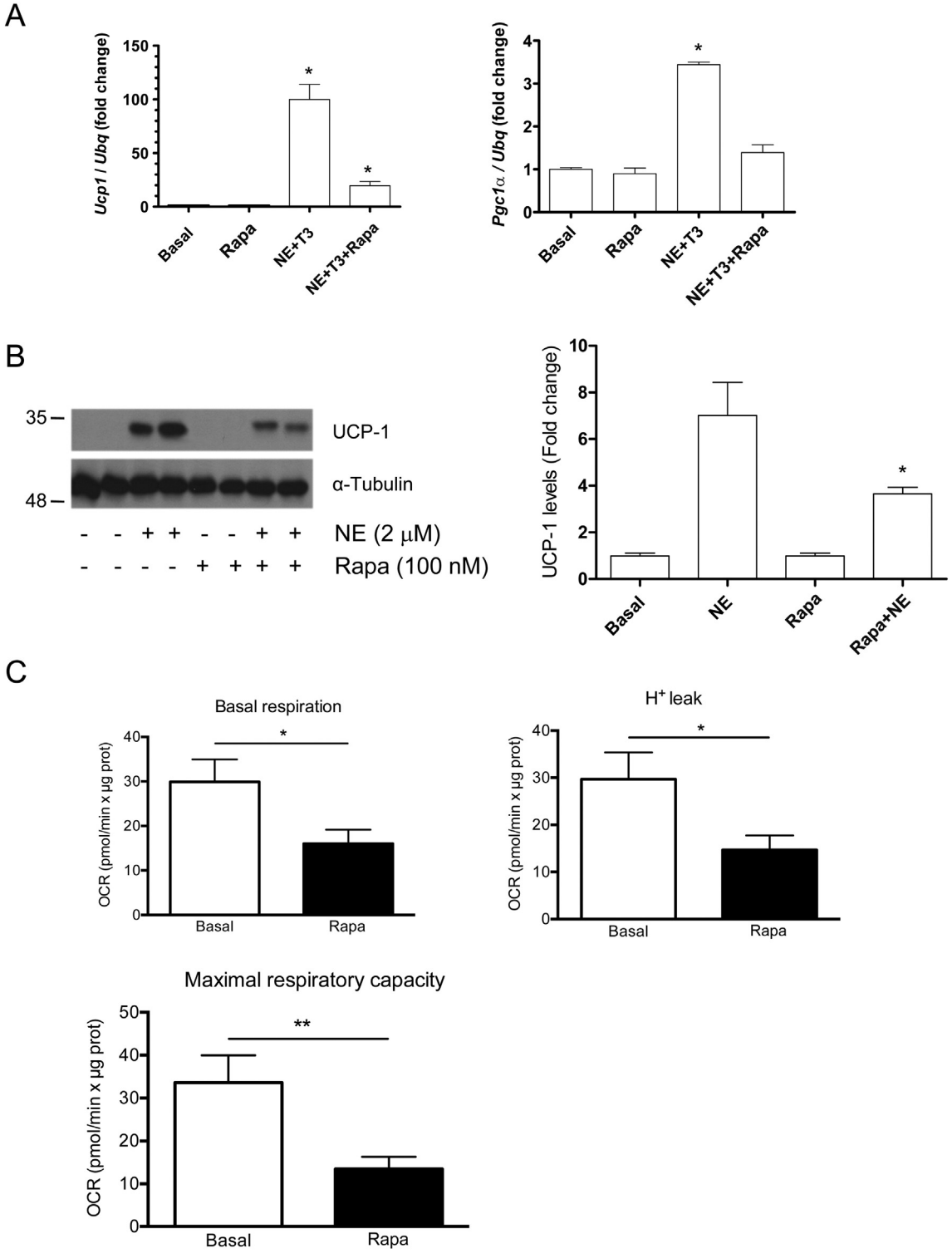

Fig. 8. Rapamycin decreased the NE-induced UCP-1 expression, basal respiration, proton leak and maximal respiration in brown adipocytes. Differentiated rat brown adipocytes were treated with rapamycin (Rapa) (100 nM) for 16 h or remained untreated and subsequently stimulated with NE (5 μM) plus T3 (1 nM) for a further 8 h. A. *Ucp1* and *Pgc1a* mRNA levels were analyzed by RT-qPCR. Results are expressed as fold change referred to NE + T_3 treatment. *$p < 0.05$ ($n = 3$ independent experiments performed in triplicate). B. UCP-1 protein levels were analyzed in differentiated mouse brown adipocytes treated with rapamycin (100 nM) for 16 h or remained untreated and subsequently stimulated with NE (5 μM) for a further 8 h. α-Tubulin was used as loading control. Results of 3 independent experiments were quantified by scanning densitometry. Results are means ± SEM. *$p < 0.05$ versus NE-stimulated cells. C. Quantification of Seahorse analysis: basal respiration, H^+ leak, and maximal respiratory capacity. Results are means ± SEM. *$p < 0.05$ versus rapamycin-stimulated cells ($n = 9$ values from 3 independent experiments performed in triplicate).

that NE at the doses used in rat brown adipocytes was also able to induce UCP-1 protein expression in mouse cells, an effect that was blunted by rapamycin.

3.7. Rapamycin decreased mitochondrial respiration in brown adipocytes

To better understand how rapamycin can affect mitochondrial activity in brown adipocytes, we assessed their respiratory profile using a XF24 Extracellular Flux Analyzer (Seahorse Biosciences). Brown adipocytes were treated with 100 nM rapamycin for 16 h and as shown in Fig. 8C, rapamycin significantly reduced not only basal respiration, but also proton leak, as well as maximal respiratory capacity in these cells.

4. Discussion

Our results demonstrate for the first time that brown adipocytes are sensitive to rapamycin action, as viewed by the impaired insulin signaling and thermogenic gene expression, strongly suggesting that in addition to white adipocytes, insulin resistance in brown adipocytes might play a major role in NODAT development. In fact, previous studies in mice deficient in the IR exclusively in brown adipocytes (BATIRKO mice) have revealed the importance of maintaining functional insulin signaling in BAT for the control of whole body glucose and energy homeostasis, since these animals developed glucose intolerance [30] and increased visceral adiposity [29].

The first evidence for a negative cross-talk between rapamycin and insulin signaling in brown adipocytes with a decrease in total IRS1 protein expression upon rapamycin treatment for 16 h was observed. IRS proteins have emerged as critical regulators of signaling pathways leading to brown adipocyte differentiation. Genetic deletion of IRS1 in mice suppressed insulin-induced Akt phosphorylation in brown preadipocytes, resulting in impaired adipogenic differentiation and thermogenic response [38–40,49]. In agreement with this, our results show a decrease in Akt phosphorylation at both Ser 473 and Thr 308 residues when brown adipocytes were pretreated with rapamycin before insulin stimulation. As a consequence, treatment of brown adipocytes with rapamycin significantly reduced insulin-induced GLUT4 translocation to the plasma membrane and glucose uptake that have been demonstrated to be dependent on Akt signaling [50]. These results agree with previous findings in vivo in rodents or ex vivo in freshly isolated human white adipocytes that have shown impaired insulin-induced glucose uptake and GLUT4 translocation upon pretreatment with rapamycin [11,13]. This is in contrast to the effects of CsA or FK506 that did not impair Akt phosphorylation, but increased the rate of GLUT4 endocytosis instead [10]. However, differential modulation of IRS proteins has been observed upon rapamycin treatment. Whereas rapamycin decreased IRS2 levels in subcutaneous human adipocytes [13], it decreased IRS1 in rat brown adipocytes. Thus, our data suggest a cellular specificity of rapamycin in triggering IRS1 or IRS2 degradation via the proteasome in brown or white adipocytes, respectively. These interesting results also reinforce the concept of the specificity of IRS1/2 proteins to transduce IR-mediated signaling in insulin-sensitive cell types and might be therapeutically useful to target insulin resistance during NODAT.

We further analyzed the molecular mechanism by which long-term rapamycin treatment decreased IRS1 protein levels in brown adipocytes. Importantly, this effect was preceded by its Ser 307 phosphorylation at early time-periods (30 min–2 h). Phosphorylation of IRS1 at Ser 307 has been extensively shown to negatively regulate insulin signal transduction since it inhibits insulin-stimulated tyrosine phosphorylation and IRS1-associated PI-3 kinase activity, potentially through the disruption of protein-protein interaction between IRS1 and the IR [51], and also by triggering proteasomal degradation of IRS1 [45]. Phosphorylation of IRS1 at Ser 307 can be induced by cellular stress, insulin, TNFα, lipids and also by the activation of mTORC1 complex, causing insulin resistance [46,52]. Our results in brown fat cells suggest that in conditions of mTORC1 inhibition by rapamycin, other/s Ser/Thr kinases might be involved in this negative feed-back mechanism. Among alternative candidates for the phosphorylation of IRS1 at Ser 307 by rapamycin, JNK1 has been extensively studied since it directly binds to IRS1 [53–54]. Moreover, JNK is activated by triggers that induce insulin resistance including hyperinsulinemia, nutrient overloading and oxidative stress [51]. We found that in differentiated brown adipocytes, either primary or immortalized, rapamycin rapidly induced JNK phosphorylation. This response, which was significantly abolished by a JNK inhibitor, correlated with IRS1 phosphorylation at Ser 307. Therefore, in addition to the direct mTORC1 complex inactivation, rapamycin might increase oxidative stress leading to an elevation of reactive oxygen species (ROS) that activate JNK which, in turn, phosphorylates IRS1 at Ser 307 in an mTORC1-independent manner. In this regard, recent findings have shown a mechanism of mTORC1 inactivation in the heart that led to an up-regulation of JNK activation and increased apoptosis [55]. Of note, neither p38 MAPK nor ERK was activated by rapamycin at early time-periods (data not shown), thus potentially excluding the involvement of these kinases in the modulation of insulin signaling our experimental conditions. Interestingly, in human subcutaneous and omental white adipocytes, phosphorylation of IRS1 at Ser 307 was significantly reduced after either 13 min or 20 h of rapamycin treatment, indicating again possible cellular specificity of rapamycin effects in brown and white adipocytes [13].

In addition to the effects in WAT, rapamycin was able to induce whole body insulin resistance and glucose intolerance with a marked impairment of the insulin signaling in other insulin sensitive tissues such as liver and skeletal muscle in Wistar rats treated for 3 weeks [12]. Furthermore, and in agreement with these previous studies, our in vivo results have demonstrated that treatment with rapamycin also impaired insulin signaling in BAT, highlighting the relevance of our study.

In mammals, BAT acts as a crucial regulator of energy metabolism through β-adrenergic-induced liberation of free fatty acids (FFAs) from triacylglycerol (TAG) by lipolysis [56–57]. Brown adipocytes use FFAs not only as substrates for oxidative respiration, but also as allosteric activators of UCP-1. In addition, Mottillo et al. [58] have reported that NE-induced lipolysis promotes the activation of peroxisome-activated receptors α and δ (PPARα and PPARδ, respectively), which resulted in *Ucp1* gene expression in BAT. Interestingly, our results show that in brown adipocytes rapamycin decreased NE or CL316243-mediated lipolysis through the inhibition of HSL phosphorylation at Ser 660. This effect is opposite to that observed in 3T3-L1 adipocytes, a cellular model of white adipose cells, where an increase in phosphorylation of HSL and lipolysis by rapamycin was observed [59], as well as in the lean phenotype of the S6K1-deficient mice [60]. A possible explanation for these differences in WAT versus BAT might be the involvement of additional modulators of HSL phosphorylation in a cellular-specific and dependent manner. In this regard, activation of the phosphatase PP2A has been reported to be responsible for dephosphorylation of HSL in isolated rat white adipocytes [61] whereas Oue et al. [62] have identified PRIP (phospholipase C-related catalytically inactive protein) as a new negative modulator of thermogenesis in brown adipocytes that down-regulates HSL phosphorylation and lipolysis. Interestingly, Liu et al. [63] found that Grb10 is a negative modulator of mTORC1 in both WAT and BAT and its deficiency in both adipose tissues suppressed lipolysis and reduced the thermogenic function. The elucidation of these and possible other mechanisms by which lipolysis could be differentially modulated by rapamycin in brown and white adipose cells in the context of NODAT deserves further investigations.

In addition to lipolysis, β-adrenergic stimulation regulates thermogenesis through transcriptional control in BAT. Accordingly, our present results clearly show for the first time the inhibition of both NE-induced *Pgc1a* and *Ucp1* mRNA levels by rapamycin in brown adipocytes. Inhibition of mTORC1 by rapamycin reduces *Pgc1a* gene expression in mouse skeletal muscle, as well as mitochondrial activity and capacity by a

mechanism mediated through the transcription factor yin and yang (YY1) [64]. Thus, inhibition of mTORC1 by rapamycin resulted in a failure of YY1 to interact with and be coactivated by PGC-1α in skeletal muscle cells [65] and, importantly, under these conditions YY1 functioned as a transcriptional repressor of insulin signaling genes [66]. In BAT, under energy-demanding conditions mediated by adrenergic signaling, YY1 increases expression of the canonical thermogenic program by binding to the promoter of the *Ucp1* gene and recruiting PGC-1α [66]. Our results suggest that the reduced levels of *Pgc1a* and *Ucp1a* mRNAs after rapamycin treatment in brown adipocytes could be mediated by the repression of the YY1-PGC-1α axis via mTORC1, which is reflected by the inhibition of UCP-1 protein levels. Moreover, it is also known that mitochondrial targets of PGC-1α involved in oxidative phosphorylation, tricarboxylic acid cycle and uncoupling respiration are downregulated by rapamycin [64]. In agreement with these results, our data clearly show reduced basal respiration, proton leak and maximal respiration in rapamycin-treated brown adipocytes.

Recruitment of BAT is actually being considered as a potential tool to combat obesity and associated metabolic complications in humans [22–23,25]. Thus, it might be reasonable to propose the use of BAT activators such as fibroblast growth factor 21 [67–68] to combat NODAT, an exciting issue for further research.

5. Conclusion

This work demonstrates that besides white adipocytes, brown adipocytes are also targeted by rapamycin action as viewed by the major impact on insulin signaling, NE effects, as well as on mitochondrial bioenergetics. Although distinct mechanisms seem to be involved in the effects of rapamycin on WAT and BAT, our results strongly suggest that dysfunction in brown adipocytes could also be a major contributor for the development of NODAT.

Supplementary data to this article can be found online at http://dx.doi.org/10.1016/j.bbalip.2016.09.016.

Conflict of interest

The authors declare that there is no duality of interest associated with this manuscript.

Contributions

AMV and EC conceived the work. AMV designed the work that led to the submission. E G-C, CdM, AIA, NP, MCD, LG, LH, DS, SC, FR, MJO and AMV acquired data and/or played an important role in interpreting the results. AMV and EC drafted the manuscript. EC, LH, DS, SC, MJO, FR and AMV revised the manuscript. All authors approved the final version.

Transparency document

The Transparency document associated with this article can be found, in online version.

Acknowledgements

This work was supported by Ministerio de Economía y Competitividad: (SAF2015-65267-R to AMV, SAF2012-32491 to MJO, SAF2013-45887-R to LH, and SAF2014-52223-C2-1-R to DS) that were cofunded by the Fondos Europeos de Desarrollo Regional de la Unión Europea [FEDER], Spain, Instituto de Salud Carlos III (FIS PI15-00448 to SC and INFLAMES PIE14/00045 to AMV), Centro de Investigación Biomédica en Red de Diabetes y Enfermedades Metabólicas Asociadas (CIBERdem, ISCIII, Spain) to AMV, Centro de Investigación Biomédica en Red Fisiopatología de la Obesidad y la Nutrición (CIBERobn-Grant CB06/03/0001) to DS and S2010/BMD-2423 (Comunidad de Madrid, Spain) to AMV and MJO and S2010/BMD-2402 to SC and 2014SGR465 (Generalitat de Catalunya, Spain) to DS. CdM was supported by the Albert Reynold Grant travel fellowship from the European Foundation for the Study of Diabetes. EC and FR were funded by FEDER through the Operational Programme Competitiveness Factors - COMPETE and by FCT - Foundation for Science and Technology PTDC/SAU-OSM/104124/2008 and strategic project UID/NEU/04539/2013. We acknowledge A. Zorzano (Barcelona, Spain) for the assistance with the Seahorse.

References

[1] R.J. Galindo, M. Fried, T. Breen, R. Tamler, Hyperglycemia management in patients with posttransplantation diabetes, Endocr. Pract. 22 (2016) 454–465.
[2] M. Hecking, J. Werzowa, M. Haidinger, W.H. Horl, J. Pascual, K. Budde, F.L. Luan, A. Ojo, A.P. de Vries, E. Porrini, G. Pacini, F.K. Port, A. Sharif, M.D. Saemann, Novel views on new-onset diabetes after transplantation: development, prevention and treatment, Nephrol. Dial. Transplant. 28 (2013) 550–566.
[3] M.R. First, S. Dhadda, R. Croy, J. Holman, W.E. Fitzsimmons, New-onset diabetes after transplantation (NODAT): an evaluation of definitions in clinical trials, Transplantation 96 (2013) 58–64.
[4] J.M. Smith, T.L. Nemeth, R.A. McDonald, Current immunosuppressive agents: efficacy, side effects, and utilization, Pediatr. Clin. N. Am. 50 (2003) 1283–1300.
[5] O.C. Alebiosu, O.E. Ayodele, Natural history and epidemiology of post transplantation diabetes mellitus, Afr. Health Sci. 5 (2005) 255–260.
[6] A. Mota, Sirolimus: a new option in transplantation, Expert. Opin. Pharmacother. 6 (2005) 479–487.
[7] K.D. Watt, Metabolic syndrome: is immunosuppression to blame? Liver Transpl. 17 (Suppl. 3) (2011) S38–S42.
[8] Y. Gueguen, L. Ferrari, M. Souidi, A.M. Batt, C. Lutton, G. Siest, S. Visvikis, Compared effect of immunosuppressive drugs cyclosporine A and rapamycin on cholesterol homeostasis key enzymes CYP27A1 and HMG-CoA reductase, Basic Clin. Pharmacol. Toxicol. 100 (2007) 392–397.
[9] V.P. Houde, S. Brule, W.T. Festuccia, P.G. Blanchard, K. Bellmann, Y. Deshaies, A. Marette, Chronic rapamycin treatment causes glucose intolerance and hyperlipidemia by upregulating hepatic gluconeogenesis and impairing lipid deposition in adipose tissue, Diabetes 59 (2010) 1338–1348.
[10] A. Fuhrmann, P. Lopes, J. Sereno, J. Pedro, D.O. Espinoza, M.J. Pereira, F. Reis, J.W. Eriksson, E. Carvalho, Molecular mechanisms underlying the effects of cyclosporin A and sirolimus on glucose and lipid metabolism in liver, skeletal muscle and adipose tissue in an in vivo rat model, Biochem. Pharmacol. 88 (2014) 216–228.
[11] P. Lopes, A. Fuhrmann, J. Sereno, M.J. Pereira, P. Nunes, J. Pedro, A. Melao, F. Reis, E. Carvalho, Effects of cyclosporine and sirolimus on insulin-stimulated glucose transport and glucose tolerance in a rat model, Transplant. Proc. 45 (2013) 1142–1148.
[12] P.C. Lopes, A. Fuhrmann, J. Sereno, D.O. Espinoza, M.J. Pereira, J.W. Eriksson, F. Reis, E. Carvalho, Short and long term in vivo effects of Cyclosporine A and Sirolimus on genes and proteins involved in lipid metabolism in Wistar rats, Metabolism 63 (2014) 702–715.
[13] M.J. Pereira, J. Palming, M. Rizell, M. Aureliano, E. Carvalho, M.K. Svensson, J.W. Eriksson, mTOR inhibition with rapamycin causes impaired insulin signalling and glucose uptake in human subcutaneous and omental adipocytes, Mol. Cell. Endocrinol. 355 (2012) 96–105.
[14] M.J. Pereira, J. Palming, M. Rizell, M. Aureliano, E. Carvalho, M.K. Svensson, J.W. Eriksson, Cyclosporine A and tacrolimus reduce the amount of GLUT4 at the cell surface in human adipocytes: increased endocytosis as a potential mechanism for the diabetogenic effects of immunosuppressive agents, J. Clin. Endocrinol. Metab. 99 (2014) E1885–E1894.
[15] P.C. Lopes, A. Fuhrmann, F. Carvalho, J. Sereno, M.R. Santos, M.J. Pereira, J.W. Eriksson, F. Reis, E. Carvalho, Cyclosporine A enhances gluconeogenesis while sirolimus impairs insulin signaling in peripheral tissues after 3 weeks of treatment, Biochem. Pharmacol. 91 (2014) 61–73.
[16] V. Shivaswamy, R.G. Bennett, C.C. Clure, B. Ottemann, J.S. Davis, J.L. Larsen, F.G. Hamel, Tacrolimus and sirolimus have distinct effects on insulin signaling in male and female rats, Transl. Res. 163 (2014) 221–231.
[17] J. Nedergaard, B. Cannon, How brown is brown fat? It depends where you look, Nat. Med. 19 (2013) 540–541.
[18] C.H. Saely, K. Geiger, H. Drexel, Brown versus white adipose tissue: a mini-review, Gerontology 58 (2012) 15–23.
[19] S. Rousset, M.C. Alves-Guerra, J. Mozo, B. Miroux, A.M. Cassard-Doulcier, F. Bouillaud, D. Ricquier, The biology of mitochondrial uncoupling proteins, Diabetes 53 (Suppl. 1) (2004) S130–S135.
[20] T.F. Hany, E. Gharehpapagh, E.M. Kamel, A. Buck, J. Himms-Hagen, G.K. von Schulthess, Brown adipose tissue: a factor to consider in symmetrical tracer uptake in the neck and upper chest region, Eur. J. Nucl. Med. Mol. Imaging 29 (2002) 1393–1398.
[21] J. Nedergaard, T. Bengtsson, B. Cannon, Unexpected evidence for active brown adipose tissue in adult humans, Am. J. Physiol. Endocrinol. Metab. 293 (2007) E444–E452.
[22] A.M. Cypess, S. Lehman, G. Williams, I. Tal, D. Rodman, A.B. Goldfine, F.C. Kuo, E.L. Palmer, Y.H. Tseng, A. Doria, G.M. Kolodny, C.R. Kahn, Identification and importance of brown adipose tissue in adult humans, N. Engl. J. Med. 360 (2009) 1509–1517.
[23] K.A. Virtanen, M.E. Lidell, J. Orava, M. Heglind, R. Westergren, T. Niemi, M. Taittonen, J. Laine, N.J. Savisto, S. Enerback, P. Nuutila, Functional brown adipose tissue in healthy adults, N. Engl. J. Med. 360 (2009) 1518–1525.

[24] M.C. Zingaretti, F. Crosta, A. Vitali, M. Guerrieri, A. Frontini, B. Cannon, J. Nedergaard, S. Cinti, The presence of UCP1 demonstrates that metabolically active adipose tissue in the neck of adult humans truly represents brown adipose tissue, FASEB J. 23 (2009) 3113–3120.
[25] M. Saito, Y. Okamatsu-Ogura, M. Matsushita, K. Watanabe, T. Yoneshiro, J. Nio-Kobayashi, T. Iwanaga, M. Miyagawa, T. Kameya, K. Nakada, Y. Kawai, M. Tsujisaki, High incidence of metabolically active brown adipose tissue in healthy adult humans: effects of cold exposure and adiposity, Diabetes 58 (2009) 1526–1531.
[26] W.D. van Marken Lichtenbelt, J.W. Vanhommerig, N.M. Smulders, J.M. Drossaerts, G.J. Kemerink, N.D. Bouvy, P. Schrauwen, G.J. Teule, Cold-activated brown adipose tissue in healthy men, N. Engl. J. Med. 360 (2009) 1500–1508.
[27] M. Chondronikola, E. Volpi, E. Borsheim, C. Porter, P. Annamalai, S. Enerback, M.E. Lidell, M.K. Saraf, S.M. Labbe, N.M. Hurren, C. Yfanti, T. Chao, C.R. Andersen, F. Cesani, H. Hawkins, L.S. Sidossis, Brown adipose tissue improves whole-body glucose homeostasis and insulin sensitivity in humans, Diabetes 63 (2014) 4089–4099.
[28] L.S. Sidossis, C. Porter, M.K. Saraf, E. Borsheim, R.S. Radhakrishnan, T. Chao, A. Ali, M. Chondronikola, R. Mlcak, C.C. Finnerty, H.K. Hawkins, T. Toliver-Kinsky, D.N. Herndon, Browning of subcutaneous white adipose tissue in humans after severe adrenergic stress, Cell Metab. 22 (2015) 219–227.
[29] A. Gomez-Hernandez, Y.F. Otero, N. de las Heras, O. Escribano, V. Cachofeiro, V. Lahera, M. Benito, Brown fat lipoatrophy and increased visceral adiposity through a concerted adipocytokines overexpression induces vascular insulin resistance and dysfunction, Endocrinology 153 (2012) 1242–1255.
[30] C. Guerra, P. Navarro, A.M. Valverde, M. Arribas, J. Bruning, L.P. Kozak, C.R. Kahn, M. Benito, Brown adipose tissue-specific insulin receptor knockout shows diabetic phenotype without insulin resistance, J. Clin. Invest. 108 (2001) 1205–1213.
[31] T. Shan, P. Zhang, Q. Jiang, Y. Xiong, Y. Wang, S. Kuang, Adipocyte-specific deletion of mTOR inhibits adipose tissue development and causes insulin resistance in mice, Diabetologia 59 (2016) 1995–2004.
[32] M. Nechad, Development of brown fat cells in monolayer culture. II. Ultrastructural characterization of precursors, differentiating adipocytes and their mitochondria, Exp. Cell Res. 149 (1983) 119–127.
[33] S. Miranda, A. Gonzalez-Rodriguez, J. Revuelta-Cervantes, C.M. Rondinone, A.M. Valverde, Beneficial effects of PTP1B deficiency on brown adipocyte differentiation and protection against apoptosis induced by pro- and anti-inflammatory stimuli, Cell. Signal. 22 (2010) 645–659.
[34] M. Kumari, X. Wang, L. Lantier, A. Lyubetskaya, J. Eguchi, S. Kang, D. Tenen, H.C. Roh, X. Kong, L. Kazak, R. Ahmad, E.D. Rosen, IRF3 promotes adipose inflammation and insulin resistance and represses browning, J. Clin. Invest. 126 (2016) 2839–2854.
[35] R. Tunduguru, T.T. Chiu, L. Ramalingam, J.S. Elmendorf, A. Klip, D.C. Thurmond, Signaling of the p21-activated kinase (PAK1) coordinates insulin-stimulated actin remodeling and glucose uptake in skeletal muscle cells, Biochem. Pharmacol. 92 (2014) 380–388.
[36] A.M. Valverde, P. Navarro, M. Benito, M. Lorenzo, H-ras induces glucose uptake in brown adipocytes in an insulin- and phosphatidylinositol 3-kinase-independent manner, Exp. Cell Res. 243 (1998) 274–281.
[37] A. Entingh-Pearsall, C.R. Kahn, Differential roles of the insulin and insulin-like growth factor-I (IGF-I) receptors in response to insulin and IGF-I, J. Biol. Chem. 279 (2004) 38016–38024.
[38] A.M. Valverde, C.R. Kahn, M. Benito, Insulin signaling in insulin receptor substrate (IRS)-1-deficient brown adipocytes: requirement of IRS-1 for lipid synthesis, Diabetes 48 (1999) 2122–2131.
[39] A.M. Valverde, M. Arribas, C. Mur, P. Navarro, S. Pons, A.M. Cassard-Doulcier, C.R. Kahn, M. Benito, Insulin-induced up-regulated uncoupling protein-1 expression is mediated by insulin receptor substrate 1 through the phosphatidylinositol 3-kinase/Akt signaling pathway in fetal brown adipocytes, J. Biol. Chem. 278 (2003) 10221–10231.
[40] M. Fasshauer, J. Klein, K.M. Kriauciunas, K. Ueki, M. Benito, C.R. Kahn, Essential role of insulin receptor substrate 1 in differentiation of brown adipocytes, Mol. Cell. Biol. 21 (2001) 319–329.
[41] A.M. Valverde, D.J. Burks, I. Fabregat, T.L. Fisher, J. Carretero, M.F. White, M. Benito, Molecular mechanisms of insulin resistance in IRS-2-deficient hepatocytes, Diabetes 52 (2003) 2239–2248.
[42] A.M. Valverde, P. Navarro, T. Teruel, R. Conejo, M. Benito, M. Lorenzo, Insulin and insulin-like growth factor I up-regulate GLUT4 gene expression in fetal brown adipocytes, in a phosphoinositide 3-kinase-dependent manner, Biochem. J. 337 (Pt 3) (1999) 397–405.
[43] R. Hernandez, T. Teruel, M. Lorenzo, Akt mediates insulin induction of glucose uptake and up-regulation of GLUT4 gene expression in brown adipocytes, FEBS Lett. 494 (2001) 225–231.
[44] R. Mayoral, A.M. Valverde, C. Llorente Izquierdo, A. Gonzalez-Rodriguez, L. Bosca, P. Martin-Sanz, Impairment of transforming growth factor beta signaling in caveolin-1-deficient hepatocytes: role in liver regeneration, J. Biol. Chem. 285 (2010) 3633–3642.
[45] J.F. Tanti, J. Jager, Cellular mechanisms of insulin resistance: role of stress-regulated serine kinases and insulin receptor substrates (IRS) serine phosphorylation, Curr. Opin. Pharmacol. 9 (2009) 753–762.
[46] T.M. Pederson, D.L. Kramer, C.M. Rondinone, Serine/threonine phosphorylation of IRS-1 triggers its degradation: possible regulation by tyrosine phosphorylation, Diabetes 50 (2001) 24–31.
[47] B.L. Bennett, D.T. Sasaki, B.W. Murray, E.C. O'Leary, S.T. Sakata, W. Xu, J.C. Leisten, A. Motiwala, S. Pierce, Y. Satoh, S.S. Bhagwat, A.M. Manning, D.W. Anderson, SP600125, an anthrapyrazolone inhibitor of Jun N-terminal kinase, Proc. Natl. Acad. Sci. U. S. A. 98 (2001) 13681–13686.
[48] A. Hernandez, R.M. de Mena, E. Martin, M.J. Obregon, Differences in the response of UCP1 mRNA to hormonal stimulation between rat and mouse primary cultures of brown adipocytes, Cell. Physiol. Biochem. 28 (2011) 969–980.
[49] Y.H. Tseng, K.M. Kriauciunas, E. Kokkotou, C.R. Kahn, Differential roles of insulin receptor substrates in brown adipocyte differentiation, Mol. Cell. Biol. 24 (2004) 1918–1929.
[50] S. Huang, M.P. Czech, The GLUT4 glucose transporter, Cell Metab. 5 (2007) 237–252.
[51] K.D. Copps, M.F. White, Regulation of insulin sensitivity by serine/threonine phosphorylation of insulin receptor substrate proteins IRS1 and IRS2, Diabetologia 55 (2012) 2565–2582.
[52] C.E. Berg, B.E. Lavan, C.M. Rondinone, Rapamycin partially prevents insulin resistance induced by chronic insulin treatment, Biochem. Biophys. Res. Commun. 293 (2002) 1021–1027.
[53] T.L. Hilder, J.C. Tou, R.E. Grindeland, C.E. Wade, L.M. Graves, Phosphorylation of insulin receptor substrate-1 serine 307 correlates with JNK activity in atrophic skeletal muscle, FEBS Lett. 553 (2003) 63–67.
[54] T. Kim, J. Wayne Leitner, R. Adochio, B. Draznin, Knockdown of JNK rescues 3T3-L1 adipocytes from insulin resistance induced by mitochondrial dysfunction, Biochem. Biophys. Res. Commun. 378 (2009) 772–776.
[55] L. Mazelin, B. Panthu, A.S. Nicot, E. Belotti, L. Tintignac, G. Teixeira, Q. Zhang, V. Risson, D. Baas, E. Delaune, G. Derumeaux, D. Taillandier, T. Ohlmann, M. Ovize, Y.G. Gangloff, L. Schaeffer, mTOR inactivation in myocardium from infant mice rapidly leads to dilated cardiomyopathy due to translation defects and p53/JNK-mediated apoptosis, J. Mol. Cell. Cardiol. 97 (2016) 213–225.
[56] B. Cannon, J. Nedergaard, Brown adipose tissue: function and physiological significance, Physiol. Rev. 84 (2004) 277–359.
[57] A. Fedorenko, P.V. Lishko, Y. Kirichok, Mechanism of fatty-acid-dependent UCP1 uncoupling in brown fat mitochondria, Cell 151 (2012) 400–413.
[58] E.P. Mottillo, A.E. Bloch, T. Leff, J.G. Granneman, Lipolytic products activate peroxisome proliferator-activated receptor (PPAR) alpha and delta in brown adipocytes to match fatty acid oxidation with supply, J. Biol. Chem. 287 (2012) 25038–25048.
[59] G.A. Soliman, H.A. Acosta-Jaquez, D.C. Fingar, mTORC1 inhibition via rapamycin promotes triacylglycerol lipolysis and release of free fatty acids in 3T3-L1 adipocytes, Lipids 45 (2010) 1089–1100.
[60] S.H. Um, F. Frigerio, M. Watanabe, F. Picard, M. Joaquin, M. Sticker, S. Fumagalli, P.R. Allegrini, S.C. Kozma, J. Auwerx, G. Thomas, Absence of S6K1 protects against age- and diet-induced obesity while enhancing insulin sensitivity, Nature 431 (2004) 200–205.
[61] S.L. Wood, N. Emmison, A.C. Borthwick, S.J. Yeaman, The protein phosphatases responsible for dephosphorylation of hormone-sensitive lipase in isolated rat adipocytes, Biochem. J. 295 (Pt 2) (1993) 531–535.
[62] K. Oue, J. Zhang, K. Harada-Hada, S. Asano, Y. Yamawaki, M. Hayashiuchi, H. Furusho, T. Takata, M. Irifune, M. Hirata, T. Kanematsu, Phospholipase C-related catalytically inactive protein is a new modulator of thermogenesis promoted by beta-adrenergic receptors in brown adipocytes, J. Biol. Chem. (2015).
[63] M. Liu, J. Bai, S. He, R. Villarreal, D. Hu, C. Zhang, X. Yang, H. Liang, T.J. Slaga, Y. Yu, Z. Zhou, J. Blenis, P.E. Scherer, L.Q. Dong, F. Liu, Grb10 promotes lipolysis and thermogenesis by phosphorylation-dependent feedback inhibition of mTORC1, Cell Metab. 19 (2014) 967–980.
[64] J.T. Cunningham, J.T. Rodgers, D.H. Arlow, F. Vazquez, V.K. Mootha, P. Puigserver, mTOR controls mitochondrial oxidative function through a YY1-PGC-1alpha transcriptional complex, Nature 450 (2007) 736–740.
[65] S.M. Blattler, F. Verdeguer, M. Liesa, J.T. Cunningham, R.O. Vogel, H. Chim, H. Liu, K. Romanino, O.S. Shirihai, F. Vazquez, M.A. Ruegg, Y. Shi, P. Puigserver, Defective mitochondrial morphology and bioenergetic function in mice lacking the transcription factor Yin Yang 1 in skeletal muscle, Mol. Cell. Biol. 32 (2012) 3333–3346.
[66] S.M. Blattler, J.T. Cunningham, F. Verdeguer, H. Chim, W. Haas, H. Liu, K. Romanino, M.A. Ruegg, S.P. Gygi, Y. Shi, P. Puigserver, Yin Yang 1 deficiency in skeletal muscle protects against rapamycin-induced diabetic-like symptoms through activation of insulin/IGF signaling, Cell Metab. 15 (2012) 505–517.
[67] M. Giralt, A. Gavalda-Navarro, F. Villarroya, Fibroblast growth factor-21, energy balance and obesity, Mol. Cell. Endocrinol. 418 (Pt 1) (2015) 66–73.
[68] M.J. Hanssen, E. Broeders, R.J. Samms, M.J. Vosselman, A.A. van der Lans, C.C. Cheng, A.C. Adams, W.D. van Marken Lichtenbelt, P. Schrauwen, Serum FGF21 levels are associated with brown adipose tissue activity in humans, Sci. Rep. 5 (2015) 10275.

PLOS | ONE

RESEARCH ARTICLE

Carnitine Palmitoyltransferase 1 Increases Lipolysis, UCP1 Protein Expression and Mitochondrial Activity in Brown Adipocytes

María Calderon-Dominguez[1,2], David Sebastián[3,4], Raquel Fucho[1,2], Minéia Weber[1,2], Joan F. Mir[1,2], Ester García-Casarrubios[5], María Jesús Obregón[5], Antonio Zorzano[3,4], Ángela M. Valverde[4,5], Dolors Serra[1,2], Laura Herrero[1,2]*

1 Department of Biochemistry and Physiology, Institut de Biomedicina de la Universitat de Barcelona (IBUB), Universitat de Barcelona, E-08028, Barcelona, Spain, **2** Centro de Investigación Biomédica en Red de Fisiopatología de la Obesidad y la Nutrición (CIBEROBN), Instituto de Salud Carlos III, E-28029, Madrid, Spain, **3** Institute for Research in Biomedicine (IRB Barcelona) and Departament de Bioquímica i Biologia Molecular, Facultat de Biologia, Universitat de Barcelona, E-08028, Barcelona, Spain, **4** Centro de Investigación Biomédica en Red de Diabetes y Enfermedades Metabólicas Asociadas (CIBERDEM), Instituto de Salud Carlos III, E-28029, Madrid, Spain, **5** Instituto de Investigaciones Biomédicas Alberto Sols (CSIC-UAM) and Instituto de Investigación Sanitaria La Paz, 28029, Madrid, Spain

* lherrero@ub.edu

OPEN ACCESS

Citation: Calderon-Dominguez M, Sebastián D, Fucho R, Weber M, Mir JF, García-Casarrubios E, et al. (2016) Carnitine Palmitoyltransferase 1 Increases Lipolysis, UCP1 Protein Expression and Mitochondrial Activity in Brown Adipocytes. PLoS ONE 11(7): e0159399. doi:10.1371/journal.pone.0159399

Editor: Miguel López, University of Santiago de Compostela School of Medicine - CIMUS, SPAIN

Received: May 5, 2016

Accepted: July 3, 2016

Published: July 20, 2016

Data Availability Statement: All relevant data are within the paper.

Funding: This work was supported by the Ministry of Spain - MINECO (SAF2013-45887-R to LH, SAF2014-52223-C2-1-R to DS and SAF-2015-65267-R to AMV that were cofunded by the Fondos Europeos de Desarrollo Regional de la Unión Europea [FEDER], SAF2012-32491 to MJO, SAF2013-40987R to AZ, and a doctoral fellowship to JFM), the Centro de Investigación Biomédica en Red Fisiopatología de la Obesidad y la Nutrición

Abstract

The discovery of active brown adipose tissue (BAT) in adult humans and the fact that it is reduced in obese and diabetic patients have put a spotlight on this tissue as a key player in obesity-induced metabolic disorders. BAT regulates energy expenditure through thermogenesis; therefore, harnessing its thermogenic fat-burning power is an attractive therapeutic approach. We aimed to enhance BAT thermogenesis by increasing its fatty acid oxidation (FAO) rate. Thus, we expressed carnitine palmitoyltransferase 1AM (CPT1AM), a permanently active mutant form of CPT1A (the rate-limiting enzyme in FAO), in a rat brown adipocyte (rBA) cell line through adenoviral infection. We found that CPT1AM-expressing rBA have increased FAO, lipolysis, UCP1 protein levels and mitochondrial activity. Additionally, enhanced FAO reduced the palmitate-induced increase in triglyceride content and the expression of obese and inflammatory markers. Thus, CPT1AM-expressing rBA had enhanced fat-burning capacity and improved lipid-induced derangements. This indicates that CPT1AM-mediated increase in brown adipocytes FAO may be a new approach to the treatment of obesity-induced disorders.

Introduction

Obesity is a major public health problem and a worldwide epidemic contributing to the development of associated pathological conditions, such as insulin resistance, type 2 diabetes, cardiovascular disease, nonalcoholic fatty liver disease, and some forms of cancer among others [1,2]. Adipose tissue has gained a crucial role in the study of the mechanisms involved in

(CIBEROBN) (Grant CB06/03/0001 to DS), the Centro de Investigación Biomédica en red de Diabetes y Enfermedades Metabólicas Asociadas (CIBERDEM), the Generalitat de Catalunya (2014SGR465 to DS, and 2014SGR48 to AZ), the Comunidad de Madrid (S2010/BMD-2423 to MJO and AMV), INTERREG IV-B-SUDOE-FEDER (DIOMED, SOE1/P1/E178) to AZ, and the European Foundation for the Study of Diabetes (EFSD)/ Janssen-Rising Star and L'Oréal-UNESCO "For Women in Science" research fellowships to LH. AZ is a recipient of ICREA-Academia (Generalitat de Catalunya) and MW is a recipient of the Ciência sem Fronteiras-CNPq fellowship (237976/2012-9). The funders had no role in study design, data collection and analysis, decision to publish, or preparation of the manuscript.

Competing Interests: The authors have declared that no competing interests exist.

Abbreviations: BAT, brown adipose tissue; CIDEA, cell death-inducing DNA fragmentation factor-α-like effector A; rBA, rat brown adipocyte cells; CHOP, C/EBP homologous protein; CPT1A, carnitine palmitoyltransferase 1A; CPT1AM, permanently active mutant form of CPT1A; EDEM, ER degradation enhancing α-mannosidase-like protein; ER, endoplasmic reticulum; FA, fatty acids; FAO, fatty acid oxidation; Mfn2, mitofusin 2; Mt-ATP6, Mitochondrial ATP synthase 6; Mt-Co1, cytochrome C oxidase I; Mt-Co2, cytochrome C oxidase II; Mt-Nd1, NADH dehydrogenase 1; Mt-Cyb, cytochrome b; NEFA, nonesterified fatty acids; OCR, oxygen consumption rate; PGC1a, peroxisome proliferator-activated receptor gamma coactivator 1 alpha; PRDM16, PR domain-containing 16; TG, triglyceride; Tim 44, translocase of mitochondrial inner membrane 44; UCP1, uncoupling protein 1; WAT, white adipose tissue.

obesity-related disorders. Adipose tissue is classified into energy-storing white adipose tissue (WAT) and brown adipose tissue (BAT), which controls thermogenesis by burning fatty acids (FA) to produce heat and defend the body against cold. Traditionally, WAT has been implicated in the pathogenesis of obesity-induced insulin resistance [2–5]. BAT has received less attention, because it is less abundant, and it was considered exclusive to rodents and human neonates. However, in the last decade, active BAT was discovered in adult humans by a combination of positron-emission tomography (PET) and computed tomography (CT) (PET-CT) [6–12]. Furthermore, it was shown that BAT is reduced in obese and diabetic patients [8]. Thus, BAT has become a leading research topic, since any strategy that can enhance BAT mass or activity may be a potential therapeutic approach to obesity-induced diabetes.

The cellular heterogeneity of fat is still under debate [13]. To date, at least two types of thermogenic adipocytes have been described in humans and rodents: the classical brown adipocytes, and beige (also called brite) adipocytes. They differ in both their developmental origin and their anatomical localization [14]. Beige adipocytes are located within the WAT and appear in response to certain stimuli such as cold exposure or β3-adrenergic signals. A recent study has identified *Zic1* and *Tcf21* as specific markers for brown and white adipocytes, respectively, while *Cd137*, *Epsti1*, *Tbx1*, and *Tmem26* would be specific for beige adipocytes [15].

Any strategy that can reduce lipid accumulation would be beneficial for the treatment of obesity and related disorders. Studies in rodents have demonstrated that BAT modulates triglyceridemia and controls lipid clearance [16–18]. The aim of our study was to enhance the thermogenic capacity of BAT by increasing its fatty acid oxidation (FAO). Our group and others have shown that increased FAO in white adipocytes and macrophages [19], liver [20–22], pancreas [23,24], neurons [25] and muscle [26–28] results in an improvement in lipid-induced derangements. Cold stimulates FAO in mice, which indicates that FAO is required for thermogenesis [29].

Here we focused on the FAO key enzyme, carnitine palmitoyltransferase 1 (CPT1). CPT1 facilitates the transfer of FAs into the mitochondria for oxidation. There are three CPT1 isoforms, with differences in kinetics, sensitivity to their physiological inhibitor malonyl-CoA, and tissue expression: CPT1A (liver, intestine, kidney, ovary, pancreas, brain and mouse and human WAT), CPT1B (BAT, heart, skeletal muscle and rat and human WAT) and CPT1C (brain and testis) [30,31]. Interestingly, BAT CPT1 activity is decreased in diabetic rats [32]. Thus, we attempted to overexpress a permanently active mutant form of CPT1A, CPT1AM, which is insensitive to malonyl-CoA [33], in a brown adipocyte rat cell line (rBA) through adenoviral infection. The choice of CPT1AM was based on the following points: 1) the CPT1A isoform has lower sensitivity to malonyl-CoA inhibition and higher affinity for the substrate than CPT1B [34]; 2) CPT1A could be differentiated from the BAT endogenous main isoform, CPT1B, and 3) CPT1AM is a permanently active mutant that would ensure constant high levels of FAO, independently of the levels of malonyl-CoA, which is usually derived from glucose metabolism and is the first intermediate in lipogenesis. This last point is particularly relevant in obesity, where in addition to high lipid levels high glucose (and therefore high malonyl-CoA) levels are present.

Here we demonstrate that CPT1AM-expressing rBA display higher FAO, lipolysis, uncoupling protein 1 (UCP1) expression, and mitochondrial respiration. Enhanced FAO in palmitate-incubated rBA reduced triglyceride content and the expression of fatty acid binding protein 4 (FABP4) and tumor necrosis factor α (TNFa), obese and inflammatory markers, respectively. We conclude that CPT1AM-expressing rBA had enhanced lipolysis and UCP1 protein expression, considered as indicators of increased thermogenesis, and showed an improvement in lipid-induced derangements. This highlights CPT1AM-mediated BAT FAO as a new approach to treat obesity and related disorders.

Materials and Methods

Materials

Norepinephrine, sodium palmitate, sodium oleate and FA-free BSA were purchased from Sigma Aldrich (St. Louis, MO). DMEM, FBS and penicillin/streptomycin mixture were purchased from Life Technologies (Carlsbad, CA). Etomoxir was kindly provided by Dr. H. P. O. Wolf (GMBH, Allensbach, Germany).

Cell culture and differentiation of brown adipocytes

Immortalized rBA from neonatal rats were generated as previously described [35]. rBA preadipocytes were grown in DMEM supplemented with 10% fetal serum, 1% penicillin/streptomycin and 2 mM HEPES. rBA were differentiated in DMEM supplemented with 10% fetal serum, 1 nM T3 and 20 nM insulin (differentiation media) until confluence (day 0). Then, cells were incubated with induction medium containing 1 μM rosiglitazone, 0.5 μM dexamethasone, 0.125 μM indomethacin and 0.5 mM isobutylmethylxanthine (IBMX) for two days. Finally, cells were incubated for a further three days in differentiation media, after which they exhibited a fully differentiated phenotype with numerous multilocular lipid droplets in their cytoplasm.

Oil Red O staining

rBA were grown and differentiated on coverslips. They were rinsed twice in PBS, fixed in 10% paraformaldehyde for 30 minutes at room temperature, and washed again in PBS. Then, cells were rinsed in 60% isopropanol for 5 min to facilitate the staining of neutral lipids, and stained with filtered Oil Red O working solution (0.3% Oil Red O in isopropanol) for 15 minutes. After several washes in distilled water, the coverslips were removed and fixed with mount medium. The intracellular lipid vesicles stained with Oil Red O were identified by their bright red color under the microscope.

Adenovirus (Ad) infection

At day 6 of differentiation, rBA were infected with AdGFP (100 moi) and AdCPT1AM (100 moi) for 48 hours in serum-free DMEM, 1% penicillin/streptomycin and 2 mM HEPES. Adenovirus infection efficiency was assessed in AdGFP-infected cells.

Western blot analysis

rBA were cultured in 12-well plates, differentiated and infected as described above. Cells were harvested in lysis buffer (RIPA), and protein concentration was determined using a BCA protein assay kit (Thermoscientific). Samples were separated on 8% and 12% SDS-PAGE gels, for CPT1A and UCP1 respectively, and then transferred onto PVDF membranes (Millipore). The following primary antibodies were used: CPT1A (1/6,000) [24], Tim 44 (1/5,000; BD Bioscience), UCP1 (1/1,000; Abcam) and b-actin (I-19; 1/4,000; Santa Cruz). Blots were incubated with the appropriate IgG-HRP-conjugated secondary antibody. Protein bands were visualized using the ECL immunoblotting detection system (GE Healthcare) and developed on an ImageQuant LAS4000 mini Fuji luminescence imagining system. For the analysis of protein expression, bands from at least three independent experiments were quantified by densitometry using Image J analysis software.

Analysis of mRNA expression by quantitative real-time PCR

Total RNA was isolated from rBA using an Illustra MiniRNA Spin kit (GE Healthcare), and cDNA was obtained using a Transcriptor First Strand cDNA Synthesis kit (Roche), following the manufacturer's instructions. Relative quantification of mRNA was performed using a LightCycler® 480 instrument (Roche) in 10 μL of reaction medium by using 6.5 ng of cDNA, forward and reverse primers at 100 nM each, and a SYBR Green PCR Master Mix Reagent kit (Life Technologies). Primer pairs are shown in Table 1. The mRNA levels were normalized to those of b-actin and expressed as fold change.

Fatty acid oxidation assay

The FAO rate was measured in rBA grown in 25-cm^2 flasks, differentiated and infected as described above. On the day of the assay, cells were washed in KRBH 0.1% BSA (FA free), pre-incubated at 37°C for 30 min in KRBH 1% BSA, and washed again in KRBH 0.1% BSA. Cells were then incubated for 3 hours at 37°C with fresh KRBH containing 11 mM glucose, 0.8 mM carnitine plus 0.2 mM [1-^{14}C] oleate (Perkin Elmer). Oxidation was measured as previously described [21].

Glycerol release

rBA were seeded, differentiated in 12-wells plates and infected as described above or incubated in the presence or absence of 5 μM norepinephrine and 180 μM etomoxir for 6 hours. Then, the cell medium was removed and glycerol levels were measured using the TG Triglyceride kit (Sigma-Aldrich), according to the manufacturer's instructions. Samples were normalized by the protein concentration present in each well.

Table 1. Quantitative real-time PCR oligonucleotides.

Gene Name	Forward	Reverse
b-actin	5'- AAGTCCCTCACCCTCCCAAAG-3'	5'AAGCAATGCTGTCACCTTCCC-3'
Cidea	5'-TGATATCCGCTGCACAAGC-3'	5'-CACCTGGGCAGCATAGGA-3'
Cd137	5'-AGCTGACAGAGACCCTGTGG-3'	5'-CACATGCACAGGACACCAA-3'
Fabp4	5'-GAGGAGACGAGATGGTGACAA-3'	5'-GCTCATGCCCTTTCGTAAAC-3'
Mt-Atp6	5'-TAAGCATAGCCATCCCCCTA-3'	5'-TTAGTTTGTGTCGGAAGCCTAGA-3'
Mt-Co1	5'-TCGGAACCCTCTACCTATTATTTG-3'	5'-CTCGAATTAGAATACTTAAAGCTGTCC-3'
Mt-Co2	5'-TAAGCATAGCCATCCCCCTA-3'	5'-TTAGTTTGTGTCGGAAGCCTAGA-3'
Mt-Cyb	5'-CCCTAGTACTATTCTTCCCAGACCT-3'	5′ -AGGGGGTTAGCGGGTGTAT-3'
Mt-Nd1	5'-CCTCAACCTAGGCATACCATTT-3'	5′ -AGGCTCATCCCGATCATAGA-3'
Pgc1a	5'- AAAGGGCCAAGCAGAGAGA-3'	5'- GTAAATCACACGGCGCTCTT-3'
Prdm16	5'-CGGATGTTCCCCAACAAAT-3'	5'-ACGCTCTTCTGTGTGGACAA-3'
Tnfa	5'-AAATGGGCTCCCTCTCATCAGTTC-3'	5'-TCTGCTTGGTGGTTTGCTACGAC-3'
Zic1	5'-AACCTCAAGATCCACAAAAGGA-3'	5'-CCTCGAACTCGCACTTGAA-3'
Cpt1a*	5'- ACAATGGGACATTCCAGGAG-3'	5'- AAAGACTGGCGCTGCTCA-3'
Cpt1b	5'- GTGACTGGTGGGAAGAGTACG-3'	5'- CTGCTTGTTGGCTCGTGTT-3'
Cpt1c	5'- GCCTGCCAATTTGTGAGAG-3'	5'- GGCAAGGCACTGTTGGTC-3'
Mfn2	5′ -ATTGGCCACACCACCAAT-3′	5′ -TGGGCTAGCTGGTTCACG-3′

* Recognizes both CPT1A and CPT1AM

doi:10.1371/journal.pone.0159399.t001

Lipid extraction from rBA

rBA were seeded, differentiated in 12-wells plates and infected as described above. Then, cells were collected for lipid extraction following Gesta *et al* protocol [36] with minor modifications: after cell lysis with 0.1% SDS, 1/2/0.12 (v/v/v) methanol/chloroform/0.5M KCl solution was added, the two phases were separated by centrifugation and the upper phase was dried with N_2. Finally, lipids were resuspended in 100% isopropanol.

Measurement of nonesterified fatty acids

Nonesterified fatty acids (NEFAs) were measured in rBA lipid extracts by NEFA-HR detection kit (Wako Diagnostics) according to the manufacturer's instructions. NEFA levels were normalized against protein content.

Seahorse bioanalyzer

The Seahorse XF24 (Seahorse Bioscience, www.seahorsebio.com) was used to measure oxygen consumption rate (OCR) in mature brown adipocytes. For a typical bioenergetic profile we used oligomycin to block ATP synthase; the uncoupler carbonyl cyanide-4-(trifluoromethoxy) phenylhydrazone (FCCP) to measure maximal respiratory capacity; followed by rotenone, the complex 1 inhibitor, and antimycin-A to leave only non-mitochondrial activity to be measured (all from Sigma-Aldrich). Cells were differentiated in customized Seahorse 24-well plates and infected as described above. Before the measurement, cells were incubated for 1 hour with XF Assay Medium (Seahorse Bioscience) plus 5 mM glucose. During the assay, we injected the following at the final concentrations shown: 0.2 μM oligomycin, 0.2 μM FCCP, 1 μM rotenone, and 1 μM antimycin-A. OCR was calculated by plotting the O_2 tension of media as a function of time (pmol/min), and data were normalized by the protein concentration measured in each individual well. The results were quantified as the average of 8–10 wells +/- SEM per time point in at least three independent experiments.

Fatty acid (FA) treatment

Sodium palmitate was conjugated with free BSA in a 5:1 ratio to yield a stock solution of 2.5 mM [27]. Cells were incubated with 0.3 mM or 1 mM of this solution or only BSA (basal control) for 24 hours.

Triglycerides measurement

Triglycerides (TG) were quantified in rBA lipid extracts using TG Triglyceride kit (Sigma), according to the manufacturer's instructions. Protein concentrations were used to normalize sample values.

Statistical analysis

Data are expressed as the mean ± SEM. Control and experimental groups were compared using Student's *t*-test (column analysis) or two-way ANOVA (grouped analysis). $P<0.05$ was considered statistically significant. All figures and statistical analyses were generated using GraphPad Prism 6 software.

Results

Characterization of rBA differentiation stage

A time-course study was performed to assess the differentiation stage of rBA. Differentiation was evaluated by Oil Red O staining, mRNA expression of BAT differentiation markers, and protein levels of UCP1. Oil Red O staining showed an increase in neutral lipid accumulation, starting at day 6 of differentiation (Fig 1A and 1B). The mRNA levels of the brown adipocyte differentiation markers CIDEA, PGC1a, PRDM16 and Zic1 increased at day 3, and peaked at day 6 of differentiation (Fig 1C). The mRNA levels of the beige adipocyte marker CD137 were unchanged (Fig 1C), which indicates that rBA did not show a beige phenotype. The proteins levels of the classical BAT marker, UCP1, were maximal at day 6 of differentiation (Fig 1D). Therefore, day 6, when cells were completely differentiated and had reached maturity, was chosen to perform the expression of CPT1AM.

In addition, we analyzed the mRNA expression pattern of CPT1 isoforms during differentiation (Fig 1E). As expected, CPT1B (the isoform most expressed in BAT), showed higher mRNA changes than the other two isoforms starting at day 3 of differentiation. CPT1A was also increased at day 3 and 6 of differentiation compared to day 0, but to a lesser extent than CPT1B. At day six of differentiation, the three isoforms were significantly increased compared to undifferentiated rBA (day 0).

Enhanced FAO in CPT1AM-expressing rBA

Fully differentiated and mature rBA (day 6) were infected with adenoviruses carrying the CPT1AM gene or GFP as a control. The efficiency of the infection was evaluated in rBA transduced with AdGFP (Fig 2A upper panel; 52.8% infected cells). CPT1A mRNA and protein levels were 9.82- and 3.52-fold higher, respectively, in CPT1AM-expressing rBA than in GFP control cells (Fig 2A lower panel and Fig 2B). The mRNA expression levels of the other CPT1 isoforms (CPT1B and CPT1C) were unaltered in CPT1AM-expressing rBA (S1A Fig and S1 Table). In turn, the FAO rate was 3.42-fold higher in CPT1AM-expressing rBA (Fig 2C). To evaluate whether the increase in FAO was related to an increase in mitochondrial content, we measured the expression of Tim 44 (translocase of mitochondrial inner membrane 44, a mitochondrial content marker), PGC1aα (a mitochondrial biogenesis marker) and Mfn2 (target gene of PGC1a). No changes were seen in any of these markers, which indicate that CPT1AM expression did not affect mitochondrial content or mitochondrial biogenesis (Fig 2D–2F). Interestingly, the mRNA expression of the mitochondrial electron transport respiratory chain (ETC) complexes such as mitochondrial NADH dehydrogenase 1 (Mt-Nd1, complex I), cytochrome b (Mt-Cyb, complex III), cytochrome C oxidase I (Mt-Co1, complex IV component), and ATP synthase 6 (Mt-ATP6, complex V), were increased in CPT1AM-expressing rBA (Fig 2G).

CPT1AM expression increases lipolysis and UCP1 protein levels

The effects of increased FAO on lipolysis and UCP1 protein levels were measured as markers of activation of thermogenesis. We measured intracellular nonesterified fatty acids (NEFAs) and glycerol release, which are two major products of lipolysis, a conventional method to quantify thermogenesis. NEFAs and glycerol levels were increased in CPT1AM-expressing rBA, indicating that CPT1AM expression stimulates lipolysis (Fig 3A and 3B). CPT1AM-expressing cells showed a 1.6-fold increase in UCP1 protein levels compared to GFP-infected cells (Fig 3C).

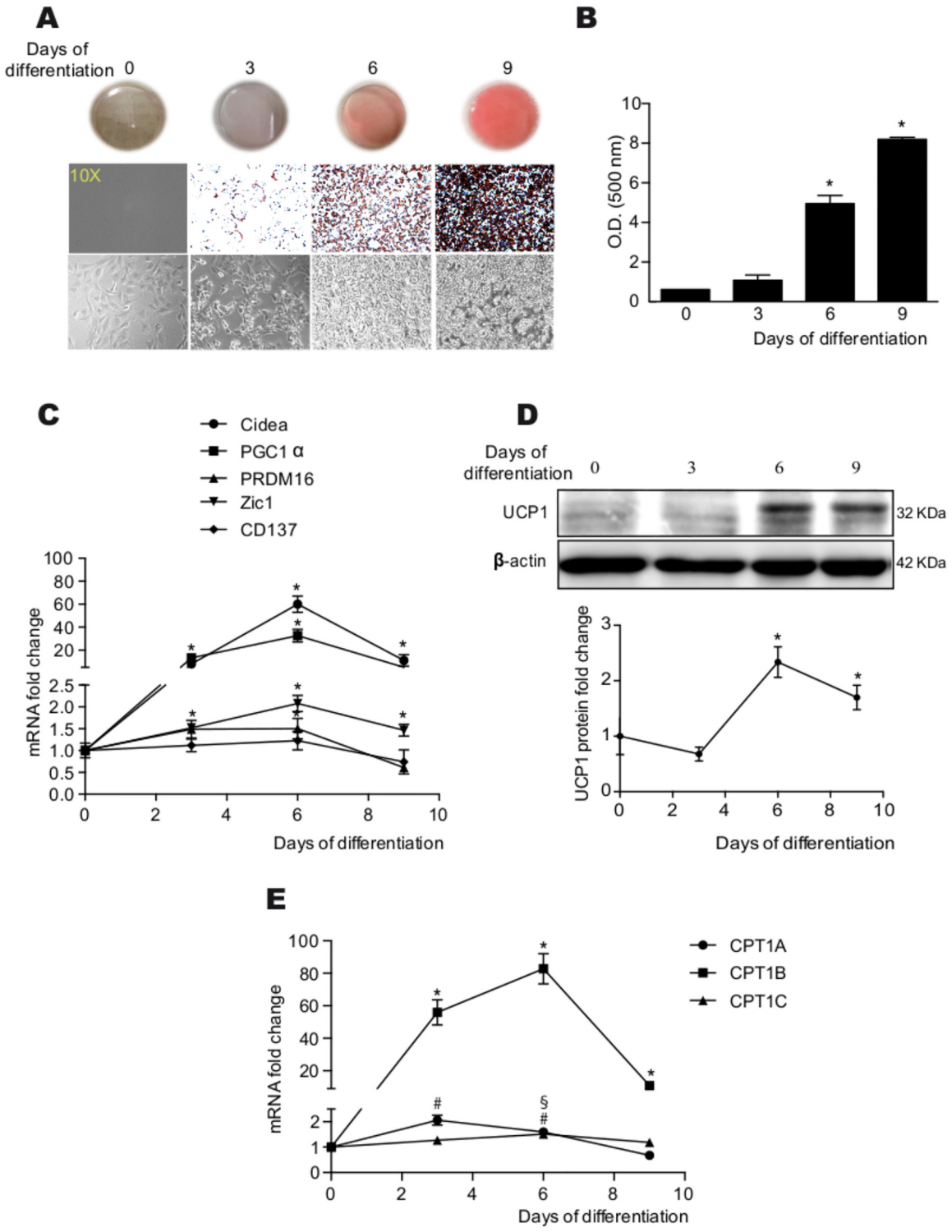

Fig 1. Assessment of rBA differentiation. (A) Oil Red O staining of rBA at different days of differentiation. (B) Quantification of the Oil Red O staining images. (C) Relative mRNA expression of brown (CIDEA, PGC1a, PRDM16, and Zic1) or beige adipocyte markers (CD137). (D) UCP1 protein expression. € Relative mRNA expression of the three CPT1 isoforms during rBA differentiation. The values represent the mean ± SEM of at least three independent experiments. *, #, § $P < 0.05$ compared with day 0 of differentiation of CPT1B, CPT1A and CPT1C, respectively.

doi:10.1371/journal.pone.0159399.g001

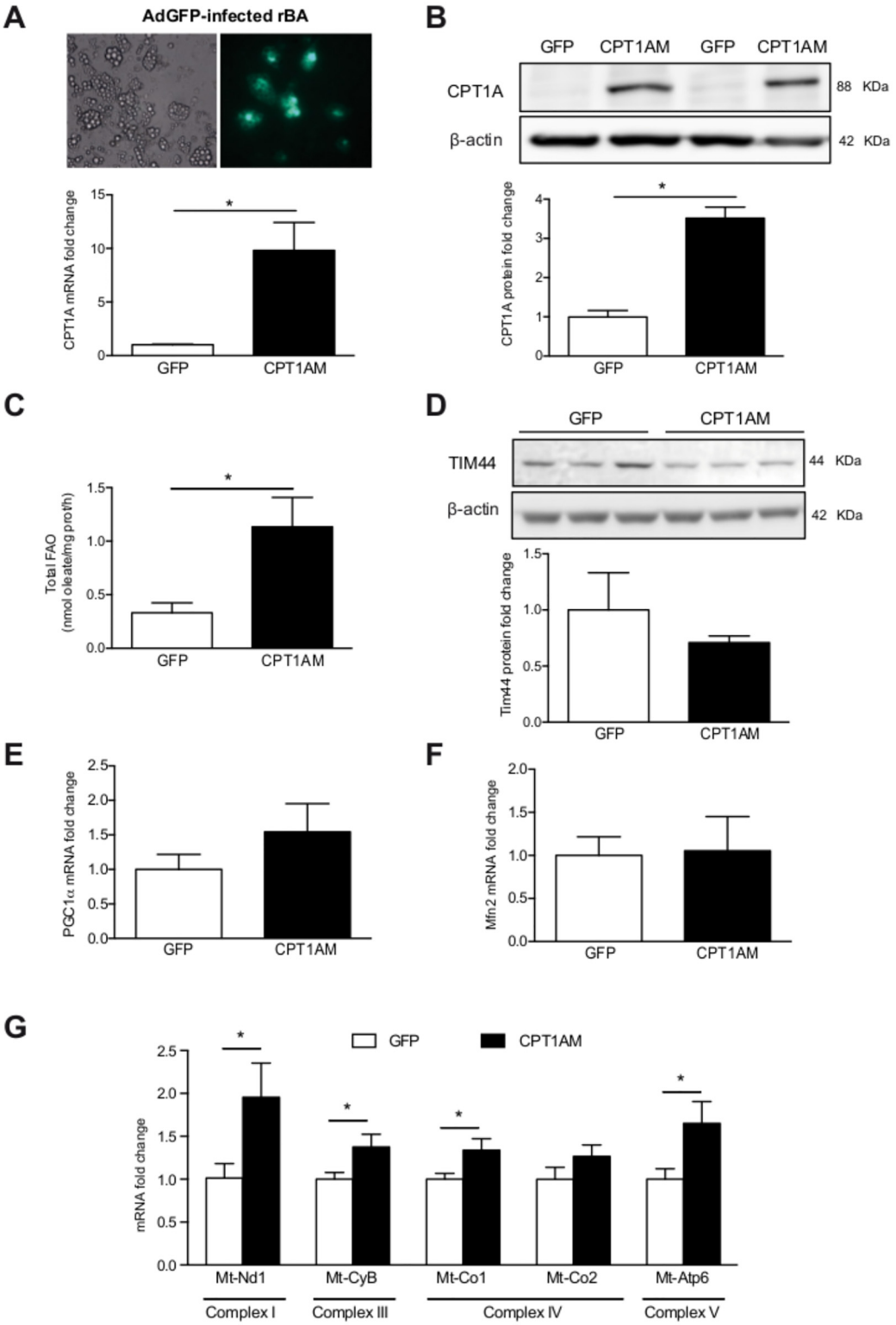

Fig 2. Enhanced FAO in CPT1AM-expressing rBA. (A) (upper panel) AdGFP-infected rBA 48h after infection. A (lower panel): Relative CPT1A mRNA expression in AdGFP- or AdCPT1AM-infected rBA. (B) Whole cell lysates from GFP- and CPT1AM-expressing rBA were subjected to immunoblot analysis with a specific antibody against CPT1A and b-actin. (C) Total FAO rate represented as the sum of acid soluble products plus CO_2 oxidation. (D) Whole cell lysates from GFP- and CPT1AM-expressing rBA were subjected to immunoblot

analysis with a specific antibody against Tim 44 and b-actin. (E-F) Relative PGC1a and Mfn2 mRNA expression in AdGFP- or AdCPT1AM-infected rBA. (G) Relative mRNA expression of the mitochondrial ETC complexes. Shown representative experiment out of 3, n = 3–4. *$P < 0.05$.

doi:10.1371/journal.pone.0159399.g002

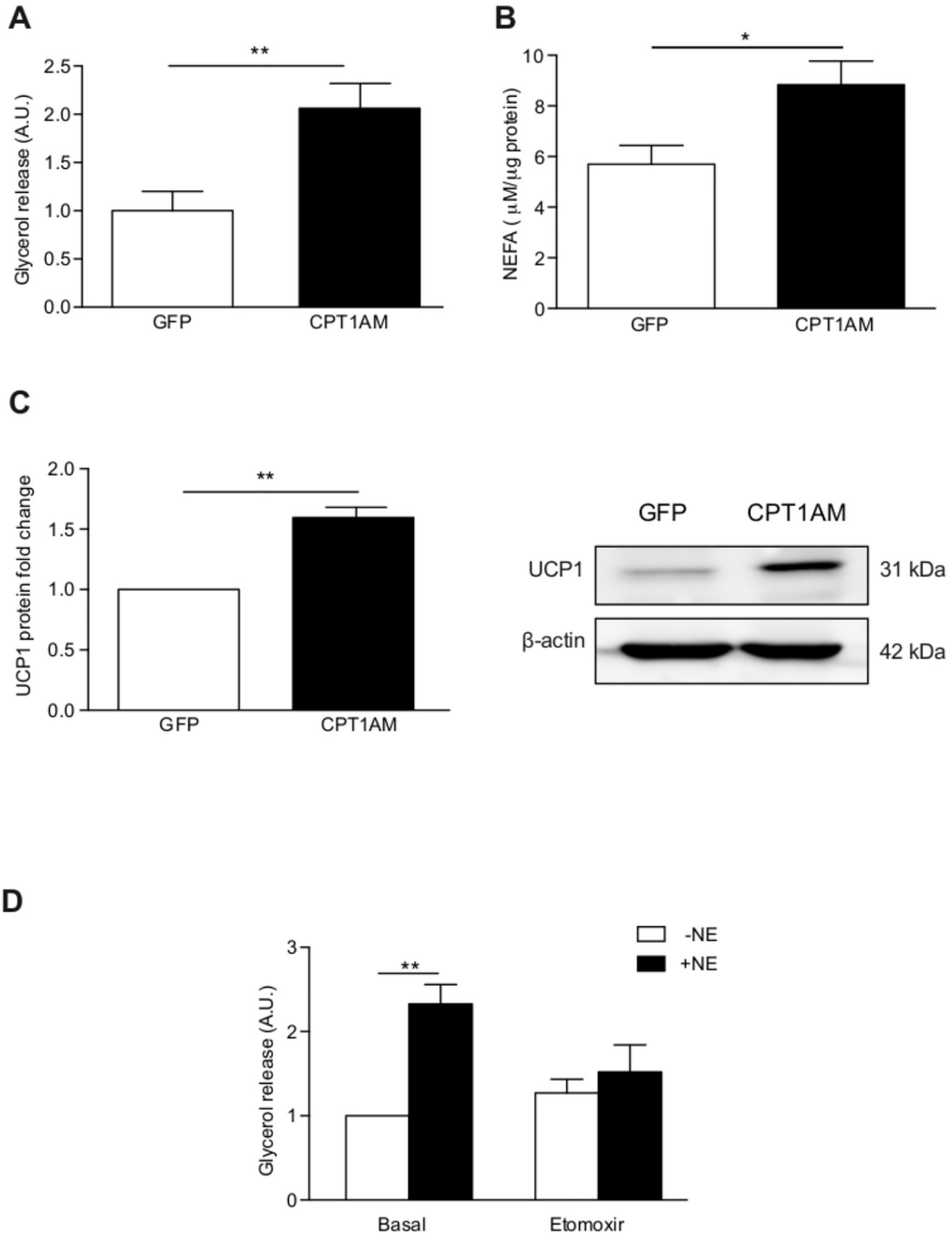

Fig 3. Enhanced lipolysis and UCP1 protein levels in CPT1AM-expressing rBA. (A, B) Lipolysis measured as glycerol release and intracellular NEFAs concentration in GFP- and CPT1AM-expressing rBA. (C) CPT1AM expression increases UCP1 protein levels. (D) Glycerol release in rBA incubated for 6 hours with or without 5 μM norepinephrine (NE) and 180 μM etomoxir. Shown representative experiment out of 3, n = 3–4. *$P < 0.05$, **$P < 0.01$.

doi:10.1371/journal.pone.0159399.g003

To further examine the role of FAO in rBA thermogenesis, rBA were stimulated with norepinephrine (NE) and incubated with or without etomoxir, an irreversible CPT1-specific inhibitor. Glycerol release was measured after 6 hours of treatment. The NE-induced increase in lipolysis was blunted in etomoxir-treated rBA (Fig 3E).

Increased mitochondrial respiration in CPT1AM-expressing rBA

The CPT1AM-induced increase in FAO, UCP1 protein levels and lipolysis prompted us to evaluate potential changes in rBA energetics. Bioenergetic studies were performed using a XF24 Extracellular Flux Analyzer (Seahorse Biosciences) to measure the mitochondrial activity. First, basal respiration was measured, followed by exposure to oligomycin, an inhibitor of ATP synthase, which allowed the measurement of ATP synthesis-coupled respiration and H^+ leak. Then, the uncoupler carbonyl cyanide 4-(trifluoromethoxy) phenylhydrazone [FCCP] was added to measure the maximal respiratory capacity, followed by the Complex I inhibitor rotenone and complex III inhibitor antimycin A, which left only non-mitochondrial respiration to be measured (Fig 4A). Interestingly, the bioenergetic profile of CPT1AM-expressing rBA revealed significant increases in overall mitochondrial respiration (Fig 4A–4F). CPT1AM-expressing rBA showed higher basal respiration (Fig 4B), H^+ leak (Fig 4C), maximal respiratory capacity (Fig 4D), ATP synthesis-coupled respiration (Fig 4E), and reserve capacity (Fig 4F) than GFP control cells.

CPT1AM expression reduces palmitate-induced derangements

The palmitate-induced increase in triglyceride (TG) accumulation was blunted in CPT1AM-expressing rBA (Fig 5A). The mRNA levels of the obesity (FABP4) and inflammatory (TNFa) markers were increased after palmitate treatment. However, CPT1AM-expressing rBA were protected from a palmitate-induced increase in FABP4 and TNFa (Fig 5B and 5C). The mRNA levels of the ER stress markers CHOP and EDEM were decreased in CPT1AM-expressing rBA compared to GFP-control cells (S1B Fig and S1 Table).

Discussion

Obesity and associated diseases such as diabetes have become a worldwide health threat. Dyslipidemia is a common characteristic shared by these metabolic disorders, and the lipid-central point of view has become popular in recent years. The finding that humans have active brown fat has raised high expectations for the treatment of obesity-induced diseases, since brown fat can dissipate caloric energy and reduce both obesity and diabetes in experimental animals [8–12,37–40]. In fact, after short-term cold exposure, brown fat is the main lipid clearance organ [16]. Thus, recent years have seen increasing interest in the regulation of BAT thermogenesis. Most of the strategies have been focused on the role of UCP1 and attempts to enhance heat production, although other authors argue that additional genes may cooperate in the thermogenic function [41].

The finding that BAT is the tissue with the highest FAO rate [42] and that the activity of the FAO rate-limiting enzyme, CPT1, is decreased in BAT of diabetic rats [32] led us to hypothesize that BAT thermogenic power could be enhanced by increasing its FAO. Thus, we overexpressed the constitutively active mutant form, CPT1AM, in rBA.

The assessment of rBA differentiation by Oil Red O staining, UCP1 protein levels and mRNA expression of several BAT differentiation markers showed that the rBA were fully differentiated and mature at day 6. Thus, day 6 was chosen for further experiments. The expression pattern of the three CPT1 isoforms (CPT1A, CPT1B and CPT1C) indicated that all were significantly increased during differentiation, especially CPT1B. Although further studies will

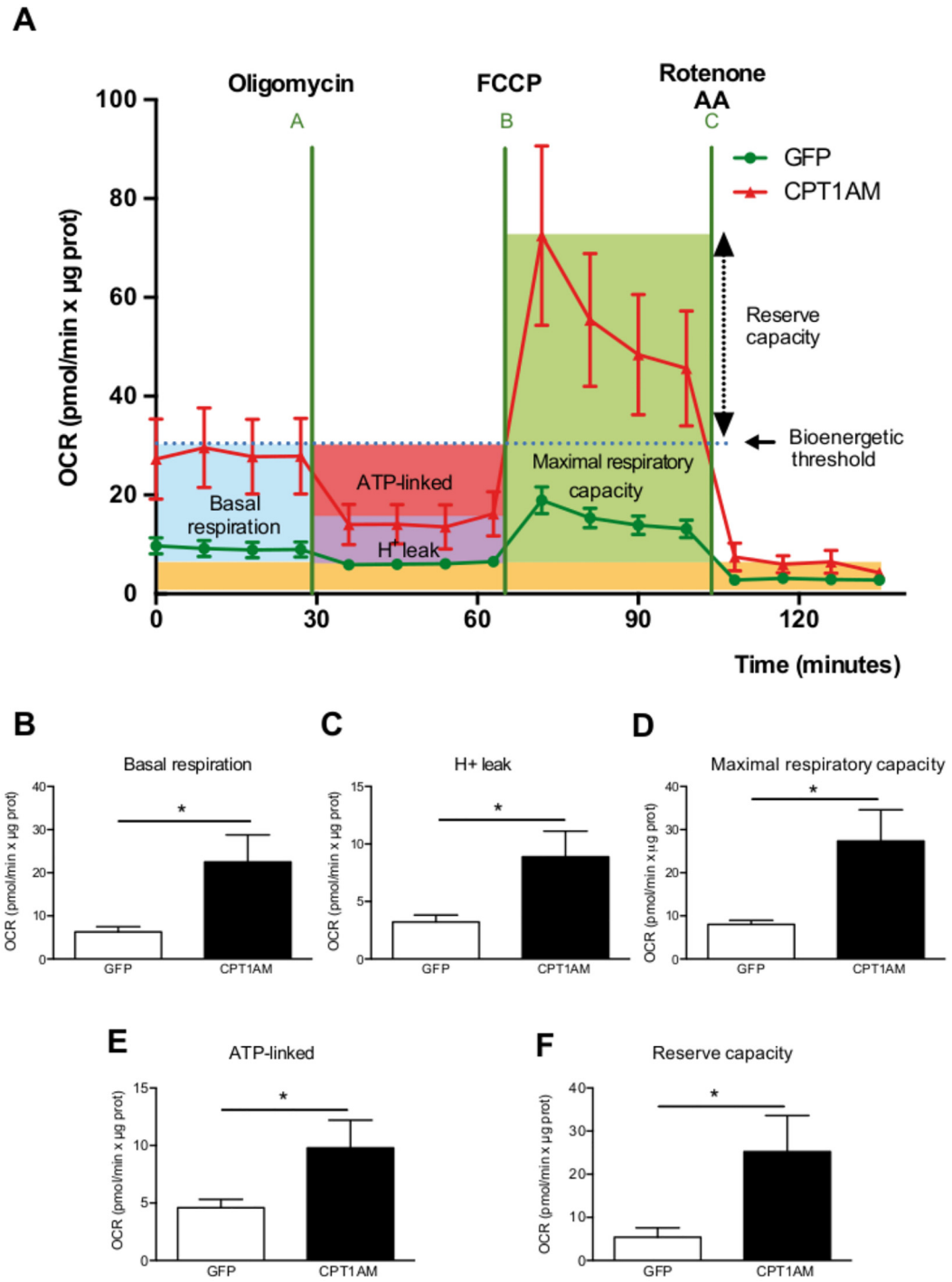

Fig 4. Increased mitochondrial activity in CPT1AM-expressing rBA. (A) Bioenergetic profile of GFP- and CPT1AM-expressing rBA. (B-F) Quantification of Seahorse analysis: basal respiration (B), H^+ leak (C), maximal respiratory capacity (D), ATP-linked (E) and reserve capacity (F). Shown representative experiment out of 3, n = 8–10. *$P < 0.05$.

doi:10.1371/journal.pone.0159399.g004

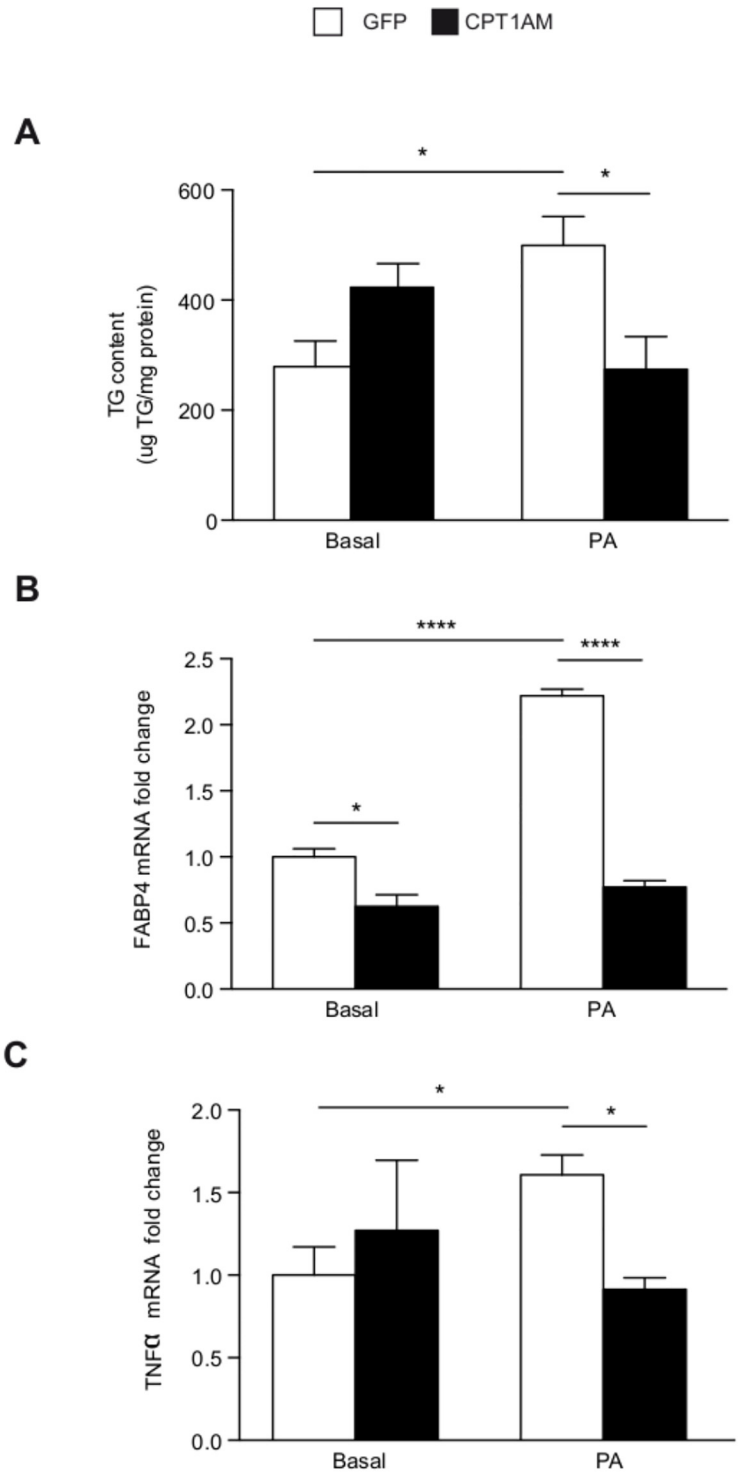

Fig 5. CPT1AM expression is able to reduce lipid-induced derangements. (A) TG content in GFP- or CPT1AM-expressing rBA treated with BSA (basal) or 1 mM palmitate (PA) for 24 hours. (B-C) Relative mRNA expression of FABP4 and TNFa in GFP- or CPT1AM-expressing rBA incubated with 1 mM (FABP4) or 0.3 mM (TNFa) PA. Shown representative experiment out of 3, n = 3–4. *$P < 0.05$, **$P < 0.01$.

doi:10.1371/journal.pone.0159399.g005

be necessary to identify the specific function of each isoform in BAT, these results implicate all three isoforms in the differentiation of brown adipocytes.

Despite BAT being the tissue with the highest FAO rate [42], here we were able to further increase FAO in rBA by the expression of CPT1AM. This was achieved without changes in mitochondrial content or biogenesis. CPT1AM-expressing cells had higher lipolysis and UCP1 protein expression, usually considered as increased thermogenesis. This indicates that CPT1AM-mediated increase in FAO could be an alternative pathway for the regulation of thermogenesis. Initially, BAT thermogenesis requires a plentiful supply of FAs as substrates [43,44]. Therefore, lipolysis is activated during this process, releasing FAs from TG. FAs could be transported into the mitochondria, be involved in the regulation of UCP1 or directly activate UCP1, which uncouples oxidative phosphorylation from ATP production, generating heat [45,46]. Although further experiments will be needed to determine UCP1 regulation during CPT1AM expression, here we have shown that FAO enhancement not only increases lipolysis in rBA, but it is also associated with increased UCP1 protein expression, whose levels are rate-limiting for thermogenesis [47]. Since FA constitute the primary substrate for BAT [48] we hypothesize that CPT1AM expression increases the provision of BAT FA by: 1) directly introducing them into the mitochondria and 2) enhancing lipolysis. The liberated FA then activate and bind to UCP1 in the inner mitochondrial membrane resulting in proton transport, heat generation, and oxygen consumption [48,49]. Thus, CPT1AM may directly or indirectly trigger lipid mobilization to provide BAT mitochondria with fuel (FA).

Several studies have demonstrated the importance of FAO in BAT. Ji *et al*. showed that $CPT1B^{+/-}$ mice developed fatal hypothermia as a result of their inability to perform thermogenesis [50]. More recently, a study in adipocyte-specific CPT2 KO mice indicated that FAO is required for the induction of thermogenic genes in BAT and cold adaptation [29]. In addition, Chondronikola *et al*. have shown that humans with higher amounts of BAT have also higher FAO during cold exposure and that BAT volume is associated with increased lipid metabolism (whole-body FA turnover and oxidation) and adipose tissue insulin sensitivity [51,52]. Here we show that etomoxir (a CPT1-specific inhibitor) blocks TG breakdown in NE-stimulated rBA. These observations indicate that lipolysis supplies substrates for thermogenesis, but when CPT1 is inhibited, free FAs are not transported into the mitochondria and lipolysis is blunted. This would support previous observations that CPT1 inhibitors suppress mitochondrial respiration [53], and that FAO plays an important role during thermogenesis. CPT1AM-expressing rBA displayed increased basal respiration, H^+ leak, maximal respiratory capacity, and reserve capacity. The increase in H^+ leak is consistent with the increase seen in UCP1 protein expression. CPT1AM-expressing rBA showed increased lipolysis (FA substrate availability) and mitochondrial ETC complexes mRNA expression. This could have contributed to the enhanced maximal respiratory capacity [54]. Reserve capacity is the difference between maximal respiratory capacity and basal respiration, and it is a useful qualitative indicator of mitochondrial energetic status [54,55]. Thus, our data indicate that enhanced FAO in brown adipocytes potentiates mitochondrial activity.

Finally, we evaluated whether enhanced FAO by CPT1AM expression in the context of obesity would improve lipid-induced derangements. Thus, we decided to mimic an obese phenotype in our cellular rBA model. Traditionally, FA incubation has been used to activate thermogenesis [56]. We tested several palmitate concentrations and different times of incubation to achieve a lipid-induced increase in TG accumulation and FABP4 and TNFa mRNA expression, similar to that previously observed in obese and lipodystrophic mice [16,57,58]. Enhanced FAO in rBA reduced TG content and FABP4 and TNFa mRNA levels, thereby protecting brown adipocytes from obesity and inflammation. These observations highlight

CPT1AM-mediated activation of FAO in brown adipocytes as a potential strategy to treat obesity-induced diseases.

In summary, we have shown that CPT1AM expression in rBA increases FAO, lipolysis, UCP1 protein levels and mitochondrial activity. Incubation of rBA with the CPT1-specific inhibitor, etomoxir, blocks NE-stimulated lipolysis. Furthermore, enhanced FAO restored the palmitate-induced increase in TG accumulation and the expression levels of obese and inflammatory markers. We conclude that enhancing the fat-burning power of brown adipocytes through CPT1AM expression may protect them from lipid-induced derangements. Thus, CPT1AM-mediated increase in lipolysis, UCP1 protein expression and mitochondrial activity in brown adipocytes may lead to a new treatment of obesity and related disorders.

Supporting Information

S1 Fig. mRNA expression levels of CPT1 isoforms and ER stress markers. (A) Relative mRNA expression of CPT1A, CPT1B and CPT1C in GFP- or CPT1AM-expressing rBA. (B) Relative mRNA expression of BiP, CHOP and EDEM in GFP- or CPT1AM-expressing rBA incubated with 1 mM palmitate (PA). See S1 Table for primer design. Shown representative experiment out of 3, n = 3–4. $^{*}P < 0.05$, $^{**}P < 0.01$.
(TIF)

S1 Table. Quantitative real-time PCR oligonucleotides.
(DOCX)

Acknowledgments

We thank Lucille Banham from the Language Services at the Universitat de Barcelona for valuable assistance in the preparation of the English manuscript and Anna Orozco for research assistance.

Author Contributions

Conceived and designed the experiments: MCD DS RF MW JFM AMV DS LH. Performed the experiments: MCD DS RF MW EGC. Analyzed the data: MCD DS RF MW JFM EGC MJO AZ AMV DS LH. Contributed reagents/materials/analysis tools: MJO AZ AMV DS LH. Wrote the paper: MCD DS RF MJO AMV DS LH.

References

1. World Health Organization (n.d.) Obesity and overweight. http://www.who.int/mediacentre/factsheets/fs311/en/ (accessed 5 January 2016).
2. Shoelson SE, Herrero L, Naaz A (2007) Obesity, inflammation, and insulin resistance. Gastroenterology 132: 2169–2180. doi: 10.1053/j.gastro.2007.03.059 PMID: 17498510
3. Samuel VT, Shulman GI (2012) Mechanisms for insulin resistance: Common threads and missing links. Cell 148: 852–871. doi: 10.1016/j.cell.2012.02.017 PMID: 22385956
4. Sun K, Kusminski CM, Scherer PE (2011) Adipose tissue remodeling and obesity. J Clin Invest 121: 2094–2101. doi: 10.1172/JCI45887 PMID: 21633177
5. Virtue S, Vidal-Puig A (2010) Adipose tissue expandability, lipotoxicity and the Metabolic Syndrome—An allostatic perspective. Biochim Biophys Acta—Mol Cell Biol Lipids 1801: 338–349.
6. Hany TF, Gharehpapagh E, Kamel EM, Buck A, Himms-Hagen J, et al. (2002) Brown adipose tissue: A factor to consider in symmetrical tracer uptake in the neck and upper chest region. Eur J Nucl Med 29: 1393–1398. doi: 10.1007/s00259-002-0902-6
7. Nedergaard J, Bengtsson T, Cannon B (2007) Unexpected evidence for active brown adipose tissue in adult humans. Am J Physiol Endocrinol Metab 293: E444–E452. doi: 10.1152/ajpendo.00691.2006 PMID: 17473055

8. Cypess AM, Lehman S, Williams G, Tal I, Rodman D, et al. (2009) Identification and importance of brown adipose tissue in adult humans. N Engl J Med 360: 1509–1517.
9. Virtanen KA, Lidell ME, Orava J, Heglind M, Westergren R, et al. (2009) Functional brown adipose tissue in healthy adults. N Engl J Med 360: 1518–1525. doi: 10.1056/NEJMoa0808949 PMID: 19357407
10. Zingaretti MC, Crosta F, Vitali A, Guerrieri M, Frontini A, et al. (2009) The presence of UCP1 demonstrates that metabolically active adipose tissue in the neck of adult humans truly represents brown adipose tissue. FASEB J 23: 3113–3120. doi: 10.1096/fj.09-133546 PMID: 19417078
11. Saito M, Okamatsu-Ogura Y, Matsushita M, Watanabe K, Yoneshiro T, et al. (2009) High incidence of metabolically active brown adipose tissue in healthy adult humans: effects of cold exposure and adiposity. Diabetes 58: 1526–1531. doi: 10.2337/db09-0530 PMID: 19401428
12. van Marken Lichtenbelt WD, Vanhommerig JW, Smulders NM, Drossaerts JM a FL, Kemerink GJ, et al. (2009) Cold-activated brown adipose tissue in healthy men. N Engl J Med 360: 1500–1508. doi: 10.1056/NEJMoa0808718 PMID: 19357405
13. Xue R, Lynes MD, Dreyfuss JM, Shamsi F, Schulz TJ, et al. (2015) Clonal analyses and gene profiling identify genetic biomarkers of the thermogenic potential of human brown and white preadipocytes. Nat Med 21: 760–768. doi: 10.1038/nm.3881 PMID: 26076036
14. Calderon-Dominguez M; Mir JF; Fucho R; Weber M; Serra D; Herrero L (2016) Fatty Acid Metabolism and the Basis of Brown Adipose Tissue Function. Adipocyte: 5:98–118. doi: 10.1080/21623945.2015.1122857 PMID: 27386151
15. de Jong JM a, Larsson O, Cannon B, Nedergaard J (2015) A stringent validation of mouse adipose tissue identity markers. Am J Physiol—Endocrinol Metab 308: E1085–E1105. doi: 10.1152/ajpendo.00023.2015 PMID: 25898951
16. Bartelt A, Bruns OT, Reimer R, Hohenberg H, Ittrich H, et al. (2011) Brown adipose tissue activity controls triglyceride clearance. Nat Med 17: 200–205. doi: 10.1038/nm.2297 PMID: 21258337
17. Festuccia WT, Blanchard P-G, Deshaies Y (2011) Control of Brown Adipose Tissue Glucose and Lipid Metabolism by PPARγ. Front Endocrinol (Lausanne) 2: 84. doi: 10.3389/fendo.2011.00084
18. Festuccia WT, Blanchard P-G, Turcotte V, Laplante M, Sariahmetoglu M, et al. (2009) The PPARgamma agonist rosiglitazone enhances rat brown adipose tissue lipogenesis from glucose without altering glucose uptake. Am J Physiol Regul Integr Comp Physiol 296: R1327–R1335. doi: 10.1152/ajpregu.91012.2008 PMID: 19211718
19. Malandrino MI, Fucho R, Weber M, Calderon-Dominguez M, Mir JF, et al. (2015) Enhanced fatty acid oxidation in adipocytes and macrophages reduces lipid-induced triglyceride accumulation and inflammation. Am J Physiol—Endocrinol Metab 308: E756–E769. doi: 10.1152/ajpendo.00362.2014 PMID: 25714670
20. Stefanovic-Racic M, Perdomo G, Mantell BS, Sipula IJ, Brown NF, et al. (2008) A moderate increase in carnitine palmitoyltransferase 1a activity is sufficient to substantially reduce hepatic triglyceride levels. Am J Physiol Endocrinol Metab 294: E969–E977. doi: 10.1152/ajpendo.00497.2007 PMID: 18349115
21. Orellana-Gavaldà JM, Herrero L, Malandrino MI, Pañeda A, Sol Rodríguez-Peña M, et al. (2011) Molecular therapy for obesity and diabetes based on a long-term increase in hepatic fatty-acid oxidation. Hepatology 53: 821–832. doi: 10.1002/hep.24140 PMID: 21319201
22. Monsénégo J, Mansouri A, Akkaoui M, Lenoir V, Esnous C, et al. (2012) Enhancing liver mitochondrial fatty acid oxidation capacity in obese mice improves insulin sensitivity independently of hepatic steatosis. J Hepatol 56: 632–639. doi: 10.1016/j.jhep.2011.10.008 PMID: 22037024
23. Rubi B, Antinozzi PA, Herrero L, Ishihara H, Asins G, et al. (2002) Adenovirus-mediated overexpression of liver carnitine palmitoyltransferase I in INS1E cells: effects on cell metabolism and insulin secretion. Biochem J 364: 219–226. PMID: 11988095
24. Herrero L, Rubí B, Sebastián D, Serra D, Asins G, et al. (2005) Alteration of the malonyl-CoA/carnitine palmitoyltransferase I interaction in the beta-cell impairs glucose-induced insulin secretion. Diabetes 54: 462–471. doi: 10.2337/diabetes.54.2.462 PMID: 15677504
25. Mera P, Mir JF, Fabriàs G, Casas J, Costa ASH, et al. (2014) Long-term increased carnitine palmitoyltransferase 1A expression in ventromedial hypotalamus causes hyperphagia and alters the hypothalamic lipidomic profile. PLoS One 9: e97195. doi: 10.1371/journal.pone.0097195 PMID: 24819600
26. Perdomo G, Commerford SR, Richard A-MT, Adams SH, Corkey BE, et al. (2004) Increased beta-oxidation in muscle cells enhances insulin-stimulated glucose metabolism and protects against fatty acid-induced insulin resistance despite intramyocellular lipid accumulation. J Biol Chem 279: 27177–27186. doi: 10.1074/jbc.M403566200 PMID: 15105415
27. Sebastián D, Herrero L, Serra D, Asins G, Hegardt FG (2007) CPT I overexpression protects L6E9 muscle cells from fatty acid-induced insulin resistance. Am J Physiol Endocrinol Metab 292: E677–E686. doi: 10.1152/ajpendo.00360.2006 PMID: 17062841

28. Bruce CR, Hoy AJ, Turner N, Watt MJ, Allen TL, et al. (2009) Overexpression of carnitine palmitoyltransferase-1 in skeletal muscle is sufficient to enhance fatty acid oxidation and improve high-fat diet-induced insulin resistance. Diabetes 58: 550–558. doi: 10.2337/db08-1078 PMID: 19073774

29. Lee J, Ellis JM, Wolfgang MJ (2015) Adipose Fatty Acid Oxidation Is Required for Thermogenesis and Potentiates Oxidative Stress-Induced Inflammation. Cell Rep 10: 266–279. doi: 10.1016/j.celrep.2014.12.023 PMID: 25578732

30. Brown NF, Hill JK, Esser V, Kirkland JL, Corkey BE, et al. (1997) Mouse white adipocytes and 3T3-L1 cells display an anomalous pattern of carnitine palmitoyltransferase (CPT) I isoform expression during differentiation. Inter-tissue and inter-species expression of CPT I and CPT II enzymes. Biochem J 327: 225–231. PMID: 9355756

31. Price N, van der Leij F, Jackson V, Corstorphine C, Thomson R, et al. (2002) A novel brain-expressed protein related to carnitine palmitoyltransferase I. Genomics 80: 433–442. doi: 10.1006/geno.2002.6845 PMID: 12376098

32. Jamal Z, Saggerson ED (1988) Changes in brown-adipose-tissue mitochondrial processes in streptozotocin-diabetes. Biochem J 252: 293–296. PMID: 3421907

33. Morillas M, Gómez-Puertas P, Bentebibel A, Sellés E, Casals N, et al. (2003) Identification of conserved amino acid residues in rat liver carnitine palmitoyltransferase I critical for malonyl-CoA inhibition: Mutation of methionine 593 abolishes malonyl-CoA inhibition. J Biol Chem 278: 9058–9063. doi: 10.1074/jbc.M209999200 PMID: 12499375

34. McGarry JD, Mills SE, Long CS, Foster DW (1983) Observations on the affinity for carnitine, and malonyl-CoA sensitivity, of carnitine palmitoyltransferase I in animal and human tissues. Demonstration of the presence of malonyl-CoA in non-hepatic tissues of the rat. Biochem J 214: 21–28. PMID: 6615466

35. Lorenzo M, Valverde a. M, Teruel T, Benito M (1993) IGF-I is a mitogen involved in differentiation-related gene expression in fetal rat brown adipocytes. J Cell Biol 123: 1567–1575. doi: 10.1083/jcb.123.6.1567 PMID: 8253851

36. Gesta S, Bezy O, Mori MA, Macotela Y, Lee KY, et al. (2011) Mesodermal developmental gene Tbx15 impairs adipocyte differentiation and mitochondrial respiration. Proc Natl Acad Sci U S A 108: 2771–2776. doi: 10.1073/pnas.1019704108 PMID: 21282637

37. Zhang Y, Xu Q, Liu YH, Zhang XS, Wang J, et al. (2015) Medium-Chain Triglyceride Activated Brown Adipose Tissue and Induced Reduction of Fat Mass in C57BL/6J Mice Fed High-fat Diet. Biomed Environ Sci 28: 97–104. doi: 10.3967/bes2015.012 PMID: 25716560

38. Liu X, Wang S, You Y, Meng M, Zheng Z, et al. (2015) Brown Adipose Tissue Transplantation Reverses Obesity in Ob/Ob Mice. Endocrinology 156: 2461–2469. doi: 10.1210/en.2014-1598 PMID: 25830704

39. Heppner KM, Marks S, Holland J, Ottaway N, Smiley D, et al. (2015) Contribution of brown adipose tissue activity to the control of energy balance by GLP-1 receptor signalling in mice. Diabetologia 58: 2124–2132. doi: 10.1007/s00125-015-3651-3 PMID: 26049402

40. Thiam AR, Farese R V, Walther TC (2013) The biophysics and cell biology of lipid droplets. Nat Rev Mol Cell Biol 14: 775–786. doi: 10.1038/nrm3699 PMID: 24220094

41. Yu XX, Lewin DA, Forrest W, Adams SH (2002) Cold elicits the simultaneous induction of fatty acid synthesis and beta-oxidation in murine brown adipose tissue: prediction from differential gene expression and confirmation in vivo. FASEB J 16: 155–168. doi: 10.1096/fj.01-0568com PMID: 11818363

42. Doh K-O, Kim Y-W, Park S-Y, Lee S-K, Park JS, et al. (2005) Interrelation between long-chain fatty acid oxidation rate and carnitine palmitoyltransferase 1 activity with different isoforms in rat tissues. Life Sci 77: 435–443. doi: 10.1016/j.lfs.2004.11.032 PMID: 15894012

43. Nedergaard J, Bengtsson T, Cannon B (2011) New powers of brown fat: Fighting the metabolic syndrome. Cell Metab 13: 238–240. doi: 10.1016/j.cmet.2011.02.009 PMID: 21356513

44. Townsend KL, Tseng Y-H (2014) Brown fat fuel utilization and thermogenesis. Trends Endocrinol Metab 25: 168–177. doi: 10.1016/j.tem.2013.12.004 PMID: 24389130

45. Smith RE (1961) Thermogenic activity of the hibernating gland in the cold-acclimated rat. Physiologist 4: 113–113.

46. Cannon B, Nedergaard J (2004) Brown adipose tissue: function and physiological significance. Physiol Rev 84: 277–359. doi: 10.1152/physrev.00015.2003 PMID: 14715917

47. Shabalina IG, Ost M, Petrovic N, Vrbacky M, Nedergaard J, et al. (2010) Uncoupling protein-1 is not leaky. Biochim Biophys Acta—Bioenerg 1797: 773–784. doi: 10.1016/j.bbabio.2010.04.007

48. Cannon B, Nedergaard J (2004) Brown adipose tissue: function and physiological significance. Physiol Rev 84: 277–359. doi: 10.1152/physrev.00015.2003 PMID: 14715917

49. Li Y, Fromme T, Schweizer S, Schöttl T, Klingenspor M (2014) Taking control over intracellular fatty acid levels is essential for the analysis of thermogenic function in cultured primary brown and brite/beige adipocytes. EMBO Rep 15: 1069–1076. doi: 10.15252/embr.201438775 PMID: 25135951

50. Ji S, You Y, Kerner J, Hoppel CL, Schoeb TR, et al. (2008) Homozygous carnitine palmitoyltransferase 1b (muscle isoform) deficiency is lethal in the mouse. Mol Genet Metab 93: 314–322. PMID: 18023382

51. Chondronikola M, Volpi E, Borsheim E, Porter C, Annamalai P, et al. (2014) Brown Adipose Tissue Improves Whole-Body Glucose Homeostasis and Insulin Sensitivity in Humans. Diabetes 63: 4089–4099. doi: 10.2337/db14-0746 PMID: 25056438

52. Chondronikola M, Volpi E, Børsheim E, Porter C, Saraf MK, et al. (2016) Brown Adipose Tissue Activation Is Linked to Distinct Systemic Effects on Lipid Metabolism in Humans. Cell Metab 23: 1200–1206. doi: 10.1016/j.cmet.2016.04.029 PMID: 27238638

53. Bukowiecki LJ, Folléa N, Lupien J, Paradis A (1981) Metabolic relationships between lipolysis and respiration in rat brown adipocytes. The role of long chain fatty acids as regulators of mitochondrial respiration and feedback inhibitors of lipolysis. J Biol Chem 256: 12840–12848. PMID: 6273408

54. Hill BG, Benavides GA, Lancaster JR, Ballinger S, Dell'Italia L, et al. (2012) Integration of cellular bioenergetics with mitochondrial quality control and autophagy. Biol Chem 393: 1485–1512. doi: 10.1515/hsz-2012-0198 PMID: 23092819

55. Chacko BK, Kramer P a, Ravi S, Benavides G a, Mitchell T, et al. (2014) The Bioenergetic Health Index: a new concept in mitochondrial translational research. Clin Sci (Lond) 127: 367–373. doi: 10.1042/CS20140101

56. Divakaruni AS, Humphrey DM, Brand MD (2012) Fatty acids change the conformation of uncoupling protein 1 (UCP1). J Biol Chem 287: 36845–36853. doi: 10.1074/jbc.M112.381780 PMID: 22952235

57. Queipo-Ortuño MI, Escoté X, Ceperuelo-Mallafré V, Garrido-Sanchez L, Miranda M, et al. (2012) FABP4 dynamics in obesity: discrepancies in adipose tissue and liver expression regarding circulating plasma levels. PLoS One 7: e48605. doi: 10.1371/journal.pone.0048605 PMID: 23139800

58. Herrero L, Shapiro H, Nayer A, Lee J, Shoelson SE (2010) Inflammation and adipose tissue macrophages in lipodystrophic mice. Proc Natl Acad Sci U S A 107: 240–245. doi: 10.1073/pnas.0905310107 PMID: 20007767

Daniel E. Francés,[1] Omar Motiño,[2] Noelia Agrá,[2] Águeda González-Rodríguez,[2,3] Ana Fernández-Álvarez,[1] Carme Cucarella,[4] Rafael Mayoral,[5,6] Luis Castro-Sánchez,[2] Ester García-Casarrubios,[2] Lisardo Boscá,[2,5] Cristina E. Carnovale,[1] Marta Casado,[4,5] Ángela M. Valverde,[2,3] and Paloma Martín-Sanz[2,5]

Hepatic Cyclooxygenase-2 Expression Protects Against Diet-Induced Steatosis, Obesity, and Insulin Resistance

Diabetes 2015;64:1522–1531 | DOI: 10.2337/db14-0979

Accumulation evidence links obesity-induced inflammation as an important contributor to the development of insulin resistance, which plays a key role in the pathophysiology of obesity-related diseases such as type 2 diabetes and nonalcoholic fatty liver disease. Cyclooxygenase (COX)-1 and -2 catalyze the first step in prostanoid biosynthesis. Because adult hepatocytes fail to induce COX-2 expression regardless of the proinflammatory stimuli used, we have evaluated whether this lack of expression under mild proinflammatory conditions might constitute a permissive condition for the onset of insulin resistance. Our results show that constitutive expression of human COX-2 (hCOX-2) in hepatocytes protects against adiposity, inflammation, and, hence, insulin resistance induced by a high-fat diet, as demonstrated by decreased hepatic steatosis, adiposity, plasmatic and hepatic triglycerides and free fatty acids, increased adiponectin-to-leptin ratio, and decreased levels of proinflammatory cytokines, together with an enhancement of insulin sensitivity and glucose tolerance. Furthermore, hCOX-2 transgenic mice exhibited increased whole-body energy expenditure due in part by induction of thermogenesis and fatty acid oxidation. The analysis of hepatic insulin signaling revealed an increase in insulin receptor–mediated Akt phosphorylation in hCOX-2 transgenic mice. In conclusion, our results point to COX-2 as a potential therapeutic target against obesity-associated metabolic dysfunction.

Insulin resistance (IR) plays a key role in the pathophysiology of obesity-related diseases such as type 2 diabetes and nonalcoholic fatty liver disease. IR is the key primary defect underlying the development of type 2 diabetes and is a central component defining the metabolic syndrome. That IR is associated with a state of chronic low-grade inflammation has been demonstrated, and inflammation is assumed to contribute in a major way to its development (1). Besides the fact that IR is characterized by complex interactions between genetic determinants and nutritional factors, it is recognized that mediators synthesized from immune cells and adipocytes are involved in the regulation of insulin action (2). Insulin acts in target cells by binding to its specific receptor and activating a cascade of intracellular signaling events that are altered in inflammation-associated IR (3).

Inflammation induces the expression of a variety of proteins, including prostaglandin–endoperoxide synthase-2, also known as cyclooxygenase (COX)-2, which catalyzes the first step in prostanoid biosynthesis. COX-2 is induced by a variety of stimuli such as growth factors, proinflammatory mediators, hormones, and other cellular

[1]Institute of Experimental Physiology (Instituto de Fisiología Experimental), Consejo Nacional de Investigaciones Científicas y Técnicas, Rosario, Argentina
[2]Institute of Biomedical Research Alberto Sols, Consejo Superior de Investigaciones Científicas-Universidad Autónoma de Madrid, Madrid, Spain
[3]CIBERDEM, Instituto de Salud Carlos III, Madrid, Spain
[4]Biomedical Institute of Valencia, Instituto de Biomedicina de Valencia-Consejo Superior de Investigaciones Científicas, Valencia, Spain
[5]CIBERehd, Instituto de Salud Carlos III, Madrid, Spain
[6]Department of Medicine, University of California, San Diego, La Jolla, CA

Corresponding author: Paloma Martín-Sanz, pmartins@iib.uam.es, or Ángela M. Valverde, avalverde@iib.uam.es.

Received 25 June 2014 and accepted 18 November 2014.

This article contains Supplementary Data online at http://diabetes.diabetesjournals.org/lookup/suppl/doi:10.2337/db14-0979/-/DC1.

D.E.F., O.M., and N.A. contributed equally to this work.

A.M.V. and P.M.-S. share senior authorship.

stresses (4). On one hand, adult hepatocytes fail to induce COX-2 regardless of the proinflammatory stimuli used, and COX-2 is induced only under prolonged aggression as a result of the drop of C/EBP-α (5) or after partial hepatectomy (6). On the other hand, Kupffer, stellate, hepatoma mouse liver cells, and fetal hepatocytes retain the ability to express COX-2 upon stimulation with lipopolysaccharide and proinflammatory cytokines (7).

Previous work has implicated COX-2 in the pathogenesis of obesity and IR. Hsieh et al. (8–10) reported muscle and fat IR improved in rats fed fructose or a high-fat diet (HFD) treated with COX-2 inhibitors. However, Coll et al. (11) found that COX-2 inhibition exacerbated palmitate-induced inflammation and IR in skeletal muscle. Our previous results (12), performed in a model of transgenic (Tg) mice constitutively expressing human COX-2 in hepatocytes (hCOX-2–Tg), demonstrated a protective role of COX-2 against liver apoptosis induced by streptozotocin-mediated hyperglycemia. These findings prompted us to screen the role of COX-2 expression in hepatocytes in a model of IR and altered energy homeostasis induced by HFD. The current study has demonstrated that expression of COX-2 in hepatocytes protects against steatosis, adiposity, inflammation, and hepatic IR in hCOX-2–Tg mice under HFD conditions by improving insulin sensitivity and glucose tolerance, enhancing Akt and AMPK phosphorylation, decreasing protein tyrosine phosphatase-1B (PTP1B) protein levels, and increasing thermogenesis and energy expenditure.

RESEARCH DESIGN AND METHODS

Animal Experimentation

The study used hCOX-2–Tg mice (25–30 g body weight; 3 months) on a B6D2/OlaHsd background along with corresponding age-matched wild-type (Wt) mice (13). Animals were treated according to the Institutional Care Instructions (Bioethical Commission from Spanish Research Council [CSIC], Spain). The hCOX-2–Tg mice and their corresponding Wt littermates were generated by systematic mating of Tg mice with B6D2F1/OlaHsd Wt mice in our animal facilities for more than seven generations.

Insulin Signaling Studies

Wt and hCOX-2–Tg mice fasted for 6 h were intraperitoneally injected with 0.75 units/kg human recombinant insulin and killed 15 min later. The liver was removed, and RNA and total protein extracts were prepared, as previously described (14).

Induction of Liver Steatosis and Obesity by HFD

Wt and hCOX-2–Tg mice were fed a regular chow diet (RCD; A04-10, Panlab, Barcelona, Spain) or a 42% HFD (TD.88137, Harlan Laboratories, Madison, WI) ad libitum for 12 weeks. Some (n = 7) of the hCOX-2–Tg mice fed the HFD were treated intraperitoneally with 10 mg/kg/day DFU, a COX-2 selective inhibitor, five times in a week during all the treatment. During HFD treatment, body weight and food and water intake were recorded every 2 days. After 12 weeks of treatment, animals were killed and the liver, epididymal white adipose tissue (eWAT), inguinal WAT (iWAT), and interscapular brown adipose tissue (BAT) were snap-frozen in liquid nitrogen and stored at −80°C or collected in a solution containing 30% sucrose in PBS or fixed in 10% buffered formalin. Plasma was obtained from the inferior vena cava.

Metabolic Measurements

Metabolic measurements were performed at the beginning of HFD treatment and at the end of week 12. Mice underwent an insulin tolerance test (ITT) and glucose tolerance test (GTT). For the ITT, after mice fasted for 6 h were intraperitoneally injected with 0.75 units/kg human recombinant insulin. Blood glucose was measured from the tail vein at 0, 15, 30, 60, and 90 min. For the GTT, mice fasted for 16 h were intraperitoneally injected with 2 g/kg glucose, and blood samples were taken at 0, 30, 60, and 90 min. Glucose levels were measured with an Accu-Check Glucometer (Roche). The homeostasis model of assessment of IR (HOMA-IR), an index of whole-body IR at the basal state, was calculated as HOMA-IR = (FPI × FPG)/22.5, where FPI is fasting plasma insulin concentration (mU/L) and FPG is fasting plasma glucose (mmol/L).

Indirect Calorimetry

At the end of week 12, independent groups of Wt and hCOX-2–Tg mice (n = 4) were analyzed by indirect calorimetry in a PhenoMaster System (TSE Systems, Bad Homburg, Germany). Mice were acclimated to the test chamber for at least 24 h and were monitored for an additional 48 h. Food and water were provided ad libitum in the appropriate devices and measured by the built-in automated instruments. VO_2 and VCO_2 measurements were taken every 10 min. The respiratory exchange ratio was calculated as: RER = VCO_2/VO_2. Energy expenditure (EE) was calculated as: EE = [3.815 + (1.23 × RER)] × VO_2 × 1.44. Data are the average values obtained in these recordings.

Cold Exposure Experiments

Three-month-old Wt and hCOX-2–Tg mice (n = 8) were acclimated at a temperature of 28°C for 1 week. Then, mice were randomly divided into two groups: one group was exposed to 4°C for 6 h in individual cages and the other group was maintained at 28°C. Mice were killed at the end of the experiment, and BAT, eWAT and iWAT depots were removed and frozen in liquid nitrogen for posterior assays.

Data Analysis

Statistical analyses were performed using SPSS 17 software. Data are expressed as means ± SE. The Student t test was applied whenever necessary, and statistical analysis of the differences between groups was performed by

one-way ANOVA, followed by the Tukey test. $P < 0.05$ was considered statistically significant.

RESULTS

COX-2–Tg Mice Are Protected From HFD-Induced Hepatic Steatosis, Obesity, and IR

To explore whether COX-2 expression in hepatocytes affects glucose tolerance and insulin sensitivity in mice, we used our previously described hCOX-2–Tg mice that constitutively express human COX-2 in hepatocytes under the control of the human apolipoprotein E promoter and its specific hepatic control region, a unique regulatory domain that directs apolipoprotein E expression in the liver (13) and that also lacks macrophage-specific regulatory regions (ME.2 and ME.1) (15), ensuring exclusive expression in liver. Prostaglandin E_2 (PGE_2), the main COX-2–derived prostanoid in the liver, is threefold increased (Supplementary Fig. 1*A* and *B*) (13). The expression of COX-2 in the liver of COX-2–Tg mice was comparable to the levels reached in fetal hepatocytes after stimulation with lipopolysaccharide (5,7) and in liver regeneration after partial hepatectomy (6,16).

Although, no differences in body weight gain were found under the RCD condition (Supplementary Fig. 1*C*), the body weight in hCOX-2–Tg mice fed the HFD did not increase as much as the corresponding Wt littermates, and the eWAT size and liver weight were significantly lower compared with those of the Wt mice (liver weight: 1.29 ± 0.05 g for hCOX-2–Tg and 1.63 ± 0.11 g for Wt; $P < 0.05$) (Fig. 1*A*–*C*). Notably, hCOX-2–Tg mice displayed a 20% lesser body weight gain without significant changes in the initial body weight or in food intake (Fig. 1*D*).

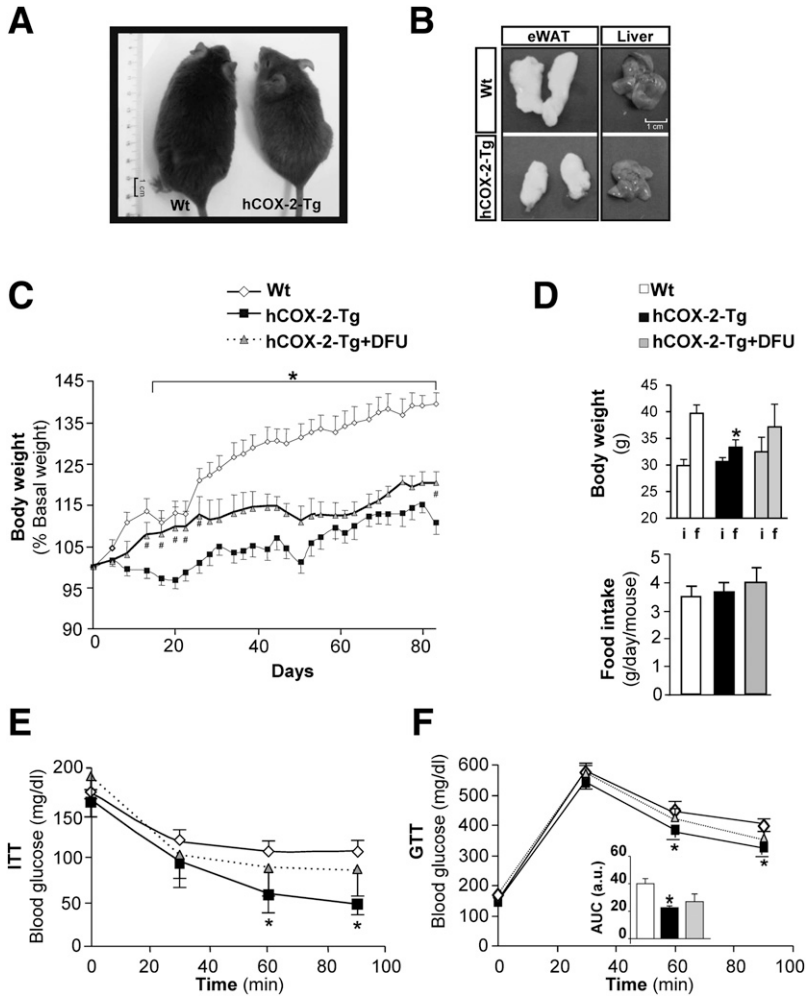

Figure 1—hCOX-2–Tg mice are protected from HFD-induced obesity, insulin, and glucose intolerances. Wt and hCOX-2–Tg mice were fed an HFD ad libitum for 12 weeks. An additional group of hCOX-2–Tg mice was treated with the COX-2 inhibitor DFU five times weekly during all HFD treatment. *A*: Representative photographs of Wt and hCOX-2–Tg mice. *B*: Representative photographs of eWAT and liver from Wt and hCOX-2–Tg mice. *C*: Body weight curve of Wt, hCOX-2–Tg, and hCOX-2–Tg+DFU mice fed an HFD expressed as percentage of basal body weight. Data are expressed as means ± SE ($n = 7$ per group). *$P < 0.05$ vs. Wt; #$P < 0.05$ vs. hCOX-2–Tg. *D*: Initial (i) and final (f) body weight and mean daily food intake. ITT after 6 h fasting (*E*) and GTT after 16 h fasting (*F*) of animals ($n = 6$ per group) after HFD. Graph represents area under the curve (AUC) during GTT. Data are expressed as means ± SE. *$P < 0.05$ vs. Wt.

Interestingly enough, hCOX-2–Tg mice treated with DFU exhibited an intermediate body weight value (Fig. 1*C*). To assess the effect of the HFD on glucose homeostasis, HFD-fed mice underwent GTT and ITT analysis (Fig. 1*E* and *F*). Plasma glucose levels (mg/dL) were similar among genotypes under the HFD condition, at 173.5 ± 6.7 for Wt, 159.2 ± 12.1 for hCOX-2–Tg, and 177.3 ± 21.2 for hCOX-2–Tg+DFU. However, under the HFD condition, hCOX-2–Tg mice displayed enhanced insulin sensitivity (Fig. 1*E*) and glucose tolerance (Fig. 1*F*) compared with the Wt. In addition, treatment of hCOX-2–Tg mice with DFU partially reversed the beneficial effects on glucose homeostasis induced by COX-2–dependent prostaglandins. ITT and GTT also revealed an enhanced insulin sensitivity and glucose tolerance in hCOX-2–Tg versus Wt mice under RCD basal conditions (Supplementary Fig. 1*D* and *E*). The effect of COX-2 expression in hepatic insulin signaling was evaluated in primary hepatocytes. As shown in Supplementary Fig. 2*A*, insulin-induced insulin receptor and Akt phosphorylations were markedly increased in hCOX-2–Tg hepatocytes. Furthermore, when Wt hepatocytes were treated with PGE_2 before insulin stimulation, Akt phosphorylation was increased, and conversely, when hCOX-2–Tg hepatocytes were pretreated with DFU, Akt phosphorylation was decreased, indicating the specificity of COX-2–dependent prostaglandins in the modulation of insulin signaling (Supplementary Fig. 2*B*).

Chronic HFD treatment causes accumulation of lipids in the liver, a process leading to fatty liver disease. Under these nutritional conditions Wt mice developed severe steatosis (Fig. 2*A*), including massive accumulation of large lipid droplets and a significant increase in liver triglyceride (TG) (Fig. 2*B*). The hCOX-2–Tg mice were protected against liver steatosis, showing fewer and smaller lipid droplets, whereas DFU administration partially reverted this effect, exhibiting an intermediate liver steatosis but including lipids microvesicles (Supplementary Fig. 3*A*). The steatosis score, as defined by Nonalcoholic Steatohepatitis Clinical Research Network Scoring System Definitions (17), was lower in hCOX-2–Tg mice (Supplementary Fig. 3*B*).

COX-2–Tg Mice Are Protected From Hepatic Inflammation and Injury

Because the increase in adipose tissue and inflammation has been linked to IR, we performed histologic examination of eWAT, and the results showed adipocyte hypertrophy with larger adipocytes in Wt mice versus hCOX-2–Tg; and again, COX-2–Tg mice treated with DFU resembled features of the Wt eWAT (Fig. 2*C*). A frequency histogram showed a shift to the left in adipocyte size in the hCOX-2–Tg mice, with a significant increase in the number of cells and a decrease in the occupied area (mean 1,168 ± 652 μm^2 for Wt and 624 ± 356 μm^2 for hCOX-2–Tg, $P < 0.05$); this process was partially reverted with the DFU treatment (748 ± 863 μm^2) (Fig. 2*D* and *E*). Moreover, as an estimation of body fat content, eWAT plus iWAT mass referred to body weight was lower in hCOX-2–Tg mice, whereas tibia length did not change between Wt and hCOX-2–Tg mice (Fig. 2*F*). These results indicate hypertrophy in eWAT from Wt mice. Cytokine eWAT expression is shown in Fig. 2*G*. As expected, higher adiponectin levels were detected in hCOX-2–Tg mice together with a significant decrease in the proinflammatory markers tumor necrosis factor-α (TNF-α) and interleukin (IL)-6.

Indeed, whereas plasma TGs were significantly elevated exclusively in obese Wt mice after the HFD, plasma cholesterol increased both in Wt and hCOX-2–Tg mice. Levels of plasma nonesterified fatty acids (NEFA) were higher in HFD-fed Wt mice than in hCOX-2–Tg mice (Table 1). Plasma insulin and leptin increased after the HFD in Wt mice, but smaller increases were found in hCOX-2–Tg mice. Furthermore, hCOX-2–Tg mice were hypoleptinemic under the RCD condition (Table 1), and adiponectin levels were elevated (20% increase) in hCOX-2–Tg mice versus Wt controls under the HFD condition. The adiponectin-to-leptin ratio was higher in hCOX-2–Tg; however, HOMA-IR was lower in hCOX-2–Tg mice under the HFD condition (Table 1). DFU treatment in the hCOX-2–Tg mice partially prevented the beneficial effects on plasmatic parameters induced by COX-2–dependent prostaglandins. In fact, plasmatic PGE_2 did not change with the HFD; however, as expected, PGE_2 levels decreased under DFU treatment (Table 1). Hepatic injury was analyzed by measuring alanine aminotransferase and aspartate aminotransferase activities, and both enzymes increased by the effect of HFD to a lesser extent in hCOX-2–Tg mice (Supplementary Fig. 4). The HFD led to a chronic inflammatory profile, which is believed to be critical for the development of glucose intolerance and IR (18). Accordingly, hepatic mRNA levels of TNF-α, Il-1β, and IL-6 were significantly enhanced in livers from HFD-fed Wt mice, whereas hCOX-2–Tg mice exhibited lower levels of these inflammatory markers (Table 2).

After detecting the differences in NEFAs levels, high-resolution magic-angle spinning magnetic resonance spectroscopy was performed to identify and quantify saturated fatty acids (Supplementary Fig. 5*A* and *B*). We found a lower value of the pool of total saturated fatty acids in hCOX-2–Tg mice compared with Wt, and this result was reversed in hCOX2–Tg+DFU (Supplementary Fig. 5*B*).

To gain insight into the molecular mechanisms implicated in COX-2 protection, we evaluated mRNA levels of transcription factors and genes involved in fatty acid oxidation, lipolysis, and lipogenesis. In hCOX-2–Tg liver, there was a significant increase of *Ppara* and *Cpt1a* under the HFD condition indicating an enhanced fatty acid oxidation. In agreement, the expression levels of genes involved in fatty acid synthesis, such as *Pparg* and *Scd1*, were markedly increased in Wt, but upregulation of these markers was lower in hCOX-2–Tg mice. Also, *Cd36* expression was lower in hCOX-2–Tg. Moreover, gene expression of COX-2–mediated responsive primary targets has been analyzed. As expected, hCOX-2–Tg mice showed an increase

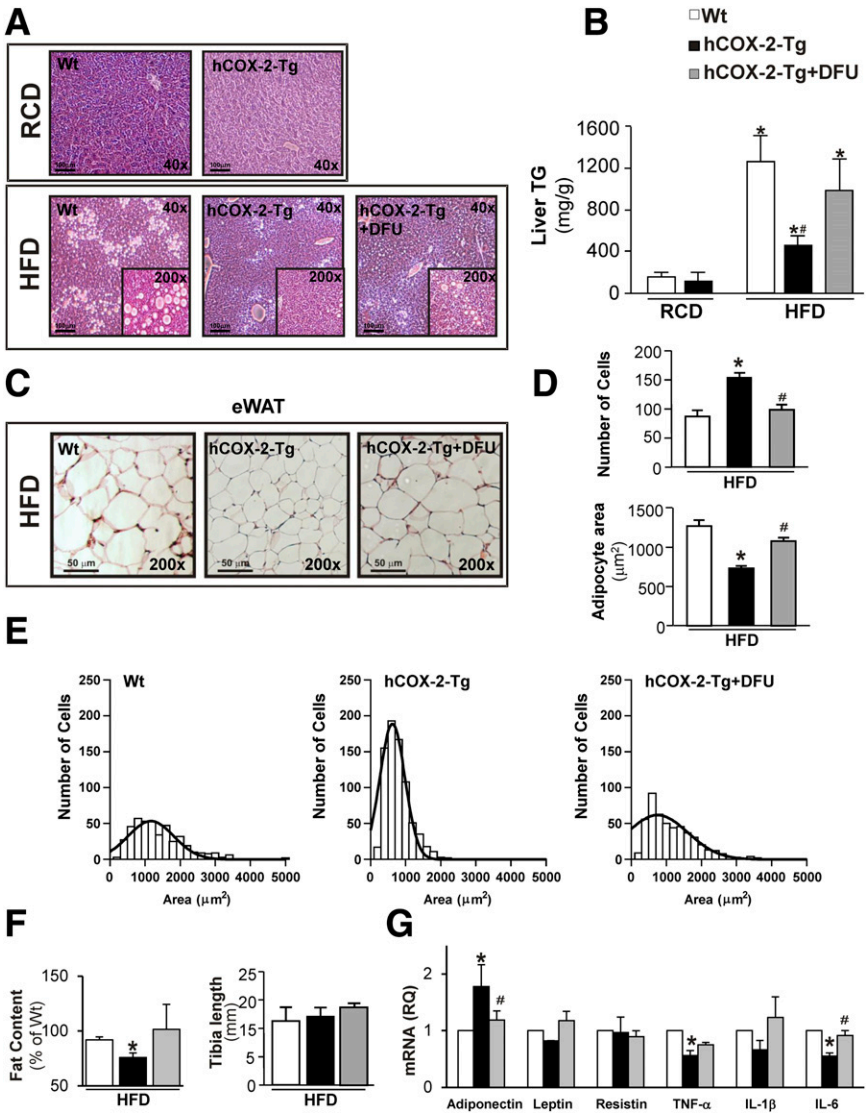

Figure 2—COX-2–Tg mice are protected from HFD-induced hepatic steatosis. *A*: Representative images of hematoxylin and eosin (H&E)-stained liver paraffin-embedded sections from Wt and hCOX-2–Tg mice under RCD and from Wt, hCOX-2–Tg, and hCOX-2–Tg+DFU mice under the HFD condition. *B*: Hepatic TG levels in all experimental groups, measured by enzymatic analysis. Data are expressed as means ± SE ($n = 7$ per group). *$P < 0.05$ vs. Wt-RCD; #$P < 0.05$ vs. Wt-HFD. *C*: Representative images of H&E-stained sections of paraffin-embedded eWAT from Wt, hCOX-2–Tg, and hCOX-2–Tg+DFU mice under the HFD condition. *D*: Number and adipocyte area expressed in μm^2 of five sections per animal ($n = 4$ per group). *E*: Frequency histograms of eWAT from HFD-fed Wt, hCOX-2–Tg, and hCOX-2–Tg+DFU mice. *F*: eWAT + iWAT fat mass content related to body weight and tibia length. *G*: mRNA levels of adipokines and proinflammatory cytokines measured in eWAT by real-time quantitative PCR and normalized to the expression of 36b4 mRNA. Values represent fold relative to Wt under the HFD condition. Data are expressed as means ± SE for four to six mice for each experimental group. *$P < 0.05$ vs. Wt-HDF; #$P < 0.05$ vs. hCOX-2–Tg-HFD.

in hepatic mRNA levels of *CyclinD1* and *Bcl2*, known target genes of COX-2, and *mPges1*, the second key enzyme that couples with COX-2 for the synthesis of PGE_2 (Table 3).

Increased EE in COX-2–Tg Mice After HFD Treatment

To determine the cause of decreased adiposity and improved insulin sensitivity in hCOX-2–Tg mice, we examined food intake and EE. The reduced adiposity of hCOX-2–Tg mice could not be explained by decreased food intake (Fig. 1*D*) but was associated with increased EE. Of note, no differences were found in basal rectal temperature by a possible pyrogenic effect of PGE_2 (Wt: 36.4 ± 0.6°C; h-COX-2–Tg: 35.8 ± 0.7°C).

VO_2 was elevated in hCOX-2–Tg mice versus Wt mice during light and dark cycles. As expected, DFU treatment of hCOX-2–Tg resembled the Wt situation (Fig. 3*A* and Supplementary Fig. 6*A*). Similar results were obtained when CO_2 production was measured, and as a consequence, EE and RER were also increased in hCOX-2–Tg mice versus Wt mice during light and dark periods (Fig. 3*B*, *C* and *E* and Supplementary Fig. 6*E*). However, no differences between genotypes were noted in locomotor activity (Fig. 3*D*).

Table 1—Biochemical and metabolic characteristics of hCOX-2–Tg mice after HFD

	RCD		HFD		
	Wt	hCOX-2–Tg	Wt	hCOX-2–Tg	hCOX-2–Tg+DFU
TG (mg/dL)	23.80 ± 2.70	23.66 ± 4.51	35.78 ± 3.08*	23.28 ± 1.89#	32.59 ± 1.63*†
Cholesterol (mg/dL)	101.78 ± 12.98	72.71 ± 10.72	232.17 ± 25.68*	147.78 ± 9.13z*#	207.90 ± 15.33*†
NEFAs (mEq/L)	18.69 ± 2.21	16.79 ± 2.77	23.44 ± 2.96*	14.17 ± 2.43#	21.69 ± 4.42*†
Insulin (ng/mL)	0.94 ± 0.30	0.72 ± 0.17	1.73 ± 0.36*	1.46 ± 0.13*	2.23 ± 0.66*
Adiponectin (pg/mL)	7.21 ± 0.72	6.99 ± 1.64	6.08 ± 1.11	8.05 ± 0.35#	4.94 ± 0.61*†
Leptin (pg/mL)	7.61 ± 2.07	3.82 ± 0.64*	24.93 ± 1.81*	21.29 ± 1.49*#	24.95 ± 0.89*†
Adiponectin-to-leptin ratio	0.95	1.83*	0.24	0.38#	0.20
HOMA-IR (AU)			19.01 ± 2.89	14.46 ± 0.92#	23.43 ± 0.63
PGE_2 (pg/mL)	9.43 ± 1.16	14.18 ± 1.10*	8.98 ± 0.35	12.04 ± 0.48*#	8.03 ± 0.34†

Plasma levels of TGs, cholesterol, NEFAs, insulin, leptin, and adiponectin from Wt, hCOX-2–Tg, and hCOX-2–Tg+DFU mice fed the RCD or the HFD for 12 weeks. The adiponectin-to-leptin ratio, HOMA-IR, plasma PGE_2 levels from Wt, hCOX-2–Tg, and hCOX-2–Tg+DFU mice fed with the RCD or HFD. Data are expressed as means ± SE for four to six mice of each experimental group. *$P < 0.05$ vs. Wt-RCD. #$P < 0.05$ vs. Wt-HFD. †$P < 0.05$ vs. hCOX-2–Tg–HFD. AU, arbitrary units.

In agreement with increased cage temperature (Fig. 3*F*), hepatic COX-2–derived PGE_2 enhanced the expression of thermogenic genes (*Ucp1*, *Dio2*, and *Prdm16*) in iWAT, suggesting induction of browning. Furthermore, thermogenic-gene expression was also increased in BAT in hCOX-2–Tg mice (Fig. 4*A*). To reinforce these data, we performed a cold acclimation experiment to assess the differential thermogenic response between Wt and hCOX-2–Tg mice. As shown in Fig. 4*B*, cold-induced *Ucp1*, *Dio2*, and *Prdm16* mRNA levels were significantly higher in iWAT of hCOX-2–Tg mice, suggesting a browning process. In BAT, the differential effects after cold exposure were found in *Ucp1* mRNA levels. These data reinforce the beneficial effects found in energy expenditure in hCOX-2–Tg mice. Also, PGE_2 was able to induce uncoupling protein 1 (UCP-1) expression in nondifferentiated BAT SVF cells (Fig. 4*C*).

Hepatic COX-2 Expression Enhances Insulin Signaling in Liver After HFD

The phosphorylation of Akt and AMPK-α were markedly reduced in obese Wt liver compared with hCOX-2–Tg mice (Fig. 5*A* and *B*). These differences in insulin signaling between Wt and hCOX-2–Tg mice after HFD could reflect differential expression of negative modulators of the early steps of insulin signaling. In this regard, PTP1B protein levels were upregulated in the liver of HFD-fed Wt mice compared with similar genotype fed the RCD, whereas this effect was not observed in hCOX-2–Tg mice. All of these data suggest that hCOX-2–Tg mice are protected against IR under the HFD condition.

Human and Mouse Liver Cells Expressing COX-2–Tg Are Protected Against Fatty Acids Exposure

To confirm whether liver cells expressing COX-2 exhibit higher insulin sensitivity and are protected against IR, CHL (human) and NCL (murine) cells, with (CHL-C, NCL-C) or without (CHL-V, NCL-V) COX-2 expression were treated with 600 μmol/L palmitate for 16 h and then stimulated with 10 nmol/L insulin for 15 min. As shown in Supplementary Fig 7*A–C*, CHL-C and NCL-C cells per se showed a higher increase in Akt phosphorylation in response to insulin than CHL-V and NCL-V cells. Moreover, when cells were treated with palmitate to induce IR, CHL-C and NCL-C exhibited a higher Akt phosphorylation in response to insulin than CHL-V and NCL-V, thus reinforcing the results obtained in vivo in hCOX-2–Tg mice.

DISCUSSION

The current study has demonstrated that constitutive expression of COX-2 in hepatocytes protects against steatosis, adiposity, inflammation, and hepatic IR in mice under HFD, implicating the lack of COX-2 expression under these circumstances as a novel key player in

Table 2—Hepatic mRNA expression of proinflammatory cytokines in hCOX-2–Tg mice

	RCD		HFD		
Gene	Wt	hCOX-2–Tg	Wt	hCOX-2–Tg	hCOX-2–Tg+DFU
Tnfa	1	0.65 ± 0.32	2.36 ± 0.79*	1.13 ± 0.38#	1.55 ± 0.66
Il1b	1	1.47 ± 0.30	3.16 ± 1.01*	1.52 ± 0.26#	1.47 ± 0.88
Il6	1	0.44 ± 0.10*	2.16 ± 0.68*	0.63 ± 0.20#	1.67 ± 0.81

Hepatic mRNA levels of proinflammatory cytokines IL-6, IL-1β, and TNF-α measured by real-time quantitative PCR normalized to the expression of 36b4 mRNA. Values represent fold relative to Wt under the RCD condition. Data are expressed as means ± SE for four to six mice of each experimental group. *$P < 0.05$ vs. Wt-RCD. #$P < 0.05$ vs. Wt-HFD.

Table 3—Hepatic mRNA expression of genes related to lipogenesis, lipolysis, and β-oxidation in hCOX-2–Tg mice

	RCD		HFD	
Gene	Wt	hCOX-2–Tg	Wt	hCOX-2–Tg
Cpt1a	1	1.15 ± 0.04	1.70 ± 0.20*	2.87 ± 0.27*#
Pgc1a	1	0.68 ± 0.22	1.00 ± 0.13	0.99 ± 0.14
Acox1	1	0.73 ± 0.20	1.92 ± 0.24*	1.18 ± 0.39
Ppara	1	1.61 ± 0.18*	2.54 ± 0.10*	4.41 ± 0.14*#
Pparg	1	0.16 ± 0.04*	5.95 ± 0.09*	2.94 ± 0.07*#
Acaca	1	0.94 ± 0.18	1.21 ± 0.36	0.89 ± 0.16
Fasn	1	1.59 ± 0.43	1.32 ± 0.72	1.09 ± 0.35
Scd1	1	0.64 ± 0.24	2.25 ± 0.23*	1.46 ± 0.09*#
Lipc	1	0.87 ± 0.17	1.05 ± 0.18	1.18 ± 0.16
Lipe	1	0.82 ± 0.08	1.70 ± 0.06*	1.80 ± 0.56
Pnpla2	1	0.97 ± 0.17	1.68 ± 0.56	2.55 ± 0.53
Cd36	1	0.67 ± 0.18	6.30 ± 0.38*	3.65 ± 0.22*#
hcox2	1	7,365.5 ± 453.8*	1.04 ± 0.43	6,749.9 ± 266.2*#
mpges1	1	1.58 ± 0.39	0.84 ± 0.35	1.68 ± 0.32*#
CyclinD1	1	1.34 ± 0.08*	1.10 ± 0.21	1.51 ± 0.25*#
Bcl2	1	1.13 ± 0.11	0.96 ± 0.20	1.57 ± 0.35*#

Hepatic mRNA levels measured by real-time quantitative PCR normalized to the expression of 36b4 mRNA. Values represent fold relative to Wt under the RCD condition. Data are expressed as means ± SE for four to six mice of each experimental group. *$P < 0.05$ vs. Wt-RCD. #$P < 0.05$ vs. Wt-HFD.

the development of obesity-associated metabolic dysfunction. Importantly, the leanness of hCOX-2–Tg mice is associated with increased systemic EE, enhanced thermogenesis, and fatty acid oxidation in the liver. Furthermore, pharmacological inhibition of COX-2 with DFU reverts to the situation of the Wt mice.

Our previous results (12), by using this transgenic model, demonstrated a protective role of COX-2 against liver injury in an experimental model of streptozotocin-mediated hyperglycemia. The current study reveals that hCOX-2–Tg mice exhibit increased insulin sensitivity in basal conditions and after HFD and are protected against HFD-induced glucose intolerance, steatosis, and adiposity. Recent studies suggested that COX-2 expression in eWAT protects against obesity by an increase in thermogenic activity (19). Moreover, this effect has been attributed principally to COX-2–derived PGE_2 (20). In agreement with this, the reduced adiposity found in hCOX-2–Tg mice under HFD could be explained as a consequence of elevated EE caused by increased substrate consumption. In this way, circulating liver-derived PGE_2 might be sufficient for the induction of thermogenic genes in adipose tissues, all of these contributing to protection against HFD-induced obesity and improvement of glucose homeostasis. This was supported by the enhanced thermogenic gene expression found in iWAT and BAT of hCOX-2–Tg mice under the HFD condition or cold exposure and by the induction of UCP-1 protein levels in brown preadipocytes stimulated with PGE_2.

Elevation of circulating fatty acids and proinflammatory adipokines secreted by WAT reduces insulin sensitivity in liver and skeletal muscle (21), and adipose tissue inflammation has been correlated with hepatic steatosis in humans (22). Our results show that hCOX-2–Tg mice did not develop the common increase in fat mass and enhanced adipocyte hypertrophy that is shown in Wt mice under the HFD condition. In agreement with these data, plasma and hepatic TGs, cholesterol, and NEFAs levels were lower in hCOX-2–Tg mice, and these mice also showed decreased plasma insulin and leptin and increased adiponectin levels. Moreover, proinflammatory markers were also lower in hepatic tissue from hCOX-2–Tg mice compared with Wt after the HFD. Altogether, these parameters indicate that the beneficial effects on obesity and glucose homeostasis in hCOX-2–Tg mice might be due to decreased inflammation.

When Wt and hCOX-2–Tg mice were fed the HFD, we found an important protection against steatosis and IR versus Wt mice. Moreover, we found significant differences in the expression of key enzymes and transcription factors implicated in lipogenesis and β-oxidation, such as *Pparg*, *Scd1*, *Ppara*, *Cpt1a*, and *CD36*, indicating an increase in β-oxidation in hCOX-2–Tg mice under the HFD condition. Recent results have implicated hepatic fatty acid translocase CD36 upregulation with IR and steatosis in nonalcoholic steatohepatitis and chronic hepatitis C (23). In addition, the positive effects of COX-2 on inflammation and IR are evidenced by the prevention of obesity through increased EE and RER.

The phosphatidylinositide 3-kinase/Akt and AMPK pathways play a central role in integrating diverse survival

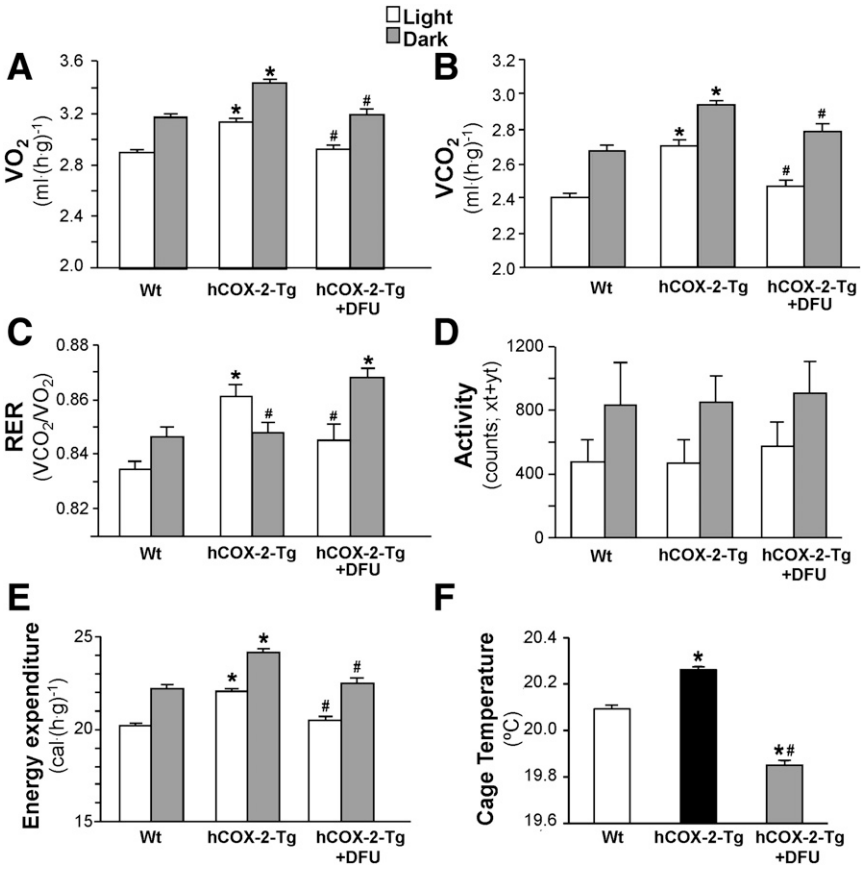

Figure 3—Increased energy expenditure in hCOX-2–Tg mice under the HFD condition. VO_2 (*A*), VCO_2 (*B*), RER (*C*), locomotor activity (*D*), EE (*E*), and average cage temperature (*F*) in HFD-fed Wt, hCOX-2–Tg, and hCOX-2–Tg+DFU mice were measured in 12-h light/dark cycles. Data are expressed as means ± SE for four mice in each experimental group. **P* < 0.05 vs. Wt-HDF; #*P* < 0.05 vs. hCOX-2–Tg-HFD.

signals. Moreover, Akt phosphorylation is a critical node of the insulin-signaling pathway, being that tyrosine-phosphorylated insulin receptor substrate-1 is an upstream mediator of its activation (1). It is known that the Akt pathway is a target of prostaglandins and that Akt phosphorylation is enhanced in the liver of hCOX-2–Tg mice compared with the Wt mice, thus reinforcing the survival pathways (12). In Wt liver, the HFD impaired insulin-stimulated Akt phosphorylation, and this effect was prevented in hCOX-2–Tg mice. This situation was paralleled in murine- and human-derived liver cells overexpressing COX-2. The increase in the phosphorylated (p)Akt-to-Akt ratio in hCOX-2–Tg mice under RCD and HFD conditions may be due, besides intracellular signaling, to a direct Akt activation through COX-2–dependent PGE_2 acting via EP2/EP4 Gβγ dimers, as reported by Rizzo (24). Notably, the effect of PGE_2 pretreatment on Akt phosphorylation observed in isolated hepatocytes confirmed that COX-2–derived prostanoids can be responsible for this effect. Thus, the improved insulin sensitivity in vivo reflected by hepatic Akt activation found in hCOX-2–Tg mice might contribute to the amelioration of HFD-derived deleterious metabolic effects as exacerbated lipogenesis and hepatic TG content.

AMPK-α1 is known to protect mice from diet-induced obesity and IR. AMPK-α1 knockdown in mice enhanced adipocyte lipid accumulation, exacerbated the inflammatory response, and induced IR (25). We showed that AMPK was phosphorylated in liver cells expressing COX-2 under basal conditions and after liver injury (16). Indeed, AMPK phosphorylation and its downstream gene *Cpt1a,* which regulates a rate-controlling step of fatty acid oxidation transferring long-chain acyl-CoA into the mitochondria, were increased in hCOX-2–Tg mice under the HFD condition. Cellular lipid content is determined by the balance between fatty acid oxidation and lipid storage as TGs. Because the ability of AMPK to induce lipid oxidation is considered an important feature for insulin sensitization (26), this might also contribute to the beneficial effects of COX-2 expression in hepatocytes on insulin sensitivity.

In addition to the molecular mechanisms mentioned above, differences in insulin signaling between Wt and hCOX-2–Tg mice after the HFD could reflect differential expression of negative modulators of the early steps of insulin signaling. Among them, PTP1B was a likely candidate given its ability to directly dephosphorylate the insulin receptor and its expression being induced by

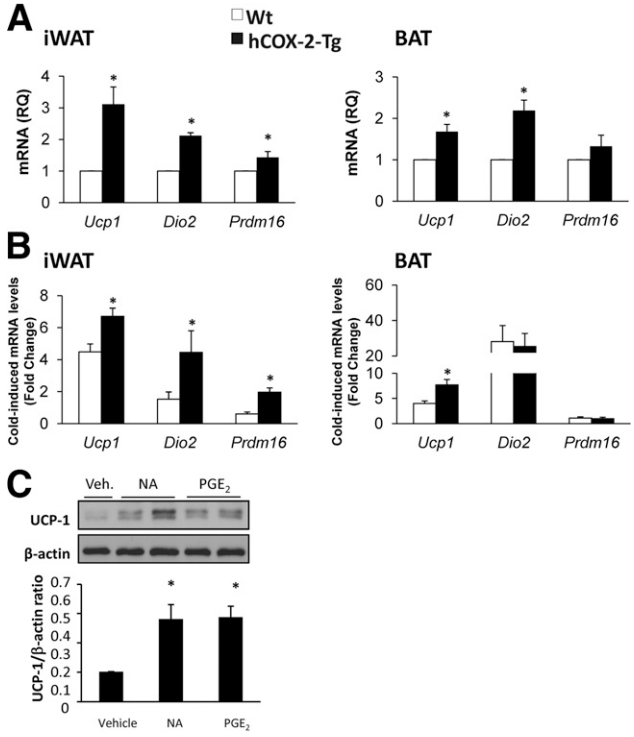

Figure 4—Enhanced thermogenic-related genes in hCOX-2–Tg mice. *A*: *Ucp1, Dio2,* and *Prdm16* mRNA levels were measured in iWAT and BAT by real-time quantitative PCR and normalized to the expression of 36b4 mRNA. Values represent fold relative to Wt under the HFD condition. Data are expressed as means ± SE for six mice of each experimental group. **P* < 0.05 vs. Wt-HFD. *B*: Mice were maintained at 28°C for 1 week and then at 4°C for 6 h. *Ucp1*, *Dio2*, and *Prdm16* mRNA levels were measured in iWAT and BAT by real-time quantitative PCR and normalized to the expression of 36b4 mRNA. Results are means ± SE for four to six mice of each experimental group. Data are expressed as fold change relative to Wt or hCOX-2–Tg at thermoneutrality. **P* < 0.05 vs. cold exposure Wt. *C*: BAT precursor stromal vascular fraction cells were stimulated with PGE_2 (1 μmol/L) or noradrenalin (NA) (1 μmol/L) as a positive control for 24 h, and UCP-1 expression was analyzed by Western blot. Data are expressed as means ± SE for three different experiments. **P* < 0.05 vs. control without stimulation.

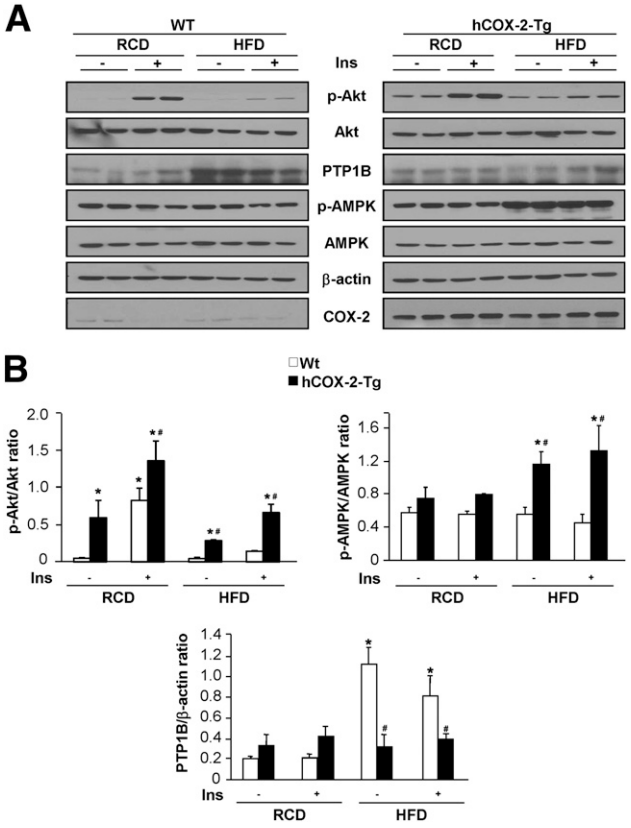

Figure 5—COX-2 expression enhances insulin signaling in liver of mice fed the HFD. *A:* Representative Western blot analysis of Wt and COX-2–Tg liver under RCD or HFD; nontreated (−Ins) or treated (+Ins) with 0.75 units/kg insulin (Ins) for 15 min before being killed. *B*: Ratios phosphorylated (p)-Akt/Akt and p-AMPK/AMPK after densitometric analysis of Western blot data normalized using β-actin as control. Data are expressed as means ± SE for four to six mice of each experimental group. **P* < 0.05 vs. Wt (−Ins); #*P* < 0.05 vs. Wt-HFD (−Ins).

inflammatory mediators (27). PTP1B-knockout mice are protected against obesity-induced inflammation and peripheral IR during aging (28). In agreement with these data, PTP1B protein was upregulated in the liver of HFD-fed Wt mice but not in hCOX-2–Tg mice, suggesting that COX-2–dependent prostaglandins might protect from the elevation of PTP1B during obesity. In addition, PTP1B modulates leptin sensitivity (29), and decreased leptin levels are found in hCOX-2–Tg mice in both RCD and HFD conditions, suggesting a possible cross talk between COX-2–derived signals and leptin.

Henkel et al. (30) reported that PGE_2 produced in Kupffer cells interrupts the intracellular insulin signaling in hepatocytes through serine phosphorylation of insulin receptor substrate-1 via EP3 receptor-dependent ERK1/2 activation. Moreover, they demonstrated that the EP3 receptor in hepatocytes is expressed at higher levels than the other isoforms (30). However, our results show that the liver of Wt and hCOX-2–Tg mice expresses comparable levels of all of the EPs receptors (EP1–4; data not shown) indicating a different molecular mechanism of action. Our in vivo data in the hCOX-2–Tg model, characterized by a continuous production of PGE_2 in the liver, clearly show enhanced insulin-mediated Akt phosphorylation partly due to decreased PTP1B levels under the HFD condition. Therefore, the view emerging from this study is that prostaglandins synthesized by other liver cells (Kupffer or stellate) are not sufficient to cope for the beneficial effects observed when hepatocytes are able to express COX-2.

In conclusion, the current study demonstrates that expression of COX-2 in hepatocytes protects against adiposity, inflammation, and hepatic IR in mice under the HFD condition, pointing to COX-2 as a potential therapeutic target against obesity-associated metabolic dysfunction. Stable analogs of PGE_2, such as 16,16dmPGE_2, resembling COX-2 overexpression (31), could be administered to treat steatosis or IR. In fact, PGE_1 and PGE_2 and

their analogs are used in the clinic to improve moderate hypercholesterolemia among other liver pathologies (32). Furthermore, these results support caution with use of COX inhibitors in patients with obesity, type 2 diabetes, or nonalcoholic fatty liver disease.

Acknowledgments. The authors thank Gerardo Pisani (Instituto de Fisiología Experimental-Consejo Nacional de Investigaciones Científicas y Técnicas), Rosario, Argentina, for his technical assistance with the immunohistochemical analysis.

Funding. This work was supported by Financing Program for Short Stays Abroad (Consejo Nacional de Investigaciones Científicas y Técnicas-Argentina) to D.E.F., by a Post-Doctoral fellowship from Consejo Nacional de Ciencia y Tecnología, México, SAF2012-39732 (Ministerio de Economía y Competitividad [MINECO], Spain) to L.C.-S., by CIBERehd (Instituto de Salud Carlos III [ISCIII], Spain) to M.C., by BFU2011-24760 (MINECO, Spain) to L.B., by S2010/BMD-2378 (Comunidad de Madrid) to L.B. and P.M.-S., by RD12/0042/0019 (ISCIII, Spain) and CIBERehd (ISCIII, Spain) to L.B. and P.M.-S., by SAF2010-16037, SAF2013-43713-R (MINECO, Spain) to P.M.-S., and by SAF2012-33283 (MINECO, Spain), S2010/BMD-2423 (Comunidad de Madrid), European Foundation for the Study of Diabetes and Amylin Paul Langerhans Grant, and CIBERDEM (ISCIII, Spain) to Á.M.V.

Duality of Interest. No potential conflicts of interest relevant to this article were reported.

Author Contributions. D.E.F., O.M., N.A., Á.G.-R., A.F-Á., C.C., E.G.-C., and Á.M.V. researched the data. L.C.-S. edited the manuscript. R.M., L.B., C.E.C., and M.C. reviewed the manuscript and contributed to discussion. Á.M.V. and P.M-S. wrote and reviewed the manuscript. Á.M.V. and P.M.-S. are the guarantors of this work and, as such, had full access to all the data in the study and take responsibility for the integrity of the data and the accuracy of the data analysis.

References

1. Tilg H, Moschen AR. Inflammatory mechanisms in the regulation of insulin resistance. Mol Med 2008;14:222–231
2. Rosen ED, Spiegelman BM. Adipocytes as regulators of energy balance and glucose homeostasis. Nature 2006;444:847–853
3. Copps KD, White MF. Regulation of insulin sensitivity by serine/threonine phosphorylation of insulin receptor substrate proteins IRS1 and IRS2. Diabetologia 2012;55:2565–2582
4. Simmons DL, Botting RM, Hla T. Cyclooxygenase isozymes: the biology of prostaglandin synthesis and inhibition. Pharmacol Rev 2004;56:387–437
5. Callejas NA, Boscá L, Williams CS, DuBois RN, Martín-Sanz P. Regulation of cyclooxygenase 2 expression in hepatocytes by CCAAT/enhancer-binding proteins. Gastroenterology 2000;119:493–501
6. Casado M, Callejas NA, Rodrigo J, et al. Contribution of cyclooxygenase 2 to liver regeneration after partial hepatectomy. FASEB J 2001;15:2016–2018
7. Martín-Sanz P, Callejas NA, Casado M, Díaz-Guerra MJ, Boscá L. Expression of cyclooxygenase-2 in foetal rat hepatocytes stimulated with lipopolysaccharide and pro-inflammatory cytokines. Br J Pharmacol 1998;125:1313–1319
8. Hsieh PS, Jin JS, Chiang CF, Chan PC, Chen CH, Shih KC. COX-2-mediated inflammation in fat is crucial for obesity-linked insulin resistance and fatty liver. Obesity (Silver Spring) 2009;17:1150–1157
9. Hsieh PS, Tsai HC, Kuo CH, et al. Selective COX2 inhibition improves whole body and muscular insulin resistance in fructose-fed rats. Eur J Clin Invest 2008;38:812–819
10. Tian YF, Hsia TL, Hsieh CH, Huang DW, Chen CH, Hsieh PS. The importance of cyclooxygenase 2-mediated oxidative stress in obesity-induced muscular insulin resistance in high-fat-fed rats. Life Sci 2011;89:107–114
11. Coll T, Palomer X, Blanco-Vaca F, et al. Cyclooxygenase 2 inhibition exacerbates palmitate-induced inflammation and insulin resistance in skeletal muscle cells. Endocrinology 2010;151:537–548
12. Francés DE, Ingaramo PI, Mayoral R, et al. Cyclooxygenase-2 overexpression inhibits liver apoptosis induced by hyperglycemia. J Cell Biochem 2013;114:669–680
13. Casado M, Mollá B, Roy R, et al. Protection against Fas-induced liver apoptosis in transgenic mice expressing cyclooxygenase 2 in hepatocytes. Hepatology 2007;45:631–638
14. Llorente Izquierdo C, Mayoral R, Flores JM, et al. Transgenic mice expressing cyclooxygenase-2 in hepatocytes reveal a minor contribution of this enzyme to chemical hepatocarcinogenesis. Am J Pathol 2011;178:1361–1373
15. Trusca VG, Fuior EV, Florea IC, Kardassis D, Simionescu M, Gafencu AV. Macrophage-specific up-regulation of apolipoprotein E gene expression by STAT1 is achieved via long range genomic interactions. J Biol Chem 2011;286:13891–13904
16. Mayoral R, Mollá B, Flores JM, Boscá L, Casado M, Martín-Sanz P. Constitutive expression of cyclo-oxygenase 2 transgene in hepatocytes protects against liver injury. Biochem J 2008;416:337–346
17. Kleiner DE, Brunt EM, Van Natta M, et al.; Nonalcoholic Steatohepatitis Clinical Research Network. Design and validation of a histological scoring system for nonalcoholic fatty liver disease. Hepatology 2005;41:1313–1321
18. Hotamisligil GS. Inflammation and metabolic disorders. Nature 2006;444:860–867
19. Vegiopoulos A, Müller-Decker K, Strzoda D, et al. Cyclooxygenase-2 controls energy homeostasis in mice by de novo recruitment of brown adipocytes. Science 2010;328:1158–1161
20. García-Alonso V, López-Vicario C, Titos E, et al. Coordinate functional regulation between microsomal prostaglandin E synthase-1 (mPGES-1) and peroxisome proliferator-activated receptor γ (PPARγ) in the conversion of white-to-brown adipocytes. J Biol Chem 2013;288:28230–28242
21. Olefsky JM. Fat talks, liver and muscle listen. Cell 2008;134:914–916
22. Cancello R, Tordjman J, Poitou C, et al. Increased infiltration of macrophages in omental adipose tissue is associated with marked hepatic lesions in morbid human obesity. Diabetes 2006;55:1554–1561
23. Miquilena-Colina ME, Lima-Cabello E, Sánchez-Campos S, et al. Hepatic fatty acid translocase CD36 upregulation is associated with insulin resistance, hyperinsulinaemia and increased steatosis in non-alcoholic steatohepatitis and chronic hepatitis C. Gut 2011;60:1394–1402
24. Rizzo MT. Cyclooxygenase-2 in oncogenesis. Clin Chim Acta 2011;412:671–687
25. Zhang W, Zhang X, Wang H, et al. AMP-activated protein kinase α1 protects against diet-induced insulin resistance and obesity. Diabetes 2012;61:3114–3125
26. Yamauchi T, Kamon J, Minokoshi Y, et al. Adiponectin stimulates glucose utilization and fatty-acid oxidation by activating AMP-activated protein kinase. Nat Med 2002;8:1288–1295
27. Zabolotny JM, Kim YB, Welsh LA, Kershaw EE, Neel BG, Kahn BB. Protein-tyrosine phosphatase 1B expression is induced by inflammation in vivo. J Biol Chem 2008;283:14230–14241
28. González-Rodríguez A, Más-Gutierrez JA, Mirasierra M, et al. Essential role of protein tyrosine phosphatase 1B in obesity-induced inflammation and peripheral insulin resistance during aging. Aging Cell 2012;11:284–296
29. Zabolotny JM, Bence-Hanulec KK, Stricker-Krongrad A, et al. PTP1B regulates leptin signal transduction in vivo. Dev Cell 2002;2:489–495
30. Henkel J, Neuschäfer-Rube F, Pathe-Neuschäfer-Rube A, Püschel GP. Aggravation by prostaglandin E2 of interleukin-6-dependent insulin resistance in hepatocytes. Hepatology 2009;50:781–790
31. Madsen L, Pedersen LM, Lillefosse HH, et al. UCP1 induction during recruitment of brown adipocytes in white adipose tissue is dependent on cyclooxygenase activity. PLoS ONE 2010;5:e11391
32. Korhonen T, Savolainen MJ, Jääskeläinen T, Kesäniemi YA. Effect of a synthetic prostaglandin E2 analogue, RS-86505-007, on plasma lipids and lipoproteins in patients with moderate hypercholesterolaemia: efficacy and tolerance of treatment and response in different apolipoprotein polymorphism groups. Eur J Clin Pharmacol 1995;48:97–102

Original article

MOLECULAR METABOLISM

SIRT1 enhances glucose tolerance by potentiating brown adipose tissue function

Marie Boutant [1], Magali Joffraud [1], Sameer S. Kulkarni [1], Ester García-Casarrubios [2,3], Pablo M. García-Roves [3,4], Joanna Ratajczak [1,5], Pablo J. Fernández-Marcos [6], Angela M. Valverde [2,3], Manuel Serrano [6], Carles Cantó [1,*]

ABSTRACT

Objective: SIRT1 has been proposed to be a key signaling node linking changes in energy metabolism to transcriptional adaptations. Although SIRT1 overexpression is protective against diverse metabolic complications, especially in response to high-fat diets, studies aiming to understand the etiology of such benefits are scarce. Here, we aimed to identify the key tissues and mechanisms implicated in the beneficial effects of SIRT1 on glucose homeostasis.

Methods: We have used a mouse model of moderate SIRT1 overexpression, under the control of its natural promoter, to evaluate glucose homeostasis and thoroughly characterize how different tissues could influence insulin sensitivity.

Results: Mice with moderate overexpression of SIRT1 exhibit better glucose tolerance and insulin sensitivity even on a low fat diet. Euglycemic-hyperinsulinemic clamps and in-depth tissue analyses revealed that enhanced insulin sensitivity was achieved through a higher brown adipose tissue activity and was fully reversed by housing the mice at thermoneutrality. SIRT1 did not influence brown adipocyte differentiation, but dramatically enhanced the metabolic transcriptional responses to β3-adrenergic stimuli in differentiated adipocytes.

Conclusions: Our work demonstrates that SIRT1 improves glucose homeostasis by enhancing BAT function. This is not consequent to an alteration in the brown adipocyte differentiation process, but as a result of potentiating the response to β3-adrenergic stimuli.

Keywords SIRT1; Energy homeostasis; Insulin resistance; Brown adipose tissue

1. INTRODUCTION

SIRT1 is a NAD^+-dependent protein deacetylase and the best studied mammalian homolog of the yeast enzyme Sir2, a protein with an established capacity to influence yeast replicative lifespan [1]. In mammals, SIRT1 targets include a constellation of transcription factors and enzymes with key roles in mitochondrial biogenesis, lipid catabolism, cholesterol homeostasis and gluconeogenesis [1]. Studies using SIRT1 activating compounds (STACs) in mammals have highlighted how SIRT1 might have pleiotropic metabolic benefits. Dietary supplementation with STACs led to increased mitochondrial biogenesis in diverse mouse tissues, including skeletal muscle and brown adipose tissue (BAT), which in turn protected against high-fat diet (HFD)-induced obesity and many of its metabolic comorbidities [2]. The specificity of these compounds, however, has been called into question and is still unclear [3]. To overcome this problem, transgenic mouse models with a moderate SIRT1 overexpression were generated. In them, a single copy of a large genomic construct (174 kb) containing the entire *Sirt1* gene in its natural genomic context was integrated [4]. This led to a 2–4-fold overexpression of SIRT1 in tissues from heterozygous mice for the transgene ($SIRT1^{Tg/-}$) [4]. While similar to wild-type (WT) mice when fed low fat diets (LFD), $SIRT1^{Tg/-}$ mice were protected against HFD-induced insulin resistance, despite similar body weight gain [4]. These observations were confirmed in an independent SIRT1 overexpressing mouse line (SirBACO) generated by the Accili lab [5]. In light of the above results, we reasoned that the generation of a homozygous transgenic mouse ($SIRT1^{Tg/Tg}$) might lead to a more marked phenotype, likely closer to that observed with STACs. Here, we describe how $SIRT1^{Tg/Tg}$ mice display enhanced energy expenditure (EE), glucose tolerance and insulin sensitivity even when fed an LFD. We demonstrate that this phenotype stems from a higher BAT activity and that $SIRT1^{Tg/Tg}$ mice do not show major muscle or liver functional changes on LFD. Using immortalized brown adipocytes from SIRT1 transgenic mice we further demonstrate that the effects of SIRT1 on BAT biology do not derive from differences in the brown adipocyte differentiation process, but from a higher response to β3-adrenergic stimuli. Altogether, our work illustrates how SIRT1 gain-of-function can improve insulin sensitivity by acting as a gauge for the BAT response to β3-adrenergic stimuli.

[1]Nestlé Institute of Health Sciences (NIHS) SA, EPFL Campus, Quartier de l'Innovation, Bâtiment G, Lausanne CH-1015, Switzerland [2]Instituto de Investigaciones Biomédicas Alberto Sols (CSIC-UAM), 28029 Madrid, Spain [3]Spanish Biomedical Research Centre in Diabetes and Associated Metabolic Disorders (CIBERDEM), 28029 Madrid, Spain [4]Diabetes and Obesity Research Laboratory, Institut d'Investigacions Biomediques August Pi i Sunyer (IDIBAPS), Barcelona 08036, Spain [5]Ecole Polytechnique Fédérale de Lausanne (EPFL), CH-1015 Lausanne, Switzerland [6]Spanish National Cancer Research Center (CNIO), Madrid E28029, Spain

*Corresponding author. Tel.: +41 (0) 21 632 6116. E-mail: carlos.cantoalvarez@rd.nestle.com (C. Cantó).

Received December 3, 2014 • Revision received December 11, 2014 • Accepted December 13, 2014 • Available online 19 December 2014

http://dx.doi.org/10.1016/j.molmet.2014.12.008

2. MATERIAL AND METHODS

2.1. Animal care

The SIRT1 transgenic model has already been described in Ref. [4]. In contrast to that publication, we used homozygote transgenic male mice $SIRT1^{Tg/Tg}$ which had been backcrossed to C57Bl/6N background. Unless otherwise specified, mice were kept in a standard temperature- and humidity-controlled environment with a 12:12-h light–dark cycle. Mice had nesting material and ad libitum access to water and commercial LFD or HFD (D12450J and D12492, respectively, from Research Diets Inc.). All animal experiments were carried according to national Swiss and EU ethical guidelines and approved by the local animal experimentation committee under licenses 2519 and 2519.1-3. For thermoneutrality studies, mice were housed in temperature controlled cabinets at 30 °C.

2.2. Animal phenotyping

All clinical tests were carried out according to standard operational procedures (SOPs) established and validated within the Eumorphia program (http://empress.har.mrc.ac.uk/) [6]. Mice were weighed and the food consumption was measured each week on the same day. Body composition was determined by Echo-MRI (Echo Medical Systems, Houston, TX, USA) and oxygen consumption (VO_2), respiratory exchange ratios (RER) were monitored by indirect calorimetry using the comprehensive laboratory animal monitoring system (CLAMS; Columbus Instruments, Columbus, OH, USA). EE was estimated using VO_2 and VCO_2 values from indirect calorimetry, using the following equation: EE (in kJ/h) $= (15.818 \times VO_2) + (5.176 \times VCO_2)$ [7]. Food intake and activity (horizontal (XD) and vertical (Z)) was also monitored using the CLAMS during a 24 h period. Daily voluntary activity was measured by providing a running wheel to the mice and monitoring the running distance. Grip tests, treadmill and cold tests were performed as previously described in Ref. [8]. Maximal running speed and VO_2 were evaluated using a calorimetric treadmill (Columbus instruments, Columbus, OH, USA) with an incremental speed protocol. During the run, VO_2 and VCO_2 were measured. The experiment was stopped when mice showed obvious signs of exhaustion. Glucose and insulin tolerance was analyzed by measuring blood glucose following intraperitoneal injection of 2 g/kg glucose or 0.3 U insulin/kg (human insulin actrapid, Lilly), respectively, after a 12 h fast. For HFD-fed mice, the insulin dose was increased to 0.75 U/Kg. Unless otherwise specified, animals were sacrificed at 8 a.m. after a 12 h fast, in order to stabilize systemic parameters and to allow the measurement of blood biochemistry in the fasting state. Blood samples were collected in EDTA-coated tubes and plasma was isolated after centrifugation. Plasma insulin was determined in plasma samples using specific ELISA kits (Merck Millipore, Darmstadt, Germany). All other plasma parameters were measured using Dimension® Xpand Plus (Siemens Healthcare Diagnostics AG, Dudingen, Suisse). Tissues were collected upon sacrifice and flash-frozen in liquid nitrogen.

2.3. Hyperinsulinemic-euglycemic clamp

Hyperinsulinemic-euglycemic clamps were performed at Phyiogenex (Physiogenex SAS, France) according to standardized procedures, following the Guide for the Care and Use of Laboratory animals and French laws. Mice ($n = 12$ per genotype) underwent a surgery procedure to insert a catheter in the femoral vein. Clamp was performed five days post-surgery on 6 h fasted mice. Following a first blood collection, mice received a bolus of D-[3-^{3}H] glucose and then radiotracer (30 μCi/min/kg) infusion started for up to 210 min. Insulin was simultaneously infused at 4 mU/kg/min for the first 100 min and at 12 mU/kg/min for the last 110 min. Glucose infusion rate was adjusted according to blood glucose levels until the two respective euglycemic steadystates were reached. Moreover, 1 h before the end of the clamp, a bolus injection of ^{14}C-2Deoxy-Glucose was performed. At the end of the 210-minute perfusion, mice were euthanized, several tissues were collected and ^{14}C-radioactivity was measured to determine glucose utilization in epididymal and sub-cutaneous WAT, brown adipose tissue, vastus lateralis skeletal muscle and liver.

2.4. Respirometry studies

Respirometry studies in homogenates from freshly extracted BAT and liver or in permeabilized EDL muscle were performed using high-resolution respirometry (Oroboros Oxygraph-2k; Oroboros Instruments, Innsbruck, Austria), as described previously in Ref. [9] with minor modifications. All respirometry experiments were performed on fresh tissues immediately following dissection. Liver and BAT were homogenized (mechanical permeabilization) in amino acid-depleted respirometry medium (0.5 mM EGTA, 3 mM $MgCl_2$, 60 mM K-lactobionate, 10 mM KH_2PO_4, 20 mM HEPES, and 110 mM sucrose, pH 7.1) and the equivalent of 2 mg wet tissue was added to the experimental chamber. Glycolytic EDL skeletal muscle was placed in relaxing buffer (in mM: 2.8 Ca_2K_2EGTA, 7.2 K_2EGTA, 5.8 ATP, 6.6 $MgCl_2$, 20 taurine, 15 Na_2 phosphocreatine, 20 imidazole, 0.5 dithiothreitol, and 50 MES, pH 7.1) immediately after dissection, and fibers were gently separated. Following sarcolemmal permeabilization in relaxing buffer supplemented with 0.005% (wt/vol) saponin, the tissue was equilibrated in respirometry medium [in mM: 0.5 EGTA, 3 $MgCl_2$, 60 K-lactobionate, 20 taurine, 10 KH_2PO_4, 20 HEPES, 110 sucrose and 0.1% (wt/vol) bovine serum albumin, pH 7.1]. Thereafter, skeletal muscle fibers were blotted for ~30 s to remove the excess of medium and 1.0–2.5 mg of tissue was added to each chamber. All the tissues were assessed in respirometry medium. Oxygen flux (denoted as "Leak" in figures) was measured by adding malate (final concentration 2 mM), pyruvate (10 mM) and glutamate (20 mM) in the absence of ADP. Complex I-driven oxidative phosphorylation (denoted as "C I" in figures) was quantified by the addition of ADP (5 mM; 0.5 mM for tests in BAT). This was followed by the addition of succinate (10 mM) for convergent electron flow through both complex I and II (denoted as "C I + II" in figures). Subsequently, carbonylcyanide-4-(trifluoromethoxy)-phenylhydrazone (FCCP) was titrated to achieve maximum flux through the electron transfer system (denoted as "ETS" in figures). Finally, electron transport through complex I (denoted as "ETS C II" in figures) and III was inhibited by the sequential addition of rotenone (0.1 μM) and antimycin A (2.5 μM), respectively. The remaining O_2 flux after inhibition with Antimycin A (O_2 flux independent of the ETS) was subtracted from the values of each of the previous steps. O_2 flux values are expressed relative to tissue wet weight per second.

2.5. Western blotting

Cells were lysed in lysis buffer (50 mM Tris–HCL pH7.5, 150 mM NaCl, EDTA 5 mM, NP40 1%, sodium butyrate 1 mM, protease inhibitors). Proteins were quantified using BCA assay (Pierce). For western blotting, proteins were separated by SDS-PAGE and transferred onto nitrocellulose membranes. Antibodies are listed in Supplemental Table 1. All spliced together non-contiguous lanes from the same gels are marked using a thin black line and noted in the figure. The images for the full, unedited gels are available upon request.

2.6. Determination of mitochondrial vs. nuclear DNA ratio

Total genomic DNA was extracted from liver, skeletal muscle (gastrocnemius) and brown adipose tissue using a DNeasy Blood and

Tissue kit (Qiagen) according to the manufacturer's instructions. Mitochondrial and nuclear DNA (COX2 and HK2, respectively) were measured by quantitative PCR using SYBR Green. Primers are listed in Supplemental Table 2.

2.7. RNA extraction and qPCR

Total mRNA from all studied tissues was extracted according to the instructions provided by the manufacturer, using TRIZOL (Life technologies). The mRNA concentration was measured using a Nanodrop 1000 (Thermo Scientific, Wilmington, MA). Conversion to cDNA was performed using SuperScript II (Life technologies) with oligo (dT2), Random Hexamers primers and RNAsine (Roche) according to the protocol provided by the manufacturer. Quantification of mRNA expression was performed using the SYBR Green real time PCR technology (Roche). Reactions were performed in duplicate in a 384-well plate using the Light Cycler (Roche). Primers are listed in Supplemental Table 2. Gene expression was normalized with β2-microglobulin and cyclophillin as housekeeping genes. Relative gene expression between genotypes was assessed through the ΔΔCt method [10].

2.8. Microarray

Illumina microarrays were used to profile the gene expression levels of approximately 25,000 genes, in the BAT of WT and SIRT1$^{Tg/Tg}$ mice ($n = 6$ per group). The mRNA samples were hybridized on a single chip and raw microarray data were analyzed using the Illumina genome studio software. The results of the microarray are available in the GEO database with the accession number GSE62324. To test for sets of related genes that might be systematically altered in SIRT1$^{Tg/Tg}$ BAT, we used a Gene Set Enrichment Analysis (GSEA), a method which combines information from the members of previously defined sets of genes (e.g. curated biological pathways) to increase signal relative to noise and improve statistical power to detect subtle changes [11]. Complete details on the method for this analysis are available on the http://www.broad.mit.edu/gsea website. Briefly, genes from the microarray were first ranked according to the expression difference (signal to noise ratio) between genotypes. The extent of association was then measured by a non-parametric running sum statistic termed the enrichment score (ES), and the maximum ES (MES) was recorded over each gene set. Permutation tests were used to assess the statistical significance of the MES, which is calculated as the fraction of the 100 random permutations of the gene list in which the top pathway gave a stronger result than that observed in the actual data. The unadjusted nominal *P* value estimates the statistical significance of a gene set without adjusting for gene set size or multiple hypothesis testing, whereas the false discovery rate (FDR) statistic adjusts for both. In this analysis, an FDR of approximately 30% was considered acceptable. The nominal *P*-values for the gene set are indicated in the corresponding panels.

2.9. Citrate synthase activity

Citrate synthase activity was performed on tissue accordingly to the protocol of Sigma's Citrate Synthase Assay Kit (CS0720).

2.10. Triglycerides and glycogen content

Triglycerides and Glycogen content were performed on tissue accordingly to the protocol of Bioassay System Assay Kit (ETGA-200 and E2GN-100, respectively).

2.11. Lipolysis

Lipolysis was determined on freshly extracted tissues using the ZenBio assay kit (LIP-3-NC), incubating the tissues in assay buffer supplemented with a vehicle or with isoproterenol 1 μM during 5 h at 37 °C under agitation and then glycerol release were measured.

2.12. Cell culture

Primary brown adipocytes cells were obtained from the interscapular BAT of WT or SIRT1 transgenic mice and immortalized as previously described in Ref. [12]. Immortalized brown pre-adipocytes were grown in "growth medium" (GM) (DMEM supplemented with 10% FBS, 20 nM Insulin, and 1.5 nM 3,3′,5 Triiodothyronine (T3)). For differentiation, cells were growth until 90% confluence with GM and next stimulated during 36 h with "differentiation medium" (GM supplemented of 0.5 μM dexamethasone, 1 μM rosiglitazone, 0.125 μM indomethacin and 0.5 mM isobutylmethylxanthine (IBMX)). Then, cells were cultivated in GM until final differentiation (day 6 of differentiation). Adipocytes are fully differentiated when they exhibited multilocular lipid droplets in their cytoplasm. For experiments, norepinephrine (A0937, SIGMA) or CL316,243 (C5976, SIGMA) were added to GM at 1 μM concentrations unless otherwise specified.

2.13. Statistical analyses

Statistical analyses were performed with Prism software (GraphPad). Differences between two groups were analyzed using Student's t test (two-tailed), and multiple comparisons were analyzed by ANOVA with a Bonferroni post hoc test. A *P*-value less than 0.05 was considered significant. Data are expressed as means ± SEM.

3. RESULTS

3.1. SIRT1$^{Tg/Tg}$ mice display higher energy expenditure and glucose tolerance

SIRT1$^{Tg/Tg}$ mice displayed a moderate SIRT1 overexpression in skeletal muscle, liver, white adipose tissue (WAT) and BAT, both at the mRNA and protein levels (Figure 1A,B). In contrast to the heterozygous mice, where changes were reported to be 2–4-fold [4], up to 10-fold increases in SIRT1 expression were observed in the WAT from SIRT1$^{Tg/Tg}$ mice. When fed an LFD, SIRT1$^{Tg/Tg}$ mice displayed a similar body weight (Figure 1C) and composition (Figure 1D) as WT mice. However, SIRT1$^{Tg/Tg}$ showed a marked increase in O_2 consumption and EE both during the light and the dark phases (Figure 1E and Figure S1A-B). The respiratory exchange ratio (RER) of SIRT1$^{Tg/Tg}$ mice was lower than in WT mice during the light phase, indicating a higher use of lipid energy substrates (Figure 1F and Figure S1C). The bigger amplitude in RER changes between the light and dark phases (Figure 1F) suggests an enhanced flexibility to shift between carbohydrate and lipid energy sources. While food intake was similar between genotypes (Figure 1G), the CLAMS analysis revealed a clear tendency to decreased activity in SIRT1$^{Tg/Tg}$ mice (Figure S1D). The lower spontaneous activity of SIRT1$^{Tg/Tg}$ mice was more evident when daily voluntary activity was analyzed in regular housing cages (Figure 1H). This is an interesting aspect, as SIRT1$^{Tg/-}$ mice also showed a tendency towards lower activity on LFD [4], and this decrease was largely significant in the SirBACO mice [5]. Also, the treatment with STACs has been reported to decrease spontaneous activity in mice [8,13]. Hence, systemic SIRT1 activation might reduce spontaneous activity, which could explain why SIRT1$^{Tg/Tg}$ mice have a similar body weight despite higher EE.

We next evaluated if the marked differences of SIRT1$^{Tg/Tg}$ mice on energy homeostasis could have an impact on glucose metabolism. Blood glucose and insulin levels were similar between WT and SIRT1$^{Tg/Tg}$ mice, either in the fed or fasted state (Table 1). SIRT1$^{Tg/Tg}$ mice, however, displayed a higher glucose tolerance (Figure 2A) and response to insulin (Figure 2B), based on intraperitoneal glucose and insulin

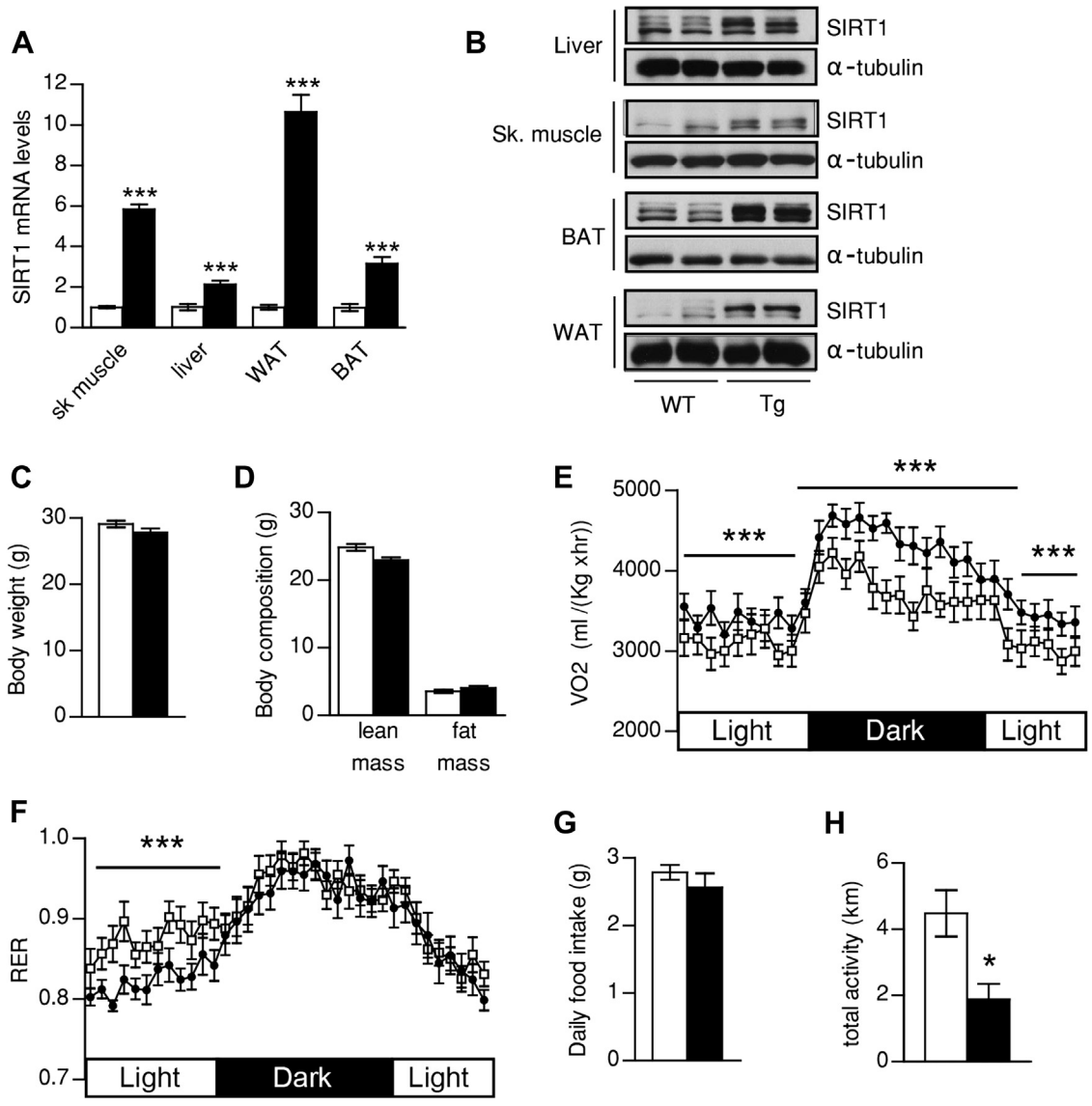

Figure 1: Evaluation of energy homeostasis in SIRT1$^{Tg/Tg}$ mice. (A, B) 20 week-old wild-type (WT) and SIRT1$^{Tg/Tg}$ (Tg) mice were sacrificed to measure (A) the mRNA and (B) protein levels of SIRT1 in the indicated tissues. (C, D) Three months old WT and Tg mice were fed ad libitum with a low fat diet and (C) body weight and (D) body composition were measured through EchoMRI. (E) Oxygen consumption (VO_2) and (F) Respiratory exchange ratio (RER) were measured by indirect calorimetry using a comprehensive laboratory animal monitoring system (CLAMS). (G) Food intake a measured during the indirect calorimetry tests. (H) Voluntary wheel running activity was measured in 20-week-old WT and Tg mice. All values are presented as mean ± SEM of $n = 10–14$ mice for each genotype. *indicates statistical significant difference between WT (white bars and circles) and Tg mice (black bars and circles) at $P < 0.05$.

tolerance tests, respectively. In order to evaluate the key tissues contributing to the higher glucose tolerance and insulin response, we performed a hyperinsulinemic-euglycemic clamp on WT and SIRT1$^{Tg/Tg}$. Both phenotypes required similar glucose infusion rates (GIR) at low insulin concentrations (4 mU/kg/min) (Figure 2C). However, when insulin levels were raised to asses peripheral glucose uptake (12 mU/kg/min), SIRT1$^{Tg/Tg}$ mice required a significantly higher GIR (Figure 2C). In these conditions, insulin equally decreased hepatic glucose production in both genotypes (Figure 2D), illustrating that differences in hepatic function do not account for the higher GIR rate. Glucose disposal rates were also calculated for individual tissues in response to the insulin challenges. Glucose uptake was similar between genotypes in skeletal muscle, liver, epididymal and sub-cutaneous WAT (Figure 2E). In contrast, BAT glucose uptake was higher in SIRT1$^{Tg/Tg}$ mice (Figure 2E) suggesting that BAT is the main responsible for the higher GIR required to maintain euglycemia in SIRT1$^{Tg/Tg}$ mice.

These observations contrast with those in SIRT1$^{Tg/-}$ mice, where higher glucose tolerance was only observed on HFD [4,5]. In this sense, SIRT1$^{Tg/Tg}$ mice also displayed a strong protection against glucose intolerance (Figure S2A) and insulin resistance

Table 1 — Blood biochemistry.

Parameters	WT ($n = 6$)	Tg ($n = 6$)
Glycemia (mg/dL) — Fed	150.63 ± 3.12	155.14 ± 6.01
Glycemia (mg/dL) — Fasted	75.67 ± 4.8	81.14 ± 5.1
Insulinemia (ng/mL) — Fed	2.73 ± 0.34	2.74 ± 0.30
Insulinemia (ng/mL) — Fasted	1.10 ± 0.21	1.05 ± 0.10
Triglycerides (mmol/L)	1.08 ± 0.13	1.50 ± 0.19
Free Fatty Acid (mmol/L)	0.63 ± 0.11	0.75 ± 0.09
Total Cholesterol (mmol/L)	2.8 ± 0.2	2.8 ± 0.2
HDL-Cholesterol (mmol/L)	2.78 ± 0.15	2.74 ± 0.25
LDL-Cholesterol (mmol/L)	0.11 ± 0.03	0.09 ± 0.02

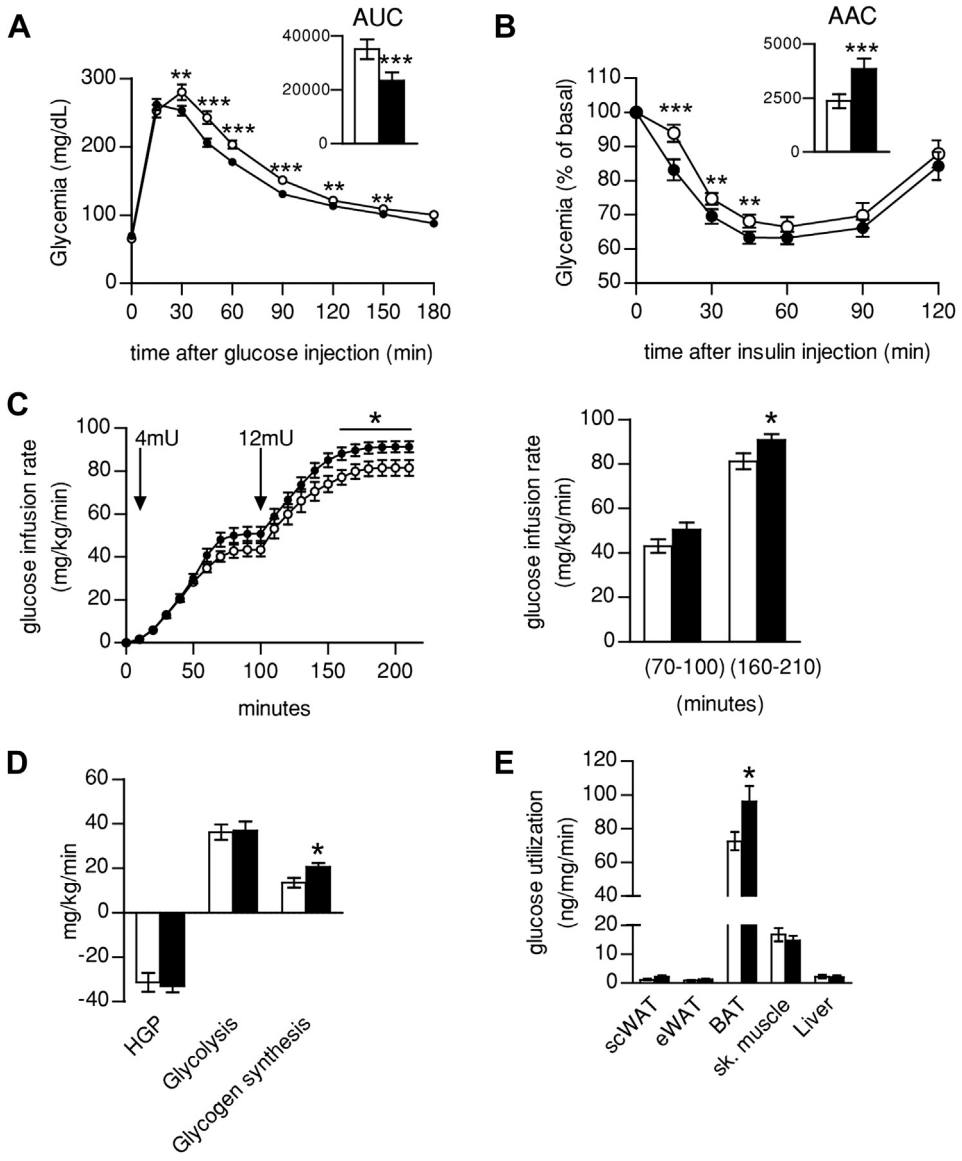

Figure 2: SIRT1 overexpression improves insulin sensitivity through higher BAT glucose uptake. (A) An intraperitoneal glucose tolerance test and (B) an intraperitoneal insulin tolerance test were performed on 4-month-old WT and Tg mice. Area under the curve (AUC) or area above the curve (AAC) calculations are present on the top right of each glucose excursion. (C–E) Hyperinsulinemic-euglycemic clamp was performed on WT and SIRT1$^{Tg/Tg}$ mice fed on low fat diet. Glucose Infusion Rate (GIR) measured at two different levels of insulin infusion (4 and 12 mU/kg/min) (C), glucose fluxes (D) and Glucose uptake in different tissues (inguinal sub-cutaneous and epididymal WAT, BAT, vastus lateralis skeletal muscle and liver) (E) are represented. All values are presented as mean ± SEM of $n = 12–14$ mice for each genotype. * indicates statistical significant difference between WT (white bars and circles) and Tg mice (black bars and circles) at $P < 0.05$.

(Figure S2B) on HFD, despite a similar body weight gain as WT mice (Figure S2C).

3.2. Skeletal muscle and liver are not affected in SIRT1$^{Tg/Tg}$ mice on low fat diet

The fact that SIRT1$^{Tg/Tg}$ mice did not display higher insulin sensitivity in skeletal muscle is in line with recent reports using transgenic models with even higher SIRT1 overexpression [14,15]. However, these results do not rule out other possible contributions of SIRT1 transgenesis to muscle metabolic properties. In this sense, mitochondrial biogenesis and higher oxidative capacity are believed to be two key metabolic actions triggered by SIRT1 in skeletal muscle [16]. To further explore these areas, we first, submitted the mice to grip and treadmill tests in order to evaluate muscle force and endurance, respectively. However, none of them were improved by SIRT1 transgenesis (Figure 3A,B). In line with this, no differences in maximal running speed or maximal VO_2 could be found between genotypes (Figure S3A-B). No structural or oxidative profile differences were observed between the gastrocnemius muscles of WT and SIRT1$^{Tg/Tg}$ mice, based on succinate dehydrogenase stainings (data not shown). WT and SIRT1$^{Tg/Tg}$ mice also showed no differences when evaluating mitochondrial vs. nuclear DNA ratios (Figure 3C), citrate synthase (CS) activity (Figure 3D) or the levels of mitochondrial-related mRNAs and proteins in gastrocnemius muscle (Figure 3E,F). The protein content of mitochondrial respiratory complex subunits was also unaffected in highly oxidative (soleus) or glycolytic (EDL) muscles (Figure S3C). Interestingly, an upregulation of several

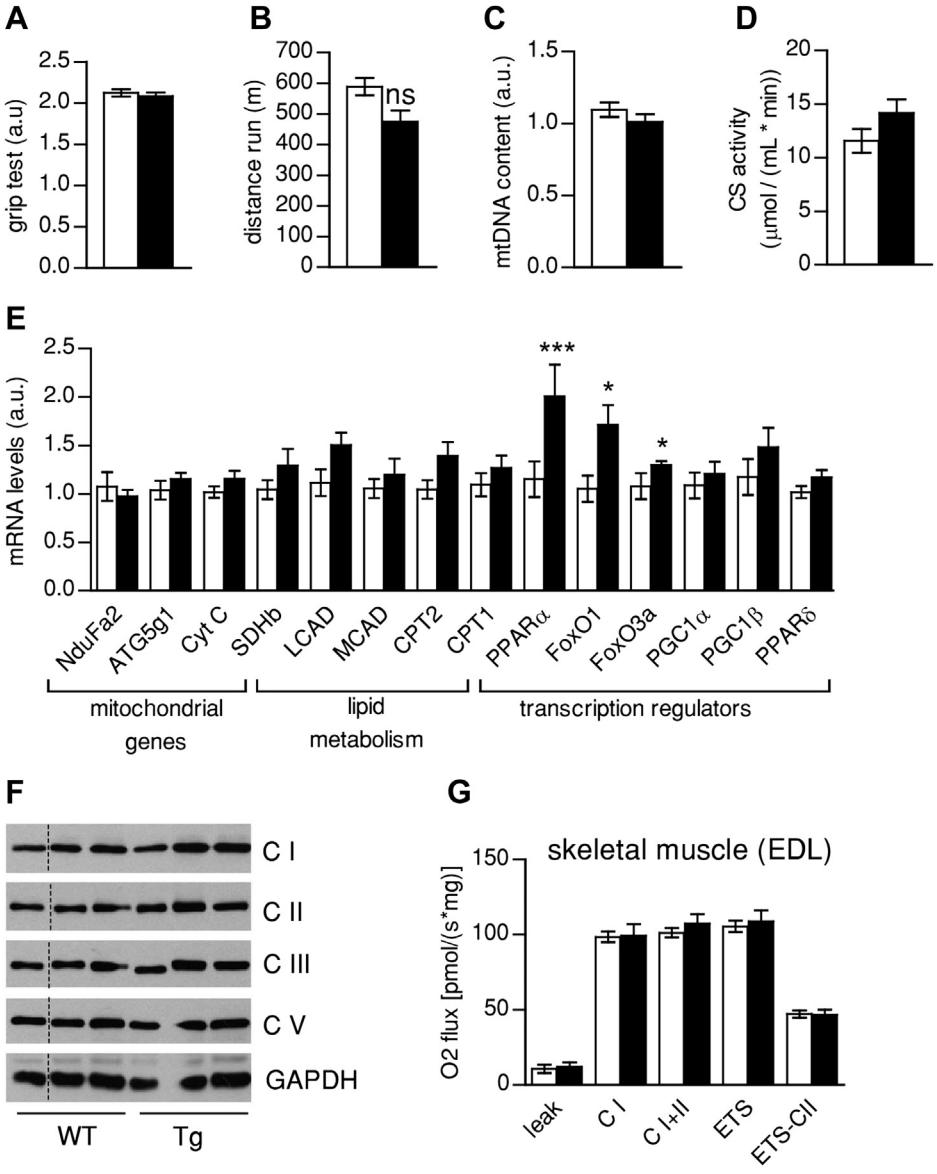

Figure 3: Muscle function is not affected by SIRT1 transgenesis. (A) Muscle force was evaluated in wild type (WT) and SIRT1$^{Tg/Tg}$ (Tg) mice through a grip test. (B) Running distance was evaluated by submitting mice to an endurance treadmill test. (C) Mitochondrial DNA content in gastrocnemius muscle was measured and normalized to nuclear DNA copy number. (D) Citrate synthase activity was measured in quadriceps muscle. (E) Total mRNA was extracted from gastrocnemius muscles and used for qPCR analysis of the markers indicated. (F) Protein analysis of mitochondrial markers in total homogenates of quadriceps muscle (thin black lines on gels are used for lanes that were run on the same gel but were non-contiguous). (G) Oxidative phosphorylation and electron transfer system capacity in permeabilitzed EDL muscle fibers of WT and Tg mice. All values are presented as mean ± SEM of $n = 8–10$ mice for each genotype. * indicates statistical significant difference between WT (white bars and circles) and Tg mice (black bars and circles) at $P < 0.05$.

transcriptional regulators, such as the *peroxisome proliferator-activated receptor-α* (PPARα) and the Forkhead O box (FOXO) 1 and 3a, was observed in SIRT1$^{Tg/Tg}$ muscles. However, the above results suggest that these changes were not enough to affect muscle endurance and mitochondrial function. To further substantiate the lack of differences in mitochondrial function between WT and SIRT1$^{Tg/Tg}$ mice, we performed respirometry analyses in permeabilized EDL muscle fibers. Uncoupled respiration (leak) through complex I, stimulated with malate, pyruvate and glutamate, was not affected by SIRT1 transgenesis (Figure 3G). Similarly, maximal respiration in the coupled state, with electron input through complex I alone (C I) or through complex I + II – after the addition of succinate – (C I + II) was comparable across genotypes (Figure 3G). Maximum electron transport system (ETS) capacity was also similar, even after the addition of the complex I inhibitor rotenone (ETS CII) (Figure 3G). Hence, no major differences in mitochondrial function could be observed in the skeletal muscle from WT and SIRT1$^{Tg/Tg}$ mice.

Next, we also examine the consequences of SIRT1 transgenesis in liver tissue on LFD. While the hyperinsulinemic-euglycemic clamp revealed no major effects of SIRT1 transgenesis in liver glucose turnover on LFD (Figure 2D,E), the liver accounts for the benefits of SIRT1 transgenesis on glucose metabolism upon HFD [4,5]. To further evaluate hepatic glucose metabolism in our SIRT1$^{Tg/Tg}$ mice on LFD diet, we challenged the mice with a pyruvate tolerance test. After the injection of pyruvate, a

gluconeogenic precursor, glucose excursions were comparable between WT and SIRT1$^{Tg/Tg}$ mice (Figure 4A). We also failed to detect differences between the two genotypes on histological Oil red'O stainings (Figure 4B) or at the level of hepatic triglyceride or glycogen content (Figure 4C,D). As in muscle, no changes could be found on mitochondrial DNA content (Figure 4E), on CS activity (Figure 4F) or at the mRNA and protein level of several mitochondrial components (Figure 4G,H). In line with the comparable response to pyruvate, the expression of key gluconeogenic genes, such as glucose 6-phosphatase (G6Pase) and phopho-enol-pyruvate carboxylase (PEPCK), was similar between genotypes (Figure 4G). As in muscle, some transcriptional regulators of lipid metabolism were upregulated, including PPARα, FOXO1 and FOXO3a (Figure 4G). Interestingly, respirometry analyses revealed a higher complex II activity in SIRT1$^{Tg/Tg}$ livers (Figure 4I). However, based on the absence of differences in hepatic metabolism upon pyruvate and insulin challenges, the physiological relevance of these increases is unclear.

3.3. Brown adipose function is improved in SIRT1 transgenic mice

The lack of effects on WAT insulin response in SIRT1$^{Tg/Tg}$ mice on LFD (Figure 2E) was in line with the absence of differences in the weight of different WAT depots (Figure S4A) or their histological aspect

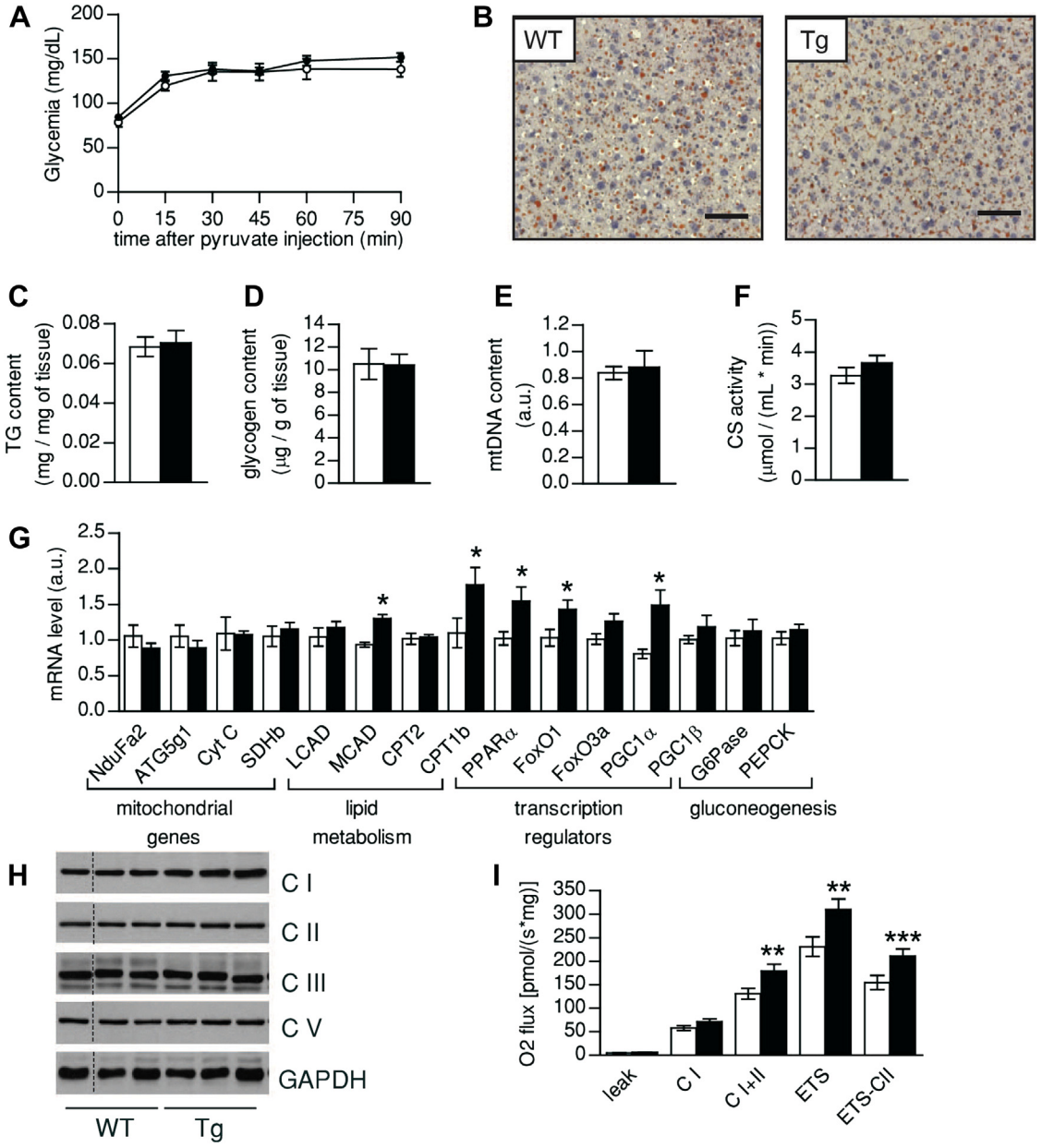

Figure 4: Hepatic function is not critically affected by SIRT1 transgenesis. (A) Blood glucose curves after a pyruvate (2 g/kg) challenge. (B) Oil Red'O staining in WT and Tg livers after an overnight fast (bar = 600 µm) (C, D) Hepatic triglyceride (C) and glycogen (D) content was measured after an overnight fast. (E) Mitochondrial DNA content was measured and normalized to nuclear DNA copy number. (F) Citrate synthase activity in liver. (G) Total liver mRNA was extracted and used for qPCR analysis of the markers indicated. (H) Protein analysis of mitochondrial markers in total liver homogenates (thin black lines on gels are used for lanes that were run on the same gel but were non-contiguous). (I) Oxidative phosphorylation and electron transfer system capacity in liver homogenates of WT and Tg mice. All values are presented as mean ± SEM of $n = 8–10$ mice for each genotype. * indicates statistical significant difference between WT (white bars and circles) and Tg mice (black bars and circles) at $P < 0.05$.

(Figure S4B). Accordingly, we found no alterations in mitochondrial function (Figure S4C) or lipolytic capacity (Figure S4D) in the WAT of SIRT1$^{Tg/Tg}$ mice.

Finally, we focused on the BAT function in SIRT1$^{Tg/Tg}$ mice, as it is the tissue most likely explaining the differences in glucose homeostasis between genotype (Figure 2E). Strikingly, the color of the BAT from SIRT1$^{Tg/Tg}$ mice was more intense (Figure 5A), likely due to a lower accumulation of lipids, as reflected in the much smaller lipid droplets observed through hematoxylin/eosin staining (Figure 5B). We next evaluated BAT thermogenic function by placing the mice at 6 °C and monitoring body temperature for 5 h. While no significant differences on the basal state, SIRT1$^{Tg/Tg}$ mice maintained better their body temperature during the cold challenge (Figure 5C), suggesting a higher thermogenic activity. As in other tissues, we found no differences between genotypes in mitochondrial DNA copy number (Figure 5D) or in the content of respiratory complexes subunits at protein and mRNA levels (Figure 5E and Figure S5A, respectively). To infer the possible mechanisms by which SIRT1$^{Tg/Tg}$ mice displayed altered BAT function, we performed microarray analyses (results available in the GEO database with the accession number GSE62324). Geneset enrichment revealed a strongly significant (nominal P-value < 0.01) increase of genes related to fatty acid metabolism and, more in particular, lipid catabolism (Figure 5F and Figure S5B). The microarray results were validated by quantitative real-time PCR (qPCR), which confirmed that genes related to β-oxidation were strongly induced in the BAT of SIRT1$^{Tg/Tg}$ mice (Figure 5G). This way, key genes for lipid oxidation, such as the long-chain acyl-CoA dehydrogenase (LCAD), the medium-chain acyl-CoA dehydrogenase (MCAD) or the carnitine palmitoyltransferase 1b

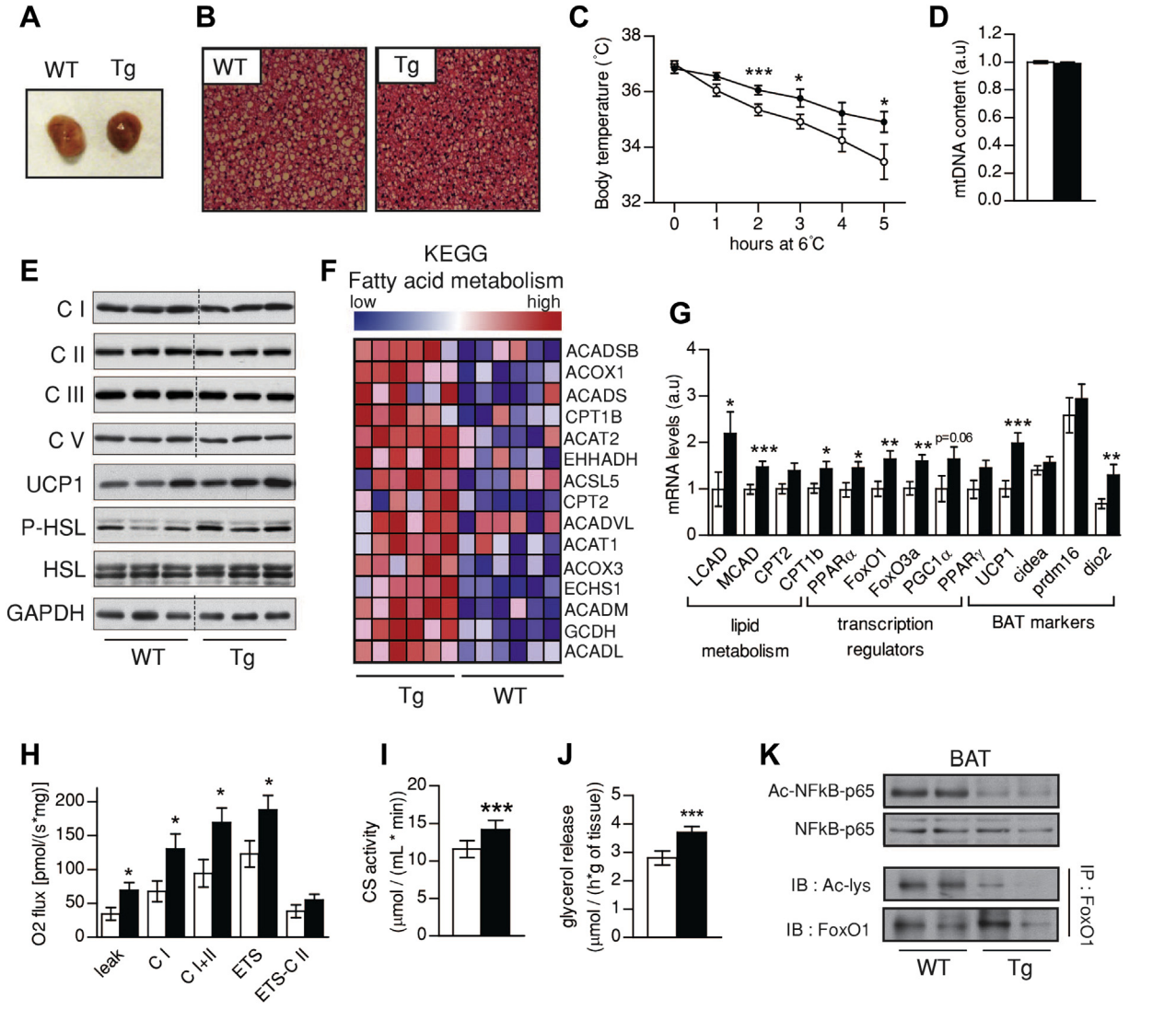

Figure 5: Brown adipose function is improved in SIRT1 transgenic mice. (A) Pictures of brown adipose tissue (BAT) from WT and Tg mice. (B) Hematoxylin and eosin stainings on the BAT of wild type (WT) and SIRT1$^{Tg/Tg}$ (Tg) mice (bar = 600 µm) (C) Brown adipose thermogenic function was evaluated by placing WT and Tg mice at 6 °C for 5 h. (D) Mitochondrial DNA content in BAT from WT and Tg mice, normalized to nuclear DNA copy number. (E) Western Blots were performed to evaluate the protein levels of proteins in BAT from WT and Tg mice (thin black lines on gels are used for lanes that were run on the same gel but were non-contiguous). (F) Gene set enrichment analyses of gene expression profiles of BAT from WT and Tg mice. (G) Total mRNA was extracted from BAT and used for qPCR analysis. (H) Oxidative phosphorylation and electron transfer system capacity in BAT. (I) Citrate synthase activity in BAT from WT and Tg mice. (J) Lipolysis was evaluated by measuring glycerol release in isolated BAT. (K) SIRT1 activity was tested in WT and Tg BAT using the acetylation status of RelA(p65) and FOXO1 as readout. All values are presented as mean ± SEM of $n = 8–10$ mice for each genotype. * indicates statistical significant difference between WT (white bars and circles) and Tg mice (black bars and circles) at $P < 0.05$.

(CPT1b), were significantly elevated in SIRT1$^{Tg/Tg}$ mice (Figure 5G). This was, again, in line with an upregulation of PPARα and FOXOs. Interestingly, the protein and mRNA levels of the uncoupling protein UCP1 were also elevated in SIRT1$^{Tg/Tg}$ BAT (Figure 5E and G, respectively). The key role of UCP1 in energy dissipation could explain the higher EE (Figure 5E,F) and thermogenic potential (Figure 5C) observed in SIRT1$^{Tg/Tg}$ mice. In line with this, respirometry analyses revealed an almost 2-fold increase in uncoupled respiration (leak) in the BAT from SIRT1$^{Tg/Tg}$ mice, and a higher maximal ETS capacity (Figure 5H). Concordantly, CS activity was also increased (Figure 5I). Finally, we examined the lipolytic rates in WT and SIRT1$^{Tg/Tg}$ BATs. The results obtained illustrate how the basal lipolytic rates in the BAT from SIRT1$^{Tg/Tg}$ are ∼20% higher than those of their control WT mice (Figure 5J). This result is in line with the higher basal phosphorylation of the hormone sensitive lipase (HSL) observed in protein homogenates (Figure 5E), and could explain the lower lipid accumulation observed through histology (Figure 5B). Also, the mRNA level of the type II iodothyronine deiodinase (*DIO2*) was also increased in the BAT of SIRT1$^{Tg/Tg}$ mice, supporting a higher catabolic rate (Figure 5G). Altogether, these data suggest that SIRT1$^{Tg/Tg}$ mice have a higher thermogenic function and lipid oxidation-related gene expression in BAT. While SIRT1 activation has been classically linked to enhanced mitochondrial biogenesis [1] mitochondrial content was not affected in the BAT from SIRT1$^{Tg/Tg}$ mice, despite a markedly higher SIRT1 activity, as testified by the reduced acetylation of NFκB and FoxO1 (Figure 5K).

3.4. SIRT1 transgenesis affects BAT response to adrenergic stimulation

We next aimed to understand whether the changes in BAT biology elicited by SIRT1 transgenesis were derived from alterations in the BAT differentiation process or on its function. For this purpose, we immortalized primary brown pre-adipocytes from WT and SIRT1 transgenic mice. SIRT1 transgenesis did not affect the cellular morphology (Figure 6A), lipid droplet accumulation (Figure S6A) and TG content (Figure 6B) of the cultured brown adipocytes. Brown adipocyte differentiation markers, such as Prdm16, Cidea and PPARγ, were similarly induced at the mRNA and protein level after differentiation between the two genotypes (Figure 6C,D). In line with this, the mRNA expression of these markers in adult BAT from WT and SIRT1$^{Tg/Tg}$ mice was also similar (Figure 6G). These analyses also confirmed that SIRT1 overexpression levels in undifferentiated and differentiated transgenic immortalized brown adipocytes are comparable to those in the SIRT1 transgenic BAT (Figures 1A,B and 6D). Hence, SIRT1 overexpression does not affect brown adipocyte differentiation. Strikingly, while *Ucp1* expression, both at the mRNA and protein level, increased upon differentiation of WT brown adipocytes, it did much less in the brown adipocytes from SIRT1 transgenic mice (Figure 6D,E). A recent publication indicated that SIRT1 can amplify the transcriptional response to PKA signaling [17]. We hence reasoned that the increased UCP1 levels observed in SIRT1$^{Tg/Tg}$ BAT could be consequent to a higher response of SIRT1 transgenic adipocytes to β3-adrenergic stimulation. To test this hypothesis, we analyzed the response of differentiated brown adipocytes to adrenergic stimulation using norepinephrine (NE) or the synthetic agonist CL316,243 (CL). Both agents induced a comparable increase in p-HSL after 5 h of treatment (Figure 6F). This indicates that early signaling responses to β3 stimulation are not altered by SIRT1 transgenesis. However, the transcriptional response of *Ucp1* to NE or CL was dramatically enhanced in SIRT1 brown adipocytes (Figure 6F,G and Figure S6B). The enhanced transcriptional response to β3 agonists in SIRT1 transgenic adipocytes was certified using another adrenergic target in the BAT, the PPARγ coactivator 1α (PGC-1α) [17] (Figure S6C). The transcriptional responsiveness of SIRT1 transgenic adipocytes to adrenergic stimulation was higher at concentrations as low as 10 nM, as testified by *Ucp1* mRNA analyses (Figure 6G). Similarly, SIRT1 transgenic brown adipocytes achieved maximal *Ucp1* transcriptional response to adrenergic stimulation at earlier time-periods than WT adipocytes (Figure 6H). Thus, our results indicate that SIRT1 grants brown adipocytes with a higher transcriptional responsiveness to β3 agonists.

3.5. Thermoneutrality blunts the differences in glucose homeostasis of SIRT1$^{Tg/Tg}$ mice

The results above illustrate that, upon adrenergic stimulation, SIRT1 transgenic adipocytes have an exacerbated transcriptional response (Figure 6G,H) that allows them to recover UCP1 protein levels to comparable levels of that of WT mice even within a few hours (Figure 6F). We reasoned that if this stimulation had a chronic character, this could lead to even further increases and explain the higher activity of BAT in SIRT1$^{Tg/Tg}$ mice. In this sense, it must be taken into account that at regular housing conditions (∼20–22 °C), mice are below thermoneutrality, which leads to a basal stimulation of the BAT thermogenic function. Considering the above results, this chronic basal adrenergic tone could be responsible for the higher BAT function, *Ucp1* expression and EE observed in SIRT1$^{Tg/Tg}$ mice. To test this hypothesis, we housed WT and SIRT1$^{Tg/Tg}$ mice at thermoneutrality (30 °C), which blunts thermogenic activity [18]. In turn, this would allow us to evaluate whether the enhancement of BAT function is responsible for the higher glucose tolerance and insulin sensitivity of SIRT1$^{Tg/Tg}$ mice on LFD. After one month at thermoneutrality, SIRT1$^{Tg/Tg}$ and WT mice were undistinguishable at the level of body weight (Figure 7A), body composition (Figure 7B) and food intake (Figure S7A). As in normal housing conditions the total activity of the SIRT1$^{Tg/Tg}$ mice was also reduced at thermoneutrality (Figure S7C). Importantly, however, thermoneutrality blunted the effect of SIRT1 transgenesis on VO_2 (Figure 7C), EE (Figure S7B) and RER (Figure S7D) that we previously observed in normal housing conditions (Figure 1E,F). In addition, thermoneutrality also abrogated the higher glucose tolerance and insulin sensitivity of SIRT1$^{Tg/Tg}$ mice (Figure 7D,E). Interestingly, a higher glycemia was clearly observed in SIRT1$^{Tg/Tg}$ mice 15 min after a glucose load (Figure 7D), even though the physiological relevance of this difference is unclear. These evidences, together with the results obtained during hyperinsuilnemic-euglycemic clamp (Figure 2E), clearly demonstrate that enhanced BAT function is the primordial event by which SIRT1$^{Tg/Tg}$ mice are granted better glucose homeostasis in regular housing conditions. Thermoneutrality increased the lipid droplet size in the BAT of both WT and SIRT1$^{Tg/Tg}$ mice (Figures 5B and 7F), and rendered both genotypes histologically undistinguishable. Similarly, the higher basal expression of lipid oxidation-related genes observed in SIRT1$^{Tg/Tg}$ mice was blunted on thermoneutral conditions (Figure 7G). Interestingly, we observed a dramatic reduction in *Ucp1* expression in the BAT of SIRT1$^{Tg/Tg}$ compared to that of WT mice (Figure 7G), which is very reminiscent of the lower *Ucp1* mRNA levels observed in cultured primary brown adipocytes. This substantiates that the higher *Ucp1* levels in mice housed at normal conditions are consequent to an exacerbated response to a basal adrenergic tone. As expected, thermoneutrality lowered uncoupled respiration (leak) in both WT and SIRT1$^{Tg/Tg}$ mice (Figures 5H and 7H). While similar respiratory profiles were observed in the BAT from WT and SIRT1$^{Tg/Tg}$ mice on thermoneutrality, we noted a tendency to a lower respiratory leak in SIRT1$^{Tg/Tg}$ mice (Figure 7H), in line with the decrease in *Ucp1* expression. Interestingly, thermoneutrality did not affect the higher Complex II activity in the livers of SIRT1$^{Tg/Tg}$ mice (Figures 4H and 7H).

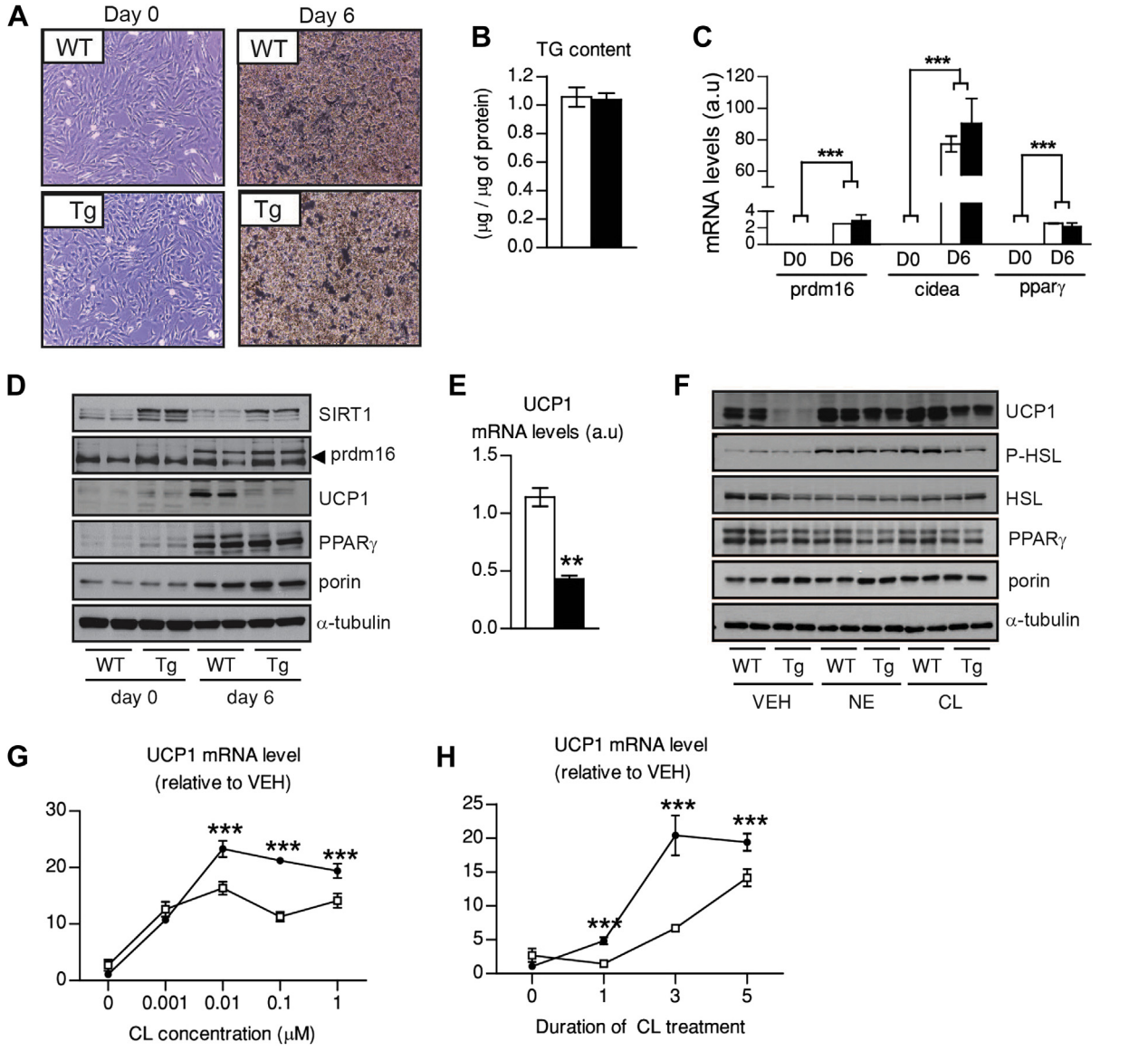

Figure 6: SIRT1 transgenic adipocytes display an exhacerbated response to β3-adrenergic stimulation. Brown pre-adipocytes from wild-type (WT) and SIRT1 transgenic (Tg) mice were isolated and immortalized. (A) The morphology of immortalized brown adipocytes was evaluated before (day 0) and after (day 6) differentiation. (B) Total triglyceride content in differentiated brown adipocytes was evaluated. (C) Total mRNA levels were extracted from pre-adipocytes and differentiated adipocytes and used for qPCR analysis. (D) Total protein extracts were used to evaluate diverse differentiation markers in differentiated and undifferentiated adipocytes. (E) *Ucp1* expression was measured in total mRNA extracts of differentiated brown adipocytes. (F) Differentiated WT and Tg adipocytes were stimulated with 1 µM of norepinephrine (NE) or 1 µM of CL316,243 (CL) during 5 h at 37 °C. Then, total proteins were extracted and used for western blot analysis. (G) WT and Tg brown adipocytes were treated with CL in a dose–response fashion for 5 h at 37 °C and then total mRNA was extracted to measure *Ucp*1 expression. (H) WT and Tg brown adipocytes were treated with 1 µM CL and incubated at 37 °C. Then, total mRNA was extracted at the times indicated to measure *Ucp1* expression. All values are presented as mean ± SEM of at least $n = 4$ independent experiments, each of them run in triplicate. * indicates statistical significant difference between WT (white bars and circles) and Tg mice (black bars and circles) at $P < 0.05$.

On one side, this testifies for the BAT-specific impact of the intervention. On the other, it argues that the increase in Complex II activity in the liver is not responsible for the better glucose tolerance of SIRT1$^{Tg/Tg}$ mice on regular housing conditions. Finally, we evaluated whether thermoneutrality also blunted the higher lipolytic rates we observed in SIRT1$^{Tg/Tg}$ mice on non-thermoneutral conditions (Figure 5J). As expected, thermoneutral conditions decreased lipolytic rates in WT mice, as noticed when comparing the values obtained in Figure 5J (white bar; 2.80 ± 0.25 mmol/(mg of tissue*h)) and at thermoneutral conditions (Figure 7I, white bar, 1.51 ± 0.22 mmol/(mg of tissue*h)). Thermoneutrality also blunted the higher lipolytic rates and HSL phosphorylation in the BAT from SIRT1$^{Tg/Tg}$ mice and made them undistinguishable from WT mice (Figure 7I).

4. DISCUSSION

While SIRT1 activation has been linked to diverse metabolic health benefits, the key tissue(s) responsible for such actions remain elusive. Mouse models with a moderate SIRT1 overexpression have shown a key protective role for SIRT1 on liver function upon HFD [4,5]. Here we describe how the expression of just one additional copy of SIRT1 to that of previous works [4,19], is sufficient to enhance BAT activity,

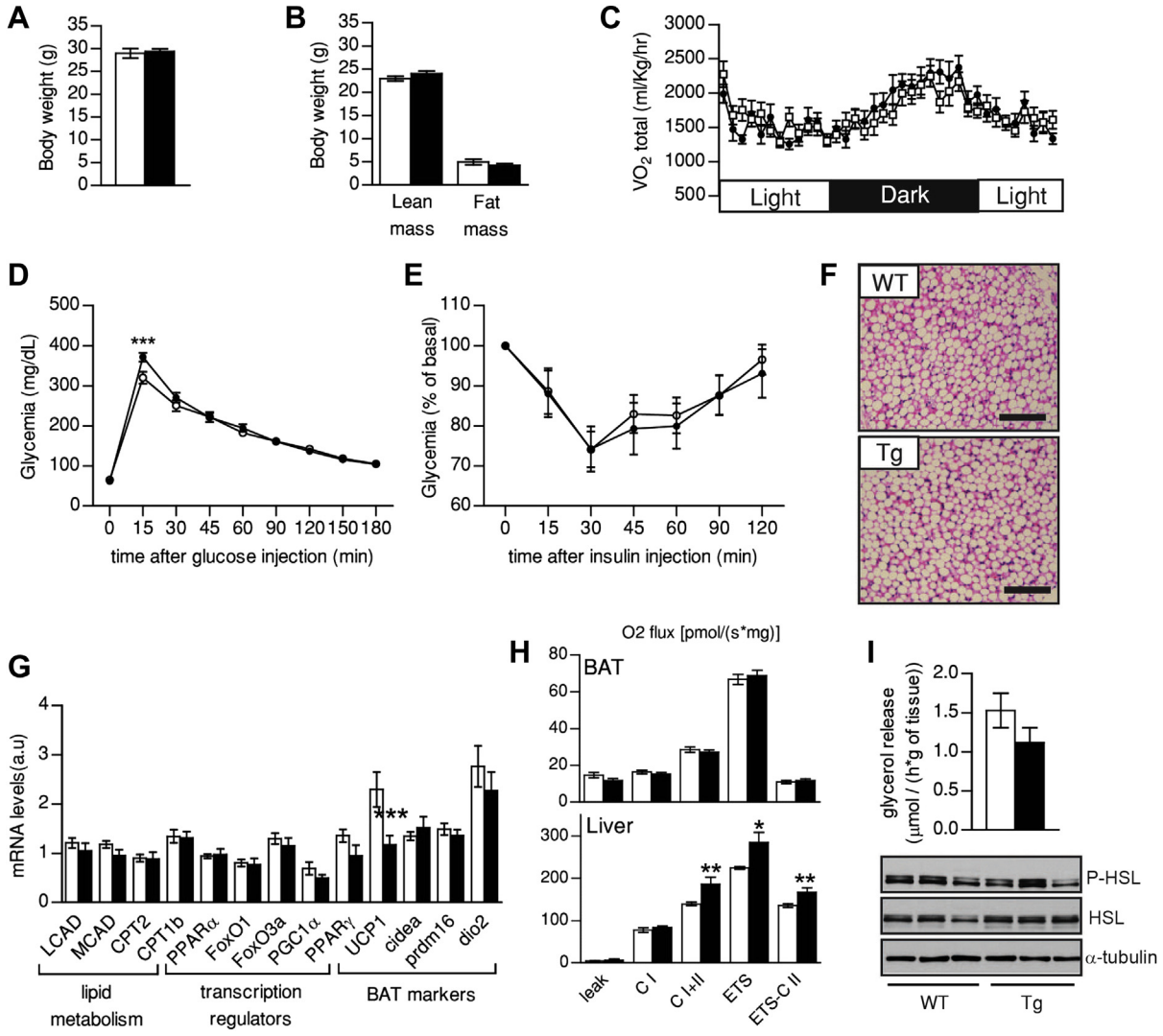

Figure 7: Thermoneutrality blunts the insulin-sensitizing effect of SIRT1 transgenesis. Three months old WT and Tg mice were fed ad libitum with low fat diet and placed at thermoneutrality (30 °C) for one month before phenotyping. Then, (A) Body weight and (B) body composition were measured using Echo-MRI. (C) O_2 consumption was evaluated using a comprehensive animal laboratory monitoring system; (D) An intraperitoneal glucose tolerance test and (E) an insulin tolerance test were performed on 4 months old mice. (F) Hematoxylin and eosin stainings of BAT from WT and Tg mice (bar = 600 μm). (G) Total mRNA was extracted from BAT and used for qPCR analysis. (H) Oxidative phosphorylation and electron transfer system capacity in BAT (top) and liver (bottom) of WT and Tg mice. (I) Lipolysis rates were evaluated by measuring glycerol release from BAT. At the bottom HSL and p-HSL levels were evaluated in total BAT protein extracts. All values are presented as mean ± SEM of $n = 12$ mice for each genotype. * indicates statistical significant difference between WT (white bars and circles) and Tg mice (black bars and circles) at $P < 0.05$.

leading to increased EE and improved glucose homeostasis even on LFD.

SIRT1 transgenesis did not affect BAT differentiation, yet it dramatically enhanced BAT transcriptional responses to β3-adrenergic stimulation. Hence, the chronic adrenergic tone taking place in mice housed below thermoneutrality drives a higher basal BAT function in SIRT1$^{Tg/Tg}$ mice. In agreement with our results, the SirBACO model has an exacerbated transcriptional response of thermogenic genes after an acute cold exposure [17]. In this case the authors proposed a mechanism in which PKA activation led to the phosphorylation of a residue in the catalytic domain of SIRT1, Ser^{434}, which led to an increase in intrinsic SIRT1 enzymatic activity [17] in the absence of changes in NAD^+ levels. In line with this, we did not observe changes in the BAT NAD^+ levels between WT and SIRT1$^{Tg/Tg}$ mice (Figure S5C). Further efforts from the Accili lab have demonstrated how SIRT1 amplifies the browning response of WAT in response to cold stimuli [20]. Altogether, these works and ours certify the ability of SIRT1 to amplify the response to β3-adrenergic stimuli. Strikingly, the SirBACO model did not display a basal BAT phenotype [5,17]. Our results on thermoneutrality, however, indicate that small differences in the adrenergic tone can even drive to opposite outcomes of SIRT1 on thermogenic gene expression. This way, SIRT1 transgenesis led to a lower *Ucp1* expression in primary brown adipocytes and in BAT from animals at thermoneutral conditions. The repressive action of SIRT1 on *Ucp1* is in line with the role of SIRT1 as an energy sensor triggering adaptations aimed to optimize energy production [1]. Accordingly, SIRT1 represses *Ucp2* expression in pancreatic β-cells [21,22]. The ability of SIRT1 to shift from a corepressing to a coactivating function on thermogenic gene sets might be determined by environmental cues enhancing, in this case, PKA signaling. In this sense, SIRT1 has also been described

as both a positive and negative regulator of PGC-1α and, hence, mitochondrial biogenesis [23,24]. In fact, the simultaneous activation of AMPK signaling is key to determine the outcomes of SIRT1 action on PGC-1α activity and mitochondrial gene expression [25]. In this sense, we did not observe changes in AMPK activity in our SIRT1$^{Tg/Tg}$ model, which might explain the lack of impact on mitochondrial gene expression (Figure S5D). This highlights how small differences in environmental conditions can critically influence SIRT1 actions, which might have strong implications not only for the evaluation of transgenic mouse models, but also for genetic association studies in humans.

Interestingly, higher EE and glucose tolerance were also observed in the first generated model of SIRT1 moderate overexpression [26]. A particularity of that model was a high expression of the transgene in WAT and BAT, but not in the liver or skeletal muscle [26]. More recently, it has been shown that the deletion of SIRT1 in adipose tissues is enough to drive body weight gain and metabolic dysfunction in mice [27]. Conversely, the selective overexpression of SIRT1 in the adipose tissues enhances EE and prevents age-related insulin resistance [28]. Our results refine all these studies by establishing SIRT1 action in the BAT as the key determinant of whole body thermogenic function, EE and glucose homeostasis. Importantly, the higher SIRT1 content did not manifest into an overt phenotype in liver or muscle. Likely, the activity of SIRT1 needs to be triggered by either hormonal or nutritional inputs. In liver, this might only take place upon HFD, when liver phenotypes are clearly observed in SIRT1 transgenic mice [4,5]. The lack of phenotype in skeletal muscle is not entirely surprising, as mice with much higher SIRT1 overexpression in muscle also fail to display any overt alteration [14,15]. Thus, endogenous SIRT1 levels might be able to account for all the necessary SIRT1 activity required to trigger metabolic adaptations in this tissue. Our results also contrast with the largely accepted notion that SIRT1 is a master regulator of mitochondrial biogenesis. In agreement with previous observations [4], the protein or mRNA levels of mitochondrial respiratory complexes were unaffected in SIRT1$^{Tg/Tg}$ tissues. This, does not rule out, however, that SIRT1 overexpression at a higher (>100-fold), non-physiological, level can impact mitochondrial gene expression [14,29].

While SIRT1 can potentially impact on multiple transcriptional programs, lipid oxidation-related gene sets were the most significantly upregulated in the BAT from SIRT1$^{Tg/Tg}$ mice. In fact, SIRT1 transgenesis increased PPARα, FOXO1 and FOXO3a expression in all tissues examined, certifying an intimate link between SIRT1 and these transcriptional regulators in the control of lipid catabolism. Previous reports have demonstrated the ability of SIRT1 to interact with PPARα and enhance its transcriptional activity on lipid catabolism-related genes [30,31]. In this model, SIRT1 would enhance PPARα activity by deacetylating PGC-1α in the PPARα transcriptional complex [30,31]. Conversely, SIRT1 deletion leads to a dramatic decrease in the expression of PPARα target genes, at least in liver [30]. FOXOs are directly deacetylated by SIRT1, an action that targets FOXO activity onto specific gene sets, including oxidative stress genes [32]. Knock-in mice expressing a FOXO1 form mimicking constitutive deacetylation displayed a marked use of lipid as energy source and enhanced lipolytic response to isoproterenol [33], in line with our findings. However, the potent effect of FOXO1 deacetylation on gluconeogenic gene expression [33] is not manifested in our SIRT1$^{Tg/Tg}$ mice. This would confirm that, despite similar overexpression levels in both tissues, SIRT1 transgenesis has a deeper impact in the BAT than in liver, at least on LFD. PPARα and FOXOs, in addition, might also constitute key mediators of the action of SIRT1 on *Ucp1* expression, as both directly regulate the *Ucp1* promoter in brown fat cells [12,34].

One key question derived from our work is: how does SIRT1 enhance insulin-stimulated glucose uptake in the BAT? One possibility is that higher lipolytic rates and prevention of fat deposition (Figure 5J and B, respectively) might spare the BAT from the accumulation of lipid species that could potentially interfere with insulin signaling, such as ceramides or diacylglycerols (DAGs) [35]. While excessive lipolysis in the WAT can be detrimental for whole body insulin sensitivity [36], this is generally associated with a lipid overflow onto other tissues. In contrast, the higher lipolytic flux in the BAT of SIRT1$^{Tg/Tg}$ mice is fully met by an increase in mitochondrial fatty acid oxidation capacity and uncoupling activity. In skeletal muscle, HSL activity seems to be a critical determinant of insulin sensitivity, as it can prevent ATGL-driven accumulation of DAGs and the consequent disruption of insulin signaling [37]. In this sense, the higher HSL activity in the BAT of SIRT1$^{Tg/Tg}$ mice might act in a similar fashion. In HFD, lower inflammation was a key mechanism by which SIRT1$^{Tg/-}$ mice retained hepatic insulin sensitivity [9]. Interestingly, in our microarrays, cytokine and inflammatory pathways were two of the most significantly downregulated gene-sets in the BAT of SIRT1$^{Tg/Tg}$ mice (Figure S5B), suggesting that a lower baseline inflammation state might also contribute to its higher insulin sensitivity. Recently, using a BAT transplantation model, it has been shown that increasing BAT function promotes an increase in FGF21 and IL-6 expression, which could act in an endocrine fashion to alter insulin sensitivity in other peripheral tissues [38]. This, however, is not the case in our model, as enhanced insulin sensitivity is not manifested in muscle or eWAT (Figure 2E). Accordingly, we failed to detect differences in BAT FGF21 or IL-6 expression between genotypes (data not shown).

A final aspect for discussion is whether SIRT1 activation *via* transgenesis is comparable to that achieved via improving NAD^+ availability. In theory, at similar NAD^+ levels, SIRT1 activity will increase directly in line with increases in expression, unless SIRT1 overexpression decreases NAD^+ content via excessive consumption. This is not the case in the BAT of SIRT1$^{Tg/Tg}$ mice, where SIRT1 activity is higher, based on the evaluation of NFκB and FOXO1 acetylation (Figure 5K), without affecting NAD^+ levels (Figure S5C). Hence, SIRT1 transgenesis should ensure a linear increase in SIRT1 activity with the level of overexpression, at least up to a certain threshold. The efficacy of NAD^+ boosting strategies on SIRT1 activity, however, depends on whether intracellular NAD^+ levels are rate-limiting for SIRT1 activity in the basal state. Dietary supplementation with the NAD^+ precursor nicotinamide riboside (NR) leads to SIRT1 activation in the BAT [39]. This suggests that basal NAD^+ levels are rate-limiting for SIRT1 activity in the BAT. However, a NAD^+ precursor will fail to activate SIRT1 if NAD^+ is not rate-limiting or in tissues with limited capacity to metabolize the precursor into NAD^+. In the case of NR, additionally, it also leads to the activation of other sirtuins, such as SIRT3, by increasing NAD^+ content in the mitochondrial compartment [39,40]. Therefore the comparison between transgenic and NAD^+-related SIRT1 gain-of-function models should be taken carefully. In the case of STACs, resveratrol and SRT1720 have major effects on BAT activity [8,13]. However, STACs have also marked effects in skeletal muscle oxidative capacity and prevent body weight gain on HFD [8,13]. None of these effects have been observed in this or previous studies using models of moderate SIRT1 overexpression [4,5]. Therefore, either STACs increase SIRT1 activity in muscle in a much more stronger fashion than the above mentioned SIRT1 gain-of-function mouse models, or some effects might be influenced by off-target actions on other molecular paths regulating energy metabolism, as discussed recently in Ref. [1].

Altogether, this manuscript describes a key physiological role of SIRT1 in BAT biology and establishes SIRT1 as a sensitive gauge for the adrenergic response of the BAT, a property that could be exploited for therapeutic approaches aimed to ameliorate glycemic control.

AUTHOR CONTRIBUTIONS

M.B., S.S.K., P.J.F.M. and C.C. have taken care of animal management, phenotyping and tissue collection. M.B., M.J., J.R. and C.C. have performed molecular biology analyses. M.B., P.M.G.R. and C.C. have performed respirometry analyses. E.G.C. and A.M.V. have immortalized primary brown adipocytes. M.B., P.M.G.R., M.S. and C.C. have experimentally conceived the project. M.B. and C.C have written the manuscript and all authors have contributed to editing duties.

ACKNOWLEDGMENTS

We thank the members of the Canto lab for exciting discussions. We thank the members of the EPFL and CNIO animal houses for technical support. We also thank the Genomic platform (P. Descombes, F. Raymond and S. Metairon) at NIHS for technical help and advice on microarray analyses. We would also like to express our gratitude to Physiogenex S.A.S. for their help with the hyperinsulinemic-euglycemic clamp. M.S. is funded by the CNIO and by grants from the MICINN (SAF), the Regional Government of Madrid, the European Research Council (CANCER&AGING; LS1, ERC-2008-AdG), the Botín Foundation, the Ramón Areces Foundation, and the AXA Foundation. P.J.F.M. is funded by the AECC. A.M.V. is funded by the following grant support: SAF2012-33283 (MINECO, Spain), Comunidad de Madrid S2010/BMD-2423, EFSD and Amylin Paul Langerhans Grant and Centro de Investigación Biomédica en Red de Diabetes y Enfermedades Metabólicas Asociadas (CIBERDEM, ISCIII, Barcelona, Spain). P.M.G.R. is funded by the following grant support: BFU2011-24679 (MINECO, Spain) and he is a recipient of a Ramon y Cajal contract: RYC-2009-05158(MINECO, Spain).

CONFLICT OF INTEREST

M.B., M.J., S.S.K., J.R. and C.C. are employees of the Nestlé Institute of Health Sciences S.A.

APPENDIX A. SUPPLEMENTARY DATA

Supplementary data related to this article can be found at http://dx.doi.org/10.1016/j.molmet.2014.12.008.

REFERENCES

[1] Canto, C., Auwerx, J., 2012. Targeting sirtuin 1 to improve metabolism: all you need is NAD(+)? Pharmacological Reviews 64(1):166–187.

[2] Baur, J.A., Ungvari, Z., Minor, R.K., Le Couteur, D.G., de Cabo, R., 2012. Are sirtuins viable targets for improving healthspan and lifespan? Nature Review Drug Discovery 11(6):443–461.

[3] Pacholec, M., Bleasdale, J.E., Chrunyk, B., Cunningham, D., Flynn, D., Garofalo, R.S., et al., 2010. SRT1720, SRT2183, SRT1460, and resveratrol are not direct activators of SIRT1. Journal of Biological Chemistry 285(11):8340–8351.

[4] Pfluger, P.T., Herranz, D., Velasco-Miguel, S., Serrano, M., Tschop, M.H., 2008. Sirt1 protects against high-fat diet-induced metabolic damage. Proceedings of the National Academy of Sciences of the United States of America 105(28):9793–9798.

[5] Banks, A.S., Kon, N., Knight, C., Matsumoto, M., Gutierrez-Juarez, R., Rossetti, L., et al., 2008. SirT1 gain of function increases energy efficiency and prevents diabetes in mice. Cell Metabolism 8(4):333–341.

[6] Champy, M.F., Selloum, M., Zeitler, V., Caradec, C., Jung, B., Rousseau, S., et al., 2008. Genetic background determines metabolic phenotypes in the mouse. Mammalian Genome 19(5):318–331.

[7] Virtue, S., Vidal-Puig, A., 2013. Assessment of brown adipose tissue function. Frontiers in Physiology, 4128.

[8] Lagouge, M., Argmann, C., Gerhart-Hines, Z., Meziane, H., Lerin, C., Daussin, F., et al., 2006. Resveratrol improves mitochondrial function and protects against metabolic disease by activating SIRT1 and PGC-1alpha. Cell 127(6):1109–1122.

[9] Holmstrom, M.H., Iglesias-Gutierrez, E., Zierath, J.R., Garcia-Roves, P.M., 2012. Tissue-specific control of mitochondrial respiration in obesity-related insulin resistance and diabetes. American Journal of Physiology. Endocrinology and Metabolism 302(6):E731–E739.

[10] Schmittgen, T.D., Livak, K.J., 2008. Analyzing real-time PCR data by the comparative C(T) method. Nature Protocols 3(6):1101–1108.

[11] Mootha, V.K., Lindgren, C.M., Eriksson, K.F., Subramanian, A., Sihag, S., Lehar, J., et al., 2003. PGC-1alpha-responsive genes involved in oxidative phosphorylation are coordinately downregulated in human diabetes. Nature Genetics 34(3):267–273.

[12] Ortega-Molina, A., Efeyan, A., Lopez-Guadamillas, E., Munoz-Martin, M., Gomez-Lopez, G., Canamero, M., et al., 2012. Pten positively regulates brown adipose function, energy expenditure, and longevity. Cell Metabolism 15(3):382–394.

[13] Feige, J.N., Lagouge, M., Canto, C., Strehle, A., Houten, S.M., Milne, J.C., et al., 2008. Specific SIRT1 activation mimics low energy levels and protects against diet-induced metabolic disorders by enhancing fat oxidation. Cell Metabolism 8(5):347–358.

[14] White, A.T., Philp, A., Fridolfsson, H.N., Schilling, J.M., Murphy, A.N., Hamilton, D.L., et al., 2014. High-fat diet-induced impairment of skeletal muscle insulin sensitivity is not prevented by SIRT1 overexpression. American Journal of Physiology. Endocrinology and Metabolism 9(307):E764–E772.

[15] White, A.T., McCurdy, C.E., Philp, A., Hamilton, D.L., Johnson, C.D., Schenk, S., 2013. Skeletal muscle-specific overexpression of SIRT1 does not enhance whole-body energy expenditure or insulin sensitivity in young mice. Diabetologia 56(7):1629–1637.

[16] Gerhart-Hines, Z., Rodgers, J.T., Bare, O., Lerin, C., Kim, S.H., Mostoslavsky, R., et al., 2007. Metabolic control of muscle mitochondrial function and fatty acid oxidation through SIRT1/PGC-1alpha. EMBO Journal 26(7):1913–1923.

[17] Gerhart-Hines, Z., Dominy Jr., J.E., Blattler, S.M., Jedrychowski, M.P., Banks, A.S., Lim, J.H., et al., 2011. The cAMP/PKA pathway rapidly activates SIRT1 to promote fatty acid oxidation independently of changes in NAD(+). Molecular Cell 44(6):851–863.

[18] Cannon, B., Nedergaard, J., 2011. Nonshivering thermogenesis and its adequate measurement in metabolic studies. Journal of Experimental Biology 214(Pt 2):242–253.

[19] Herranz, D., Munoz-Martin, M., Canamero, M., Mulero, F., Martinez-Pastor, B., Fernandez-Capetillo, O., et al., 2010. Sirt1 improves healthy ageing and protects from metabolic syndrome-associated cancer. Nature Communications(1) (Article number 3). http://www.nature.com/ncomms/journal/v1/n1/full/ncomms1001.html.

[20] Qiang, L., Wang, L., Kon, N., Zhao, W., Lee, S., Zhang, Y., et al., 2012. Brown remodeling of white adipose tissue by SirT1-dependent deacetylation of Ppargamma. Cell 150(3):620–632.

[21] Moynihan, K.A., Grimm, A.A., Plueger, M.M., Bernal-Mizrachi, E., Ford, E., Cras-Meneur, C., et al., 2005. Increased dosage of mammalian Sir2 in pancreatic beta cells enhances glucose-stimulated insulin secretion in mice. Cell Metabolism 2(2):105–117.

[22] Bordone, L., Motta, M.C., Picard, F., Robinson, A., Jhala, U.S., Apfeld, J., et al., 2006. Sirt1 regulates insulin secretion by repressing UCP2 in pancreatic beta cells. PLoS Biology 4(2):e31.

[23] Rodgers, J.T., Lerin, C., Haas, W., Gygi, S.P., Spiegelman, B.M., Puigserver, P., 2005. Nutrient control of glucose homeostasis through a complex of PGC-1alpha and SIRT1. Nature 434(7029):113–118.

[24] Nemoto, S., Fergusson, M.M., Finkel, T., 2005. SIRT1 functionally interacts with the metabolic regulator and transcriptional coactivator PGC-1{alpha}. Journal of Biological Chemistry 280(16):16456–16460.

[25] Cantó, C., Gerhart-Hines, Z., Feige, J.N., Lagouge, M., Noriega, L., Milne, J.C., et al., 2009. AMPK regulates energy expenditure by modulating NAD+ metabolism and SIRT1 activity. Nature 458(7241):1056–1060.

[26] Bordone, L., Cohen, D., Robinson, A., Motta, M.C., van Veen, E., Czopik, A., et al., 2007. SIRT1 transgenic mice show phenotypes resembling calorie restriction. Aging Cell 6(6):759–767.

[27] Chalkiadaki, A., Guarente, L., 2012. High-fat diet triggers inflammation-induced cleavage of SIRT1 in adipose tissue to promote metabolic dysfunction. Cell Metabolism 16(2):180–188.

[28] Xu, C., Bai, B., Fan, P., Cai, Y., Huang, B., Law, I.K., et al., 2013. Selective overexpression of human SIRT1 in adipose tissue enhances energy homeostasis and prevents the deterioration of insulin sensitivity with ageing in mice. American Journal of Translational Research 5(4):412–426.

[29] Price, N.L., Gomes, A.P., Ling, A.J.Y., Duarte, F.V., Martin-Montalvo, A., North, B.J., et al., 2012. SIRT1 is required for AMPK activation and the beneficial effects of resveratrol on mitochondrial function. Cell Metabolism 15(5):675–690.

[30] Purushotham, A., Schug, T.T., Xu, Q., Surapureddi, S., Guo, X., Li, X., 2009. Hepatocyte-specific deletion of SIRT1 alters fatty acid metabolism and results in hepatic steatosis and inflammation. Cell Metabolism 9(4):327–338.

[31] Planavila, A., Iglesias, R., Giralt, M., Villarroya, F., 2011. Sirt1 acts in association with PPARalpha to protect the heart from hypertrophy, metabolic dysregulation, and inflammation. Cardiovascular Research 90(2):276–284.

[32] Brunet, A., Sweeney, L.B., Sturgill, J.F., Chua, K.F., Greer, P.L., Lin, Y., et al., 2004. Stress-dependent regulation of FOXO transcription factors by the SIRT1 deacetylase. Science 303(5666):2011–2015.

[33] Banks, A.S., Kim-Muller, J.Y., Mastracci, T.L., Kofler, N.M., Qiang, L., Haeusler, R.A., et al., 2011. Dissociation of the glucose and lipid regulatory functions of Fox01 by targeted knockin of acetylation-defective alleles in mice. Cell Metabolism 14(5):587–597.

[34] Barbera, M.J., Schluter, A., Pedraza, N., Iglesias, R., Villarroya, F., Giralt, M., 2001. Peroxisome proliferator-activated receptor alpha activates transcription of the brown fat uncoupling protein-1 gene. A link between regulation of the thermogenic and lipid oxidation pathways in the brown fat cell. Journal of Biological Chemistry 276(2):1486–1493.

[35] Petersen, K.F., Shulman, G.I., 2006. Etiology of insulin resistance. American Journal of Medicine 119(5 Suppl. 1):S10–S16.

[36] Girousse, A., Tavernier, G., Valle, C., Moro, C., Mejhert, N., Dinel, A.L., et al., 2013. Partial inhibition of adipose tissue lipolysis improves glucose metabolism and insulin sensitivity without alteration of fat mass. PLoS Biology 11(2):e1001485.

[37] Badin, P.M., Louche, K., Mairal, A., Liebisch, G., Schmitz, G., Rustan, A.C., et al., 2011. Altered skeletal muscle lipase expression and activity contribute to insulin resistance in humans. Diabetes 60(6):1734–1742.

[38] Stanford, K.I., Middelbeek, R.J., Townsend, K.L., An, D., Nygaard, E.B., Hitchcox, K.M., et al., 2013. Brown adipose tissue regulates glucose homeostasis and insulin sensitivity. Journal of Clinical Investigation 123(1): 215–223.

[39] Canto, C., Houtkooper, R.H., Pirinen, E., Youn, D.Y., Oosterveer, M.H., Cen, Y., et al., 2012. The NAD(+) precursor nicotinamide riboside enhances oxidative metabolism and protects against high-fat diet-induced obesity. Cell Metabolism 15(6):838–847.

[40] Brown, K.D., Maqsood, S., Huang, J.Y., Pan, Y., Harkcom, W., Li, W., et al., 2014. Activation of SIRT3 by the NAD(+) precursor nicotinamide riboside protects from noise-induced hearing loss. Cell Metabolism 20(6): 1059–1068.

